To Nunún

"Here in Norway we would say that you are like a potato[1]*,*
it's good to be like a potato"

Asgeir J. Sørensen, to me

"Now we have to wait for another transect. This is a bit boring",
"That is ok. Out on sea, boring is good".

talking with Frode Volden

[1]The potato is probably the most recurrent element of the Norwegian cuisine, being usually combined with most of the dishes. Metaphorically speaking, to be like a potato means to fit into many situations or, like in this case, many projects of different nature.

Abstract

This thesis concerns several aspects of the automatic system that controls the behavior of Remotely Operated Vehicles (ROVs), and elaborates the data collected during the operations. It presents the algorithms used to develop the motion control system implemented in the NTNU AUR-Lab's fleet of ROVs, and to accomplish sea operations in collaboration with academic and industrial partners. The required improvements of such system, and the need for a higher level of autonomy in the field of marine robotics, have been the main drivers of this thesis. The participation in field work and practical missions, the collaborations with scientists with different backgrounds, and the current vision of the marine robotics community and of the centre for Autonomous Marine Operations and Systems (NTNU AMOS), have contributed to direct this research towards the nodes which the author considered crucial.

This thesis presents contributions to the different modules of a control system for ROVs. A control system takes as input reference and sensor signals, using them to produce a proper control action in order to obtain the desired vehicle motion. The characteristics of the input signals are therefore important for the behavior of the whole control system feedback chain. For such reason, a signal processing module is developed and implemented, with the purpose of filtering out the outliers often produced by acoustic positioning systems. The sensor signals need to be merged and filtered, in order to produce a complete and reliable estimation of the vehicle. This problem, known as the navigation problem, can be solved by model-based or kinematic observers (estimators). Moreover, underwater vehicles are utilized in various use-modes and with different environmental conditions. These aspects can be taken into account in the design of the observer module. In fact, a bank of observers can be designed so that it is possible to switch between the single algorithms to improve the accuracy of the estimation. A so-called multi-objective observer, based on the nonlinear passive filter, is designed for this purpose. The reference signal, which is often a destination point in space or a line to be followed, cannot always be fed into the control system. A guidance module is often used to produce intermediate desired states that converge to the ultimate goal. This module is designed so that environmental disturbances, as well as kinematic and dynamic constraints, can be automatically taken into account during the process. In this context, an Integral Line Of Sight (ILOS) algorithm has been implemented and tested on an ROV system. The users are also part of the control chain, although they are often not formally included in the system architectures. This is important to have in mind, since the behavior of the human operators influences

the performance of the vehicle. An important task for those who design control systems is to provide the operators with both necessary and sufficient information, and a way to efficiently steer and control the vehicle. In this context, an innovative Human-Machine Interface (HMI), which uses the Head-Mounted-Display (HMD) technology, has been developed and implemented, with the purpose of improving the state-of-art of the ROV interfaces.

The camera technology mounted on the AUR-Lab fleet of vehicles is also included in this work, not only to produce data of valuable importance for the end users, but also to produce useful information for the control system itself. Underwater mapping is presented as an application of this technology, together with the development of underwater off-line and real-time mosaics. Underwater photomosaics and camera information can be used to give important information on the morphology of the terrain. With such information, the vehicle can be automatically steered giving priority to those areas with a greater density of Object Of Interest (OOIs). An attempt to understand the best direction of the vehicle, based on camera information, is proposed.

A path-planning system is necessary to define the mission of a vehicle. In a context of increased autonomy, underwater vehicles have the necessity of being equipped with a fast and safe autonomous planning and replanning systems. In this work, a system to automatically plan and re-plan the path of a marine vehicle (possibly underactuated) is proposed and developed. The system has been first developed to plan surface vessel paths. Then, the system has been improved including a fast, automatic re-planning procedure, and finally extended to be used in the underwater three-dimensional environments.

This work also presents some examples of practical operations, which have been performed along the Norwegian coastline by AUR-Lab engineers, technicians and scientists, in collaboration with different end-users commissioning the work (companies, other researchers, institutions). Some details of such operations, their critical aspects and the goals of the key people involved are described in this thesis, as well as the operations of AUR-Lab, which successfully merges the academic need for scientific development and the end user's needs.

Acknowledgements

In the following, the list of the contributors for the work described in this thesis is presented. I would like to underline that this thesis would not have been possible without the collaboration of any single person that is cited in the following.

Collaborations related to Chapter 2

Fredrik Dukan is the person that started the ROV DP system project back in 2010, carried its responsibility for the first years and passed it to me some years ago. Stein Nornes is the one who inherited the same responsibility after my duty was over. We have cooperated to keep the system working, efficient and free of bugs (or at least we tried hard). Since the system was launched there have been many other people collaborating on it. Marianne Kirkeby, Steffen Kørte, Phat Truong, Espen Tolpinrud, and Daniel de Almeida Fernandes have contributed to discuss, develop and test the algorithms for the system.

The discussions with Anastasios M. Lekkas about the HiPAP system behavior during full-scale missions, brought to the development of the outlier detection algorithm.

The student Fabio Dezi is thanked for the collaboration on the multi-objective observer.

Walter Carahija and Signe Moe are thanked to involve me in the guidance work concerning the ILOS algorithms.

Eirik Valle and Michel Rejani Miyazaki are thanked for the great effort they did to help me integrating the Oculus Rift system into the 30K system.

Collaborations related to Chapter 3

For the work included in this chapter, I must thank Martin Ludvigsen, who asked me to process some pictures on a cruise towards Ormen Lange. That is how (unexpectedly) this work began. Many students have collaborated with me along the process, Francesco Celiberti, Paolo Pencarelli, Fernando Mosciaro are some of those.

Ingrid M. Hansen, Geir Johnsen, Øyvind Ødegård, and Fredrik Skoglund helped me for the development of the underwater mosaics and during the cruises work.

Collaborations related to Chapter 4

Anastasios M. Lekkas is thanked to suggest the usage of Voronoi diagram for the path planning of marine vehicles. His constant supervision has been essential to develop all

the work related with surface vessel and underwater vehicle's path planning.

Jeevith Hegde is thanked for the discussions and cooperation related to safety for UUVs.

Collaborations related to Chapter 5

Many should be thanked for the help during the hard work on the vessel Gunnerus: Frode Volden has been one of the persons I had more fun working with. A special thank goes to Christian Malmquist, an example of a professional which can perform greatly in stressful situations with an incredible calm. All the members of the Gunnerus crew has been always helping are highly thanked: Arve Knudsen, Svenn Ove Linde, Mats Reppe.

The students Jostein Follestad, Eirik Valle and Fredrik Sandved are thanked for the work with the Neptunus project. Was very fun working with you.

Personal Acknowledgments

A five-year-long process cannot be accomplished without the support of a lot of people. My adventure in Trondheim allowed me to collect new knowledge and experience on the field, and gave me also the chance of getting to know a lot of wonderful people, which I would like to thank in the following lines.

Asgeir deserves the biggest *thank you*, since he has not been only my work-supervisor, but he has also helped me answering questions and giving me suggestions about my life outside the department, being constantly available. Moreover, he brought me to Trondheim three times: to start my master thesis, to start my PhD, and to continue it when I was almost deciding to take another direction. I am very grateful for that.

Thank you to my co-supervisors Martin Ludvigsen and Sauro Longhi for the support and help during these years. The former taught me a lot about ROV technology.

During the latest months and while ultimating this thesis, some people were extremely helpful for many different reasons. To this purpose, would like to say *thank you* to Ingrid Schjølberg, Ingrid Utne, Roger Skjetne, Marilena Greco and Jannike Gripp.

At Marine Technology I had the pleasure to meet many cool people from all over the world. We shared experiences, thoughts, points of view. Daniel, Bo Zhao, Vijay, Sepideh, Rikard, Isar have been the ones I started my adventure with. Siri, Martin, Jit, Saša, Øyvind, Sandro, Sabah enlarged the group soon after. Then AMOS started, and brought in a lot of new colleagues: Michel, Stein, Claudio, Mikkel, Øyvind, Dennis, Bård, Astrid, Petter, Ida, Jan Tore are some of them. I shared a little part of my everyday with all of you, and I am very happy that I had the chance of doing so.

I must also say *thank you* to Erik Dyrkoren, Borja, and the rest of the team at BluEye Robotics. I have been on board for few months (after months planning meetings) seeing a new and exciting company being finally shaped.

Tasos, Svenn Are, Albert, Michel and Daniele have been very, very good friends. *Thank you* for all the help and support. I must also thank Andreas for a sentence that he told me before leaving my goodbye party. He said that he was sad that I was leaving, because I

became a bit one of the “old pillars" of the PhD group. This sentence says a lot about how much the over-consumption of alcohol can shape sentences but still, I want to believe that I also left something positive to my ex colleagues and friends at Marine.

For a long period I had the pleasure of sharing my office with Fredrik. *Thank you* for being a great officemate and colleague, and for giving me the chance of joining him at his new and exciting start-up company: Norwegian Subsea.

Marin Technology gave me also the chance of meeting some people that were not only cool. But also musicians (which adds the adverb “super” in front of “cool”): Tasos, Daniel, Geir, Kasper, Matteo, Andreas, Erlend and Tore. We had so much fun at the rehearsals and on stage, *thank you* for our 20 minutes of fame.

Although may be not so noticeable to everybody, Trondheim hides a lot of Italians behind its corners. I had the chance of meeting and sharing a lot of funny moments with many of them. Fabio, Luca O., Mister G, Simone, Luca R., Luca F., Alessandro, Nick, Mauro, Francesco, Stefano, Elena & Andrea and Massimiliano are some of the Italian crew.

Giorg, Mattia, Mallu, Stefano, Nico, Gimmy, Scoccio, Pasqua and Michi deserve a *thank you* for the long-distance support, and for the warm welcome that I found everything I was putting my feet back on the little Italian town where I come from.

A *thank you* to all the others which came into my life for chance, and made it so much richer. Filippo and Thomas have been incredible friends, always there when I needed: we had interminable discussions about everything and nothing at the same time. Runa has been a great flatmate and friend. Hildegunn gave me a place to stay for my defence-days and helped with MaurTek AS, that will be such a great company one day. Renata helped me correcting the thousand typos hidden in these pages. Kalle and Julia have been great friends, too bad our lives kept us almost constantly far apart since the Erasmus times. And then Helene, Marta, Seniz, Einar and Maria with which I shared a lot of time.

A *thank you* also to my second boss, Frode, which tried to find a girlfriend for me, warning me that the more I wait the less available girls I will find. I hope there are still some left cause, up to today, nothing much has changed.

A big *thank you* goes to my family. Which was there when I needed to talk more than humanly acceptable, or when I was disappearing for interminable periods. They have always understanding, always helping, always close.

At last, a *thank you* to myself. I have been my best friend and my worst enemy at the same time. I went through very happy and very tough moments, but I am aware that I became stronger and wiser then when I started, which in itself is already a good achievement. And I made it to these days, with a thesis which I am soon going to discuss. I swear I didn’t think this was going to happen until Asgeir wanted it on his desk as soon as possible. He finally had it, maybe not *as soon* as he actually expected but well, here it is:

I made it!

Trondheim, December 2016 *Mauro Candeloro*

Nomenclature

VEHICLES AND PAYLOAD

AUV	Autonomous Underwater Vehicle
ASV	Autonomous Surface Vessel
CMROV	Consumer-market ROVs
CTD	Conductivity, Temperature, Depth
DVL	Doppler Velocity Log
IMU	Inertial Measurement Unit
MRU	Marine Reference Unit
MSROV	Mid-sized ROV
OCROV	Observation Class ROV
PMT	Photon Multiplier Tube
ROV	Remotely Operated Vehicle
UBAT	Underwater BAThyphotometer
UHI	Underwater Hyperspectral Imaging
USV	Unmanned Surface Vessel
UUV	Unmanned Underwater Vehicle
WCROV	Work class ROV

SOFTWARE AND INTERFACES

GUI	Graphical User Interface
HMI	Human-Machine Interface
HMD	Head-Mounted Display
OO	Object Oriented

ALGORITHMS AND MATHEMATICS

2D	Two-dimensions or two-dimensional, depending by the context.
3D	Three-dimensions or three-dimensional, depending by the context
AOI	Area Of Interest
CTA	Closest Time of Approach
CTE	Cross-Track-Error
CPA	Closest Point of Approach
DOF	Degree Of Freedom
ECF	Explicit Complementary Filter
EKF	Extended Kalman Filter

FOV	Field Of View
(I)LOS	(Integral) Line Of Sight
LKF	Linear Kalman Filter
POA	Projected Obstacle Area
RANSAC	RANdom SAmple Consensus
SIFT	Scale-invariant feature transform

PEOPLE AND ORGANIZATIONS

AMOS	centre for Autonomous Marine Operations and Systems
AUR-Lab	Applied Underwater Robotics Laboratory
IEEE	Institute of Electrical and Electronics Engineers
ISO	International Organization for Standardization
NORSOK	Norsk Sokkels Konkurranseposisjon (Norwegian Offshore standards)
NTNU	Norges Teknisk-Naturvitenskapelige Universitet (Norwegian University of Science and Technology)
WHOI	Woods Hole Oceanographic Institution

SYSTEMS AND ARCHITECTURES

DP	Dynamic Positioning
GNSS	Global Navigation Satellite System
HD	High Definition
HiPAP	High Precision Acoustic Positioning
HW	HardWare
INS	Inertial Navigation System
LBL	Long Base Line
SSBL	Super Short Base Line
SW	SoftWare
USBL	Ultra Short Base Line

OPERATIONS

COLREG	International Regulations for Preventing Collisions at Sea
LMP	Lawn Mower Pattern
MCM	Mine Counter Measures
OaG	Oil and Gas
OOI	Object Of Interest

OTHERS

DC	Direct Current
HMI	Hydrargyrum Medium-arc Iodide
PVC	Poly Vinyl Chloride

Contents

List of Figures

Part I

Thesis Overview

Chapter 1

Introduction

This thesis regards control system algorithms and operations for underwater vehicles. Remotely Operated Vehicles (ROVs) will be mainly cited, although many of the algorithms can also be used for Autonomous Underwater Vehicles (AUVs) or Unmanned Surface Vehicles (USVs). Contributions are related with the development of several modules of the NTNU Applied Underwater Robotics Laboratory (AUR-Lab) ROVs' motion control system, of path-planning systems for USVs and Unmanned Underwater Vehicles (UUVs) and of underwater mapping and photomosaics.

The ROV motion control system was developed during the last years with the contributions of PhD candidates, master students, postdoctoral researchers and professors. The AUR-Lab ROVs are described in Subsection 1.2.5. These vehicles, and their Dynamic Positioning (DP) motion control system, were used to provide some of the results showed in this thesis. In other cases, simulation results are used to validate the proposed algorithms. The participation to several full-scale missions outside the Norwegian coastline allowed the author to gain experience as an ROV pilot, and as the responsible person for the control system, the collection of data and the data analysis. Part of this experience is mentioned to illustrate the needs and goals of the operators, engineers and end-users.

Section 1.1 presents the motivations of this work, placing it in the bigger picture of an offshore operation. Note how UUVs are great engineering products, but they are relevant only in connection with the needs of scientists and end-users working within the ocean space. Consequently, their perspective will be taken into account. Section 1.2, tries to give an overview of the characteristics of the UUVs, going into details of the ROV class. This section will concern: UUV and ROV classifications (Subsection 1.2.1), some historical glimpses of the ROV technology (Subsection 1.2.2), ROV applications (Subsection 1.2.3), ROV payload components (Subsection 1.2.4), the AUR-Lab ROV fleet (Subsection 1.2.5), the new class of consumer-market ROVs (Subsection 1.2.6) and the autonomy perspective (Subsection 1.2.7). Section 1.3 describes the structure of this thesis, and Section 1.4 describes the main scientific contributions of this thesis. Finally, Section 1.5 lists the papers which contain the main algorithms, methods and contributions on which this thesis is built. Section 1.6 shows the media interest in this work.

1.1 Motivation

Figure 1.1 summarizes an offshore operation scenario, and shows the mutual cooperation of underwater and surface vehicles, researchers and scientific equipment. The operations themselves are influenced by the marine environment: the motion of the water acts as a disturbance towards the vehicles, while biological and artificial Objects Of Interest (OOIs) are hidden under its depths. In the following description, the *italic font* represents a direct reference to the elements showed in Figure 1.1.

Engineers, technicians and operators run the technical aspects of the mission from the surface vessel's *control room*, assuring that the vehicles (e.g. ROVs, AUVs) perform their tasks properly and that data is correctly gathered. Scientists and end-users follow the operations, interpreting and analyzing the data, and giving indications for the mission's next steps. Meanwhile, the AUV and the ROV perform the designated operations, which may involve sampling, mapping or inspecting underwater OOIs. Vehicles can be programmed to work together, in more complex *coordinated operations*. Such integrated missions can proficiently reach their goals if all their components can work synchronously towards a common goal, despite the difficulties introduced by the underwater environment. The ability of estimating the real state of the vehicles, of optimally actuating their thrusters, of *planning a proper trajectory* to be followed while simultaneously counteracting for *environmental and external forces*, are all necessary elements in this context.

This thesis discusses and proposes methods and algorithms which help to improve the operations that often need to be carried out in the aforementioned scenario. The personal participation of the author in several full scale missions generated suggestions on what was needed or could be improved in order to increase the vehicles' performance, and also to better gather and analyze the data for the end-users. This push towards a general improvement of the mission operations and a better end-users' satisfaction has been the main drive for the following steps of this thesis. It is important to underline that, although the thesis is mainly focused on providing tools aimed for seabed operations, they find applications and needs also in water column applications, as it will be clearer when treating the users' point of view and field operations.

In this big and complex picture, this thesis tries to contribute by answering the following research questions:

- How can the ROV Control System be efficiently improved to increase its performance in connection to the real mission's characteristics and the operator's needs?
- Which tools can be developed to give the end-users a comprehensive information about the underwater environment? Could these tools be used actively and autonomously from the ROV Control System during the operations?
- How could the mission and path planning phases be designed to increase the mission's autonomy?

Possible answers to these questions are given respectively in Chapters 2, 3, and 4. Chapter 5 describes few examples of full-scale missions. Chapter 6 states the conclusions.

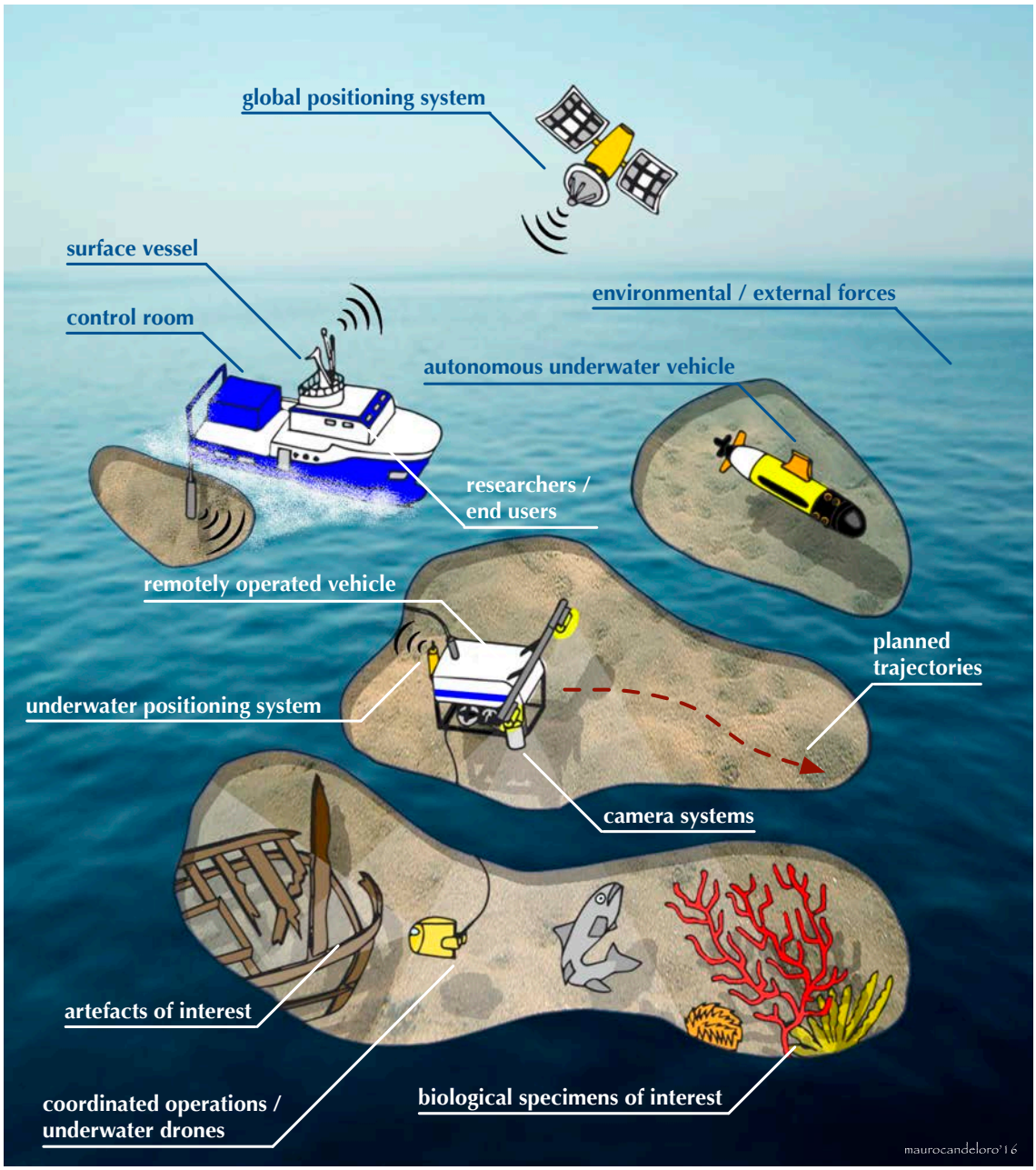

Figure 1.1: Representation of the main elements which compose the scenario treated in this thesis. In fact, this work mainly concerns ROVs and their motion control systems, which requires the integration and cooperation of a certain payload and navigation sensors. Many aspects are relevant and applicable for AUVs also. Surface vessels are required to operate ROVs, since they carry the control room, support the communication and provide the missing connection link with a global positioning system. It is important to remember that underwater vehicles are tools, that would not have much use without OOIs to be investigated, mapped or sampled. The importance of the end-users' perspective is underlined. Some attempts of developing a multi-vehicle system for a coordinated operation will also be briefly treated. The latter has also been the starting point of the development of an innovative underwater-drone prototype. [Illustration by Mauro Candeloro]

1.2 Background

In the following, some information about UUVs and their applications are given, mainly focusing on their characteristics and on the operations performed by their ROV sub-class. Many extensive reviews about the state-of-art of UUVs and ROVs can be found in literature [1, 2, 3]. Notice that the information concerning the overview presented in the next subsections, has been mainly inspired by [4]. The information about the ROV classifications (Subsection 1.2.1), about the ROV applications (Subsection 1.2.3) and about the ROVs' main components (Subsection 1.2.4), are presented altogether in Figure 1.5, which gives a visual and summarizing overview of the characteristics of this technology.

1.2.1 UUVs: Characteristics and Classifications

The US Navy's UUV Master Plan [3] defines UUVs as:

> *"Self-propelled submersible whose operation is either fully autonomous [...] or under minimal supervisory control and is untethered except, possibly, for data links such as a fiber-optic cable."*

This definition emphasizes the absence of tethering and the operator's level of intervention in the vehicles' operations, mainly depicting what is known as an AUV. Notice that ROVs are also normally classified as an UUV subclass, both in the scientific and industrial community. A simple definition of ROV is provided by [5]:

> *"An underwater vehicle physically linked, via the tether, to an operator that can be on a submarine or on a surface ship. The tether is in charge of giving power to the vehicle as well as closing the manned control loop."*

It is important to notice that the differences between the AUV and ROV subclasses are deeply influenced, but goes beyond the presence or absence of tethering:

AUVs are characterized by the absence of tethering, characteristic that *breaks the physical connection* between the operators and the vehicle. This absence of link is also underlined by the term *autonomous*, included in the acronym. The absence of a physical tethering requires the presence of on-board batteries, which, in turns imposes a limit on the duration or the geographical extension of the operations. The hydrodynamic shape and the absence of the tether drag allow for higher speed and the possibility of covering longer distances. The limited power those vehicles can exercise on external elements and their underactuation make AUVs generally unsuited for manipulation operations, where the ability of exercising a discrete force while keeping a steady position is required.

ROVs are characterized by the presence of the tether, which is underlined by the terms *remotely operated* in the acronym. The presence of this continuous physical link with a support vessel clearly reduces their level of autonomy, but gives them, ideally, unlimited power and the possibility to carry out infinitely long operations. The presence of

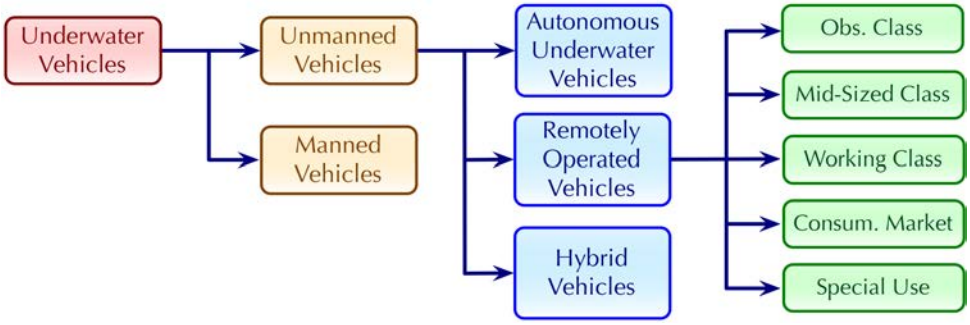

Figure 1.2: Classification of UUVs based, respectively, on the presence of humans on board, design characteristics and operations.

the tether increases the drag, which reduces the effectiveness of any hydrodynamic design (which is often limited to the most practical box-shape). The high power that they can exercise, their ability of carrying heavy and cumbersome payloads, and a dexterous hydraulic manipulator, together with the Dynamic Positioning (DP) possibilities, allow them to perform heavy manipulation or construction work, among other tasks.

Due to the limitations that affect these classes of vehicles, hybrid solutions are being studied and developed, in order to overcome the limitations and increase the effectiveness of the operations. This is made possible from the parallel development of wireless higher-bandwidth optic/acoustic communication links, and lighter (and more efficient) battery systems. An example is the ROV Nereus, developed by the Woods Hole Oceanographic Institution, which is the first cost-effective technology that can reach the deepest spots in the oceans [6]. Other examples are the Bluefin Robotics, or the H-ROV [7, 8].

Figure 1.2 shows how UUVs can be divided in subclasses depending on size, presence of humans on board, and design characteristics. The ROV subclass can be further divided in many ways, depending on the characteristics which are taken into consideration. Size can be a good classifying parameter, since it is directly related with the thrust capabilities, the payload weight and the depth rating [4]. This allows to define:

Observation Class ROVs *(OCROVs)*: Smaller vehicles weighing up to 100 Kg, mainly used for shallow waters inspection and mapping tasks. Their payload is often limited to cameras and a small grasper[1]. The depth-rating is also limited to few hundreds meters.

Mid-sized ROVs *(MSROVs)*: extended version of the OCROVs: heavier, rated for higher depths and with higher payload capabilities. They often carry a hydraulic manipulator. They are built to perform observation tasks and light intervention work.

Work class ROVs *(WCROVs)*: heavy vehicles running on high voltage power supplies from the surface. Usually, they have hydraulic propulsion and a 6 DOFs dexterous manipulation devices, which give them the ability to perform heavy work.

[1] A grasper is a simple device which consists of a pincer-shape end-effector tool which can pick up and hold an object. Usually, it is mounted on a non-extensible, fixed, metal arm.

***Consumer-market ROVs** (CMROVs)*: a new category of ROVs, which is becoming commercially available as the author is writing his thesis. Their weight generally allows a single person to carry the needed equipment by himself. The power supply is given by on-board batteries, while the payload often consists of only an inspection and navigation camera. Their low cost makes them affordable for the masses (see Subsection 1.2.6).

Special-use vehicles: all the other vehicles that cannot be described by the previous definitions and that include ad-hoc design due to the peculiarity of their operation. For instance, underwater non-swimming vehicles (i.e. crawling or towed vehicles), or vehicles which are built for special operations (i.e. the exploration of particularly deep trenches).

1.2.2 ROVs: from *"nothing but a problem"* to an *"industry need"*

The development of innovative technologies often follows a common thread: the dream and effort of some visionary, the investment from the governments (which see a potential in these "dreams"), the understanding of the idea's benefits from the industrial society, and the rapid development due to the involvement of a larger number of private companies. Finally, the diffusion and the employment of the technology in the everyday operations. The ROV development follows this thread too, as briefly explained in the following paragraphs. More information can be found in [4, 9, 10].

As any technology in its birth-phase, the ROV technology was not easy to develop during its initial stage, since many, peculiar, new challenges needed to be faced. This is well stated in the following quote [11]:

> *"ROVs were nothing but a problem: their bottles leaked, their hydraulics failed, sunlight damaged them, they were too noisy and unreliable, were hard to control and needed constant maintenance."*

This is not difficult to imagine, since it is still not easy to design, assemble and operate an underwater vehicle from scratch (see the failing experience in Subsection 5.2).

Dimitri Rebikoff is credited to have developed the first ROV (the *PODDLE*, in 1953), for archaeological research. The Royal Navy developed the ROV *Cutlet*, to recover torpedoes and mines (in the 1950s). In the same years, the US Navy started also to develop this class of vehicles, and succeeded to produce *XN-3*, *CURV* (Cable-Controlled Underwater Recovery Vehicle) and *CURV III*, between the 1960s and the 1970s. The US Navy was initially moved by the need of recovering military equipment which was lost on the sea bottom. Following missions showed the effectiveness of such vehicles for this purpose: *CURV* was able to recover a nuclear bomb lost in the Mediterranean Sea after the 1966 Palomares B-52 crash, while *CURV III* saved the pilots of a sunken submersible off Cork, Ireland, the Pisces in 1973, with only minutes of air remaining. These vehicles performed missions in depths of 900 m: it was clear that such technology could perform much harder tasks if scientists were able to go over the limitations of this first generation of vehicles and expand their workspace and capabilities.

The US Navy kept on improving this technology, both in the direction of big and performing vehicles, but also in the new direction of small-sized observation vehicles. *Pontoon Implacement Vehicle* (with the aim of recovering sunken submarines) falls in the former category, while the *SNOOPY* ROV and its electric version (the *Electric SNOOPY*, both produced in the 1970s), fall in the latter one. The US Navy-funded company HydroProducts developed two of the first ROVs targeted for offshore work: the RCV-225 (Eyeball) and the RCV-150 (both in the early 1970s). The aim was to proceed towards smaller solutions, still capable of performing work for the offshore industry.

In the late 1970s, other nations started funding projects aimed to the development of ROVs: France, Finland, UK and Soviet Union were some of those. In these years, it was possible to notice a strong change in the trend: while, between the 1950s-1970s, the governments were the ones investing on the development of the ROV technology (85% of the produced vehicles were government-funded), private investments took over in the late 1970s, and private companies started the developing process (96% of the produced vehicles came from the private industry). This handover spread worldwide, and in most of the Americans, European and Asian nations, a number of companies entered competition, highly increasing the technology development speed.

The development of ROVs became, in the 1980s, an actual *need* for the offshore industry, which started to use ROVs to install, operate and maintain its infrastructures at high depths (up to 3000m depth). Notice that, in the same decade, the ROV development had a temporary deceleration, due to a serious drop in the price of oil and a global economic recession, which was not much different of what the world is experiencing nowadays.

Development and research kept on exploring the small-and-affordable ROV category, but the challenge of developing ROVs for extreme applications and depths was strong. The Deep Sea System International *MiniRover* was the first real low-cost, observation-type ROV (1983), followed by the Deep Ocean Engineering's *Phantom* (early 1980s). At the same time, the US Navy set the target of reaching a depth of 20000 feet (6279m), which was successfully reached from *CURV III* (1973) and by the *Advanced Tethered Vehicle (ATV)* (1988), both developed by the Space and Naval Welfare System. In 1995, the ROV *Kaiko*, developed in Japan, reached the deepest point of the Mariana Trench, setting a record that cannot be beaten.

From the 1990s, the *Schilling Robotics UHD ROV* set high standards for industrial offshore operations, starting the production of vehicles which are still proficiently used. Many other companies are nowadays producing ROVs for offshore operations. Among the biggest ones, it is possible to mention the Dutch Deep Ocean Engineering Inc., the French ECA Robotics, the American FMC Technologies Schilling Robotics and Oceaneering International, the Canadian International Submarine Engineering Ltd. (ISE), the Chilean Mariscope, the English SAAB Seaeye and the Italian Saipem America.

The 1990s also saw the beginning of the development of a new category of ROVs, made possible by the advances in the development of microelectronics and sensor technology, and the related price reduction. This category, namely micro-ROVs, is populated

by small-dimension, less-expensive vehicles, which could perform observation tasks and limited manipulation work. Although some first attempts were already done in 1983, with the Deep Sea System International *Mini Rover*, *VideoRay* was the first company finding a real market for those platforms. Today, many others compete on the same market: SeaBotix and Deeptrekker are two relevant examples.

Finally, and only in the latest months, many companies are starting to see new possibilities in a brand new market share. Following the direction firstly dictated by the aforementioned micro ROVs, and the huge success that aerial drones have had in the latest years among robotics and exploration enthusiasts, the development towards low-cost solutions has been pushed even forward. The main target is to develop vehicles which can be accessible even for hobbyist or enthusiasts. More information about this interesting chapter of the ROV history can be found in Subsection 1.2.6.

1.2.3 ROVs Applications

A brief list of common ROVs applications is reported in the following. Some applications specifically require ROVs, while other can be performed also by other kind of UUVs. Operations which require a certain strength, high power, the presence of heavy or cumbersome payload, or the ability for the vehicle to be able to keep its position despite of external factors are usually carried out by ROVs.

Science applications: public and private research organizations need to gather ocean-related data over time, for analyzing natural processes and comparing their development over time. Mapping of resources and OOIs is a very important and common task. Often, biological specimens or geological samples need to be collected and brought to the researchers for further tests.

Fisheries and Aquaculture applications: fish farming is a growing industry, allowing the production of higher quantity of fish at lower prices. For a country like Norway, it even constitutes one of the main incomes. ROVs are required to check the mooring lines, find holes in the nets, retrieve dead fish for sanitary purposes.

Military/Security/Safety applications: many operations are required in these fields. Some concern the retrieval or inspection of military objects. Mine Counter-Measures (MCM) operations is one of the tasks that can be completed through a disposable (inexpensive) ROV which triggers an explosion, or by a more powerful ROV with a dexterous manipulator that can deliver an explosive charge, arm it and escape. To provide port security, vehicles that are able to inspect vulnerable locations to verify the presence of any threat are needed. ROVs can also be used for public safety operations, for instance by inspecting a wreck to find trapped people, dead bodies, or to rescue trapped divers.

Inspection/Repair/Maintenance applications: these applications cover many industries, from wind to fish farms, from offshore Oil & Gas infrastructures to bridges' pillars. These

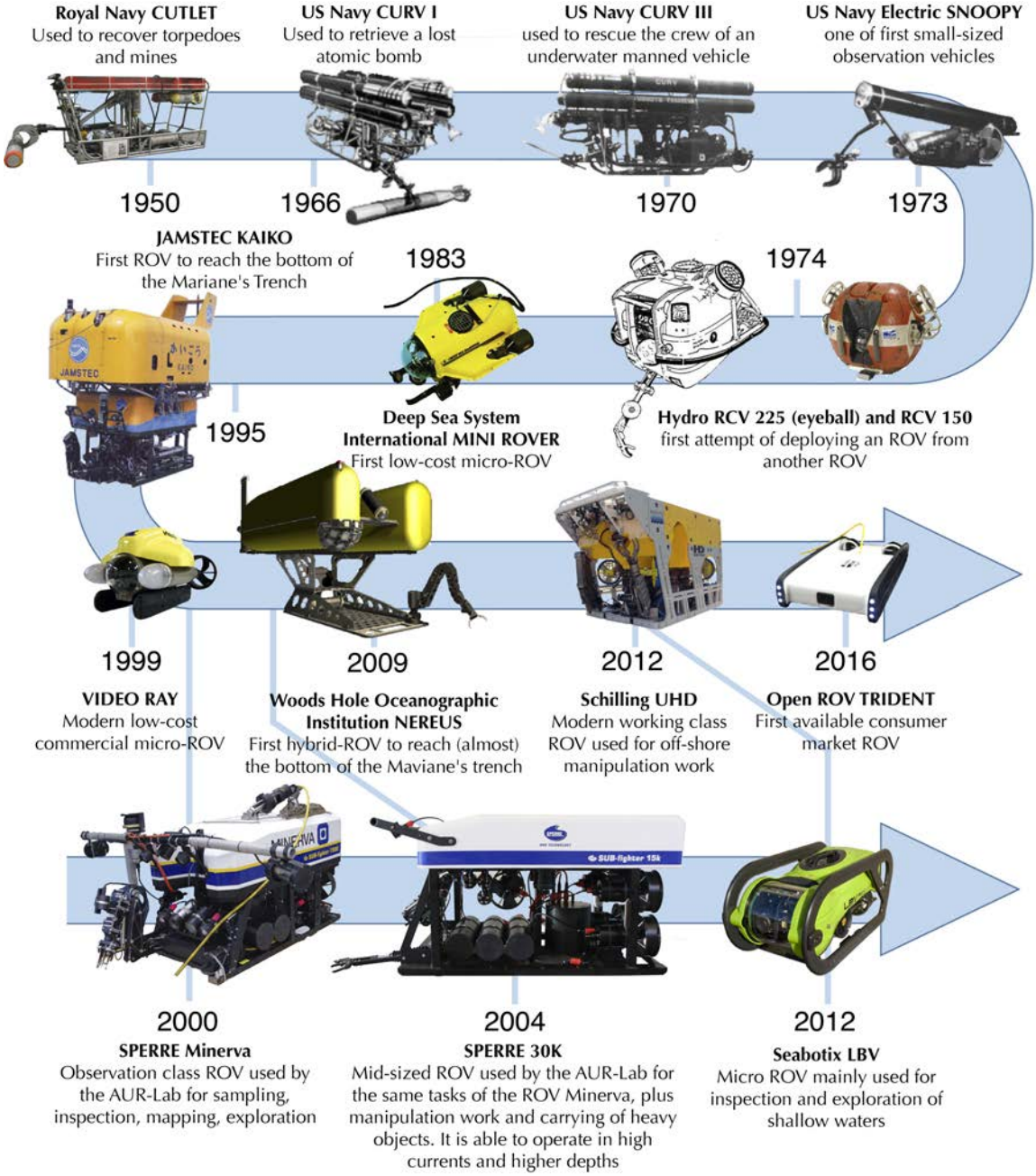

Figure 1.3: Brief overview of the ROV-technology history. The first attempts of creating ROVs were carried by governments-related projects, with main goal of rescuing and recovering lost military equipment down to depths of 1000m. The first attempts showed the effectiveness of this technology, turning on the interest of many private companies. First low-dimensions and high-performance ROVs started to be developed, together with multi-ROV systems and hybrid systems. The ROVs are, nowadays, a needed tool for the construction, inspection and maintenance of the oil&gas infrastructures at high-depths. In the latest years, the development of the new micro-ROV technology started, opening to new market possibilities, which look towards the masses. The second arrow shows the history line of the AUR-Lab fleet. The Sperre Minerva has been the first observation class ROV, followed by the mid-sized Sperre 30K and, finally, by the micro ROV from Seabotix. [Illustration by Mauro Candeloro]

systems need periodic inspection and maintenance. Depending by the needs of the specific task and the depth in which this is performed, different ROVs and tools are selected.

Construction/Drilling support applications: for construction applications, heavy pieces of equipment (e.g. cables, pipelines) may require to be moved or put into place. Heavy and powerful vehicles are consequently needed. During a drilling operation, ROVs may contribute from the first drill bit penetration to the well completion. For these tasks, ROVs may be equipped with two manipulators: one can keep the ROV steady in place, while the other performs the operation. New regulations (introduced after the Gulf of Mexico disaster) require a second ROV waiting in standby in the area, ready to intervene if needed.

1.2.4 ROVs main Components

In Figure 1.4 it is possible to see the payload of the AUR-Lab ROVs. This is quite a standard sensor-payload for OCROVs or MSROVs that are controlled from a motion control system. In the following, the main components are briefly listed and described, restricting the overview to the payload currently mounted on the AUR-Lab vehicles.

Lights

- Halogen Lights: positioned to illuminate the Field Of View (FOV) of the cameras, provide the main source of light for the operators to see the ROV surroundings. Since they can provide a relatively low illumination (18-33 Lumens[2]), several may be required around the camera systems. They provide high power only on wavelengths which are above 550 nm: consequently, the colors of the illuminated objects will be perceived warmer than they actually are.
- HMI (Hydrargyrum Medium-arc Iodide) Lights: provide a higher light intensity (70-100 Lumens) and more diffuse light. For this reason they are mounted on a top beam, far from the center of the ROV, so that a larger area in front of the vehicle can be illuminated. They provide nearly constant power all over the light spectrum, with nearly daylight characteristics, which reduces the colors distortion.
- Strobe Lights: provide high-intensity flashes of light lasting for few milliseconds. They are often used in conjunction with still-picture cameras, in order to produce a high-level of illumination which lasts only for the camera shots.

Manipulation System

- Manipulator: depending by the needs, they can span from simple grabbers (which allows to pick objects from the sea bottom or an anchorage solution), to more complex ones. In Figure 1.4 the ROV is equipped with a 4 DOFs hydraulic manipulator which provides a 2 DOFs rotation motion around its shoulder, 1 DOF around its elbow and 1 DOF on its wrist. Its end-effector is constituted by a grabbing pinch and cutter. More

[2]The lumen is the SI derived unit which measures the total quantity of visible light emitted by a source.

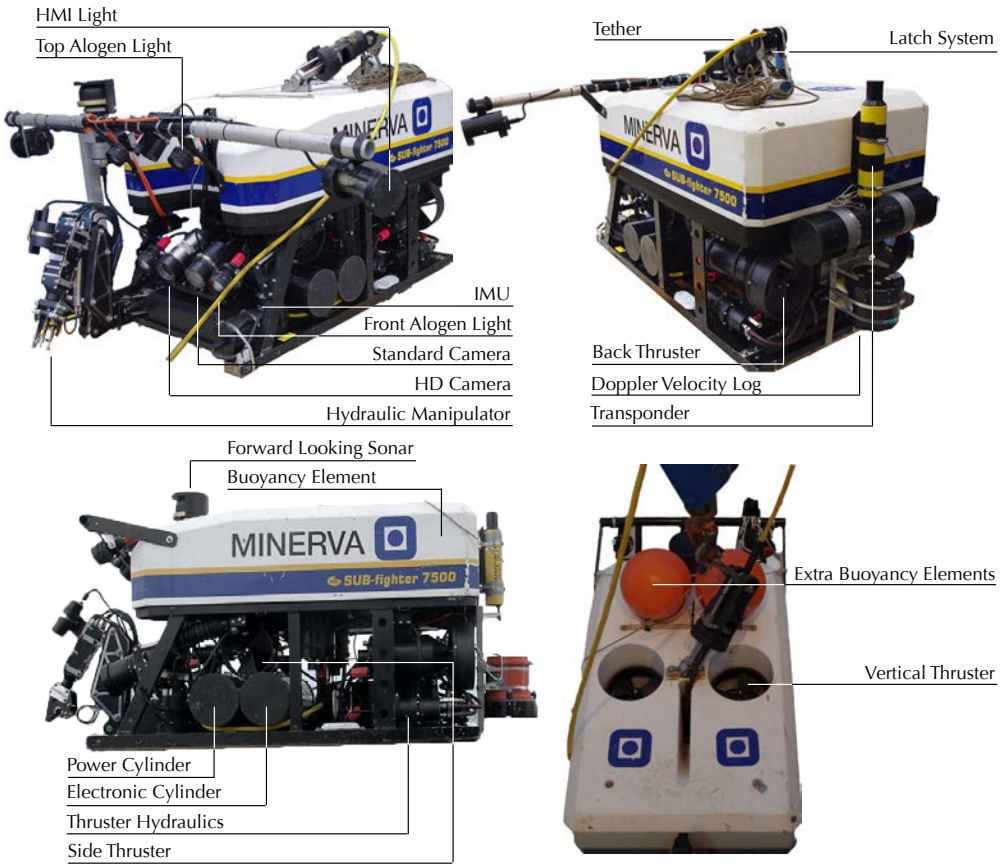

Figure 1.4: ROV main payload components. The front, back, side and top view of the ROV Minerva are shown respectively from the top left to the bottom right.

sophisticated vehicles provide dexterous 6 DOFs manipulators, where a 3 DOFs wrist provides higher agility.

- Hydraulic system: manipulators often require a hydraulic system, composed by a hydraulic motor, valve package and a compensator system. Notice that the whole components needed to build a functional manipulator system highly increase the weight of the vehicle. On the 30K system, a 6 DOFs Kraft Raptor manipulator system contributes for almost half of its 2000 Kg weight.

Navigation Sensors

- Transponder: one of the ends of an USBL (Ultra Short Base Line), SSBL (Super Short Base Line) or a LBL (Long Base Line) system. It is mounted on the vehicle and powered by internal batteries, it responds to acoustic signals transmitted from the transducers towards a known direction with a known phase. The transducers are mounted either on a support vessel (SSBL system), or positioned on the seafloor (LBL system). By triangulating the signals bouncing back to the different transducers (of which the positions are known), the position of the underwater vehicle can be calculated.

- Doppler Velocity Log (DVL): an acoustic sensor which provides a resolved velocity over bottom. The sensor is able to transmit an array of (normally) four sonar beams in a downward direction, towards the bottom. Given the position of the beam transmitters and the beams' echo return frequency the Doppler shift (which is linked to the vehicle's speed over ground related to the water column) can be measured.
- Inertial Motion Unit (IMU): a sensor suite which includes accelerometers, magnetometers and gyros. These sensors provide, respectively, accelerations, magnetic field and speed rate for every axis. If combined, variation in the vehicle's speed and position can be calculated. Notice that the fusion of the IMU with velocity or position sensors helps reducing (or eliminating) the estimation drift due to the integration.
- Pressure Sensor: a sensor which measures the pressure of the water against a flexible membrane mounted on the sensor itself. Pressure and depth are related by known mathematical formulation, which also depends by the latitude and salinity of the water.
- Still Picture / Video Cameras: produce pictures or videos that can be used as visual feedback to control the vehicle, or as a motion estimation aid. Some pictured elements, like features, objects, or light patterns, can be isolated and compared at following time instant to calculate their displacement, and consequently the vehicle's velocity vector.

Propulsion Elements

- Thrusters: are the elements which provide propulsion to the underwater vehicles. The number and position on the frame are important to guarantee maneuverability and controllability of the vehicle and define the number of DOF that the operator can actively control. Electrical motors are mainly used for underwater vehicles, where the type of electrical motor (e.g. DC permanent magnet, DC brush-less, AC motors) depends by the vehicle's application. Hydraulic motors can be employed for special applications.

Structural Elements

- Frame: provides a platform for mounting the necessary components. Its size strictly depends by the application of the vehicle and influences the amount and kind of payload the vehicle can carry.
- Buoyancy: provides compensation for the weight of the ROV structure itself, with the purpose of obtaining a (near) neutrally buoyant vehicle, so that the vertical thrusters can be only actuated to modify the depth of the vehicle, without the need of compensate for its weight. PVC or other rigid plastic foam materials are commonly used. Their structural specifications are related with the vehicle's operating depth.

Mapping Sensors

- Imaging Sonar: a forward-looking sonar, usually mounted on the bow of the ROV, helps the operator providing a wide overview of the area in front of the vehicle. A set of short acoustic pulses are emitted, those which hit the objects in the sonar's FOV bounce back to be received again from the sensor. The image formed by the reflections,

which will be shaped by the intensity of the reflections themselves, can cover an area with a radius of hundreds meters.

- Still Picture Cameras: are usually high-resolution cameras, which can provide pictures of the sea-bottom at a certain interval.
- Video Cameras: cameras which provide continuous and real-time video to the operators sitting in the support vessel. They can monitor the surroundings of the vehicle or focus on some critical equipment (e.g. the manipulator). Some should be pointed forward so that the visual feedback can be used to steer the vehicle. Due to the light absorbance characteristics of the water, turbidity and lack of natural light, underwater cameras can only show an area of few meters in front of the vehicle.
- Underwater Hyperspectral Imaging (UHI) Cameras: cameras whose digital sensor provides high sensitivity on the whole light spectrum (not only around the Red/Green/Blue channels), including the non-visible wavelengths. This equipment is very relevant for underwater mapping. In fact, due to the richer amount of color information that this sensor is able to collect, it is possible to obtain a richer optical footprint for a single specimen to the purpose of automatic recognition and mapping.

Tethering System

- Tether: the cable that connects the support vessel with the underwater vehicle. Its main roles are: send power and control signals to the vehicle and send real-time sensors and video data to the *top-side*. Consequently, the power requirements, the signal characteristics and the mechanical requirements of the tethered link itself, are the main aspects that influence its design. A tether is a complex system composed by optical fibers to transmit high-speed/wide-band signals, power cables (which diameters is proportioned to the power requirements of the vehicle), and many layers that provide isolation, mechanical resistance and flexibility.

1.2.5 Minerva and 30K, the AUR-Lab's ROVs

As of December 2016, the AUR Lab ROVs fleet is composed by the ROVs Minerva, SF 30k, and Seabotix LBV. In the following, the main characteristics of the first two ROVs are listed. For more information and details refer to [13, 14, 9, 15] and Article A.

ROV Minerva is an OCROV, designed and produced by Sperre AS for NTNU in 2003. The base model for Minerva is called "SUB-Fighter 7500". It is used for biological research and sampling, as well as development of new control technology, archaeological and geological surveys (see Chapter 5). Minerva is 1.44m long, 0.82m wide and 0.8m high, and weighs 450kg. It is equipped with five 1.5kW thrusters, each providing between 300N and 340N thrust force. Two of the thrusters are vertical, two provide forward and backward thrust, and the last one is a tunnel thruster providing lateral thrust. This ROV cannot be actively actuated in pitch and roll. This is not a problem for the control purposes since the ROV is considered passively stable on these DOFs. The ROV carries

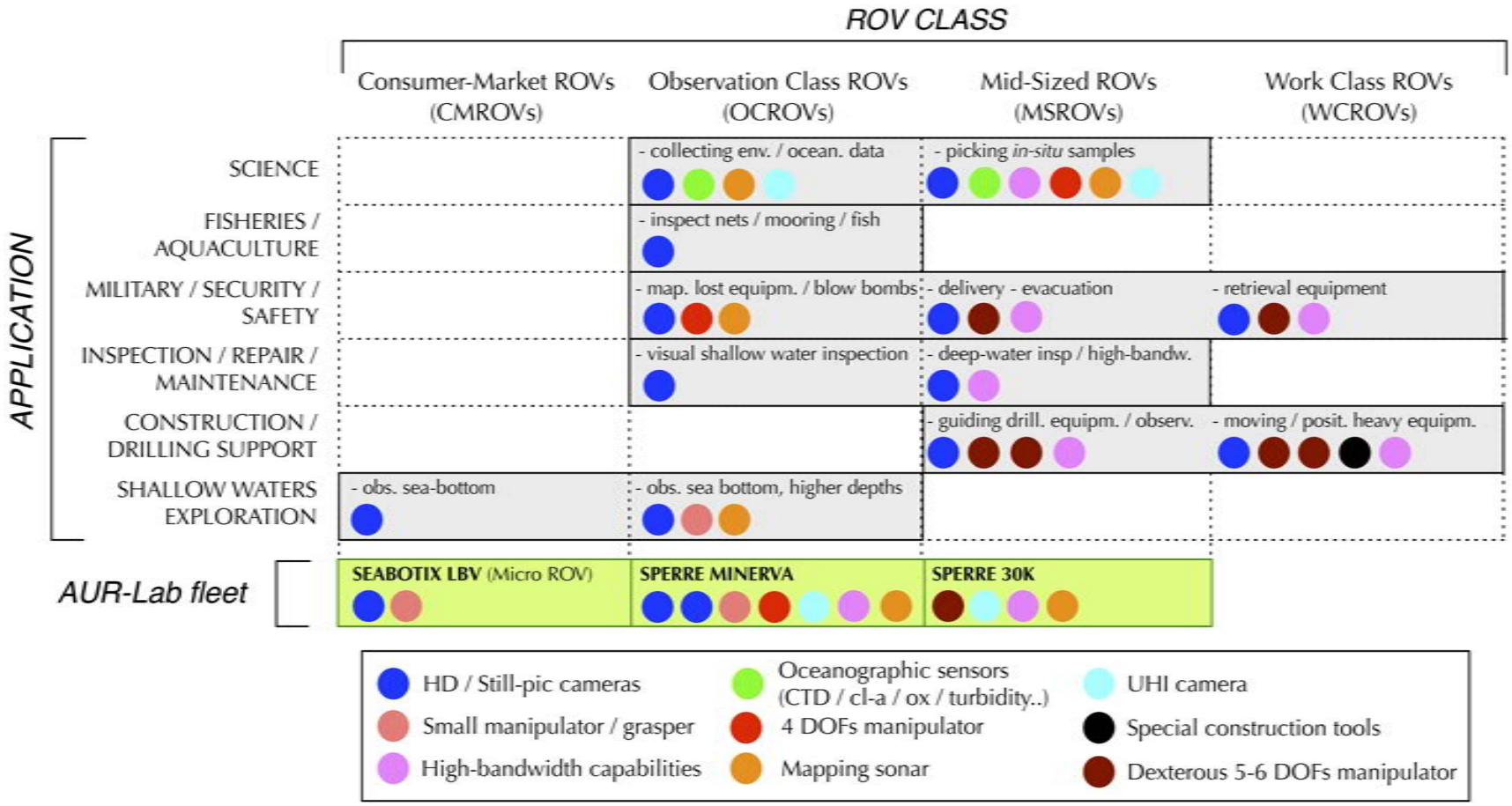

Figure 1.5: The classifications and descriptions about the ROV technology, concerning their size-related classification (Subsection 1.2.1), main components (Subsection 1.2.4) and applications (Subsection 1.2.3), are here summarized to provide to the reader a simple overview. Notice that this overview provides some clarifying examples, and it does not have the goal of completeness. [12] can provide the latest NORSOK standards, which are a comprehensive and complete set of guidelines, which defines ROVs operations, equipment and classifications.

Figure 1.6: AUR-Lab ROVs, respectively Minerva and 30k. The two ROVs are very similar in the design, which is basically scaled up for in the 30k version, which also adds a vertical truster. In the current configuration, the AUR-Lab 30k carries a Raptor manipulator. Navigation sensors payload, thrusters characteristics, lights, structural elements, electronic elements are very similar.

a manipulator without position feedback, a sonar, four lights, four cameras and a range of sensors measuring depth, heading, accelerations, velocity over ground, relative position. The umbilical connecting the ROV to the winch is 600m long.

ROV SUB-Figher 30000 (also called SF 30k), is a MSROV produced by Sperre AS. It has a length of 2.5m, a width of 1.5m, a height of 1.6m and has a weight of 1850kg. There are six 3kW thrusters installed on the ROV, disposed on a similar configuration of ROV Minerva, with the addition of a third vertical thruster. This ROV is also underactuated in pitch and roll, but presents the same characteristics of passive stability. A Kraft Raptor manipulator is installed onto this ROV. The SF 30k is connected to the support vessel winch with a 1000m long umbilical cable. The maximum listed working depth for ROV SF 30k is 3000m, which is constrained by the umbilical.

1.2.6 The New Class of Consumer-Market ROVs

The incredible success that commercial aerial drones have achieved in the latest years is witnessed by the self-explanatory trend reported in Figure 1.7. Drone companies understood that people are interested in buying vehicles which could be *fun* to control and, at the same time, shoot HD pictures (or videos) from otherwise unaccessible points of view. This awareness opened up a rich market and started a tight competition among the companies. It was not difficult to foresee that people would start asking themselves if the same could be applied to the underwater environment.

It is in fact known that the “ocean space” is widely unknown: even Mars is more extensively mapped. Due to this fact, the underwater environment still hides many secret and fascinating creatures, plants and wrecks, which people would like to explore or witness. Moreover, the worldwide spread of social platforms gives people the chance to gather and share data, feeling a member of a *global explorer community*. All these aspects pushed more competitors to start developing cheap and small solutions for enthusiast explorers.

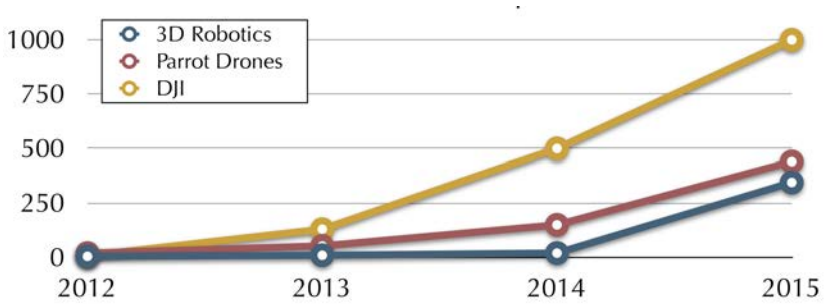

Figure 1.7: (Approximated) revenues of the major aerial drones companies in the latest years (in million $) [16]. Notice how DJI has been able to double its revenue every year.

The characteristics of such ROVs can be summarized as follows: they must be *cheap* (affordable by enthusiasts), *light* (a person should be able to operate them without the need of special equipment), able to operate *for a certain time* (generally more than a hour), *reach depths that trigger a certain interest* in the user (generally down to, at least, 20m).

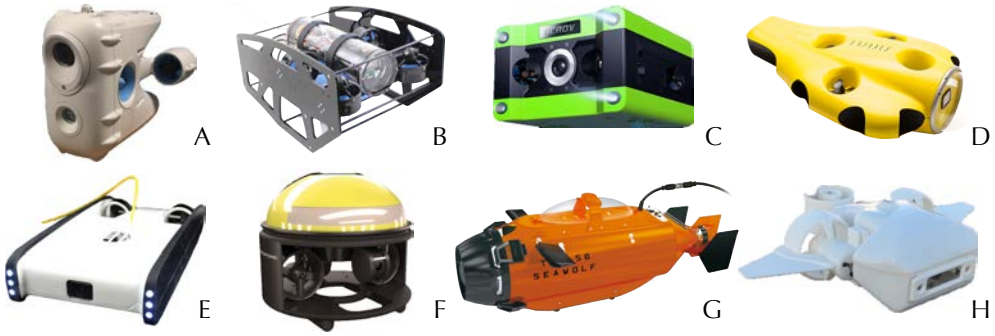

Figure 1.8: Many companies are starting to fill the ROV's market share for mass consumers since 2015. Most popped up in 2016, while some are reaching the shops shelves only these days. The development of small and low-cost HD cameras, small sensors and efficient and small thrusters and batteries, allow for the reduction of costs, which is the main driver for this market.

Since an untrained operator should be able to operate such vehicles, new interfaces need to be developed. HMD (see Subsection 2.5.1), tablet and cell phone interfaces are rapidly becoming the new standards for the underwater exploration experience. The resemblance with the videogaming interface makes them intuitive and easy to use, especially for the youngest generations.

Researchers and professors from NTNU have seen the same opportunity, starting an adventure in which the author of this thesis participated. This is briefly described in Subsection 5.2. Only the next years will unveil if this new ocean adventure will have the same fortune as the sky one.

	Name	Thr.	DOFs	Weight	Depth (max)	Tether	Price (approx.)	Batt. time
A	BluEye	4	4	13 Kg	100 m	Yes	2400 US$	4h
B	BlueROV	6	6	3.7 Kg	100 m	Yes	1290 US$	-
C	CCROV	6	6	4.5 Kg	100 m	Yes	2700 US$	1 h
D	IBubble	6	3	5 Kg	60 m	No	2000 US$	1 h
E	OpenROV	3	3	2.9 Kg	100 m	Yes	1500 US$	3 h
F	SeaDrone	5	up to 6	5 Kg	100 m	Yes	3900 US$	3 h
G	SeaWolf	1+fins	3	7.7 Kg	10 m	Yes	1000 US$	50 min
H	Fathom One	3(custom.)	3(custom.)	2 Kg	45 m	Yes	600 US$	1 h

Table 1.1: Main characteristics of available (or soon available) underwater ROVs for the consumer market, whose cost spans between 1000 US$ and 4000 US$. The letters in the first column refers to the pictures in Figure 1.8 (data updated in October, 2016).

1.2.7 Towards the Future, an Autonomy Perspective

A relevant aspect for the further development of the UUV and ROV technologies is autonomy. Autonomy is becoming an essential part of the modern control systems, aiming to improve the efficiency, safety and reduce the cost of the vehicles and operations. This is a general statement, which concerns many kinds of vehicles and applications [17]. Tesla, Volvo, Toyota and other major car producers are starting to include autonomous systems into their cars [18, 19, 20]. Those systems are able to take control of the cars and keep constant speed along highways, automatically slow down, wait in queues, or recognize street signs and indications. The driver supervision is still constantly required for safety reasons. Flying drones are already equipped with a certain level of autonomy, and are widely used for military operations [21]. The usage of autonomy in the military, automotive and other fields, opens up many interesting, moral questions [22]. In the latest years, many applications concerning surface vessels and underwater vehicles have been developed and announced [23, 24]. [25, 26] propose autonomous strategies for underwater mine countermeasures, [27] underline the importance of autonomy for underwater archeology, [28] discusses autonomy in relationship to response plans for maritime accidents.

Although the term *autonomy* may sound familiar and easy to grasp, it contains many different shades and can be interpreted using different points of view. Look, for instance, at what was included in [29]:

> *"To avoid a prolonged debate over how much "intelligence" is required for a vehicle to be considered "autonomous", the committee elected to include within the scope of this report all relevant vehicles that do not have a human onboard."*

This statement clearly underlines the presence of contradictory points of view, which are difficult to summarize in a compromising definition. The discussion is consequently cut with the following obliging statement:

$$\boxed{\text{No human on board} \Rightarrow \text{Autonomous system}}$$

which may look like an oversimplification of the problem. In fact, it is obvious that an airplane, which is able to plan its' descent and finally land itself despite external forces, is autonomous to some extent, despite the fact that pilots are still required to supervise (and take responsibility for some parts of) the operation.

It is not difficult to end up in the difficult terrain of defining the line between what is *automatic* and what is *autonomous*. AUVs are still called *Autonomous* Underwater Vehicles, although, in the opinion of the author, their degree of autonomy is not much higher than the one incorporated in ROVs (which are still defined as "remotely operated"). Both classes of vehicles are often run by pre-planning a mission, which implies the definition of a list of operations which are defined by operators prior to the mission start, and are carried out *automatically*. It is obvious that here the term *autonomous* mainly refers to the absence of the tether (which may be seen as a robotic version of a "leash"). But is the absence of the cable enough to define a system "autonomous"?

$$\boxed{\text{No tether} \Rightarrow \text{Autonomous system}}$$

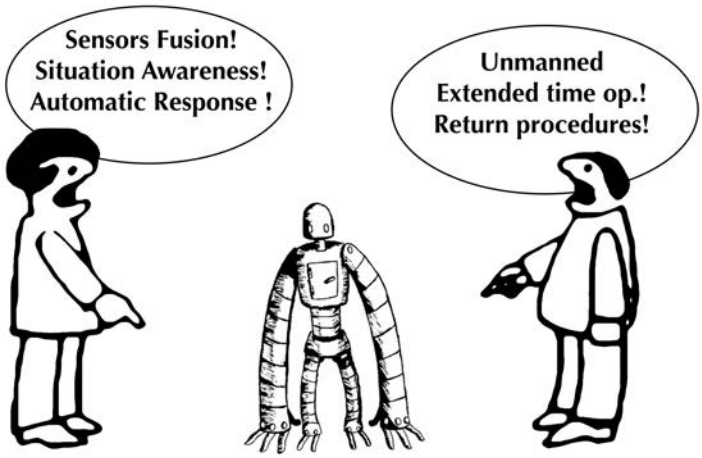

Figure 1.9: There is a wide discussion around the word "autonomy". Although it is difficult to establish which ones are the "sufficient" conditions that ultimately define an autonomous system, the formulated definitions are definitely helping to establish those conditions which are surely necessary to the achievement of such systems.

The answer is probably "no". In fact many other definitions, which consider other aspects, can be found in literature. An example is:

> *"Intelligent systems due to their ability to manage unexpected events and unstructured and uncertain environments. This means integrating mathematical models with real-time data from sensors and instruments and allowing algorithms with optimized response to be designed and embedded in computer systems."*

$$\left.\begin{array}{r}\text{Situational Awareness}\\ \text{Response ability}\\ \text{Information fusion}\end{array}\right\} \Rightarrow \text{Autonomous system}$$

From [23]:

> *"Capable of operating without operator input for extended periods of time. Implicit in this description is the requirement that the UUV's sortie accomplishes its assigned goal and makes the appropriate rendezvous for a successful recovery."*

$$\left.\begin{array}{r}\text{Extended time operations}\\ \text{Proper return procedures}\\ \text{No humans onboard}\end{array}\right\} \Rightarrow \text{Autonomous system}$$

From [30]:

> *"Autonomy or Autonomous behavior is a contentious term in reference to unmanned vehicles due to the poor understanding of whether something acting without outside commands is doing so through its own ability to make decisions or through a method of decision making pre-programmed into it. It is a quality which is rather abstract in nature and rather difficult to measure."*

$$\text{Ability of self-decision} \Rightarrow \text{Autonomous system}$$

The previous definitions confirm the difficulty on establishing what exactly an autonomous system is, and the current debate on a definition that would simply embrace all these aspects (see Figure 1.9). Nevertheless, it is important to focus on the *elements* on which these definitions focus on, because, despite of the fact that the arrival point may be blurry, it is sure that all the mentioned elements are aiming towards the right direction.

In this context, the work of the researchers is not only going towards the development of control systems and algorithms solving specific control problems, but also towards the design of architectures and "reorganization" of the modules in layers, which allows to meet the *necessary* requirements mentioned above. For instance, [31] proposes an architecture which merges the underwater operations scenario, the required payload, control aspects and operations methods with the autonomy aspects and levels. [32] proposes an autonomy architecture for unmanned vehicles, while [33] reviews the existent architectures, analyzing the evolution of the levels of autonomy definitions in literature. [34] discusses autonomy in the context of ROV operations.

It is not the purpose to discuss the level of autonomy into details, since there is as much debate about it in the literature, as there is concerning the definition of autonomy. This is quite obvious, since the decomposition of a concept into levels can be easily done only by considering a certain aspect of that technology to progressively classify it. Consequently, many equivalent level-architectures can be formulated. The most accepted and utilized

is, perhaps, the one described by the USA National Research Council, which proposes four levels based on decreasing amount of human intervention in the system operation. In the context of marine vehicles and operations, an example of architecture and levels of autonomy can be found in [29, 31].

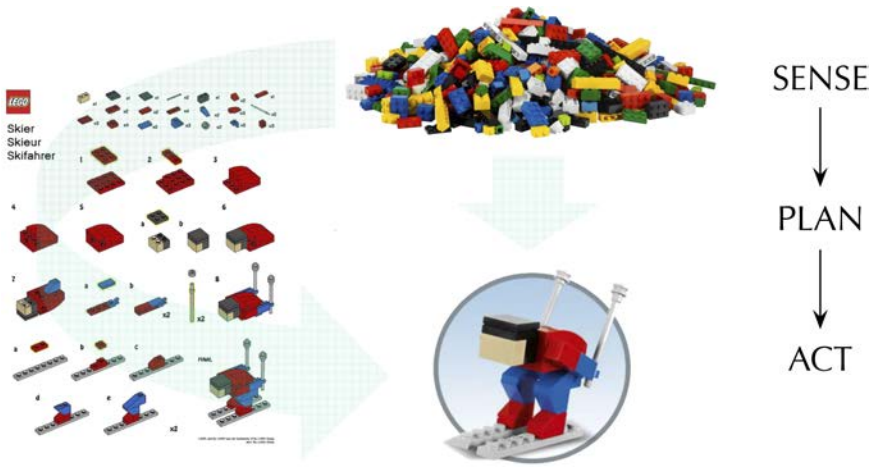

Figure 1.10: One interpretation of autonomy can be described with the "own ability to make decisions" [30], e.g. once the vehicle senses the environment, it can reach its goals without following a pre-defined list of tasks. Considering the Lego example, an "automatic" robot would follow a set of predefined instructions, while an "autonomous" one would feel the bricks, understand by itself the optimal way of putting them together to reach the goal. The philosophical interpretation of such logic is not easy: how abstract should the vehicle's controlling software be to lose the direct connection between the lines of code and the final decision performed by the vehicle?

In the context of this thesis, *autonomy* is seen as a driver towards *smarter* systems. Agreeing with the definition in [30], a system can be called autonomous if it is able not only to follow a series of preprogrammed instructions, but also to "self-define" its next tasks by itself (see Figure 1.10). Although this distinction can open up many philosophical discussions, this work is intended to improve the UUV and ROV technology by providing tools for a better understanding of the environment, which can result in an higher participation of the robot in the decision-making process and ability of planning tasks of the operations without human assistance, such as the definition of a path to follow to reach a target.

1.3 Thesis Structure and Outline

This thesis is divided in two parts: Part I provides an overview of the treated topics, while Part II provides the list of papers which support the discussion presented in Part I. Both Part I and II covers four main topics; each one of them treats one of the aspects that are visually represented in the scenario illustrated in Figure 1.1. The reader will easily see how all those parts are interconnected, as complementing pieces of the same jigsaw puzzle. Figure 1.11 shows the aforementioned complementarity of the treated topics.

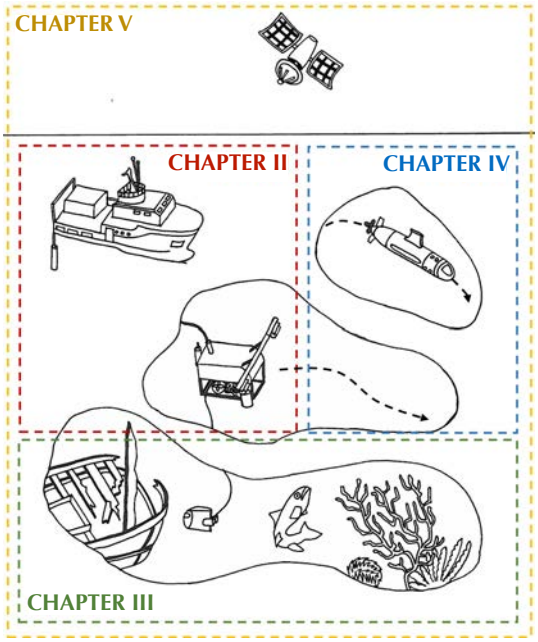

Figure 1.11: This illustration divides Figure 1.1 to visually show the content of the different parts of this thesis, and how their complementarity in the overall picture.

CHAPTER II - ROV Control System
This chapter presents and discusses the motion control system developed from PhD candidates, students and researchers of the NTNU AUR-Lab. An overview and a brief discussion about its development is presented. Here, the author contributed with the development of several modules, algorithms, tests and data collection and analysis.

CHAPTER III - Camera Payload
This chapter treats the camera payload, especially underlining the usage of still-picture cameras for the purpose of mapping and automatic planning.

CHAPTER IV - Path Planning System
This chapter treats the design and development of an automatic path-planning and replanning system that can be proficiently used from USVs or UUVs. This has been developed in sequential steps, starting from the development of a two-dimensional path-planning system, a fast replanning system, and the extension to the underwater domain.

CHAPTER V - Missions on the Field
This chapter presents some example of real operations performed with the AUR-Lab, in collaborations with academic and industrial partners. The attempt of developing a novel micro-ROV for the purpose of performing a coordinated mission is described.

CHAPTER VI - Conclusions and Further Work
This chapter summarized the main conclusions of this thesis, and suggests some ideas to improve the presented work.

1.4 Contributions

In the following, a brief list of the scientific contributions of the papers is presented.

CHAPTER II - *ROV Control System* (Article A)

- Development of a statistical signal processing module, to detect and eliminate outliers. Such outliers are commonly produced by acoustic positioning systems due to the presence of steep underwater cliffs, artificial metallic artifacts and so on (**Article B**);
- Implementation, comparison and analysis of several observer modules, tested on the NTNU AUR-Lab fleet. Moreover a multi-objective observer for UUVs has been developed, implemented and simulated (**Article C**, **Article D**);
- Development, implementation and test of a novel HMI for ROVs, which was, at the knowledge of the authors, the first attempt of controlling an ROV with such technology (at the time of the publication). Full-scale observation and manipulation operations have been conducted to show the effectiveness of such approach (**Article E**).

CHAPTER III - *Camera Payload*

- Design, development and implementation of a real-time mosaicking software, which works as an add-on of the motion control system of the ROV (**Article F**);
- Design, development and simulation of a novel real-time path-planning system based on camera feedback, which steer the UUV trying to cover as much OOIs as possible (**Article G**);

CHAPTER IV - *Path Planning System*

- Development of a novel two-dimensional path-planning system, which produces a flyable path which considers safety, kinematic and dynamic constraints. Simulations are shown to prove the effectiveness of such system (**Article H**);
- Depth constraints are added in the path-planning phase, and a real-time replanning system is designed. The replanning phase respects the International Regulations for Preventing Collisions at Sea (COLREG). Simulations shown the effectiveness of the system (**Article I**);
- Development of an innovative path-planning and replanning system for UUVs, in the context of underwater operations on a subsea factory. A novel set of traffic rules have been developed (**Article J**).

CHAPTER V - *Missions on the Field*

- Participation and description of the end-user perspective, in scenarios related with full-scale operations, in cooperation with academic and industrial partners (**Article K**, **Article L**). The development of a micro-ROV, for the purpose of coordinated operations is also briefly described.

1.5 List of Papers

In the following, the list of the papers which compose the second part of this thesis, organized following the already mentioned chapters, is reported.

CHAPTER II - *ROV Control System*

- **Article A** - *Book Chapter*
  A.J. Sørensen, F. Dukan, M. Ludvigsen, D.A Fernandes and **M. Candeloro**. Development of Dynamic Position and Tracking System for the ROV Minerva. In G.N. Roberts, R. Sutton editors, *Further Advances in Unmanned Marine Vehicles*, Chapter 6, pages 113-128. Institution of Engineering and Technology (IET), 2012.

- **Article B** - *Conference's Proceedings*
  A.M. Lekkas, **M. Candeloro** and I. Schjølberg. Outlier Rejection in Underwater Acoustic Position Measurements Based on Prediction Errors. In *Proceedings of the 4th IFAC Workshop on Navigation, Guidance and Control of Underwater Vehicles (NGCUV)* IFAC-PapersOnLine, volume 48 (2), pages 82-87, Apr 2015.

- **Article C** - *Conference's Proceedings*
  M. Candeloro, A.J. Sørensen, S. Longhi and F. Dukan. Observers for Dynamic Positioning of ROVs with Experimental Results. In *Proceedings of the 9th IFAC Conference on Manoeuvring and Control of Marine Craft (MCMC)* IFAC-PapersOnLine, volume 9 (1), pages 85-90, Sept 2012.

- **Article D** - *Conference's Proceedings*
  M. Candeloro, F. Dezi, A.J. Sørensen and S. Longhi. Analysis of a Multi-Objective Observer for UUVs. In *Proceedings of the 3rd IFAC Workshop on Navigation, Guidance and Control of Underwater Vehicles (NGCUV)* IFAC-PapersOnLine, volume 3 (1), pages 343-348, Apr 2012.

- **Article E** - *Conference's Proceedings*
  M. Candeloro, E. Valle, M.R. Miyazaki, R. Skjetne, M. Ludvigsen and A.J. Sørensen. HMD as a new Tool for Telepresence in Underwater Operations and Closed-Loop Control of ROVs. In *Proceedings of MTS/IEEE OCEANS*, Oct 2015.

CHAPTER III - *Camera Payload*

- **Article F** - *Conference*
  S.M. Nornes, **M. Candeloro**, Ø. Ødegård, G. Johnsen and A.J. Sørensen. Photomosaic camera as simultaneous data collector and navigation aid on Unmanned Underwater Vehicles. *Ocean Optics XXII*, Oct 2014.

- **Article G** - *Conference's Proceedings*
  M. Candeloro, F. Mosciaro, A.J. Sørensen, G. Ippoliti and M. Ludvigsen. Sensor-based Autonomous Path-Planner for Sea-Bottom Exploration and Mosaicking. In *Proceedings of the 10th IFAC Conference on Manoeuvring and Control of Marine Craft (MCMC)* IFAC-PapersOnLine, volume 48 (16), pages 31-36, Aug 2015.

CHAPTER IV - *Path Planning System*

- **Article H** - *Conference's Proceedings*
  M. Candeloro, A.M. Lekkas, A.J. Sørensen and T.I. Fossen. Continuous Curvature Path Planning using Voronoi diagrams and Fermat's spirals. In *Proceedings of the 9th IFAC Conference on Control Applications in Marine Systems (CAMS)* IFAC-PapersOnLine, volume 9 (1), pages 132-137. Sept 2013.

- **Article I** - *Journal*
  M. Candeloro, A.M. Lekkas and A.J. Sørensen. A Voronoi-Diagram-Based, Dynamic Path-Planning System for Marine Underactuated Vessels. Submitted for the second review to the *IFAC Control Engineering Practice*, 2016.

- **Article J** - *Conference's Proceedings*
  M. Candeloro, A.M. Lekkas, J. Hegde and A.J. Sørensen. A 3D Dynamic Voronoi Diagram-Based Path-Planning System for UUVs. In *Proceedings of the MTS/IEEE OCEANS*, Sept 2016.

CHAPTER V - *Missions on the Field*

- **Article K** - *Journal*
  G. Johnsen, **M. Candeloro**, J. Berge and M. Moline. Glowing in the dark: discriminating patterns of bioluminescence from different taxa during the Arctic polar night. In *Polar Biology*, volume 37 (5), pages 707-713, May 2014.

- **Article L** - *Conference's Proceedings*
  M. Ludvigsen, T. Thorsnes, R.E. Hansen, A.J. Sørensen, G. Johnsen, P.A. Lågstad, Ø. Ødegård, **M. Candeloro**, S.M. Nornes and C. Malmquist. Underwater vehicles for environmental management in coastal areas. In *Proceedings of MTS/IEEE OCEANS*, May 2015.

The following papers are not included in this collection:

- *Conference's Proceedings*
  W: Caharija, **M. Candeloro**, K.Y. Pettersen and A.J. Sørensen. Relative Velocity Control and Integral LOS for Path Following of Underactuated Surface Vessels. In *Proceedings of the 9th IFAC Conference on Manoeuvring and Control of Marine Craft (MCMC)* IFAC-PapersOnLine, volume 45 (27), pages 380–385, Sept 2012.

- *Journal*
  W. Caharija, K.Y. Pettersen, A.J. Sørensen, **M. Candeloro** and J.T. Gravdahl. Relative velocity control and integral line of sight for path following of autonomous surface vessels: Merging intuition with theory. In *Journal of Engineering for the Maritime Environment*, volume 228 (2), pages 180-191, May 2014.

1.6 Educational / Media Coverage

Along the process there has been interest of some media in many of the activities related with this work, which is listed in the following:

Usage of an OCROV equipped with a UHI camera, the innovative sensor, together with an advanced motion control system have been interesting for many newspapers. Here it is an example: [35];

AUR-Lab's Discovery of a WWII bomber outside Trondheim's fjord, the news had a certain relevance since those bombers were known to be in the fjord, but never found. The news went on many Norwegian and international newspaper: [36] is one example;

The test of the novel ROV interface, which uses a HMD to provide the possibility for a sole operator to control the ROV itself and a dexterous manipulator. Discovery Channel Canada has been interested, and the news was reported by other media [37, 38];

The collaboration with BluEye Robotics AS, started with the student project connected with the development of Neptunus. Now the company is reality and it's included in one of the most promising start-ups in Norway. The author collaboration was limited to the first prototype [39].

Chapter 2

ROV Control System

This chapter will introduce and discuss the topics presented in the Article A: *Development of Dynamic Position and Tracking System for the ROV Minerva* (Section 2.1), Article B: *Outlier Rejection in Underwater Acoustic Position Measurements Based on Prediction Errors* (Section 2.2), Article C: *Observers for Dynamic Positioning of ROVs with Experimental Results* and Article D: *Analysis of a Multi-Objective Observer for UUVs* (Section 2.3), Article E: *HMD as a new Tool for Telepresence in Underwater Operations and Closed-Loop Control of ROVs* (Section 2.5). Section 2.4 will briefly present the development and implementation of an Integral Line-Of-Sight (ILOS) algorithm for ROVs. The related articles of this last work are not included in this collection.

2.1 A DP System for ROVs

During the last years a complete DP system for ROVs has been designed, developed and tested on the NTNU AUR-Lab ROVs. The project has been carried on through a coordinated effort of PhD candidates, professors, technical personnel and students, and it has been both a useful test platform for new control algorithms and also a necessary tool to perform full-scale missions. The main responsibility of the developing, implementing and testing phases has been carried on by postdoctoral researchers and PhDs, in chronological order: Martin Ludvigsen, Fredrik Dukan, Daniel de Almeida Fernandes, the author of this thesis, and Stein Nornes.

In this thesis, some aspects of the structure of the software will be given, while more details can be found in [13, 9] and in Article A. The product of a software development process over a long time which involved a large group of developers, clearly ends up in a complex and articulated product, which could be extensively described only by dedicated software manual. In the next few pages a high-level overview of the system is given, going in detail only for these parts which directly refer to the attached papers. Moreover, as well said in [9], a software governing the real-time activity of a complex vehicle such as

Figure 2.1: Manual control for ROV Minerva. The two joysticks control the motion of the vehicle and allows to activate the functions of auto-heading and auto-depth. The buttons allows to turn on/off the payload devices, modify their orientation and so on.

an ROV, contains a large number of logic algorithms, exception handling, drivers, communication protocols and so on. Those elements, which usually take the highest amount of time in the development process, will not be treated in the following pages.

The DP system for underwater vehicles is a relatively new application, and is widely inspired by the historically more diffused DP systems for surface vessels and ships. This can be clearly seen in the marine industry, where the market for more complex DP systems for underwater vehicles has only found its development in the latest years. This is nicely summarized by the words of Richard Vandervoort[1], stated only few years ago [40]:

> *"The only real automatic controls present on modern work-class ROVs, used in offshore oil and gas exploration, are auto heading, auto depth and auto altitude. It really depends on pilot skills to do good piloting."*

It is possible to say that things have rapidly moved forward in the latest years, and now it is more common for companies to produce and sell ROVs which are equipped with more than only the basic control functions. Industrial development in the areas of Graphical User Interfaces (GUI) and vision-assisted systems are becoming essential to efficiently perform the more complicated operations which are nowadays required.

The company Oceaneering, for instance, offers HD video technology, offshore video streaming, remote on-shore control, and *computer-aided piloting*. The latter involves the possibility to *fly* the ROV with a command-based system involving automated steps, instead of using the traditional joystick. By analyzing the real-time video, the software sends the ROV control system positioning data from the video to control the thrusters and move the ROV. Kevin Kerins[2] underlines the importance of a DP system [41]:

> *"Computer-aided piloting is much more efficient than a human pilot can achieve unaided, which in turn reduces the potential damage to tooling, manipulators, and most importantly, the customer's subsea assets. This new ROV capability revolutionizes efficiency in the deployment of tools and navigation from point to point".*

[1] Chief of ROV operation & underwater robotics for the Marine Institute, Newfoundland, Canada
[2] Senior Vice President, Remotely Operated Vehicles (ROV), Oceaneering

Other industrial examples of DP systems, can be found in [4]. In the academia, many systems were developed in the latest years, few examples are: the system from Johns Hopkins University [42], from Limerick University [43, 40], from Girona University [44], and from multi-academies collaborations [45, 46]. The University of Porto has developed DUNE, which is a portable modular software architecture that provides a communications, navigation, control, maneuvering, plan execution and vehicle supervision to AUVs, ROVs, AUVs, UAVs [47]. The University of Girona developed the Remotely Operative System (ROS), which is an open source system which provides hardware abstraction, low-level device control, implementation of commonly used functionality, message-passing between processes and so on [48]. The open-source philosophy makes the sharing of code and the debugging easier, characteristics which made it possible for this system to be utilized for a variety of applications, including also the marine ones [49].

Notice that the development of a proper DP system for underwater vehicles must face many challenges, such as the modeling of the vehicle, the tether cable, the external forces and the design of the navigation, guidance and control algorithms. In [50] these challenges are underlined.

2.1.1 Main Objectives and Timeline

The DP system has been firstly designed to provide a better controlling tool for the Minerva and 30K ROVs. These ROVs (see Subsection 1.2.5) were produced by Sperre AS[3] together with a manual control which includes the auto heading and auto depth functions. As already mentioned, these simple control tools have been the standard in the ROV industry since the beginning of the employment of such vehicles, as showed in Figure 2.1. For academic and research purposes, this standard is not enough to obtain the required precision, accuracy and repeatability. The main objective of the DP system design process have been to produce the possibility of:

- easily integrate new navigation sensors in the system to improve performance;
- easily integrate new payload instruments to collect end-users data;
- have a synchronized system where navigation, end-users and surface data could be easily compared and retrieved;
- easily maneuver the vehicles, leaving the low-level control to the system;
- define some high-level routines which could be activated when common mission should be performed;
- display the useful information, avoiding redundancy or excessive complexity.

The current system has been obtained through sequential improvement steps, where new functionalities were added. The continuous full-scale testing procedures on the fjord and the collaboration with academic and industrial partners gave vital feedback and ideas during the process. The testing of several control algorithms suggested also new strategies to improve the control performances. Figure 2.2 proposed the main steps of the DP system

[3] Sperre AS is a Norwegian ROVs manufacturer [15].

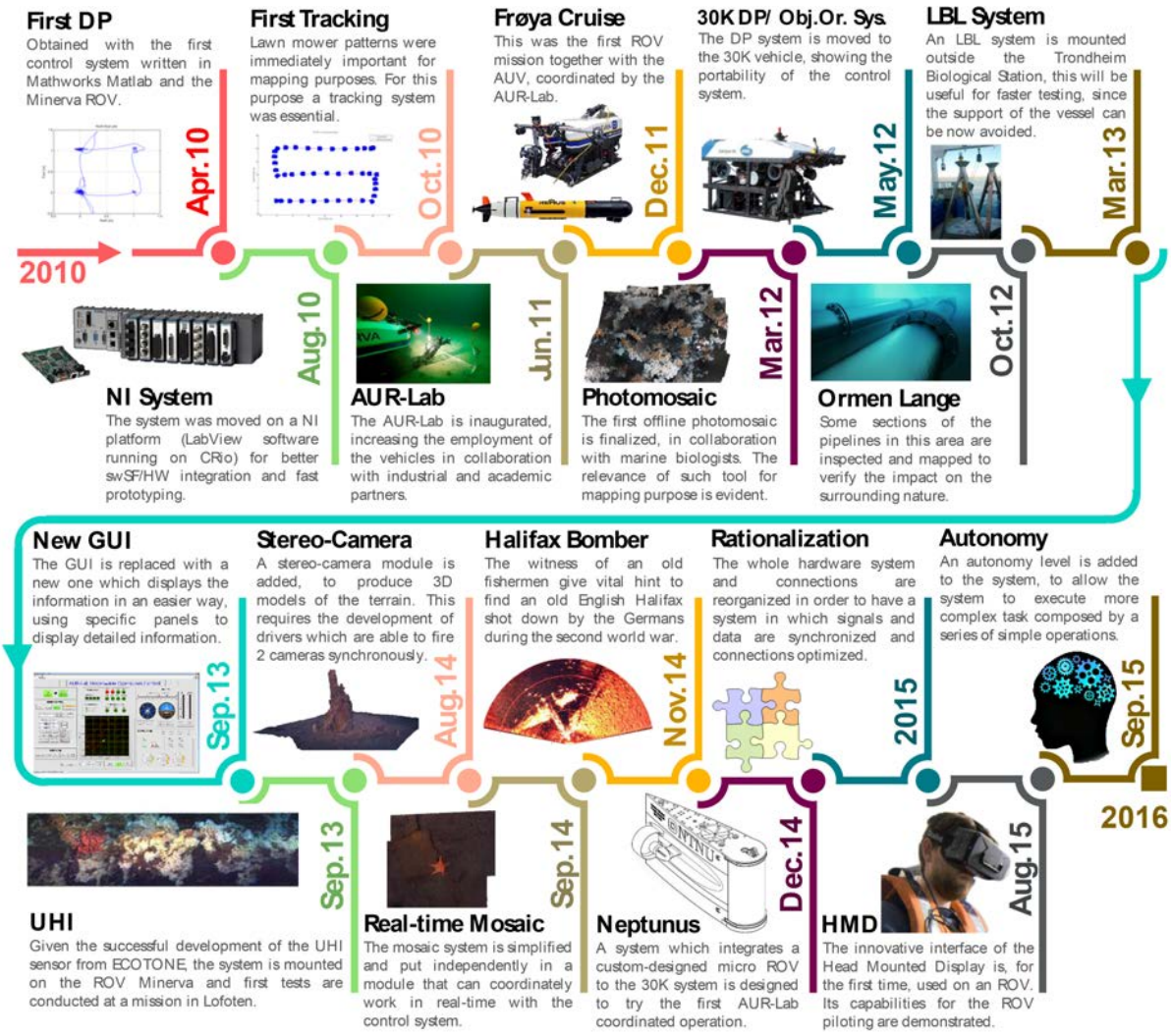

Figure 2.2: Timeline of the main steps of the DP Control System development. Having the vehicle standing in a fixed position despite of external loads (namely, DP) was the first objective. Tracking was the following goal, where a set of waypoints could be reached in a predefined sequence. These tools allowed to operate the ROVs for industrial missions (e.g. during the Frøya and the Ormen Lange cruises) since they could be used to provide accurate data or to perform manipulation operations. The system was redesigned in May of 2013, when it was clear that a modular, object-oriented, structure could have been beneficial for a cleaner and easier growth of the system. The LabView object-oriented solution met these needs. It was clear that the ROV system had a great importance in the quality of data, although the postprocessing of the latter was not less important. This pushed towards the development of modules such as the stereo-vision one and the off-line and real-time photomosaic modules. A special UHI camera was also installed in the system, and tested on cruises. ROV exploration missions brought to the discovery of a second world war Halifax bomber, a quite important historical discovery. A project which involved several students brought to the development of a new concept for micro-ROVs. The development of software systems can never disregard the users' point of view, consequently, efforts have been put on the development of an innovative, full-immersive HMD interface. In the latest period, some effort has also been put to rationalize the whole hardware-connections system to improve the synchronization of the data and the efficiency of the whole system. Moreover a simple autonomy layer has been added on top of the DP system modules, to try increasing the abstraction of the user inputs.

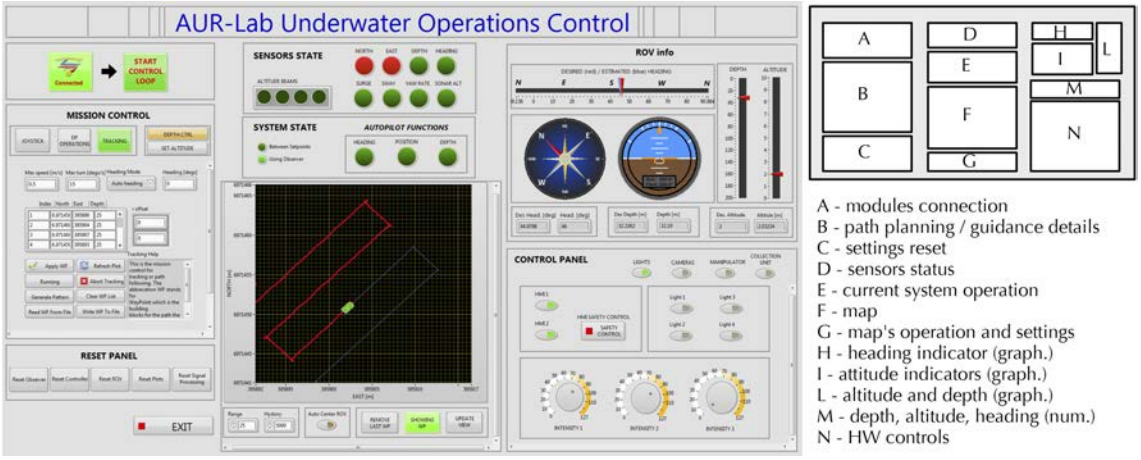

Figure 2.3: Main interface of the system. The different graphical elements and their functions, are listed in the dedicated legend. The main interface has been designed to summarize all the necessary and sufficient information that the operator needs to run the most common operations.

development. Figure 2.14 shows the connections between interfaces, hardware, computer systems, sensors (and so on), and gives a glimpse of the whole architecture.

In Article A, details about the main components composing the DP system architecture (Figure 2.5) are discussed, together with their theory, implementation and experimental results. The DP system has been evolving since the publication of this article, but the described control architecture still constitutes the main core of the current system.

2.1.2 Modularity and Architecture

The DP control system has been built over the principles of modularity and Object Oriented Programming (OOP). Those two elements allowed to physically and logically separate the main modules which compose the software. In this way, it was possible to easily design new add-on features which could work in parallel (also on different machines) and exchange information with each other and with the control system itself. The constitutive blocks of the control feedback loop are showed in Figure 2.5: they communicate and exchange information by using structured information organized in different sub-classes, which inherits their properties from two main classes: the *vessel* class, which includes the main control modules, and the *supervisor* class, which includes logic, synchronization, and communication variables. With this strategy, it is possible to add a different implementation for any module (e.g. a new observer, or controller) simply by adding a new *instance* of that module's predefined subclass.

On an higher level, the system can be decomposed in four main software components, which can be run independently. These components utilize TCP/IP or UDP protocols for communication and information exchange. In this way the inclusions of new features can be done in a simple way: the real-time mosaic module (see Chapter 3) is one example

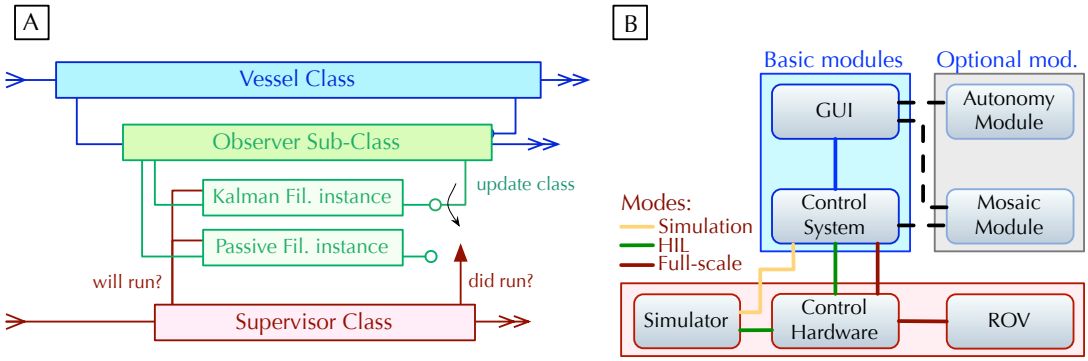

Figure 2.4: (A) OOP methodology: every module of Figure 2.5 is implemented as a subclass instance, which update the parent class at every iteration. (B) shows the modularity of the system. The basic modules are required for the system to run, optional modules can be activated. Depending by the configuration of the other modules, the software can be used for simulations (yellow connection), HIL testing (green connections), or full scale experiments (red connections).

(see Figure 2.4, A). Following the same principle the hardware and software components can be connected in different configurations to simply allow for software simulations, Hardware-In-the-Loop (HIL) testing and real operations (Figure 2.4, B).

2.1.3 Final Release and Requirements

The developed software has always been, and steel is, in a constant development phase. This is due to the continuous modifications which are required to face new challenges, test new algorithms and so on. The main feedback for the improvement of the system has always been the control performance, and the software engineering point of view has not been the first priority for the team. This is due to the fact that the development of a final release would require the deployment of the whole system on the real time computer, and an extensive an thorough series of tests. In other words, this would require to invest a dedicated and relevant amount of resources to the process. It is nevertheless important to indicate that the software should ideally reach the stage of a "Release 1.0", which would require a proper requirement analysis and a performance verification in accordance with the ISO or IEEE system engineering standards [51, 52, 53].

2.2 Signal Processing Module

The signal processing module is the main interface between the navigation sensors and the control algorithms. It is clear how the quality of the input signals is crucial to the performance of the rest of the control chain. In fact, inaccurate state estimations can cause the guidance system to generate wrong or discontinuous reference trajectories and consequently inaccurate moments and forces for the task in hand. Any anomaly of the

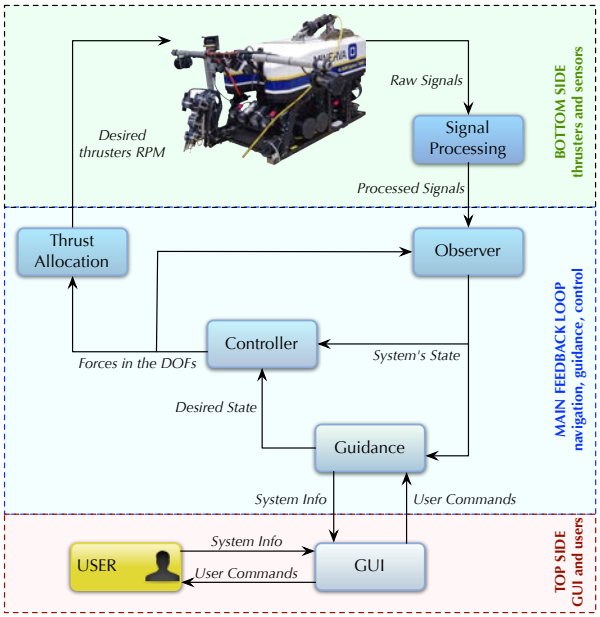

Figure 2.5: Main modules which compose the DP system for the AUR-Lab ROVs, the progression from top-side to bottom-side is also showed. Some of the blocks report also the related section, in which the development of the related algorithms is reported.

input signals should be detected and isolated, and missing information should be filled in. It is necessary to intervene on the top of the control chain so that the errors would not be dragged along the feedback loop and amplified (see Figure 2.5).

In the following, a brief state of art of the most common signal processing algorithms, and the one proposed to filter out outliers coming from the Kongsberg HiPAP (High Precision Acoustic Positioning) [54], which is presented in Article B: *Outlier Rejection in Underwater Acoustic Position Measurements Based on Prediction Errors*, are introduced.

2.2.1 Challenges and State of Art

Many misbehaviors can effect the sensor signals. Occurrence of outliers, signals with zero variance or with an unexpectedly high variance, the presence of high-derivative moments, are just few examples of problems which could occur (Figure 2.6).

There are different signal processing algorithms which helps providing an accurate and clean signal to the DP system, which can be classified as algorithms for *individual*, or *multiple signals* [55]. A wide literature covers this topic: it is possible to cite the *windowing algorithm* or the *variance-based methods* [56, 57, 58] for the individual signal case. Algorithms such as *voting* or *weighting* can solve the multiple signals problem [55]. *Change detection algorithms* aim to detect faulty signal behaviors by comparing its statistical characteristics with the outcome of a mathematical model describing its theoretical

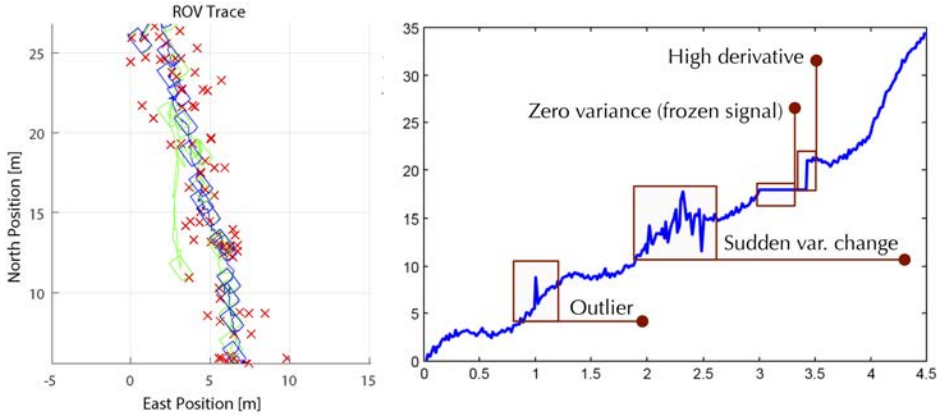

Figure 2.6: Hardware failures or the difficulty of measuring a physical variable (e.g. due to multiple reflections of acoustic signals) can produce undesired signal behavior. It is beneficial to detect the faulty behavior early in the control chain, not to compromise the quality of the control action. (A) shows an a series of outliers in the measures (red crosses) which bring to erroneous jumps in the state estimation (green line and boxes). This can be avoided with the proposed algorithm (blue line and boxes). (B) shows typical problems related with measured signals.

dynamics [59, 60]. Few statistical and model based algorithms have been developed for the ROV Minerva at the beginning of the DP system development [61]. [62] treats the problem of filtering of underwater LBL positioning system measurements.

2.2.2 Application to the 30K ROV

Underwater navigation poses great challenges, due to the lack of a precise global navigation system, like the GNSS (Global Navigation Satellite System), publicly available from 1994 for aerial and terrain applications. Consequently, acoustic positioning systems such as the USBL or the LBL positioning systems must be used.

The work of Article B was an attempt to solve the *outliers problem*, that often compromises the quality of the acoustic signals produced by the USBL or LBL systems. The navigation in the proximity of steep underwater cliffs or underwater wrecks seemed to amplify the problem, probably due to the multiple reflections phenomena [4]. [63] defines an outlier as:

> *"an observation which deviates so much from other observations as to arouse suspicions that it was generated by a different mechanism".*

The goal of Article B is to investigate the efficacy of fusing the USBL acoustic positioning system and DVL measurements, which are typically available onboard ROVs, for outlier detection and rejection purposes. An Extended Kalman Filter (EKF) is employed as the navigation filter. This, gives the full state estimates, detects and reject outliers before they enter the EKF. To obtain the desired outlier rejection, a number of χ^2 statistical tests are implemented every time a new measurement is available [64]. These tests aim at

evaluating the significance of the residuals which are the outcome of the predicted and measured values. In order to overcome the limitation of a fixed threshold, a dynamic value can be used to perform the statistical tests, defining a certain time window which is monitored over time. The outcome of this signal processing algorithm can be also used to understand if further actions must be taken, such as commanding the ROV to enter DP mode, until the acoustic positioning system returns to behave properly.

The algorithm is tested on full-scale data, collected in the Trondheim fjord. The method and related results are further explained in Article B. An example of the benefits of feeding the *observer module* with a properly filtered signal, it is showed in Figure 2.6.

2.3 Observer Module

The design of the observer module is strictly related with the *navigation* problem and it becomes critical for underwater vehicles due to the limitations imposed by the water media, which puts strict constraints on the communication links between the operators and the vehicle itself. Navigation can be defined as the process of calculating (or estimating) the state variables of a system given the available sensor measurements and (if available) the model of the system. The importance of this block is clear, since it is fundamental to reconstruct an accurate estimation of the state of the system in order to stabilize it.

A brief state of art of the most common observers, and a brief introduction of Article C: *Observers for Dynamic Positioning of ROVs with Experimental Results* and Article D: *Analysis of a Multi-Objective Observer for UUVs* are presented in the following.

2.3.1 Challenges and State of Art

The lack of a global positioning system imposes certain limitations in the underwater domain. The only efficient long-distance communication link available underwater is the acoustic one, which suffers from the problems mentioned in the previous section. Consequently, other sensors must be used to reconstruct the vehicle's state.

Vehicles with slow dynamics and the ability of carrying large payload may use mechanical and highly precise gyroscopes and accelerometers to derivate velocity and position of the vehicle. Cheaper and smaller electronic versions can constitute a lighter alternative, which can be easily strapped-down to the vehicle. Measurements of turn rates and accelerations can be integrated to provide an estimation of the unknown variables[4]. Other sensors information (e.g. the one provided by the DVL, pressure sensor and so on) can be *fused* together to provide a complete state estimation and reduce the drifting (see Subsection 1.2.4 or [4] for more information on navigation sensors). Mathematical models

[4]The procedure of determining the position of a vehicle without direct measurement of such state variable, is called *dead reckoning*.

can also be utilized to obtain the required sensor fusion. This can improve the quality of the estimation by compensating for sensors losses, and by filtering the measurement noise. On the other hand, a model-based observer introduces a certain phase lag due to its dynamics, while a pure kinematic observer can sense the forces as soon as they are exercised, producing immediate estimations.

Independently by the employment of a model, the estimation of the state through sequential integrations will always lead to an estimation drifting, unless the information of the absolute position of the vehicle is accessible at a certain point: LBL, SSBL or GPS systems can provide a reset of the estimation drift, when available.

An *observer*[5], is an algorithm which is built to fuse the sensor information and provide a state estimation, solving the navigation problem for a certain system. As mentioned, an observer will provide *reconstruction* of unmeasured signals, *estimation* of external disturbances, and *filtering* of the measurement noise. A review of the most common observers algorithms can be found in [65, 66]. [67, 68, 69, 70] propose marine applications. Kalman filtering has two main limitation: the high number of parameters to be tuned, and the unproven mathematical stability for certain applications. For such reasons, *passive filters* have been developed: [71] is able to prove global stability results, [72] describes passive observers for ships while [73, 74, 75] treat underwater vehicles. Notice that many adaptive algorithms, which aim to update on-line the Kalman Filter gains depending on the estimation error, have been developed [76, 42, 77].

2.3.2 Application to Minerva and 30K ROVs

Different observers have been designed for the ROV Minerva with the purposes of determine strength and weaknesses, comparing the performance, optimizing the tuning for the missions in the fjord. In [78] a model-based particle filter for state estimation and fault diagnosis is designed and tested, [9] proposed a sensor-based Explicit Complementary Filter (ECF) for the attitude estimation of the vehicle. In Article C, a Kalman filter applied on a linearized version of the model dynamics (LKF, Linear Kalman Filter) and on the nonlinear model (EKF) are presented. In the same work, a nonlinear passive observer is also designed and tested. An adaptive tuning technique which updates the Kalman filter gains on-line is also tested. Full-scale performance of these observers designed on the ROV model are compared, both in stable sensors conditions and in case of sensors drop-out (Figure 2.7 shows an example of full-scale results of the EKF). In case of the positioning system drop-out, the alignment of the sensors used for the integration of the state variables play a fundamental role in the accuracy of the state estimation itself. Techniques for the online estimation of such misalignments can be implemented to reduce the estimation error [79].

[5] In this section, the terms *observer* and *filter*, are used as synonyms.

2.3.3 A Multi-Objective Observer

In Article D the different ROV operation characteristics are taken in account to develop an observer which could adapt to their peculiarities. Wave and current effects are estimated to improve the performance of the state observer, while the vehicle speed is taken in account to include or exclude nonlinear terms in the system dynamics. In order to do so, a supervisor algorithm switches between a DP and a tracking observer. Simulation results show the performance of the approach.

It is worth noting that a switching system such as the one developed in Article D, would require a further analysis to investigate the effects of the switching procedure on the stability of the system. For this applications the error dynamics of every observer model are asymptotic stable (as showed in the appendix of Article D). Moreover, the switching time is greater than the decay time of the initial error of all states in every observer model (a proper hysteresis method should be implemented to avoid high switching frequencies). In general, the switching should be sufficiently slow so as to allow the transient effects of the error dynamics to dissipate after each switch. This qualitative analysis, confirmed by the simulations, should be validated by a complete stability proof in further work.

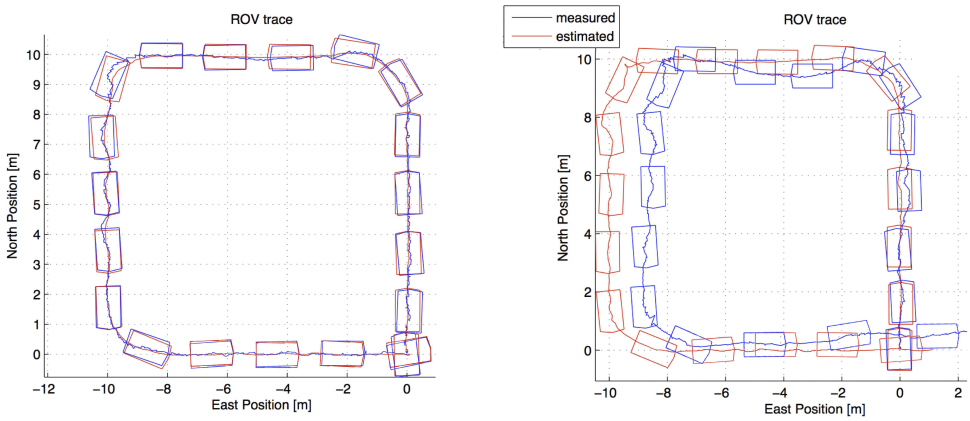

Figure 2.7: Example of Kalman Filtering applied to the ROV Minerva. Blue line and shapes indicate the measured position, red lines and shapes the estimated one. (A) shows the algorithm running with working position sensors, while (B) shows the algorithm running on dead-reckoning.

2.4 Guidance Module

Guidance algorithms are required to produce a reference signal to provide to the controllers, in order for the vehicle to reach the desired position, speed, or any desired configuration of the state variables. As stated in [80]:

> *"The process for guiding the path of an object towards a given point, which in general may be moving".*

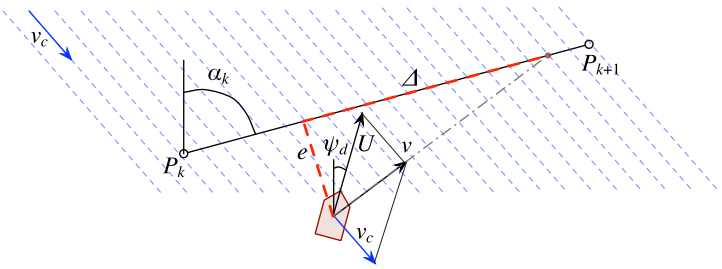

Figure 2.8: The main elements which compose the LOS guidance algorithm are reported in figure. The vehicle is converging to the line which connects the waypoints P_k and P_{k+1}, by reducing the cross track error e. The desired heading ψ_d must take in account the direction of the sea current v_c, since the underactuation cannot stabilize for the lateral forces independently.

Another relevant definition is given in [66], and it states:

> *"Guidance is concerned with the transient motion behavior associated with the achievement of the motion control objectives so that the mission specifications and the vehicle dynamics are all simultaneously observed".*

Some guidance algorithms have been implemented and utilized to steer the Minerva and 30K ROV through following waypoints, lawn mower patterns, or simple lines: [81], proposed a reference models for the Minerva ROV, [82] proposed a *reference generation scheme*, [9] proposed a constant-jerk reference model, a modification to the Line-Of-Sight (LOS) algorithm for fully actuated vehicles, and a method to produce a reference method through joystick inputs. These guidance algorithms are related to *path following*, which is a motion control scenario where the ship has to follow a predefined path without any time constraints [66].

In the following, a brief state of art of the most common path following algorithms for marine vessels is presented. Moreover, the application of the algorithms presented in [83, 84] to the ROV Minerva is showed. Some theoretical hints are given, since the development of this algorithm for the ROV Minerva has not been included in any manuscript.

2.4.1 Path Following Algorithms

It is possible to find many examples of control strategies for underactuated marine vehicles with the purpose of path following, as in [85, 86, 87, 88]. The LOS strategy is an algorithm widely used for path following, because of its simplicity and its intuitive interpretation. In fact, it is easily ascribable to the behavior of a ship commander, which directs his ship toward a certain point along the path which is *ahead* the current position. In this way, the path can be smoothly approached while the cross track error decreases, without any sudden steering. Moreover, the ILOS algorithm has been proven to ensure convergence to the desired path by allowing the vehicle to side-slip to counteract the effects of the current, application and stability analysis are also reported in [83, 84, 89, 90, 91, 92].

This may require a disturbance estimation phase in the control chain [93, 94, 74, 75]. Other techniques to overcome the effects of the disturbances, or to improve robustness, can be found in [95, 96].

2.4.2 Application to the ROV Minerva

[83, 84] present an integral LOS algorithm designed for the path following of straight lines in the presence of environmental disturbances and ocean current is designed. In order to try the ILOS in its original configuration the lateral thruster of the Minerva ROV has deactivated by acting on the thruster allocation matrix, reducing also the energy consumption of the vehicle.

Traditional LOS algorithms provides a desired heading for the vehicle based on the direction of the desired path, the cross-track error of the vehicle, and the *lookahead distance*, which defines the point of the path in which the guidance aim at a certain instant. If the vehicle is subjected to environmental disturbances, this approach results in a stationary deviation, which can be compensated by modifying the desired heading to take in account of the relative velocity of the vehicle, which contains the effects of the current.

The implemented ILOS guidance law is given by:

$$\psi_d = \alpha_k - \tan^{-1}\left(\frac{e + \sigma e_{int}}{\Delta}\right), \tag{2.1}$$

where e_{int} is the integral component, the α_k is defined in the figure above and the lookahead distance $\Delta > 0$ is a design parameter. Moreover, the integral term is utilized only if the absolute value of the cross-track error is under a certain threshold, which is defined to be of the order of magnitude of $0.5 - 1$m. Notice that the guidance block had been modified without producing other modifications to the rest of the control chain. In order to do so, the ψ_d and the constant velocity reference $u = u_d, v = 0$ are introduced in the kinematics, in order to calculate a position reference for the next control step. This reference is then given to a nonlinear PID controller (as in Article A), which produces the thrust vector. Finally, the thrust is allocated through the thruster allocation matrix $T_{con} : F = T_{con}^{\dagger} \cdot \tau$, which has been modified to exclude the lateral thruster (so that the thruster vector is reduced to $F = [F_{vert}, F_{port}, F_{stb}]$ and the T_{con} to a 4×3 matrix), in order to operate the ROV as an underactuated vehicle.

2.4.3 Examples of Full-Scale Results

Figure 2.10 show some results from a full-scale test aimed to tune the ILOS algorithm designed to let the ROV follow the two red lines cyclically. The tuning was focused to find the parameters of Δ and σ which could provide better performances respecting the stability constraints given by the related theory presented in [83, 84]: $0 < \sigma < 1$ and $\Delta \geq 5$. Notice that these theoretical constraints have been found by doing an analogous

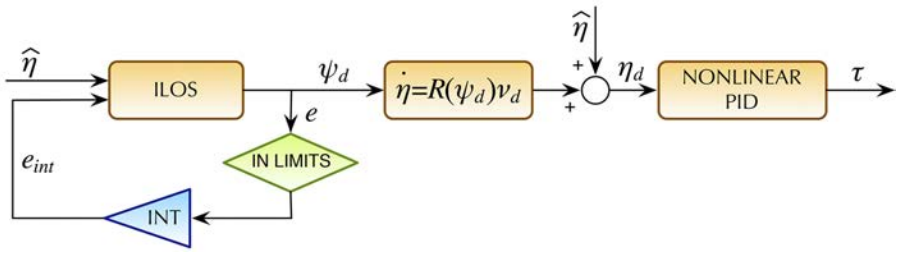

Figure 2.9: Block diagram of the implemented guidance and control system: the ILOS produces a desired heading, the correspondent desired position for the next time step is calculated by using the vehicle kinematics. A nonlinear PID stabilizes the vehicle on the new commanded position.

stability analysis as in [83, 84], considering a scaled model of the vehicle. Due to the simplifications related to the hydrodynamic effects, to the vehicle's model, and to the water and current speed, these constraints should represent a useful indication, but full scale test should be used to validate them. It is possible to see how, by increasing Δ, the approach to the lines becomes faster, producing a very oscillatory motion for $\Delta = 3$. σ weights the integral action which, in turns, build up the heading offset which is used to counteract the currents.

2.5 An Innovative Guidance and Interface Module

As mentioned in Section 2.1, ROV systems are sold with standard control interfaces, which may include control panels (with on/off buttons for the payload devices), different joysticks (to control the vehicle's motion), displays and dedicated GUIs (to feedback to the user the system's states, provide video and error messages), dedicated control panels for the manipulator controls, and so on (see Figure 2.11). The development of low-cost ROVs and underwater drones (see Subsection 1.2.6) and the understanding that an intuitive interface can deeply influence the quality and the outcome of the operations, have pushed companies to think towards innovative solutions.

In the work presented in Article E: *HMD as a new Tool for Telepresence in Underwater Operations and Closed-Loop Control of ROVs*, an innovative interface technology has been used to control the ROVs. In the following, the goal of this work is briefly described.

2.5.1 Head Mounted Displays, History and Perspectives

An innovative control interface has been proposed, included in the DP system and tested in full-scale experiments together with the ROV 30k. In particular, the goal has been to

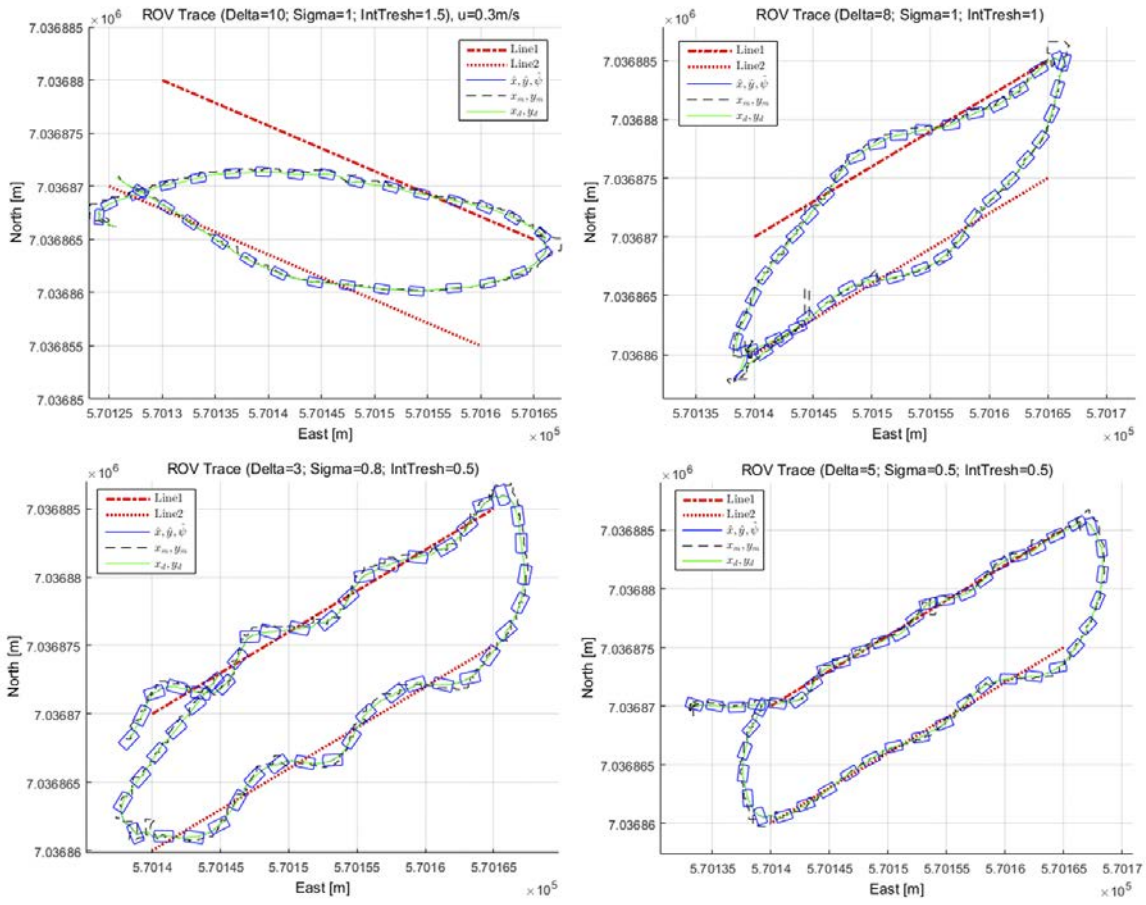

Figure 2.10: Four different results of the ILOS applied to the ROV Minerva, obtained while tuning the parameters σ and Δ. Desired surge speed is kept constant at $u_d = 0.3\frac{m}{s}$. Values around $\sigma = 0.5, \Delta = 5$ were giving best results, agreeing with the expected theoretical results.

Figure 2.11: Most common ROV control interfaces. (A) shows the combined ROV-manipulator interface that is provided by Sperre AS together with the ROV Minerva and 30k. (B) shows the control panel case used to control small OCROVs (e.g. VideoRay, Saab Seaeye). (C) shows the GUI developed together with the AUR-Lab control system (see Figure 2.3). (D) and (E) show two examples of common off-the-shelf video-gaming joysticks, which are common for fast and low-cost developing and prototyping of DP systems.

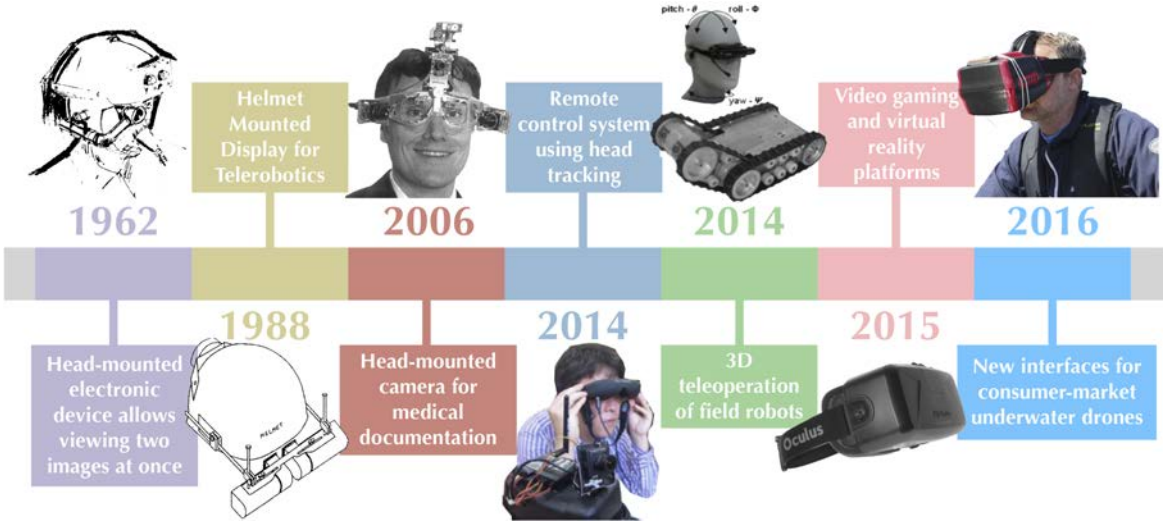

Figure 2.12: The history of HMDs starts in the 1960s, when the new technology was used to provide stereoscopic view to aircrafts pilots. In 1988 new solutions were developed for telerobotics. The development slowed down in the following years, finding new life in the 2000s, when new applications were introduced, due to the higher maturity of the needed technology and lower costs.

control the vehicle with an off-the-shelf Oculus Rift Head-Mounted Display[6]. A Head (or Helmet) Mounted Display (HMD) is, as the name implies, a device (containing one or more displays) which is attached to the head (or the helmet) of an operator. To the best knowledge of the authors, this has been the first attempt to control an ROV by using the HMD technology. As the author is writing this thesis, more and more consumer-market ROVs are introducing this technology to provide an immersive interface to their users.

As for many other technologies, the HMD technology has its roots many decades ago, a development which was "paused" due to the expensive and inadequate technology, and that experienced a new bloom due to the technology advances (a brief history is showed Figure 2.12). Due to the costs decrease of inertial sensors and Micro-Electro-Mechanical Systems (MEMS), most of the HMDs available in the market have integrated inertial sensors to track the user's head attitude, which provides a valid feedback to be used for control purposes.

2.5.2 Application to the 30K ROV

The proposed solution intuitively integrates the Oculus Rift HMD by interfacing the measured rotation of the operator's head to the motion of the vehicle itself. The hands of the operator becomes free to perform other operations, such as controlling the manipulator. With this new interface, it has been possible to provide to the ROV pilot:

[6]The Oculus Rift HMD is produced by Oculus VR, an American virtual-reality technology company. The company is property of Facebook since November, 2014.

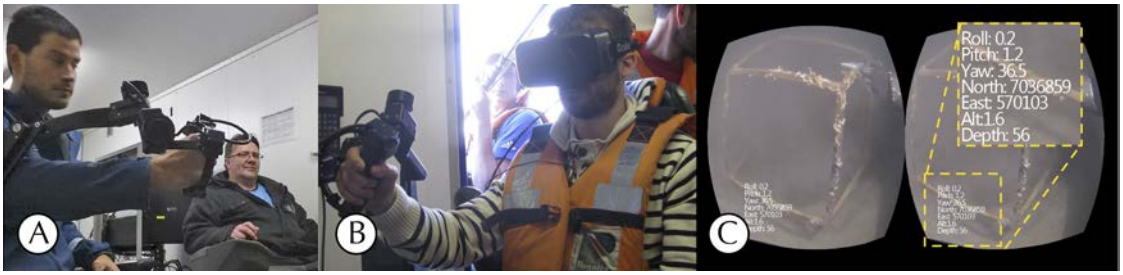

Figure 2.13: Full-scale test of an ROV manipulation work. (A) shows the operation carried from two operators. (B) shows the operator performing the same operation using the HMD. (C) shows the operator's view, which is a stereoscopic video, with an overlay containing the ROV state.

A more immersive experience, which would have increased his situational awareness.
A more intuitive interface, which relates the motion of the vehicle to the head's motions.
The perception of depth, which allows to perform more efficient manipulation operations.
The complete control over the vehicle and manipulator, at the same time.

The DP architecture is showed in Figure 2.14. The *Oculus Rift PC* generates the video stream from the ROV to the Oculus Rift, merging the attitude information coming from the ROV navigation payload, providing to the user a full understanding of the ROV state. Moreover, it receives the information related to the head rotations, which are given as control input to the DP system. Three guidance algorithm (defined in Article E) are associated to the HMD motion, in order to give a smooth and feasible input to the system.

This technology has been proven in full scale: an inspection operation has been carried out on a wreck outside Trondheimsfjorden in order to prove the HMD control effectiveness for the steering of the vehicle. Moreover, manipulation operations carried by one, or more, operators have been compared. Figure 2.13, (A) and 2.13, (B) show the two cases, in which it is possible to see that the HMD technology creates the possibility for the operator to successfully accomplish a manipulation operation by himself. By doing so, the operation was showed to be more effective, due to the lack of communication problems.

2.5.3 Human-In-The-Loop and Further Challenges

When an operator is actively involved in the operations of an highly automated system, it should necessarily be considered *part* of the system itself. In these cases, it is common to talk about "human-in-the-loop". Although the analysis of the reciprocal effects that the operator and the system have on each other has not been yet considered on this work, it is important to mention the importance of such aspects [97] and of the need of systematically model the human-system interaction [98]. In particular, a quantitative analysis of the benefit that the operator has by using the HMD technology, and the physical strains that this technology produces on the operator himself should be addressed. [99] analyses the impact of the military aircrafts' autonomous systems on the pilot, producing a sim-

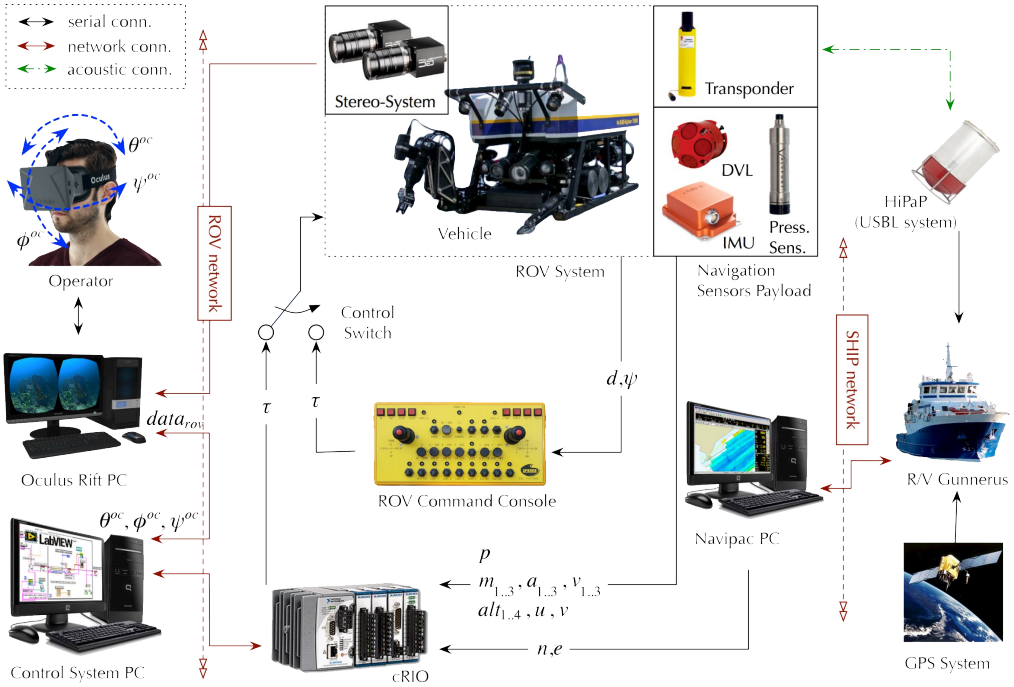

Figure 2.14: Hardware connections and information flow during the HMD interface test. The left part shows the modification that the new interface required. A dedicated computer distributes the required information between the control system PC, the stereo-camera system and the HMD. The nature of the communication links and the main shared variables are showed.

ulation model which quantifies the workload and performance level of the pilots. Long operations which involve the constant supervision of an operator can bring to a decrease of his attention level: [100] analyses this problem, monitoring the psychophysiological state of the operator.

As first step in this direction, thorough tests on a number of experienced and not experienced pilots should be performed. In this way, the effectiveness of the HMD approach could be compared with the classical joystick approach. Tests on longer missions could detect the appearance of strain effects on the operator, while tests on delicate operations would evidence the effects of this stress on the operator effectiveness. Finally, the effect of motion-sickness, which is a common effect occurring during the usage of HMD devices, should be analyzed and quantified [101, 102].

Chapter 3

Automatic Mapping and Planning

This chapter will introduce and discuss the topics presented in the Article F: *Photomosaic camera as simultaneous data collector and navigation aid on Unmanned Underwater Vehicles* (Section 3.1), and Article G: *Sensor-based Autonomous Path-Planner for Sea-Bottom Exploration and Mosaicking* (Section 3.2). A brief state of art of the most common photomosaics application its discussed. Moreover, the photomosaics system and the automatic sensor-based path-planner is briefly presented.

3.1 Mapping through Photomosaicking

In this chapter, the real-time photomosaic mapping technique developed as an add-on to the ROV DP system, is briefly described. The development has been inspired by the off-line mosaicking software developed at Woods Hole Oceanographic Institution (WHOI) used during the NTNU AUR-Lab full-scale operations to deliver optical mapping of wreck sites, coral reefs or others artifact or natural OOIs, see[103], and references therein. Figure 3.3 is an example. This mosaicking tool required the collection of imaging data during the missions and the following stitching of the pictures, to be done after the completion of the mission. This approach has been proven to be valid in terms of quality of the result, but unsatisfying as a tool to be actively used *during* the offshore missions. In fact, errors in the definition of the lawn-mower pattern could bring to incomplete data collection, which would be only discovered when it was too late (see, for instance, Figure 5.4). It was clear that this issue could have been avoided with an on-line approach. Once this became available, also new opportunities appeared possible: the high-level imaging data could be used as a feedback to modify the mission, in order to direct the vehicle towards areas of higher interest (see Section 3.2).

3.1.1 Challenges and State of Art

Photomosaic is an optical technique that allows mapping of large areas, preserving high spatial resolution. Photomosaics can span from underwater, to terrestrial, to aerial and space applications. Widely known are the mosaics which are automatically produced by the NASA rover on Mars, or the ones picturing large continental and offshore areas, coming from satellites. In the following, only the underwater application will be treated, underlining the challenges related to this domain.

The photomosaic technique can be used underwater to provide a qualitatively good and uniform representation of an underwater habitat, which is valuable for mapping and monitoring applications, and useful for the end-users of various fields. On the other hand, using the results quantitatively it is not trivial, since any picture added to the mosaic process has to be scaled and stretched in order to obtain a seamless final mosaic. This process adds errors in the represented dimensions and distances. Another problem arises from sloping sea bottoms, where the result can be strongly altered: straight artifact can become clearly bended in the final mosaic. In these cases, a photogrammetry approach through stereo-vision, like the one in [104], can be preferred. The underwater domain hides many challenges related to vision and imaging:

Natural light intensity is highly reduced by seawater. It is not rare that the light conditions do not allow to collect satisfying imaging data already at 10m depth.
Artificial light is needed. This often brings to non uniform illumination of the scene and moving shadows.
Natural light is non-uniformly attenuated by seawater, due to the water absorption spectrum, which mainly impacts the shortest wavelengths. Consequently, the images acquire a *greenish* tone.
Back scattering, which is produced from the artificial high-intensity light, reducing the contrast of the pictured objects and increasing the blur effect. In general, underwater pictures lacks of well-defined contours.

Photomosaicking techniques have their root back in 1986, when first attempts to put together pictures to represent a wide scenario were made [105]. [106] proposes the first feature detection and matching algorithm. Successive works are manly focusing on reducing the error accumulated when stitching an higher number of images, reducing the false matches and excluding outliers [107, 108, 109]. [110] is able to automatically build a big-scale mosaic (the biggest at the time, as the author claims) by using only images information. More recent work can be found in [111, 112, 113]. The formers produced the offline mosaicking software which have been inspiring the real-time mosaic software developed by the author of this thesis, and the latter produced methods and tools to utilize mosaicking techniques for biology and archeology applications. In [114], groups of underwater vehicles are used to autonomously build underwater maps.

3.1.2 Development of the Real-time Photomosaic Software

As mentioned, the WHOI software has been replaced with a real-time mosaicking software. Although the creation of real-time mosaics cannot be as precise[1], the advantage of having a continuous data flow, which instantaneously increases the previously built map, is preferred in this context. In the next list, the tasks which creates the real-time photomosaicking software are briefly explained. These steps are also represented in Figure 3.6, for a better comprehension. Notice that approximatively 800 ms are required to add a new picture to the mosaic, which makes it feasible for low-speed, real-time applications and a vehicle altitude between two to three meters. The time required to accomplish some of the most time-consuming steps of the mosaicking process are indicated in the following list for completeness[2] (and refers to the process in Figure 3.1).

1. ***Image acquisition and configuration***. Consists in shooting the picture with the optimal camera settings (depending by the available light, speed of the vehicle and altitude), and storing the imaging data in memory.

2. ***Image pre-processing***. The raw images are pre-processed to remove the vignetting effect[3]. This is caused by the light field produced by the ROV itself. The shadow pattern must be identified and corrected for. Colors are also corrected with a color mean filter, in order to compensate for the loss of the red channel. The images are converted to greyscale, to increase the processing speed of the following steps.

3. ***Feature-extraction***, *($\Delta t < 300$ ms)*. In order to merge two following pictures, it is necessary to find unequivocally identifiable characteristics of the images (*features*). The features must be rotation, scale or illumination independent (since the ROV will inevitably rotate, change its altitude and seabed illumination). A Scale-Invariant Feature Transform (SIFT) algorithm can perform this task.

4. ***Feature-description***, *($\Delta t < 300$ ms)*. Every feature is described in relationship with his surrounding information, in order to associate a "unique" fingerprint to it. The amount of information used in this descriptions depends by the desired level of accuracy and the computational time that is possible to tolerate. The output is generally a numerical vector of hundreds of elements for every feature, describing the image histogram of the neighborhood region.

5. ***Feature matching***, *($\Delta t < 40$ ms, 450 matches found)*. Two features which have the same descriptor (given a certain tolerance) in two following pictures are considered to represent the same physical point and matched. The distance between the matched features is also used to confirm the matching.

[1] The off-line process allows, for instance, to perform tasks such as global optimization and the processing and merging of parallel transects. Those operations cannot be properly performed in real-time for the heavy data-processing involved.

[2] The specified tasks are obtained with a computer equipped with two quad-core Intel i7 processor, 2.30GHz, 16GB RAM, 256GB solid state hard-drive, and the Window 7 Operative System.

[3] In photography, the term *vignetting* refers to the lower amount of light which usually illuminates the contours of the picture, creating the effect of a dark "frame".

6. ***Outliers-removal***, *($\Delta t < 50$ ms, 83% matches eliminated)*. The outliers removal step aims to remove the matchings which cannot be justified by the physical motion of the vehicle. Introducing outliers in the process compromises both the local and global registration[4] of the images. The main contribution of the author has been made in this step. The outlier-removal strategy is based upon the following three steps, which are possible thanks to the real time access to the ROV state data produced by the control system, which runs in parallel:

   - **Progression**. If the ROV is moving straight, the y-coordinate of the features should be increasing, i.e. $y_1 < y_2$, where y_2 is the feature position in the second image, while y_1 is the position of the same feature in the first image.
   - **Direction**. Knowing the ROV speed vector, heading and altitude, and making the hypothesis of a locally flat seafloor, it is possible to predict the position of the features in the second image of the pair. The constraint is relaxed allowing a certain error circle around the aforementioned predicted position.
   - **Bijective correspondence**. Some feature can have multiple matchings in the second image of the pair, due to very similar features descriptors. If more than one fall in the predicted position circle, only the closest to its center is kept, in order to keep a bijective correspondence.

7. ***Mathematical Transformation***, *($\Delta t < 90$ ms, 4 final matches selected)*. This step aims to find the mathematical transformation[5] to be applied to the picture. The transformation changes the figure proportions so that it can be correctly superimposed to the mosaic. In particular, every set of three feature matches is compatible with a unique transformation of the picture. The transformation which minimizes the error over the whole set of feature matchings should be chosen. An implementation of the *RANdom SAmple Consensus* (RANSAC) statistical method excludes the feature matchings which produces the higher error. This procedure brings to the elimination of all the matchings, except the best fitting four.

8. ***Warp and global registration***. Once the homography have been computed, the software applies the transformations (cumulative transform and warping) to the last picture, and connects it to the mosaic:

   - **Cumulative transform**. The relative transform (result of all the consecutive local transformations) is calculated, in order to place the picture into the global frame;
   - **Warping**. The image is geometrically *transformed* by applying the cumulative transform.

   Notice that, whenever a new picture is added, more memory must be allocated to store the new mosaic. Consequently, the dimension of the new mosaic must be calculated at the end of every step, before it is stored in memory. Once this is done, the last image

[4] In this context, the term *registration* refers to the process of associating a relative (*local registration*), or absolute (*global registration*) position to an image.

[5] In this work, both the affine and the projective transformation, which are both *homography* transformations described by 3×3 matrices, have been implemented. The former gives generally better results for flat terrains.

is *globally registered*, and placed in the mosaic. Transparency effects or more sophisticated blending techniques could be included to produce a seamless image. Notice that those steps are not fitting the real-time requirement of the case (so the edges of the pictures will be visible in the final mosaic).

More information about the process can be found in Article F, in which the author of this thesis has produced the explained real-time software, results, implementations details and summarizing pictures. Other details can be also found in [115, 116].

3.1.3 Results and Unresolved Issues

Full scale real-time mosaics, show that the algorithm was successfully able to generate images with relatively low distortion (see Figure 3.2). Notice that this statement is qualitative, since a quantitative analysis of the mapping error has not been done. Further work in this sense may provide the usage of the software on a test dataset, which could allow to compare the results, and calculate the geometrical errors introduced by the mosaicking process. Despite of the lack of a proper error quantification, the tool has been proven to be undoubtedly useful for the end-user, which could immediately understand the topology of the sea bottom, and replan the mission in case of unsatisfying progress.

The main issue associated with the development of this tool has been the memory allocation. In fact, only mosaics up to 50 pictures could be generated, before the memory was completely utilized. Such software requires a better memory allocation techniques, which allow to store the results in the permanent memory, and keep a low-quality version displayed. For time reasons, this has not been successfully achieved, and it is indicated as the necessary further work.

3.1.4 User Perspective: a Biology Analysis

Geir Johnsen, marine biology professor at NTNU, has been asked to analyze the final mosaic, in order to evaluate the amount of information that would be possible to extrapolate. The quality and the final result have been satisfying. In particular it was possible to make the following conclusion:

From the ca. 200 m photo mosaic map of the Tautra ridge it was estimated that 30% *was covered by orange and white alive Lophelia,* 15% *by dead and* 45% *covered by substrate. The substrate consisted mainly of pieces of dead Lophelia, called Lophelia rubble. Within the rubble, was sediment that appeared to be of of a softer character. The brownish sediments are believed to be sand, while the brighter gray sediments can be bacterial mat. Dead and alive Lophelia were not distinguished to separate zones, but surrounded each other in colonies [117]. Although not consistent, the distinct Lophelia colonies tended to grow in an eastern direction, towards the main current coming from south west probably for food supply and avoidance of sedimentation. Most taxa had its main distribution restricted to one part of the reef. A wide range of organisms is known to inhabit specific*

Figure 3.1: Main steps of the real-time mosaicking procedure illustrated in Subsection 3.1.2. Color correction and transformation into one-channel image (A, B, C),feature detection and description (D, E),feature matching (F), outliers removal and RANSAC (G,H), mathematical transformation, homography (I), warping and global registration (L).

Figure 3.2: Examples of real-time mosaics built while running a transect with the ROV Minerva. The navigation data from the control system has been used to improve the feature matching process and obtain a more correct matching. The ROV usually moves at $0.2 - 0.3\frac{m}{s}$ *at a constant altitude of* $1 - 3m$ *depending by the light conditions and depth. Altitude and speed are mutually selected in order to provide around 30% of overlapping between sequential pictures.*

zones of the reef [118]. The porifera (sponge) Mycale lingua was the dominating species on living corals, filtrated around the coral branches. Sponges are known to be bioeroding Lophelia reefs, which can be regulating reef growth and expansion [118]. The fish Sebastes viviparus and the squat lobster Munidopsis serricornis were observed beneath branches of alive Lophelia. Fewer organisms were associated with dead corals, but Demospongiae indet was abundant. Demospongiae indet. and the starfish Henricia sp. was the most common species on Lophelia rubble.

3.2 Autonomous Path Planning Strategy

A natural idea has been to utilize the imaging information (which, at this point, was available real time), in order to steer the vehicle towards the areas with a higher density of OOIs. This may be especially useful for biological or archaeological application, where the data related to certain OOIs (e.g. corals or artifacts) must be prioritized. Challenges, a brief state of art and an introduction to the Article G: *Sensor-based Autonomous Path-Planner for Sea-Bottom Exploration and Mosaicking*, are given in the following.

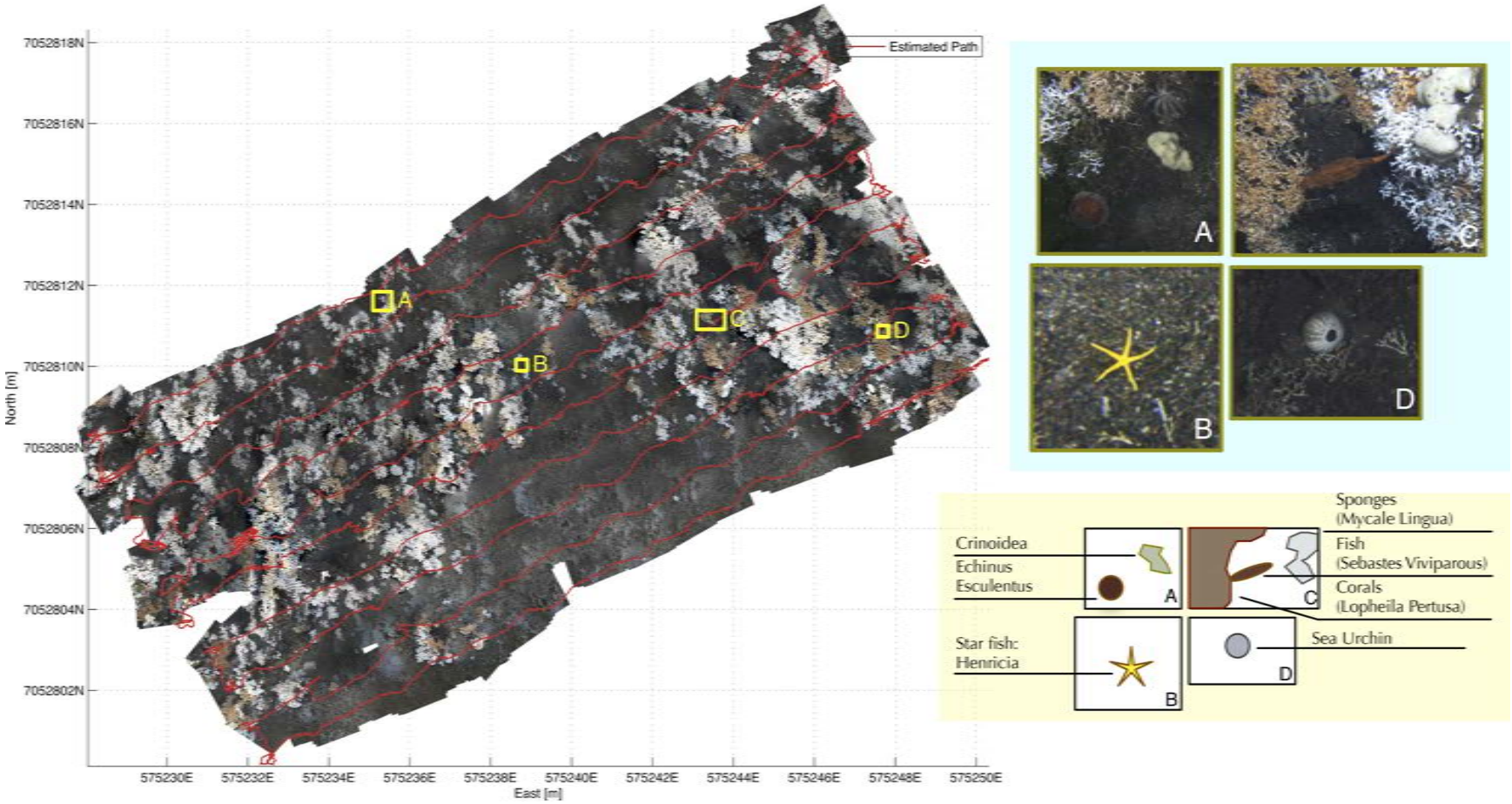

Figure 3.3: Photomosaic of a coral reef in Trondheimsfjord. The mosaic consists of 10 *transects and* 1500 *pictures, and covers a seabed area of* $200m^2$ *(*$10m \times 20m$*). The ROV speed has been constant at* $0.2\frac{m}{s}$*, with a constant altitude of* $1.5m$*. As described in Subsection 3.1.4, many information can be extracted for such representation of the sea bottom, which makes this kind of mapping useful for biological and archaeological qualitative analysis, for instance. The path of the ROV during the mapping, is also indicated (red line).*

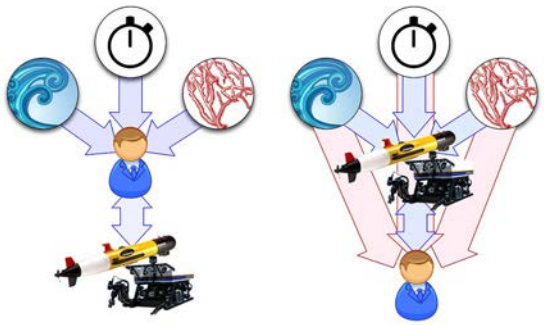

Figure 3.4: Increasing the level of autonomy, brings to a "role inversion" between the user and the vehicles. If, on a standard configuration, the user plans the mission considering the goals in relationship with the environmental and time constraints, on an autonomous operation the vehicles could access the system data, suggest solutions to reach its goal, and be able to change them.

3.2.1 Challenges and State of Art

Mapping missions are often carried in areas where information about the OOIs are little, and the environment is unstructured and often poorly known. This is true both for ROVs, and AUVs missions. The degree of autonomy and the possibility of changing its preplanned route becomes fundamental for an untethered vehicle, due to the battery constraints and the lack of real-time feedback of high level data (e.g. video, imaging, or sonar data), given by the bandwidth limitations of the acoustic link. For those reasons, a dynamic path planning which can take in account information from the surrounding environment, can become a good tool to reach the operations success. Notice that, as showed in Figure 3.4, this pushes towards a change in the overall idea of the system: the vehicle becomes the central decisional node, moving the user to the "side of the picture".

A standard approach to a sea-bed mapping mission is to define a Lawn-Mower Pattern (LMP) prior to its start, to cover a certain area of dimensions depending by the energy or time constraints of the vehicle. Data from the sea bottom are collected and stored by the vehicle during the mission, in order to be analyzed only after its recovery: the information about the environment, which is collected along the mission, is not actively used *during* the mission itself. It is often required a mission re-planning and a further mission attempt (for example if the area occupied by the OOIs has not be completely covered).

A wide literature concerning general theory and techniques for path-planning applications can be found (as described in Chapter 4). [119, 25, 26] propose strategies aimed to the autonomous underwater land demining, which involves the steps of autonomous detection, identification, and mission replanning. [120] combines sensing and autonomous path-planning for group of underwater vehicles. [121] treats automatic tracking and mapping of biological specimens of interest.

3.2.2 Application to ROV Mosaicking Operations

The online path planner proposed here is inspired from [122, 123, 124], and applied to the case of UUVs, for the purpose of mapping underwater OOIs. The strategy proposed for ROV mosaicking applications, aims to automate the research and photo-mosaicking missions, by using a sensor-based on-line path-planner based on still picture camera data feedback, in order to improve the mission outcome by increasing the quantity and quality of acquired data.

In particular the algorithm ultimate goal is to automatically steer the vehicle utilizing the visual information collected by the still-picture camera in order to maximize the coverage of the OOIs presents in the area. This is done by moving the vehicle (preferably) along parallel lines, in order to ease the parallel process of on-line mosaicking.

Figure 3.5 shows this idea: the real-time mosaicking tool, which is integrated in the GUI to provide an immediate feedback to the user (which can utilize to change the mission plan), can also be interfaced with an higher-level mission re-planning module. The visual information could automatically be used to steer the vehicle.

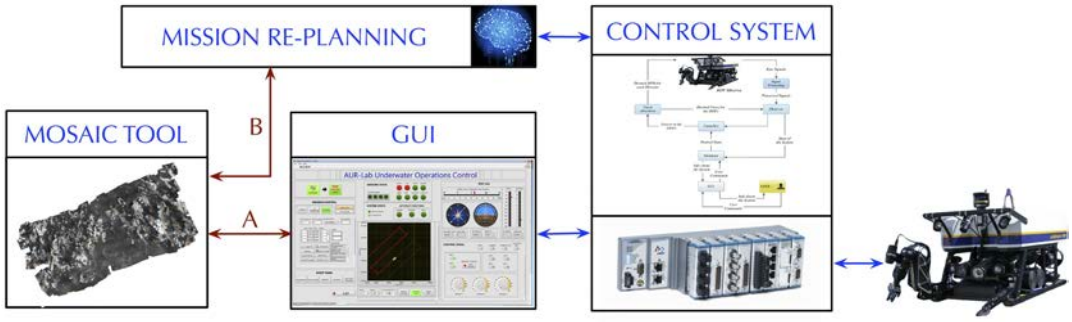

Figure 3.5: The modularity of the ROV Control System allowed to run a real-time photomosaic system during the navigation. This would allow the user to have a higher situational awareness (link A in figure). By extrapolating relevant information from such high-level user data, it is possible, for the vehicle, to change its path increasing efficiency (link B in figure).

In particular, the proposed planner has the characteristics of providing waypoints instead of a continuous heading reference to obtain a LMP-behavior (see Figure 3.6). The new waypoints are chosen taking in account:

- ***Heading changes***: a new waypoint along the current direction is prioritized in order to decrease the heading changes. Heading changes which would produce lawn-mower-like paths are prioritized.
- ***Collected information***: the information extracted from the images is taken in account to understand the distribution of OOIs.
- ***Memory of previously collected information***: the past information is taken in account to go back to unvisited areas with high probability of containing OOIs.

These three terms are quantified and optimized to define the waypoint to be reached at every step. Moreover, the initially defined area should be prioritized if all the discovered OOIs have been mapped. Finally, the vehicle should be able to reach its starting position before its energy does not allow it to navigate further.

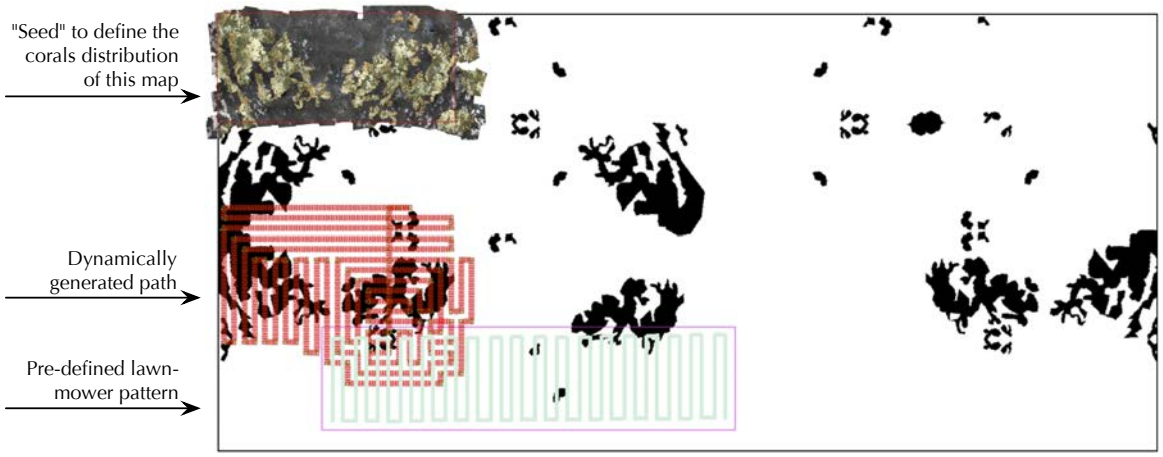

Figure 3.6: Example of real-time replanning by using feedback from the images. The vehicle redirect its path (red lines) in order to cover as much corals as possible. The corals are represented as black spots in the map, generated from the "seed" given by the distribution in Figure 3.3.

3.2.3 Unresolved Issues and Possible Developments

The proposed autonomous path planning strategy has been studied at a preliminary stage, and for this reason relies on strong assumptions which, cannot be neglected. The simulations have been carried on a two dimensional flat map. Non-zero inclination of the seabed, three-dimensional objects, high turbidity of the water or irregular camera's FOV needs to be considered in further work to obtain a more complete approach. A necessary improvement would be the following: the method relies on the subdivision of the map in a grid of equally sized and distributed cells, to which a probability is associated. A grid composed by cells with different dimensions or shapes may be necessary in case of irregular, non-flat terrain.

Notice also that the work in Article G states the Assumption for which the OOIs should be *homogeneously distributed*. This assumption legitimate the principle for which searching in the neighborhood of an OOIs would increase the chances of finding other OOIs. If, on the other hand, the objects would be sparse and randomly distributed on the area, better performance of the automatic path planning over the standard lawn-mower pattern method could not be guaranteed. The possibility of relaxing this hypothesis keeping the effectiveness of the solution should be also investigated.

Chapter 4

Path-Planning/Replanning Systems

This chapter will introduce and discuss the topics presented in the Article H: *Continuous Curvature Path Planning using Voronoi diagrams and Fermat's spirals*, the Article I: *A Voronoi-Diagram-Based, Dynamic Path-Planning System for Underactuated Marine Vessels* (Section 4.3) and Article J: *A 3D Dynamic Voronoi Diagram-Based Path-Planning System for UUVs* (Section 4.4). A brief state of art of the most common path-planning algorithms, and the relevance for autonomy is discussed. The path-planning systems are discussed in their main points.

4.1 Challenges and State of Art

In Subsection 1.2.7, some autonomy aspects were mentioned, and it was clear how many details must be considered, with the aim of obtaining a highly autonomous system. In fact, many open issues are still to be addressed in order to make the current autonomous systems safe and effective enough for their actual employment, especially if a certain interaction with humans or artifacts is required. In the same subsection, some examples of new autonomous applications were discussed, including few examples taken from the marine field. Two of the challenging phases which need to be further investigated are the path-planning and replanning phases, which are crucial knots to be untied. Their solution becomes particularly complicated when there are uncertainties in the surrounding environment and safety constraints have to be guaranteed. In fact, planning of operations is underlined by many as a substantial limitation that prevents systems to reach a higher autonomy level. As stated in [125]:

> *"automation of planning processes has been a central problem in the field of artificial intelligence for more than 30 years [...]"*

This is also confirmed by the fact that all the vehicles which could produce not negligible damages during their operations are still required to have a human crew on board in charge of all the phases of the missions. In these cases, the robot has the control of the low-level

tasks, while high-level mission planning or delicate maneuvers (e.g. landing or taking off, in the case of aircrafts), are still responsibility of the human crew.

Extensive research was conducted in the latest years concerning the topic of path-planning and obstacle avoidance (or local replanning). Literature reviews can be found in [126, 127, 128]. [129] presents a complete and recent review of motion planning algorithms for marine vessels and vehicles, [130] presents an application of dynamic path-planning and obstacle avoidance for an AUV, [131] considers the case of multiple vehicles. [132] proposes a nice discussion which treats the most common maneuvers and missions for underwater applications, and a method to automatically generate paths is discussed.

Path-planning algorithms can be classified as *global path-planning algorithms* (which evaluate the whole information available on a certain area), or *local path-planning algorithms* (which take into account the surrounding of the vehicle). Examples of methods concerning the former class are: the *rapidly-exploring random tree* [133], the *Voronoi diagram* [134], the *visibility graphs* [135], the *potential field method* [136, 137], the *occupancy grid methods* [138] and optimization methods, such as the *A* algorithm* [139, 140, 141, 142, 143]. Dynamic programming methods aimed to the solution of the Hamilton-Jacobi equations are also commonly used: the *fast marching methods* [144], and the methods based on *semi-Lagrangian approximations* [145] are two example of such techniques. These methods are widely used for the purpose of path and trajectory planning, as in [146]. [147] uses the fast marching algorithm with the Voronoi diagram, [148] uses it to produce trajectories with curvature constraints. Examples of the local path-planning algorithms class are the *dynamic window* [149], the *virtual force field* [150], its modified version *modified virtual force field* [137], and the *velocity obstacle* method [151].

As in [152], it is possible to build methods which combine the benefits of the two classes. In those cases, it is possible to talk about *dynamic path-planning*, which also includes the system presented in Article H, Article I and Article J.

4.2 The Geometric Elements

The proposed path-planning system generates paths composed by straight segment and curved segment. The former are generated through a Voronoi diagram, while the latter are spirals or circular arcs. In the following, these elements are briefly described.

4.2.1 Creating a roadmap: the Voronoi diagram tool

Voronoi diagrams have been used for many applications since the beginning of the 20th century, and many possibilities have been found in the path-planning problems for mobile robot autonomous environment exploration [153]. The Voronoi diagram is still very used in many path-planning applications, including the marine field. [154] uses it in connection

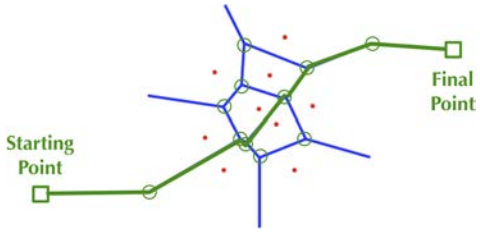

Figure 4.1: In (A), a simple example shows the generator points (red dots), the edges (blue lines), and the vertexes (green dots) of the Voronoi diagram. It is possible to see how the edges are maximally distant to all the generator points (which can be considered the obstacles), so that they can be chosen as path segments to connect a $starting$ to a $final$ point.

with multi-robots systems, [155, 156, 157, 158, 159] are recent examples covering the marine field. This number of possibilities is due to three main aspects:

- The Voronoi diagram is a geometrical tool that divides the geometrical space in such a way that the borders of the regions are maximally distant from all the obstacles in the cluttered environment (see Figure 4.1);
- It is an algorithm that has $\boldsymbol{O}(n)$ complexity, while the majority of other mathematical tools can solve the same problem with quadratic complexity;
- Mobile robots' kinematics allows them to change heading without affecting the other DOF (degrees of freedom), so they can easily run a path composed only by a sequence of straight lines (which is a natural outcome of this tool).

More details about the usage of the Voronoi diagram as a tool to provide the roadmap for the path-planning approach presented in this work can be found in Article H. Article J shows the initial Voronoi roadmap generated over the large area also reported in Figure 4.4. Article I explains the basics of the *convex hull method*, which can be used to rapidly generate the Voronoi diagram in n-dimensions [160].

4.2.2 Smoothen the Paths: Fermat Spiral and Dubins Path

As previously mentioned, the construction of the path should reflect the dynamics and kinematics properties of the vehicle, in order to ease the task of the control system and provide higher performance. For mobile robots, or even ROVs (or in general fully actuated vehicles), it is possible to design paths with discontinuous curvature: those vehicles can easily stop at the end of a straight line, direct the heading towards a new waypoint and then start moving again towards it (e.g. lawn-mower pattern path). This may be impossible for underactuated vehicles, since the motion of some DOFs can influence the others (coupled dynamics), making it impossible for the vehicle to keep the position, while rotating its heading. Consequently, the path geometry needs to be modified to make it *flyable*[1]: this can be achieved providing a continuous curvature.

[1]The term *flyability* defines the kinematic and dynamic ability of a vehicle to navigate along a certain path, as defined in [128].

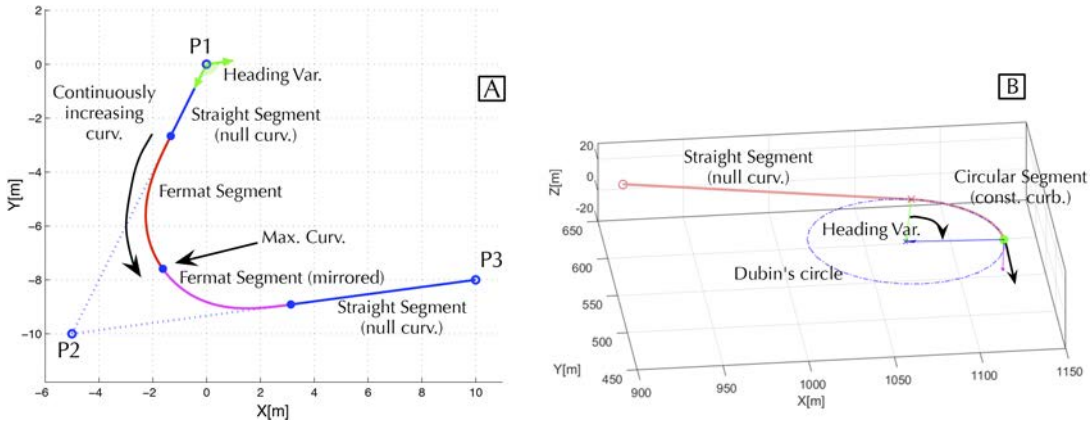

Figure 4.2: (A) illustrates an example of Fermat spiral, while (B) shows an example of 3D Dubins path. The main constitutive elements and characteristics of the paths are illustrated.

For this purpose, the generated paths will be composed by straight segments which are connected through spiral segments to *smoothen* the discontinuities. The curvature of the resulting path will be zero along the straight segments, it will continuously increase at most at the maximum feasible curvature of the vehicle, and finally decrease continuously to zero to join a new straight line. By using spirals segments instead of circular arcs, curvature continuity is achieved, see Article H, Article I, or [161, 128, 162].

If, in 2D, it has been proven that the Dubins path is the shortest path connecting two given points [163], in 3D the matter of defining the shortest path connecting a starting with a final point with given initial and final tangents, is more complicated [164]. Nevertheless, Dubins path[2] has been extensively used in many robotics applications, and many examples could be also found for applications in 3D. Some examples of applications which mainly target UAVs can be found in [165, 166, 167, 168, 169].

In Article J, Dubins paths are used to smoothen the discontinuities. Although the consequent final path does not have the characteristic of curvature continuity, this strategy was preferred because it brought to a faster development of the algorithms. This aspect will become critical when the guidance and control modules will be also integrated into this system. The missing implementation of the guidance and control modules at this stage (suggested as further work), made the curvature continuity aspect less relevant.

4.3 Path-planning and Replanning System for USVs

Given the mathematical tools described in the previous section, it is possible to describe the structure of the path-planning and replanning system for surface and underwater vehicles, starting with the former case. The following description will follow step by step

[2]In this chapter, *3D Dubins path* only indicates a path defined in the 3D-space, which is composed by straight and circular segments.

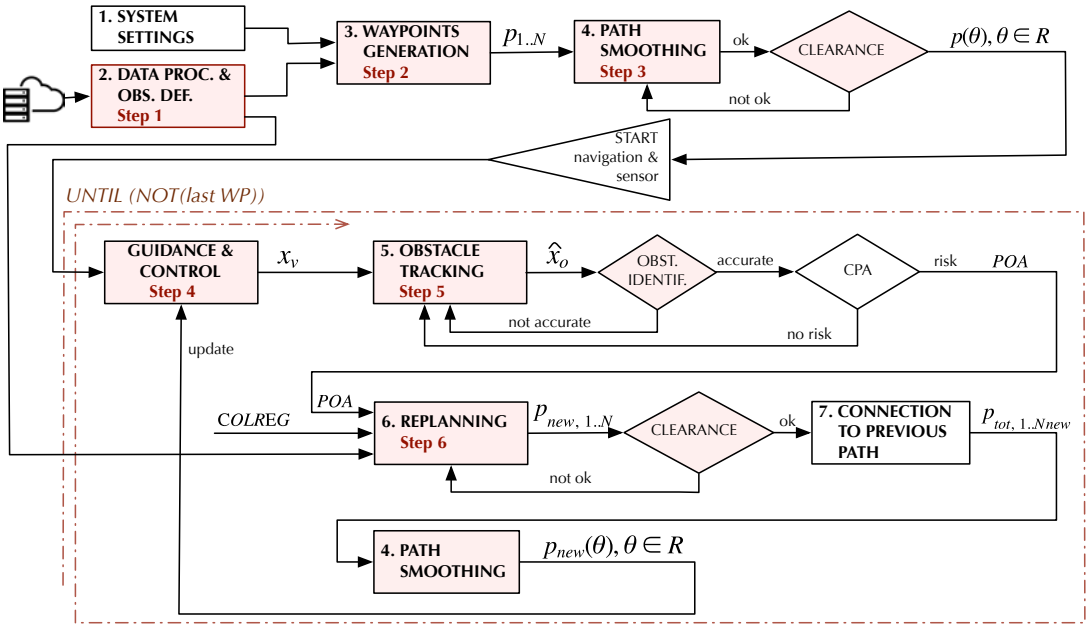

Figure 4.3: The block diagram represents the logical flow of the algorithm. The upper part is executed offline, while the red dashed line contains what runs in a loop. The text in red indicates the list item of Section 4.3 which briefly explains the related block.

the diagram flow represented by Figure 4.3, which models both systems for surface and underwater vehicles. The main steps are summarized in the following:

1. **Data Processing and Obstacles Definition Phase**

   In order to use the Voronoi diagram tool, it is necessary to choose proper *generator points*, as mentioned in Subsection 4.2.1. Moreover, to keep the computational time of the algorithms low, a simple structure to define the obstacles must be found. For those two reasons, polygonal structures compose a simplified model of the mapped obstacles (e.g. islands, mainland), and of the unmapped obstacles (e.g. vehicles or artifacts). The polygonal structures vertexes also naturally define the points set which composes the generator points set for the Voronoi diagram.

   The output of this first step are the polygons and related vertexes defining the models of the maps and the known obstacles.

2. **Waypoint Generation Phase**

   As mentioned above, the Voronoi diagram is a tool to produce a *roadmap* containing paths (sequences of Voronoi edges connecting the starting with the final waypoint) which are maximally distant from the obstacles. Given this roadmap, three steps need to be performed:

   (a) Find the waypoints in the roadmap which assure the shortest path;

(b) Verify the compatibility of the chosen path with the the clearance constraints[3];
(c) Reduce the waypoints to decrease the complexity, length and direction changes.

The shortest path is determined by using the Yen modification [170] of the Dijkstra optimization algorithm [171]. This algorithm is able to find the *k-shortest* paths. In this way, suboptimal solutions can be found if the optimal solution do not respect the preassigned clearance constraints. More details about the implementation of this algorithm can be found in Article H, Article I, and references therein.

The output of this step is a list of waypoints which provides a polygonal path, connecting the initial with the final waypoints, respecting the required clearance constraints.

3. **Path Smoothing Phase**

At this stage, the polygonal path is smoothed at the edges of every composing segment by using Fermat spirals, in order to provide curvature continuity along the whole path. The curved links are designed by considering the minimum possible curvature, to provide smooth heading changes. This step requires a further clearance check, because the path may vary significantly in the proximity of its vertexes after the linking curves are added. If the check is positive, the curvature may be increased until both the kinematic constraints of the vehicle, and the clearance requirements, are met.

The output of this step is a parametrized[4], curvature continuous path linking the initial and final waypoints.

4. **Guidance and Control Phase**

In this work, the 3 DOFs vessel model presented in [66] is considered, which expresses the horizontal plane motion in terms of the relative surge and sway. Given the path and the dynamics of the vehicle, the cross-track error needs to be minimized trough the following control objective:

$$\lim_{t \to +\infty} y_e(t) = 0. \tag{4.1}$$

A LOS algorithm with an additional disturbance rejection term (which minimizes the cross-track error dynamics) defines the desired heading of the vehicle [172].

The output of this module is the actual motion of the vehicle, which would bring it towards the final waypoints along the whole path.

5. **Obstacle Tracking and Identification Phase**

During the navigation of the vehicle along the path an unpredicted moving vehicle or an unmapped piece of land can be detected. Proceeding along the predefined route may be risky. The risk must be evaluated and a new route must be found if it is not

[3] Two clearance constraints are considered: the *shore clearance*, which assures that the vehicle will not collide with the shore, and the *sea-depth level clearance*, which assures that the vehicle will not fall into *grounding* (the collision with the sea-bottom).

[4] A parameterized curve in the plane is a function that assigns to each q in some given interval $[a, b]$ a point along the path. In particular $r(a)$ corresponds to the initial point of the path, while $r(b)$ corresponds to the last.

possible to safely proceed along the original path. To this purpose, an *obstacle tracking* algorithm is designed to estimate the state of the detected obstacles. A Kalman filter is built on a constant velocity dynamical model [173], in order to rapidly track moving or fixed obstacles during the navigation [174]. To produce realistic results, a detection sensor (a sonar) is modeled to produce noisy measurements in the local sonar frame.

This step produces an estimation of the detected obstacle(s) states, the related estimation error, and an indication about the necessity of the path-replanning.

6. **Replanning Phase and Rules of Navigation**

   If a risk of collision is determined, the path must be replanned. The replanning procedure utilizes the same concepts of the planning procedure, in a smaller scale. This idea of *scalability* of the algorithm is at the basis of this path-planning and replanning system.

   Obstacles that are estimated to have a certain, (non negligible) velocity (*moving obstacles*), can be approximated by projecting on the map the probable positions of the vehicle in the near future (i.e. Projected Obstacle Area (POA), [141, 142]). This area can be successively extended to forbid paths which would not respect the International Regulations for Preventing Collisions at Sea (COLREG) [175] which are rules that surface vessel must respect to resolve traffic or collision-risk situations. Once the map is updated with the obstacles detected along the vehicle's way, the algorithm that was used to provide the initial path is used again on a smaller area centered on the current position of the target vessel (replanning area).

   The outcome of this module is a local deviation from the original path, which is smoothly connected to it at both ends. Once the obstacle is safely passed, the vehicle rejoins the original path, so that a new analysis of the whole map is not required.

Figures 4.4, (A) and 4.4, (B) show the path planning procedure on a wide map ($45000 \times 65000\mathrm{m}^2$). Figure 4.4, (C) shows an example of replanning on the same map. A detailed discussion of the results can be found in Article H and Article I.

4.4 Path-planning and Replanning System for UUVs

The path-planning and replanning system for underwater vehicles is an extension built on the system developed for surface vessels. The system follows approximately the same steps, with the following few modifications:

Obstacle Modeling: maps, underwater environmental obstacles, floating artifacts or other moving obstacles must be modeled with 3D geometries. The vertexes of polyhedrons are considered to be the *generator points* of a 3D Voronoi diagram;
Roadmap Creation: the Voronoi diagram is extended to 3D, so that the roadmap can produce compatible paths with the underwater environment;

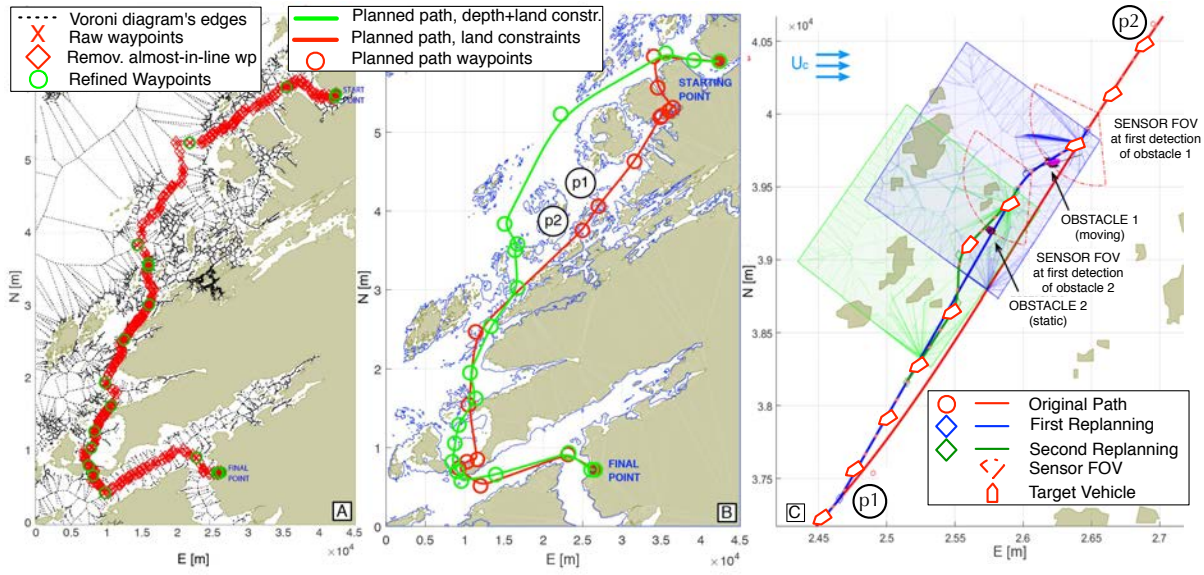

Figure 4.4: Details of the path-planning system. (A) shows the waypoints after the refinement steps (indicated, respectively, with red crosses, diamond crosses, and green circles). Voronoi diagram edges are also showed. (B) shows the paths obtained considering the water-depth constraints (green line), or the land constraints (red line). (C) shows a detail of (B), and the replanning.

Smoothing Curve: Dubins curves are used to smoothen the underwater path. This procedure produces a continuous path;
Waypoint simplifications, heuristics and other implementation details: all those steps have been extended to 3D, taking into account the third dimension when it was necessary.

Further details and simulation results are presented in Article J. The extension to the underwater domain (3D case) has been only done considering the static (path-planning/replanning) case, since the guidance and control modules (i.e. the *dynamic element*) have not been added to the system. It is believed that an extension to the same guidance and control modules utilized in 2D is straight forward and will be done as further work.

4.4.1 Rules for a Safe Underwater Navigation

Safe underwater navigation rules for UUVs are proposed by adapting the COLREGS (from the marine industry), and the TCAS (from the aviation industry), with the purpose of avoiding collisions with other physical structures, natural objects, or other vehicles in the subsea environment [175, 176, 177]. In the process of defining a path-replanning system for UUVs, it was natural to propose new rules for this context. In particular, when these two aforementioned safety philosophies are applied to UUVs, high level safety navigation rules can be derived for 3D underwater applications.

A set of navigation rules provides decision support basis to the UUV during different collision scenarios. In particular, they are divided among rules to be considered for static

obstacles and for moving obstacles, for crossing to the left or right, and for higher and lower position of the obstacle, relative to the target UUV. An idea is given in Table 4.1. These rules are applied during the replanning phase.

Direction of movement	Obstacle position in horiz. plane (wrt UUV)	Obstacle position in vert. plane (wrt UUV)	Safe navigation rules
Obstacle moving in opposite direction of UUV	Crossing left	Higher altitude	UUV descends, obstacle climbs.
	Crossing left	Same altitude	UUV climbs, obstacle descends.
	Crossing left	Lower altitude	UUV climbs, obstacle descends.

Table 4.1: Safe navigation rules in presence of a moving obstacle proceeding in the opposite direction as the UUV, crossing left, for varying altitudes.

4.4.2 Unresolved Issues and Possible Developments

The modeling of the detection sensors and the tracking algorithm have not been the focus of this project and impose a limitation on the formal description of the replanning procedure. In particular, it is not possible to formulate with precision when and how accurately an obstacle could be detected during real-life implementation, which at the moment is a limiting factor. For this reason, the replanning procedure only relies on estimating the CPA and the CTA on the basis of two strong assumptions on the detecting sensor and the states of the UUV and the obstacles:
Assumption 1. The speed of the vehicle is supposed to be known.
Assumption 2. In the horizontal 3-DOF case, the tracking algorithm produces a certain estimation of the obstacles which enters the FOV of the sensor, whereas in the underwater case the state of the obstacle is supposed to be known as soon as it enters the fixed FOV.

The geometrical constraints are included in the replanning procedure and, if the system is not able to find a flyable alternative in the replanning area, a new replanning trial would be required. The replanning procedure iteratively proposes new safe replanning alternatives until the CPA becomes so small that the related CTA does not allow for a new trial. If this process cannot result in a final positive resolution of the problem, the vehicle will be forced to a safe stop. It is worth noting that a conservative estimation of the time required from the replanning algorithm can be calculated. Consequently, given the state of the UUV and obstacle, also the number of possible trials can be estimated. Further work in this direction would necessarily require a formal statement of the requirements in terms of stating the necessary conditions which would bring to the certain replanning. These would involve conditions on:

- Uncertainties in the knowledge of the state of the UUV;
- Uncertainties in the knowledge of the state of the obstacle(s);
- Characteristics of the detection sensor;
- Geometrical shape of the surrounding environment;
- Kinematic constraints of the UUV;
- Minimum CPA tolerated.

Chapter 5

Field Operations and Technology Users

This chapter will briefly introduce the NTNU AUR-Lab mission goals, in connection with end-users, which do not necessarily work directly with technology and engineering. As previously mentioned, the development of underwater vehicle technology and solutions for the autonomy challenges are mainly devoted to the achievement of a better understanding of the ocean, to its exploration, and to the exploitation of its resources. Some examples of missions in which the author has participated are reported as examples.

This chapter is supported by two articles; Article L: *Underwater vehicles for environmental management in coastal areas* concerns the usage of underwater vehicles to continuously and cooperatively perform coastal mapping and monitoring missions. It describes the main methodologies, vehicles and operations which characterize the missions carried out by NTNU scientists. Article K: *Glowing in the dark: discriminating patterns of bioluminescence from different taxa during the Arctic polar night* is an example of an end-user application, which is directed to verify the possibility of exploiting the underwater vehicles to obtain data of biological interest.

As mentioned in the introduction, this thesis focuses primarily on providing tools aimed to seabed operations. However, it is necessary to mention that the tests were performed on the seabed mainly to provide visual feedback to the operator, often useful for safety reasons, and to provide a quantitative analysis of the methods. This does not put constraints on the possible applications for most of the tools, which could be easily used to provide support for missions in the water column.

5.1 NTNU AUR-Lab's Operation Objectives

In [178], the *vision* of AUR-Lab is described in connection with *knowledge* and *technology*. The former is required to develop the latter and, on the other hand, the former cannot

be verified or validated without the latter. Clearly, technology and knowledge need to be developed and applied in parallel, to really produce an outcome. From this report, it is clear how AUR-Lab is built on a continuous collaboration with partners, and aims to fill the gap between disciplines. The author of this thesis has been mainly collaborating with scientists coming from the field of:

- control engineering;
- geology;
- marine biology;
- maritime archeology;
- underwater system design,

in order to help providing with them the technology they need, in terms of:

- test platforms;
- methods for data processing;
- instrument carriers;
- better quality of services;
- interpretation of data,

in order to:

- develop new algorithms and methodologies;
- explore, map and sample biological OOIs;
- explore, map and sample archaeological OOIs;
- explore, map and sample geological OOIs;
- increase the understanding of deep seas, polar environment and the fjord ecosystem.

In particular, Article L shows the context in which the work that brought to this thesis found inspiration and application. Moreover, it describes the equipment, the geographical area in which the operations were performed, the deployed vehicles, the experimental methods and set-up, a lists of operation examples and the related results.

Notice that many other research groups, which work with marine vehicles, deploy a fleet of different surface, underwater, and aerial vehicles with similar objectives and characteristics. The research group at University of Porto (FEUP) has been working in the direction of multi vehicle operations through the Underwater Systems and Technology Laboratory (LSTS) for years, involving multi-institution collaborations [179, 180, 181]. Other examples involving institutions as MBARI (Monterey, USA), PLOCAN (Canary Islands, Spain) [182], WHOI (Woods Hole, USA), NSF (Arlington, USA) [183], MARUM (Bremen, Germany), SARTI (Catalunya, Spain) [184] can be found. Many other examples could be listed, which would just emphasize how the development of innovative vehicles, coordinated missions and autonomy, together with joint collaborations with scientific partners with heterogeneous background and common interests, can be the only way to achieve more efficient ocean mapping and monitoring strategies.

Figure 5.1: Some pictures from the Neptunus project. (A) Process of integration of the micro-ROV Neptunus, with the MSROV 30K. (B) The innovative design of the vehicle. (C) A CAD design table.

5.2 ROV Neptunus

A project which is worth mentioning is the Neptunus project, which the author of this thesis have been supervising. The team was composed by three students, and the goal has been the realization of a new design for micro ROVs. In particular, a commercial system has been improved, and new ideas to produce a new vehicle to be commercialized have been proposed. As a matter of fact, this project has been one of the first steps which brought to the development of the NTNU spin-off company BluEye ROV, in which the author helped developing the first prototype, namely *P0* [185]. The development of Neptunus (which is illustrated in Figure 5.1, B) started utilizing the software and hardware architecture of the OpenROV (last version can be found in [186]), which have been modified to obtain higher performance. To mention some of the modifications to the existing system, the interface has been improved, providing the possibility of controlling the vehicle also from portable devices. The tether was substituted with a full Ethernet cable, so that the interfacing boards (a board which would interface the Ethernet and twisted pair protocols, which was pointed out as one of the weakest elements of the system) could be removed. Moreover, the system was completely redesigned following an hydrodynamic approach, which could lead to better navigation performances. In particular, the shell has been designed with the *foil* characteristics, successively 3D-printed (Figure 5.1, C). The performance in terms of navigability and stability were incredibly improved. More information on this project can be found in [187, 188, 189].

This project was finalized to also provide the possibility for a bigger ROV, to have an *extended eye*: in particular the team plan was to connect Neptunus to the 30K ROV, which would carry it as a normal payload. When approaching a wreck or other OOIs, the small dimensions of Neptunus could be used to explore the inside of the wrecks, entering spaces that would be inaccessible for industrial ROVs. The team has been successful in the first part of the plan, and the systems were successfully interfaced in December, 2014 (Figure 5.1, A): Neptunus could be controlled indirectly, through the 30K system. Unfortunately, the planned mission (which aimed to explore the Herkules wreck, outside Trondheimsfjorden), was not successful due to a fault in the electronics casing, which let water in when a certain depth was reached.

Figure 5.2: An hyperspectral image example. The UHI technology can collect information which is not limited to the RGB (Red-Green-Blue) channels. This increasing sensibility can be used to produce OOIs fingerprints to be automatically detected and mapped. Courtesy of Ecotone AS.

5.3 The Biologists' Point-Of-View

Many missions aimed to provide data to biologists, which are mainly interested in monitoring and mapping biological OOIs: fish, coral reefs, zooplankton and seaweed are just few examples. In September 2013, the author controlled the ROV Minerva for the LoVe cruise, in collaboration with Statoil and Ecotone AS, with the objective of integrating the innovative underwater hyperspectral camera technology on an ROV to autonomously map biological OOIs (see Figure 5.2) [190]. The objective was to evaluate the performance of such technology and to collect imaging data of the hard bottom coral forest, cold water corals, soft bottom sponges, and deep water sea pens.

In January 2013, the author joined a biology expedition to the arctic with the goal of showing that an abundance of marine life populates the ocean also during the dark season. This work is described in Article K. Although this article did not directly produce tools to be integrated in the ROV system, the study of such technology has been the first step to that direction. Analogously to what was achieved by Ecotone AS, this methodology could enable autonomous UUV missions aiming to map the arctic life in the water column through the measurements of bioluminescence patterns.

The procedure, methods and results are well reported in Article K, and can be briefly summarized as follows: a bathyphotometer[1] and a CTD (Conductivity-Temperature-Depth) sensor were deployed below surface in Kongsfjorden, Svalbard, in order to continuously collect data over a timespan of 51 hours. In this period of time, the bathyphotometer

[1]The *Underwater BAThyphotometer* (UBAT), consists of a water inlet and outlet which sucks (flushes) a certain amount of water into (from) a chamber. A *Photon Multiplier Tube* (PMT) is placed in the chamber, and measures the bioluminescence as photons$\cdot s^{-1}$

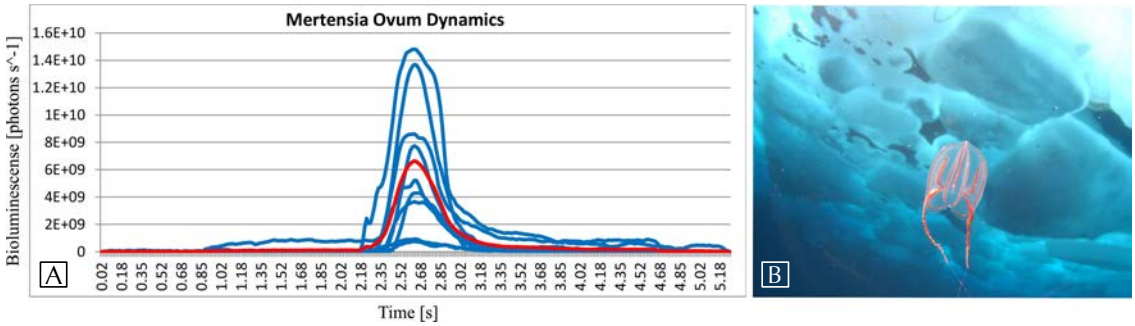

Figure 5.3: Some images from the arctic expedition aimed to measure bioluminescence of marine organisms. (A) shows the bioluminescence patterns of some individuals of the Mertensia Ovum species, and their average (red line). (B) shows an individual of the Mertensia Ovum species.

sucked sea water into its chamber, measured the intensity of the lights in the chamber, and flushed the water, continuing the cycle at regular intervals. The measured light could only be generated inside the chamber from living organisms, which reacted to the stress produced by the bathyphotometer by emitting certain bioluminescence patterns. In other words, by measuring the emitted light, it was possible to measure the amount of organisms (mainly zooplankton, or jelly) populating the flow of water. Moreover, by defining a *fingerprint* for the bioluminescence dynamic of every taxa, it was possible to show that the population composition characteristics could be automatically given. An example of the bioluminescence dynamics of the jelly Mertensia Ovum is showed in Figure 5.3.

5.4 The Archaeologists' Point-Of-View

One of the missions which was mainly devoted to archaeological studies of the area was the one conducted in 2012 in Ormen Lange, an area located 120 Kilometers northwest of Kristiansund, in the southern Norwegian sea. In-depth information about such mission can be found in [191]. Many pipelines populate the sea bottom of this area, and are the source of concern for biologists and archaeologists which must verify that the underwater infrastructure does not compromise the environmental conditions and stability. For this purpose, the NTNU AUR-Lab was called to perform a survey with the goal of verifying the state of the site, especially focusing on the ancient wrecks that were individuated years before. In fact, a Norwegian law state that:

> *"The State shall have the right of ownership of boats more than 100 years old, ships' hulls, gear, cargo and anything else that has been on board, or parts of such objects, when it seems clear under the circumstances that there is no longer any reasonable possibility of finding out whether there is an owner or who the owner is. The authority appointed under the Act may dig up, move, examine or raise objects as described in the first paragraph, regardless of who is the owner, and take other steps to preserve the object or take it into safekeeping [...]."*

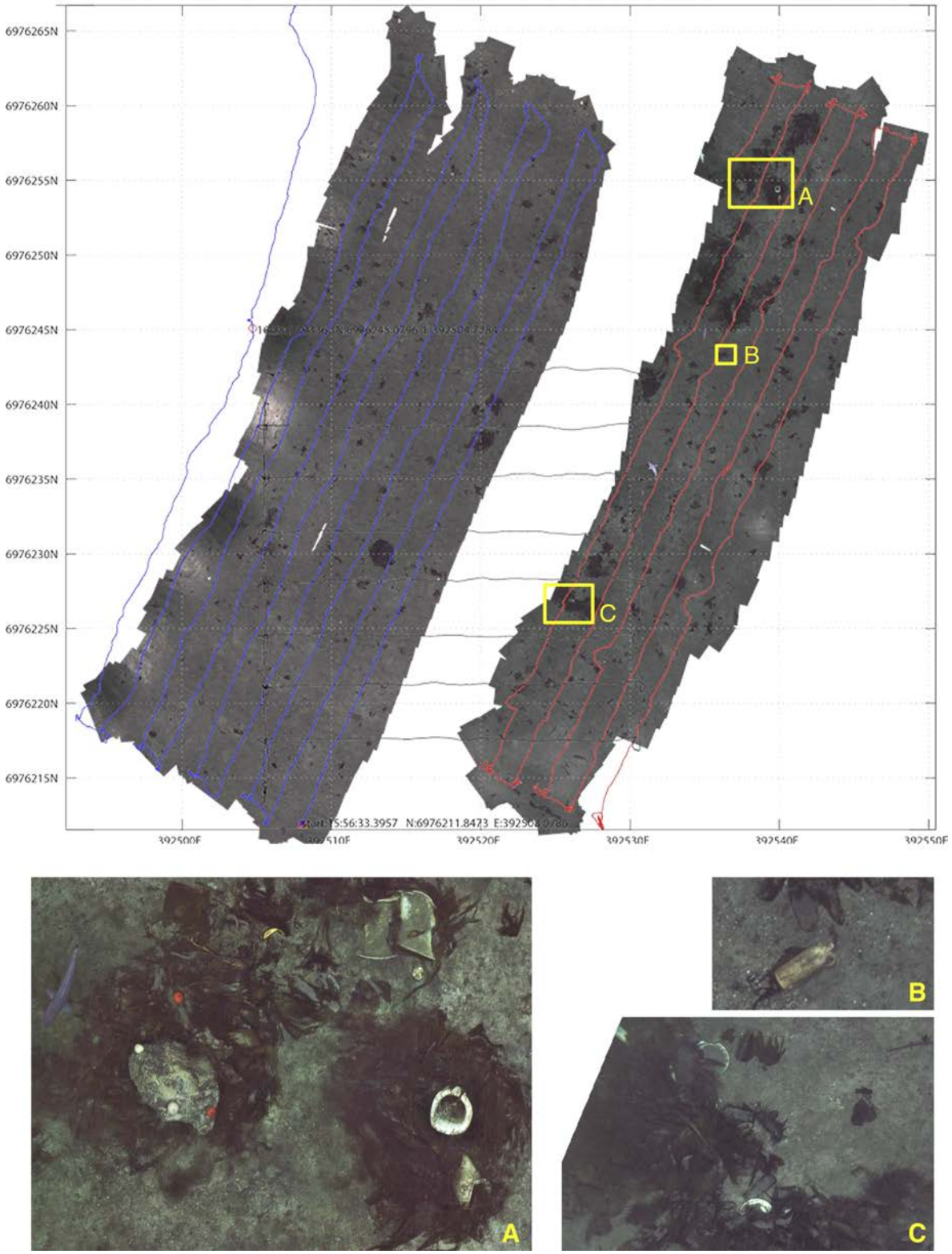

Figure 5.4: One of the mosaics developed to study the preservation conditions of the $18th$ *century ship-wreck located in the Ormen Lange gas field area, Norway. Unfortunately, due to a wrong mission planning, it was not possible to collect the data of the main wreck area, but some OOIs are still identifiable. The mosaic covers an area of approximatively* $3000m^2$.

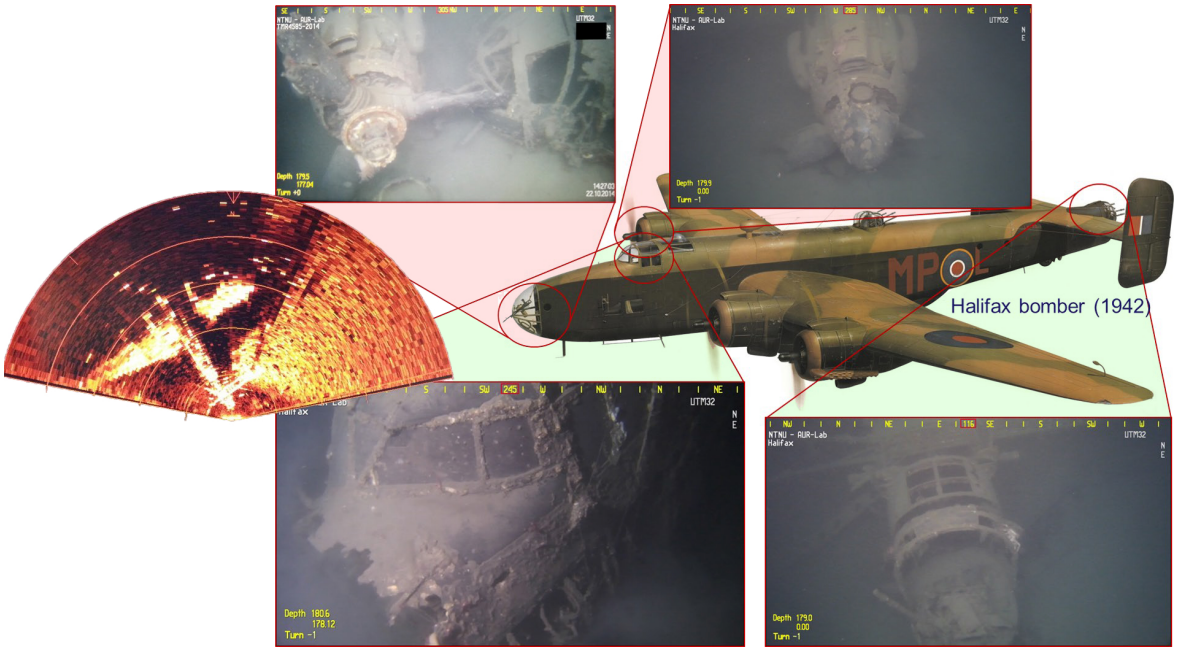

Figure 5.5: The Halifax bomber which was discovered in Trondheimsfjorden in October, 2014. The left picture shows the view from the ROV forward looking sonar, tens of meters away from the wreck location. The pictures on the right show an illustration of the airplane, with underwater pictures taken from the ROV.

In fact, during the marine archaeological surveys in 2003, an $18th$ century shipwreck of approximately 90 feet length was discovered close to the proposed route for the Ormen Lange pipeline at a depth of 170 meters. As the wreck was confirmed to be more than 100 years old, it is protected under the aforementioned law. During the mission, sediment traps were used to analyze the sea bottom, water and currents were characterized, the wrecks' wood has been sampled, and video and still-picture imaging data collected. Moreover, multi-beam data from an echo-sounder mounted on the ship was collected. The author has produced 2 large photomosaics of the area during this mission (one is proposed in Figure 5.4, where it is possible to notice few artifacts such as bottles, dishes, pieces of the wreck structure and so on). The main part of the wreck has not been pictured for some errors in the mission planning, which produced a wrong coverage of the site (this was also one of the main motivations for the development of the real-time mosaic module discussed in Subsection 3.1.2).

Notice that natural biological degradation was reported, especially for those parts of the hull which were not covered in sediments (one cause are parasites, such *Teredo Navalis*, a wood borer). There were no indications of damage being caused by human activity such as trawling or other intrusive underwater actions [191].

5.5 The Historians' Point-Of-View

Part of the side operations of the NTNU AUR-Lab, in which the author of this thesis participated, has been the one dedicated to discovery and exploration. Those missions cannot have dedicated time, since it is generally difficult to be sure of the result, or even to approximate when a positive result could come. It is natural that such high uncertainty discourages the employment of such expensive infrastructure. In October 2014, new information about a bomber which was shot down by the German army during World War 2 reached the AUR-Lab, and the discovery mission was organized together with an ROV training mission. Luckily, the information was accurate, and, after a brief search, it was possible to see a clear image on the sonar (see Figure 5.5), which allowed to finally discover and map the wreck which was lost for more than 70 years. Notice that, for such missions, autonomy is the only key which can prevent both incredibly high investments per mission, and incredibly high mission failure rates.

Chapter 6

Conclusions and Further Work

The research questions formulated at the beginning of this thesis have been pushing the author along the red thread which links the Control System for ROVs with the end users' needs. The former provides the technology which controls the platforms carrying the payload instrumentation which provides the required data to the latter. On the other hand, the collected data is also useful for the mission planning itself, and can be used during the missions in order to reach an increased autonomy level. The autonomy aspect has been also investigated, and strategies to define paths, or redefine them in the case of unexpected events, have been proposed. The author tried to put this work into the context of actual missions, providing examples taken from full-scale operations.

6.1 Concluding Remarks

Stating that the research questions have been answered cannot be done in absolute terms. The author tried to give one *possible answer* to them, maybe opening the way for further improvements which can make such answers more and more complete. In the following, concluding remarks and observations related to the presented work are stated.

> *How can the ROV Control System be efficiently improved to increase its performance in connection to the real mission's characteristics and the operator's needs?*

The ROV Dynamic Control system was integrated with modules that improved its performance. New solutions covering the whole control chain were designed, tested, and integrated into the system. Moreover, the users' experience was improved towards the study of innovative interfaces, in parallel with proper guidance algorithms. The fact that new ROV companies are investing in the HMD technology is a confirmation that this innovative research was directed towards the right path.

> *Which tools can be developed to give the end users a comprehensive information about the underwater environment? Could these tools be used actively*

and autonomously from the ROV Control System during the operations?

The photomosaic strategies were clearly needed from the first full-scale tests. The development of those algorithms for real-time applications was a strong push not to be ignored, and the usefulness of such tools was proven during full scale missions. This gave also the tools to investigate autonomy strategies that can direct the ROVs based on the sensed environment, which has suggested an interesting development towards missions characterized by higher decisional autonomy.

How could the mission and path planning phases be designed to increase the mission's autonomy?

The autonomy of the operation was mainly attacked through the point of view of the mission and path planning. Many aspects must be considered to actually achieve an autonomous system. Nevertheless, mission and path-planning are still two of the most critical tasks. For this reason, novel path-planning and replanning techniques which could be used both with ASVs and with UUVs were developed, showing promising results.

6.2 Further Work

The author of this thesis would like to focus on the following points, which he thinks would be the necessary steps required to push this work further:

- The control system should be analyzed with proper performance indexes, optimized and exported to a reliable release version.
- The contribution on switching observers and the promising simulation results must be strengthen with a formal stability proof.
- The HMD technology should be systematically tested with a selected number of non-expert and expert operators which should face the same mission with standard and HMD interface. Comparative results with the current joystick technology, both in terms of time and quality, should be collected to state more qualitative conclusions;
- The real-time mosaicking algorithm should be improved to store in the background the full-resolution data, while displaying a lower-resolution representation of the map. In this way bigger maps could be built without encountering memory problems;
- The automatic path-planning algorithm based on imaging should be formulated in a more rigorous way, include the guidance module and be dynamically tested. The integration with the mosaicking algorithm and full scale tests are also required. Moreover, the direction of the path should take currents into account, and the system should be completed with the picture analysis and OOIs detection;
- The path-planning and re-planning systems should be tested in full-scale to prove the effectiveness of the methods. This would also require the modeling of a sensor and the development of an obstacle detection module. Moreover, the conditions which assure a feasible solution for the replanning problem should be formally stated.

Bibliography

[1] O. Yildiz, A.E. Yilmaz, and B. Gokalp. State-of-the-Art System Solutions for Unmanned Underwater Vehicles. *Radioengineering*, 18(4):590–600, 2009.

[2] J. Yuh. Design and Control of Autonomous Underwater Robots: a Survey. *Autonomous Robots*, 8(1):7–24, Jan 2000.

[3] US Navy. The Navy Unmanned Undersea Vehicle (UUV) Master Plan. Technical report, PEO Littoral Combat Ships, Nov 2004.

[4] R.D. Christ and R.L. Wernli, editors. *The ROV Manual (Second Edition)*. Butterworth-Heinemann, Oxford, second edition edition, 2014.

[5] G. Antonelli. *Underwater Robots*. 2006.

[6] A.D. Bowen, D.R. Yoerger, C. Taylor, R. McCabe, J. Howland, D. Gomez-Ibanez, J.C. Kinsey, M. Heintz, G. McDonald, D.B. Peters, B. Fletcher, C. Young, J. Buescher, L.L. Whitcomb, S.C. Martin, S.E. Webster, and M.V. Jakuba. The Nereus hybrid underwater robotic vehicle for global ocean science operations to 11,000m depth. In *Proceedings of MTS/IEEE OCEANS*, pages 1–10, Sept 2008.

[7] J. Elvander and G. Hawkes. Advanced Hybrid ROV For Marine Renewable Technologies. http://goo.gl/UNG9TG, 2013. Accessed: 30-09-2016.

[8] G. Meinecke, V. Ratmeyer, and J. Renken. HYBRID-ROV - Development of a new underwater vehicle for high-risk areas. In *Proceedings of MTS/IEEE OCEANS*, pages 1–6, Sept 2011.

[9] F. Dukan. *ROV Motion Control Systems*. PhD thesis, Department of Marine Technology, Norwegian University of Science and Technology, Trondheim, Norway, 2014.

[10] Wikipedia. Remotely operated underwater vehicle. https://goo.gl/MiyNIi, 2016. Accessed: 30-09-2016.

[11] R.L. Wernli. *Operational Effectiveness of Unmanned Underwater Systems*. 1998.

[12] Norwegian Oil and Gas Association, The Federation of Norwegian Industries. NORSOK STANDARD: Remotely Operated Vehicle (ROV) services. Technical report, Jan 2016.

[13] F. Dukan, M. Ludvigsen, and A.J. Sørensen. Dynamic positioning system for a small size ROV with experimental results. In *Proceedings of MTS/IEEE OCEANS*, pages 1–10, 2011.

[14] V. Berg. Development and Commissioning of a DP system for ROV SF 30k. Master's thesis, Department of Marine Technology, Norwegian University of Science and Technology, Trondheim, Norway, 2012.

[15] Sperre A.S. Company website. http://sperre-as.com/, 2016. Accessed: 30-09-2016.

[16] DroneLife. Drone Sales Numbers: Nobody Knows, So We Venture A Guess. http://goo.gl/o6Hdme, 2016. Accessed: 30-09-2016.

[17] D. Carrington. Winds of climate change will make transatlantic flights longer, study shows. *The Guardian*, Jan 2016.

[18] Toyota. Integrated Safety Management Concept. http://goo.gl/sEbruk, 2015. Accessed: 30-09-2016.

[19] The Economist. If Autonomous Vehicles Rule the World. http://goo.gl/nfxVP5, 2015. Accessed: 30-09-2016.

[20] Volvo. Collision Avoidance Package. http://goo.gl/ZGkjC7, 2015. Accessed: 30-09-2016.

[21] P. Scharre and M.C. Horowitz. An introduction to autonomy in weapon systems. *Center for a New American Security (CNAS)*, Feb 2015. working paper.

[22] J.F. Bonnefon, A. Shariff, and I. Rahwan. The social dilemma of autonomous vehicles. *Science*, 352(6293):1573–1576, June 2016.

[23] M.L. Seto. *Marine Robot Autonomy*. Springer, 2013.

[24] Rolls-Royce. Autonomous Ship Research Project. http://goo.gl/wHhZiU, Aug 2015. Accessed: 30-09-2016.

[25] M.S. Wiig, T.R. Krogstad, and Ø Midtgaard. Autonomous identification planning for mine countermeasures. In *Proceedings of the IEEE/OES Autonomous Underwater Vehicles*, pages 1–8, Sept 2012.

[26] T.R. Krogstad and M.S Wiig. Autonomous Survey and Identification Planning for AUV MCM Operations. In *Proceedings of the Undersea Defence Technology Conference*, June 2014.

[27] Ø. Ødegård, S.M. Nornes, M. Ludvigsen, T.J. Maarleveld, and Sørensen A.J. Autonomy in Marine Archaeology. In *Proceedings of the 43rd Annual Conference on Computer Applications and Quantitative Methods in Archaeology (CAA)*, volume 1, pages 857–865, 2016.

[28] J.B. Sousa, G.A. Gonçalves, and F.L. Pereira. Autonomous vehicles in the response to maritime incidents. In *Proceedings of the 2nd IFAC Workshop on Navigation, Guidance and Control of Underwater Vehicles (NGCUV)*, volume 41, pages 67 – 72, Apr 2008. IFAC-PapersOnLine.

[29] Committee on Autonomous Vehicles in Support of Naval Operations, Naval Studies Board, Division on Engineering and Physical Sciences, National Research Council. *Autonomous Vehicles in Support of Naval Operations*. 2005.

[30] Wikipedia. Autonomy. https://en.wikipedia.org/wiki/Autonomy, 2016. Accessed: 30-09-2016.

[31] M. Ludvigsen and A.J. Sørensen. Towards integrated autonomous underwater operations for ocean mapping and monitoring. *Annual Reviews in Control*, 2016.

[32] M.S. Wiig, T.R. Krogstad, and R.A. Løvlid. Decision Autonomy Architecture for Unmanned Vehicles. In *Specialists Meeting on "Intelligence & Autonomy (Robotics)" (IST127), NATO STO*, 2016.

[33] M. Vagia, A.A. Transeth, and S.A. Fjerdingen. A literature review on the levels of automation during the years. what are the different taxonomies that have been proposed? *Applied ergonomics*, 53(A):190–202, Mar 2016.

[34] I. Schjølberg and I.B. Utne. Towards autonomy in ROV operations. In *Proceedings of the 4th IFAC Workshop on Navigation, Guidance and Control of Underwater Vehicles (NGCUV)*, volume 48, pages 183 – 188, Apr 2015. IFAC-PapersOnLine.

[35] S.I. Ekra. Kartlegger havbunnen i Barentshavet med nytt superkamera. http://goo.gl/DI3MQW, 2014. Accessed: 30-09-2016.

[36] B. Sved. NTNU kartlegger bomber, miner og skipsvrak i Trondheimsfjorden. http://goo.gl/x7WUMM, 2014. Accessed: 30-09-2016.

[37] A.S. Midling. Discovery Channel Canada visits NTNU and Trondheim Fjord. http://goo.gl/6KZA74, 2015. Accessed: 30-09-2016.

[38] Discovery Channel Canada. Daily Planet - Underwater vehicles, Nov 2015.

[39] B.T. Andersen. Christines drone kan revolusjonere forståelsen av havet. http://goo.gl/EmFCPL, Oct 2015. Accessed: 30-09-2016.

[40] E. Omerdic, D. Toal, and G. Dooly. OceanRINGS: Smart Technologies for Subsea Operations. In *Advances in Marine Robotics*. LAP LAMBERT Academic Publishing, 2013.

[41] Oceaneering. ROV Automated Control Technology. http://goo.gl/UCez4g, 2016. Accessed: 30-09-2016.

[42] D.A. Smallwood and L.L. Whitcomb. Model-based dynamic positioning of underwater robotic vehicles: theory and experiment. *IEEE Journal of Oceanic Engineering*, 29(1):169–186, Jan 2004.

[43] E. Omerdic, D. Toal, S. Nolan, and H. Ahmad. ROV LATIS: next generation smart underwater vehicle, 2012.

[44] D. Ribas, N. Palomeras, P. Ridao, M. Carreras, and A. Mallios. Girona 500 AUV: From Survey to Intervention. *IEEE/ASME Transactions on Mechatronics*, 17(1):46–53, Feb 2012.

[45] S.L. Fraga, J.B. Sousa, A. Girard, and A. Martins. An automated maneuver control framework for a remotely operated vehicle. In *Proceedings of MTS/IEEE OCEANS*, volume 2, pages 1121–1128, Aug 2001.

[46] A.R. Girard, J.B. Sousa, and J.E. Silva. Autopilots for Underwater Vehicles: Dynamics, Configurations, and Control. In *Proceedings of MTS/IEEE OCEANS*, pages 1–6, June 2007.

[47] Faculdade de Engenharia da Universidade do Porto (FEUP). DUNE. https://goo.gl/hmx9m3, 2016. Accessed: 30-09-2016.

[48] ROS: Robot Operating System. https://goo.gl/FD0VSX, 2016. Accessed: 30-09-2016.

[49] Robots using ROS. http://goo.gl/tYw8rk, 2016. Accessed: 30-09-2016.

[50] E.C. De Souza and N. Maruyama. Intelligent UUVs: Some issues on ROV dynamic positioning. *IEEE Transactions on Aerospace and Electronic Systems*, 43(1):214–226, Jan 2007.

[51] M. Chemuturi. *Requirements Engineering and Management for Software Development Projects*. 2013.

[52] P. Bourque and R.E. Fairley. *Guide to the Software Engineering Body of Knowledge*. Third edition edition, 2014.

[53] US Department of Defense. *Systems Engineering Fundamentals*. 2016.

[54] Kongsberg Maritime. HiPAP (High Precision Acoustic Positioning). https://goo.gl/KsfWPt, 2016. Accessed: 30-09-2016.

[55] A.J. Sørensen. *Marine Control Systems - Propulsion and Motion Control of Ships and Ocean Structures. Lecture Notes, UK-13-76*. Department of Marine Technology, NTNU, Jan 2013.

[56] Å. Grøvlen, A.J. Sørensen, and M.F. Aarset. Aspects of Dynamic Positioning: Impacts of Signal Processing and Local Thrust Control in an Integrated Power, Automation and Positioning System. *IMCA Station Keeping Seminar & Workshop*, 1998.

[57] J. Gertler. *Fault Detection and Diagnosis in Engineering Systems*. CRC Press, May 1998.

[58] Oppenheim A. *Signals and Systems*. Massachusetts Institute of Technology: MIT OpenCourseWare, 2011.

[59] F. Gustafsson. *Adaptive Filtering and Change Detection*. Wiley, July 2000.

[60] M. Blanke, M. Kinnaert, J. Lunze, and M. Staroswiecki. *Diagnosis and Fault-Tolerant Control*. Springer, 2006.

[61] L. Standardi. Signal Processing and Change Detection applied to ROV in DP system. Master's thesis, Dipartimento di Ingegneria dell'Informazione, Universitá Politecnica delle Marche, Ancona, Italy, 2010.

[62] B.B. Stovner, T.A. Johansen, T.I. Fossen, and I. Schjølberg. Three-stage filter for position and velocity estimation from long baseline measurements with unknown wave speed. In *Proceedings of the American Control Conference (ACC)*, pages 4532 – 4538, July 2016.

[63] D.M. Hawkins. *Identification of outliers*. Springer, 1980.

[64] F. Gustafsson. *Statistical Sensor Fusion*. Studentlitteratur, 2010.

[65] D. Simon. *Optimal State Estimation: Kalman, H∞, and Nonlinear Approaches*. John Wiley & Sons, Inc., 2006.

[66] T.I. Fossen. *Handbook of Marine Craft Hydrodynamics and Motion Control*. John Wiley and Sons Ltd., 2011.

[67] J.G. Balchen, N.A. Jenssen, E. Mathisen, and S. Sælid. A Dynamic Positioning System Based on Kalman Filtering and Optimal Control. *Modeling, Identification and Control (MIC)*, 1(3):135–163, 1980.

[68] J.G. Balchen, N.A. Jenssen, E. Mathisen, and S. Sælid. Dynamic positioning of floating vessles based on kalman filtering and optimal control. In *Proceedings of the 19th IEEE Conference on Decision and Control (CDC)*, pages 852–864, Dec 1980.

[69] S. Sælid, N. Jenssen, and J. Balchen. Design and analysis of a dynamic positioning system based on kalman filtering and optimal control. *IEEE Transactions on Automatic Control*, 28(3):331–339, Mar 1983.

[70] D.M. Steinke and B.J. Buckham. A Kalman filter for the navigation of remotely operated vehicles. In *Proceedings of MTS/IEEE OCEANS*, volume 1, pages 581–588, Sept 2005.

[71] T.I. Fossen and A. Grovlen. Nonlinear output feedback control of dynamically positioned ships using vectorial observer backstepping. *IEEE Transactions on Control Systems Technology*, 6(1):121–128, Jan 1998.

[72] T.I. Fossen and J.P. Strand. Passive Nonlinear Observer Design for Ships Using Lyapunov Methods: Full-Scale Experiments with a Supply Vessel. *Automatica*, 35:3–16, Jan 1998.

[73] J.C. Kinsey and L.L. Whitcomb. Model-Based Nonlinear Observers for Underwater Vehicle Navigation: Theory and Preliminary Experiments. In *Proceedings of the IEEE International Conference on Robotics and Automation (ICRA)*, pages 4251–4256, Apr 2007.

[74] J.E.G. Refsnes. *Nonlinear Model-Based Control of Slender Body AUVs*. PhD thesis, Department of Marine Technology, Norwegian University of Science and Technology, Trondheim, Norway, 2007.

[75] J. Refsnes, A.J. Sørensen, and K.Y. Pettersen. A 6 DOF nonlinear observer for AUVs with experimental results. In *Control Automation, 2007. MED '07. Mediterranean Conference on*, pages 1–7, June 2007.

[76] L. Jetto and S. Longhi. Development and experimental validation of an adaptive extended Kalman filter for the localization of mobile robots. *IEEE Transactions on Robotics and Automation*, 2(2), Apr 1999.

[77] Y. Yang and W. Gao. An optimal adaptive kalman filter. *Journal of Geodesy*, 80(4):177–183, July 2006.

[78] B. Zhao. *Particle Filter for Fault Diagnosis: Applications to Dynamic Positioning Vessels and Underwater Robotics*. PhD thesis, Department of Marine Technology, Norwegian University of Science and Technology, Trondheim, Norway, 2015.

[79] Wanli Li, Lundong Zhang, Fuping Sun, Li Yang, Mingjian Chen, and Ying Li. Alignment calibration of IMU and Doppler sensors for precision INS/DVL integrated navigation. *Optik - International Journal for Light and Electron Optics*, 126(23):3872 – 3876, 2015.

[80] N. Shneydor. *Missile Guidance and Pursuit, Kinematics, Dynamics and Control*. Elsevier, 1998.

[81] S.O. Kørte. Guidance & Control Strategies for UUVs. Master's thesis, Department of Marine Technology, Norwegian University of Science and Technology, Trondheim, Norway, 2011.

[82] D.A. Fernandes. *An output feedback motion control system for ROV*. PhD thesis, Department of Marine Technology, Norwegian University of Science and Technology, Trondheim, Norway, 2015.

[83] W. Caharija, M. Candeloro, K.Y. Pettersen, and A.J. Sørensen. Relative velocity control and integral los for path following of underactuated surface vessels. In *Proceedings of the 9th IFAC Conference on Manoeuvring and Control of Marine Craft (MCMC)*, volume 9, pages 380–385, Sept 2012.

[84] W. Caharija, K.Y. Pettersen, A.J. Sørensen, M. Candeloro, and J.T. Gravdahl. Relative velocity control and integral line of sight for path following of autonomous surface vessels: Merging intuition with theory. *Journal of Engineering for the Maritime Environment*, 228(2):180–191, Mar 2014.

[85] F.A. Papoulias. Bifurcation analysis of line of sight vehicle guidance using sliding modes. *International Journal of Bifurcation and Chaos*, 1(4):849–865, Dec 1991.

[86] K.Y. Pettersen and Lefeber E. Way-point tracking control of ships. In *Proceedings of the 40th IEEE Conference on Decision and Control (CDC)*, volume 1, pages 940–945, Dec 2001.

[87] L. Lapierre, D. Soetanto, and A. Pascoal. Nonlinear path following with applications to the control of autonomous underwater vehicles. In *Proceedings of the 42nd IEEE Conference on Decision and Control (CDC)*, volume 2, pages 1256–1261, Dec 2003.

[88] T.I. Fossen, M. Breivik, and R. Skjetne. Line-of-Sight path following of underactuated marine craft. In *Proceedings of the 6th IFAC Conference on Manoeuvring and Control of Marine Craft (MCMC)*, pages 224–249, Sept 2003.

[89] E. Borhaug, A. Pavlov, and K.Y. Pettersen. Integral LOS control for path following of underactuated marine surface vessels in the presence of constant ocean currents. In *Proceedings of the 47th IEEE Conference on Decision and Control (CDC)*, pages 4984–4991, Dec 2008.

[90] M. Breivik and T.I. Fossen. Guidance Laws for Autonomous Underwater Vehicles, 2009.

[91] M.S. Wiig, K.Y. Pettersen, and T.R. Krogstad. Uniform Semiglobal Exponential Stability of Integral Line of Sight Guidance Laws. In *Proceedings of the 10th IFAC Conference on Manoeuvring and Control of Marine Craft (MCMC)*, volume 48, pages 61–68, Aug 2015.

[92] M.S. Wiig, K.Y. Pettersen, and T.R. Krogstad. Integral Line-Of-Sight Guidance of Underwater Vehicles Without Neutral Buoyancy. volume 49, pages 590–597, Sept 2016.

[93] P. Encarnação, A. Pascoal, and M. Arcak. Path following for autonomous marine craft. In *Proceedings of the 5th IFAC Conference on Manoeuvring and Control of Marine Craft (MCMC)*, pages 117–122, Aug 2000.

[94] V. Bakaric, Z. Vukic, and R. Antonic. Improved basic planar algorithm of vehicle guidance through waypoints by the line of sight. In *First International Symposium on Control, Communications and Signal Processing (ISCCSP)*, pages 541–544, Mar 2004.

[95] G. Antonelli, F. Caccavale, S. Chiaverini, and G. Fusco. A novel adaptive control law for underwater vehicles. *IEEE Transactions on Control Systems Technology*, 11(2):221–232, Mar 2003.

[96] A. Aguiar and A. Pascoal. Modeling and control of an autonomous underwater shuttle for the transport of benthic laboratories. In *Proceedings of MTS/IEEE OCEANS*, volume 2, pages 888–895, Oct 1997.

[97] M.M. Cummings. Man versus Machine or Man + Machine? *IEEE Intelligent Systems*, 29(5):62–69, Sept 2014.

[98] M.L. Cummings and A.S. Clare. Holistic modelling for human-autonomous system interaction. *Theoretical Issues in Ergonomics Science*, 16(3), Mar 2015.

[99] A.J. Stimpson, J.C. Ryan, and M.L. Cummings. Assessing Pilot Workload in Single-Pilot Operations with Advanced Autonomy. In *Proceedings of the Human Factors and Ergonomics Society Annual Meeting*, pages 675–679, Sept.

[100] M. Boyer, M.L. Cummings, L.B. Spence, and E.T. Solovey. Investigating Mental Workload Changes in a Long Duration Supervisory Control Task. *Interacting with Computers*, 27(5), May 2015.

[101] J. Barrett. Side Effects of Virtual Environments: A Review of the Literature. Technical report, Defence Science and Technology Organization Canberra (Australia), Nov 2004.

[102] O. Merhi, E. Faugloire, M. Flanagan, and T.A. Stoffregen. Motion sickness, console video games, and head-mounted displays. *Human Factors*, 49(5), Oct 2007.

[103] M. Ludvigsen. *An ROV toolbox for optical and acoustical seabed investigations*. PhD thesis, Department of Marine Technology, Norwegian University of Science and Technology, Trondheim, Norway, 2010.

[104] S.M. Nornes, M. Ludvigsen, Ø. Ødegård, and A.J. Sørensen. Underwater Photogrammetric Mapping of an Intact Standing Steel Wreck with ROV. In *Proceedings of the 4th IFAC Workshop on Navigation, Guidance and Control of Underwater Vehicles (NGCUV)*, volume 48, pages 206 – 211, Apr 2015. IFAC-PapersOnLine.

[105] R. Haywood. Acquisition of a Micro Scale Photographic Survey Using an Autonomous Submersible. In *Proceedings of MTS/IEEE OCEANS*, pages 1423–1426, Sept 1986.

[106] F. Aguirre, J.M. Boucher, and J.J. Jacq. Underwater navigation by video sequence analysis. In *Proceedings of the 10th International Conference on Pattern Recognition*, volume 2, pages 537–539, June 1990.

[107] R.L. Marks, S.M. Rock, and M.J. Lee. Real-time video mosaicking of the ocean floor. In *Proceedings of the IEEE Symposium on Autonomous Underwater Vehicle Technology*, pages 21–27, July 1994.

[108] S.D. Fleischer. *Bounded-Error Vision-Based Navigation of Autonomous Underwater Vehicles*. PhD thesis, Stanford University, Stanford, CA 94305, 2000.

[109] R. Garcia, C. Xevi, and J. Battle. Detection of matchings in a sequence of underwater images through texture analysis. In *Proceedings of the IEEE International Conference on Image Processing (ICIP)*, volume 1, pages 361–364 vol.1, 2001.

[110] O. Pizarro and H. Singh. Toward large-area mosaicing for underwater scientific applications. *IEEE Journal of Oceanic Engineering*, 28(4):651–672, Oct 2003.

[111] H. Singh, J. Howland, and O. Pizarro. Advances in large-area photomosaicking underwater. *IEEE Journal of Oceanic Engineering*, 29(3):872–886, July 2004.

[112] H. Singh, C. Roman, O. Pizarro, and R. Eustice. *Advances in High Resolution Imaging from Underwater Vehicles*, pages 430–448. Springer Berlin Heidelberg, 2007.

[113] M. Ludvigsen, B. Sortland, G. Johnsen, and H. Singh. Applications of Geo-Referenced Underwater Photo Mosaics in Marine Biology and Archaeology. *Oceanography*, 20(4):140–149, Dec 2007.

[114] A.C. Kapoutsis, G.V. Salavasidis, S.A. Chatzichristofis, J. Braga, J. Pinto, J.B. Sousa, and E.B. Kosmatopoulos. The NOPTILUS project overview: A fully-autonomous navigation system of teams of AUVs for static/dynamic underwater map construction. In *Proceedings of the 4th IFAC Workshop on Navigation, Guidance and Control of Underwater Vehicles (NGCUV)*, volume 48, pages 231 – 237, Apr 2015. IFAC-PapersOnLine.

[115] P. Pencarelli. Improvement of Underwater Photomosaic Technique using ROV Navigation Data and Bathymetry Information . Master's thesis, Dipartimento di Ingegneria dell'Informazione, Universitá Politecnica delle Marche, Ancona, Italy, 2014.

[116] F. Celiberti. Vision-Aided Inertial Navigation for ROV based on Homography Filtering and Estimation. Master's thesis, Dipartimento di Ingegneria dell'Informazione, Universitá Politecnica delle Marche, Ancona, Italy, 2014.

[117] P.B. Mortensen, M.T. Hovland, and J.H. Fosså. Species diversity and spatial distribution of invertebrates on deep-water lophelia reefs in norway. In *Proceedings of the 10th International Coral Reef Symposium*, pages 1849–1868, 2006.

[118] J.M. Roberts, A.J. Wheeler, and A. Freiwald. Reefs of the deep: the biology and geology of cold-water coral ecosystems. *Science*, 2006.

[119] E.U. Acar, H. Choset, Y. Zhang, and M. Schervish. Path planning for robotic demining: Robust sensor-based coverage of unstructured environments and probabilistic methods. *The International Journal of Robotics Research*, 22(7 - 8):441 – 466, July 2003.

[120] P.B. Sujit, D.E. Lucani, and J.B. Sousa. Bridging Cooperative Sensing and Route Planning of Autonomous Vehicles. *IEEE Journal on Selected Areas in Communications*, 30(5):912–922, June 2012.

[121] J. Pinto, M. Faria, J. Fortuna, R. Martins, J.B. Sousa, N. Queiroz, F. Py, and K. Rajan. Chasing fish: Tracking and control in a autonomous multi-vehicle real-world experiment. In *Proceedings of MTS/IEEE OCEANS*, pages 1–6, Sept 2013.

[122] L. Paull, S. SaeediGharahbolagh, M. Seto, and H. Li. Sensor driven online coverage planning for autonomous underwater vehicles. In *Proceedings of the IEEE/RSJ International Conference on Intelligent Robots and Systems (IROS)*, pages 2875–2880, Oct 2012.

[123] L. Paull, S. Saeedi, M. Seto, and H. Li. Sensor-Driven Online Coverage Planning for Autonomous Underwater Vehicles. *IEEE/ASME Transactions on Mechatronics*, 18(6):1827–1838, Dec 2013.

[124] C. Cai and S. Ferrari. Information-Driven Sensor Path Planning by Approximate Cell Decomposition. *IEEE Transactions on Systems, Man, and Cybernetics, Part B: Cybernetics*, 39(3):672–689, June 2009.

[125] D.P. Watson and D.H. Scheidt. Autonomous systems. *Johns Hopkins APL Technical Digest*, 26(4), 2005.

[126] Z. Zeng, L. Liana, K. Sammut, F. He, Y. Tang, and A. Lammas. A survey on path planning for persistent autonomy of autonomous underwater vehicles. *Ocean Engineering*, 110(A):303–313, Dec 2015.

[127] S.M. LaValle. *Planning Algorithms*. Cambridge University Press, New York, NY, USA, 2006.

[128] A. Tsourdos, B. White, and M. Shanmugavel. *Cooperative Path Planning of Unmanned Aerial Vehicles*. Wiley, 2010.

[129] A. Caiti. *Motion Planning for Marine Control Systems*. Springer London, London, 2014.

[130] G. Antonelli, S. Chiaverini, R. Finotello, and R. Schiavon. Real-time path planning and obstacle avoidance for rais: an autonomous underwater vehicle. *IEEE Journal of Oceanic Engineering*, 26(2):216–227, Apr 2001.

[131] L. Chrpa, J. Pinto, M. A. Ribeiro, F. Py, J.B Sousa, and K. Rajan. On mixed-initiative planning and control for autonomous underwater vehicles. In *Proceedings of the IEEE/RSJ International Conference on Intelligent Robots and Systems (IROS)*, pages 1685–1690, Sept 2015.

[132] M. Kothari, J. Pinto, V.S. Prabhu, P. Ribeiro, J.B. Sousa, and P.B. Sujit. Robust mission planning for underwater applications: Issues and challenges. In *Proceedings of the 3rd IFAC Workshop on Navigation, Guidance and Control of Underwater Vehicles (NGCUV)*, volume 45, pages 223 – 229, Apr 2012. IFAC-PapersOnLine.

[133] S.M. Lavalle. Rapidly-Exploring Random Trees: A New Tool for Path Planning. Technical report, Computer Science Dept., Iowa State University, Nov 1998.

[134] P. Bhattacharya and M.L. Gavrilova. Voronoi diagram in optimal path planning. In *Proceedings of the 4th IEEE International Symposium on Voronoi Diagrams in Science and Engineering (ISVD)*, pages 38–47, July 2007.

[135] T. Lozano-Pérez and M.A. Wesley. An algorithm for planning collision-free paths among polyhedral obstacles. *Communications of the ACM (CAMC)*, 22(10):560–570, Oct 1979.

[136] O. Khatib. Real-time obstacle avoidance for manipulators and mobile robots. In *Proceedings of the IEEE International Conference on Robotics and Automation (ICRA)*, volume 2, pages 500–505, Mar 1985.

[137] S.M. Lee, K.Y. Kwon, and J. Joh. A fuzzy logic for autonomous navigation of marine vehicles satisfying COLREG guidelines. *International Journal of Control Automation and Systems*, 2(2):171–181, June 2004.

[138] A. Elfes. Sonar-based real-world mapping and navigation. *IEEE Journal on Robotics and Automation*, 3(3):249–265, June 1987.

[139] P.E. Hart, N.J. Nilsson, and B. Raphael. A Formal Basis for the Heuristic Determination of Minimum Cost Paths. *IEEE Transactions on Systems Science and Cybernetics*, 4(2):100–107, July 1968.

[140] D. Dolgov, S. Thrun, Montemerlo M., and Diebel J. Path Planning for Autonomous Vehicles in Unknown Semi-structured Environments. *The International Journal of Robotics*, 29(5):485–501, Jan 2010.

[141] J. Larson, M. Bruch, and J. Ebken. Autonomous navigation and obstacle avoidance for unmanned surface vehicles. *Society of Photo-Optical Instrumentation Engineers (SPIE) Conference Series*, 6230:623007, May 2006.

[142] J. Larson, M. Bruch, J. Ebken, J. Rogers, and R. Webster. Advances in autonomous obstacle avoidance for unmanned surface vehicles. 2007.

[143] W. Naeem, G.W. Irwin, and A. Yang. COLREGs-based collision avoidance strategies for unmanned surface vehicles. *Special Issue on Intelligent Mechatronics (LSMS2010 & ICSEE2010)*, 22(6):669–678, Sept 2012.

[144] J.A. Sethian. Fast Marching Methods. *Society for Industrial and Applied Mathematics (SIAM) Review*, 41(2):199–235, 1999.

[145] M. Falcone and R. Ferretti. *Semi-Lagrangian Approximation Schemes for Linear and Hamilton-Jacobi Equations*. Society for Industrial and Applied Mathematics, Philadelphia, PA, 2013.

[146] J.N. Tsitsiklis. Efficient algorithms for globally optimal trajectories. *IEEE Transactions on Automatic Control*, 40(9):1528–1538, Sept 1995.

[147] S. Garrido, L. Moreno, M. Abderrahim, and F. Martin. Path Planning for Mobile Robot Navigation using Voronoi Diagram and Fast Marching. In *Proceedings of the IEEE/RSJ International Conference on Intelligent Robots and Systems (IROS)*, pages 2376–2381, Oct 2006.

[148] Ryo Takei and Richard Tsai. Optimal Trajectories of Curvature Constrained Motion in the Hamilton–Jacobi Formulation. *Journal of Scientific Computing*, 54(2):622–644, 2013.

[149] D. Fox, W. Burgard, and S. Thrun. The dynamic window approach to collision avoidance. *IEEE Robotics Automation Magazine*, 4(1):23–33, Mar 1997.

[150] J. Borenstein and Y. Koren. The vector field histogram-fast obstacle avoidance for mobile robots. *IEEE Transactions on Robotics and Automation*, 7(3):278–288, June 1991.

[151] P. Fiorini and Z. Shiller. Motion planning in dynamic environments using the relative velocity paradigm. In *Proceedings of the Proceedings of the IEEE International Conference on Robotics and Automation (ICRA)*, volume 1, pages 560–565, May 1993.

[152] J. van den Berg, D. Ferguson, and J. Kuffner. Anytime Path Planning and Replanning in Dynamic Environments. In *Proceedings of the Proceedings of the IEEE International Conference on Robotics and Automation (ICRA)*, pages 2366 – 2371, May 2006.

[153] F. Aurenhammer. Voronoi diagrams - a survey of a fundamental geometric data structure. *ACM Computing Surveys*, 3:345–404, 1991.

[154] G. Antonelli, S. Chiaverini, and A. Marino. A coordination strategy for multirobot sampling of dynamic fields. In *Proceedings of the Proceedings of the IEEE International Conference on Robotics and Automation (ICRA)*, pages 1113–1118, May 2012.

[155] C.M. Gold. The use of the dynamic Voronoi data structure in autonomous marine navigation. pages 217–220, 1998.

[156] S.A. Bortoff. Path planning for uavs. In *Proceedings of the American Control Conference (ACC)*, volume 1, pages 364–368, Sept 2000.

[157] P. Chandler, S. Rasmussen, and M. Pachter. Uav cooperative path planning. In American Institute of Aeronautics and Astronautics, editors, *Proceedings of the AIAA Guidance, Navigation, and Control Conference and Exhibit*, Aug 2000.

[158] J.S. Bellingham, M. Tillerson, M. Alighanbari, and J.P. How. Cooperative path planning for multiple UAVs in dynamic and uncertain environments. In *Proceedings of the 41st IEEE Conference on Decision and Control (CDC)*, volume 3, pages 2816–2822, Dec 2002.

[159] I.R. Goralski and C.M. Gold. Maintaining the Spatial Relationships of Marine Vessels Using the Kinetic Voronoi Diagram. In *Proceedings of the 4th IEEE International Symposium on Voronoi Diagrams in Science and Engineering (ISVD)*, pages 84–90, July 2007.

[160] C.B. Barber, D.P. Dobkin, and H. Huhdanpaa. The Quickhull Algorithm for Convex Hulls. *ACM Transactions on Mathematical Software*, 22(4):469–483, 1996.

[161] A.M. Lekkas. *Guidance and Path-Planning Systems for Autonomous Vehicles*. PhD thesis, Department of Marine Technology, Norwegian University of Science and Technology, Trondheim, Norway, 2014.

[162] A.R. Dahl. Path Planning and Guidance for Marine Surface Vessels. Master's thesis, Department of Engineering Cybernetics, Norwegian University of Science and Technology, Trondheim, Norway, 2013.

[163] L.E. Dubins. On Curves of Minimal Length with a Constraint on Average Curvature, and with Prescribed Initial and Terminal Positions and Tangents. *American Journal of Mathematics*, 79(3):497–516, 1957.

[164] H.J. Sussmann. Shortest 3-dimensional paths with a prescribed curvature bound. In *Proceedings of the 34th IEEE Conference on Decision and Control (CDC)*, volume 4, pages 3306–3312 vol.4, Dec 1995.

[165] G. Ambrosino, M. Ariola, U. Ciniglio, F. Corraro, A. Pironti, and M. Virgilio. Algorithms for 3D UAV Path Generation and Tracking. In *Proceedings of the 45th IEEE Conference on Decision and Control (CDC)*, pages 5275–5280, Dec 2006.

[166] K. Yang and S. Sukkarieh. 3D smooth path planning for a UAV in cluttered natural environments. In *Proceedings of the IEEE/RSJ International Conference on Intelligent Robots and Systems (IROS)*, pages 794–800, Sept 2008.

[167] G. Ambrosino, M. Ariola, U. Ciniglio, F. Corraro, E. De Lellis, and A. Pironti. Path Generation and Tracking in 3-D for UAVs. *IEEE Transactions on Control Systems Technology*, 17(4):980–988, July 2009.

[168] S. Hota and D. Ghose. Optimal geometrical path in 3d with curvature constraint. In *Proceedings of the IEEE/RSJ International Conference on Intelligent Robots and Systems (IROS)*, pages 113–118, Oct 2010.

[169] Y. Lin and S. Saripalli. Path planning using 3D Dubins Curve for Unmanned Aerial Vehicles. In *Proceedings of the International Conference on Unmanned Aircraft Systems (ICUAS)*, pages 296–304, May 2014.

[170] J.Y. Yen. An algorithm for finding shortest routes from all source nodes to a given destination in general networks. *Quarterly of Applied Mathematics*, 27:526–530, 1970.

[171] E.W. Dijkstra. A note on two problems in connexion with graphs. *Numerische Mathematik*, 1:269–271, 1959.

[172] A.M. Lekkas and T.I. Fossen. Trajectory tracking and ocean current estimation for marine underactuated vehicles. In *IEEE Conference on Control Applications (CCA)*, pages 905–910, Oct 2014.

[173] D. Lerro and Y. Bar-Shalom. Tracking with debiased consistent converted measurements versus EKF. *IEEE Transactions on Aerospace and Electronic Systems*, 29(3):1015–1022, July 1993.

[174] I. Karoui, I. Quidu, and M. Legris. Automatic Sea-Surface Obstacle Detection and Tracking in Forward-Looking Sonar Image Sequences. *IEEE Transactions on Geoscience and Remote Sensing*, 53(8):4661–4669, Aug 2015.

[175] International Maritime Organization (IMO). The International Regulations for Preventing Collisions at Sea. https://goo.gl/7mPxS7, 1977. Accessed: 30-09-2016.

[176] US Department of Transportation and Fedreal Aviation Administration. Introduction to TCAS II, Version 7.1. http://goo.gl/nnkmQn, 2011. Accessed: 30-09-2016.

[177] J.K. Kuchar and A.C. Drumm. The Traffic Alert and Collision Avoidance System (TCAS). *MIT Lincoln Laboratory Journal*, 16(2), 2007.

[178] AUR-Lab. Strategy for NTNU Applied Underwater Robotics Laboratory (AUR-Lab) 2015. Technical report, 2015.

[179] J.B. Sousa. Concepts and tools for coordination and control of networked ocean-going vehicles. In *Proceedings of the IEEE/OES Autonomous Underwater Vehicles*, pages 1–6, Sept 2010.

[180] J.B. Sousa, J. Pereira, J. Alves, M. Galocha, B. Pereira, C. Lourenço, and M. Portuguesa. Experiments in multi-vehicle operations: The Rapid Environmental Picture Atlantic exercise 2014. In *Proceedings of MTS/IEEE OCEANS*, pages 1–7, May 2015.

[181] J.B. Sousa, K. Rajan, J. Pereira, M. Incze, J. Pinto, J. Alves, P. Lourenco, K. Pelekanakis, M. Galocha, J. Fontes, A. Munafo, and R. Petroccia. Rapid Environmental Picture Atlantic Exercise 2015: a Field Report. In *Proceedings of MTS/IEEE OCEANS*, Sept 2016.

[182] J. Rio S. Martinez E. Delory T. O'Reilly L. Frommhold J. Pearlman, S. Jirka. Oceans of Tomorrow Sensor Interoperability for In-Situ Ocean Monitoring. In *Proceedings of MTS/IEEE OCEANS*, Sept 2016.

[183] J. Pearlman, A. Wiliams, S. Simmons, F. Chavez, and B. Houtman. A research coordination network for ocean observations. In *Proceedings of MTS/IEEE OCEANS*, pages 1–4, May 2015.

[184] D.M. Toma, J. del Rio, S. Jirka, E. Delory, J. Pearlman, and C. Waldmann. NeXOS smart electronic interface for sensor interoperability. In *Proceedings of MTS/IEEE OCEANS*, pages 1–5, May 2015.

[185] BluEye AS. BluEye ROV. http://www.blueye.no/, 2016. Accessed: 30-09-2016.

[186] OpenROV. OpenROV v.2.8 kit. http://goo.gl/zPTWCX, 2016. Accessed: 30-09-2016.

[187] J. Follestad. Design of an ROV for the consumer market. Master's thesis, Department of Marine Technology, Norwegian University of Science and Technology, Trondheim, Norway, 2015.

[188] F. Sandved. Remote control and automatic path-following for C/S Enterprise I and ROV Neptunus. Master's thesis, Department of Marine Technology, Norwegian University of Science and Technology, Trondheim, Norway, 2015.

[189] E. Valle. Marine Telepresence System. Master's thesis, Department of Marine Technology, Norwegian University of Science and Technology, Trondheim, Norway, 2015.

[190] G. Johnsen. Underwater hyperspectral imaging, 2013. US Patent 8,502,974.

[191] F. Skoglund. Ormen Lange Shipwreck: Environmental Monitoring Project - Final Report. Technical report, 2014.

Part II

Articles

Article A

Development of Dynamic Position and Tracking System for the ROV Minerva

A.J. Sørensen, F. Dukan, M. Ludvigsen, D.A. Fernandes and **M. Candeloro**

This article is a book chapter of
G.N. Roberts, R. Sutton editors *Further Advances in Unmanned Marine Vehicles*,
Chapter 6, pages 113–128, Institution of Engineering and Technology (IET), 2012.

DEVELOPMENT OF DYNAMIC POSITIONING AND TRACKING SYSTEM FOR THE ROV MINERVA

Asgeir J. Sørensen, Fredrik Dukan, Martin Ludvigsen,
Daniel de Almeida Fernandes and Mauro Candeloro

Norwegian University of Science and Technology (NTNU)
Department of Marine Technology and Centre for Ships and Ocean Structures (CeSOS)
Trondheim, NORWAY
Email: Asgeir.Sorensen@ntnu.no

1. Introduction

The Applied Underwater Robotics Laboratory (AUR-Lab) was established by the Norwegian University of Technology and Science (NTNU) late 2009. AUR-Lab facilitates a new arena for multi- and interdisciplinary research and education in marine underwater robotics, marine biology, chemistry and archaeology addressing various science areas in the ocean space such as environmental and climate monitoring, marine biology, archaeology, exploration and exploitation of minerals, gas and oil. The AUR-Lab infrastructure enables professors, post doctors, researchers, PhD candidates and MSc students in technology, biology and archaeology to develop new knowledge, solutions and methods conducting marine operations, mapping, monitoring and research in the ocean.

During 2010 and 2011 a group of MSc students, PhD candidates and NTNU researchers have developed a dynamic positioning (DP) and tracking system for a remotely operated vehicle (ROV). The DP system is in particular designed for research and educational purposes making it easy to re-design and test control strategies, sensor configurations and tool packages including manipulators.

In this paper, which is an extension of Dukan et al. (2011), experience from this development and scientific results verified experimentally on a small size ROV called Minerva will be presented. Minerva is a SUB-fighter 7500 ROV operated from the NTNU Research Vessel (RV) Gunnerus, see Figure 1. Minerva was built for NTNU in 2003 by Sperre AS, Norway.

Figure 1. RV Gunnerus and ROV Minerva.

ROVs are used in a variety of subsea work tasks from small hand deployable ROVs to large work class ROVs for heavy intervention work at subsea offshore installations. Common for all types is that many applications instead of being manually controlled could have been performed with higher accuracy and efficiency with an automatic positioning control system. Today, most industrial ROVs are equipped with automatic heading and depth control only (Christ and Wernli, 2007). A pilot controls the thrust from a command console with joysticks. However, commercial DP systems for unmanned underwater vehicles are introduced to the market as presented by Mair and Tena (2011). In Smallwood and Whitcomb (2004) research results using model-based controller design for DP and trajectory tracking of underwater robotic vehicles are presented. In this paper and in Fossen (2011) references to earlier work on DP for underwater vehicles can be found. As proposed in these works control modes such as station keeping and tracking should be automated. Then the pilot can focus on monitoring and planning of operations that demand human intervention or decision making similar as for surface vessels. The degree of pilot interaction can depend on the various user modes. Position and orientation feedback is needed for closed-loop DP control system. For most practical subsea navigation tasks this means that an acoustic positioning reference system is needed. Slow update rates and inaccuracies in position measurements due to varying conditions in the water column motivate the use of a velocity sensor as well as observers for state estimation. In order to carry the needed instrument packages and tools such as transponder, Doppler velocity log (DVL), compass, manipulators etc., the ROV must have sufficient payload capacity. Minerva, as seen in Figure 1, is a small size ROV, but large enough to carry the needed sensor suite for the DP control system. Minerva is the test bed for the development of the control system presented in this paper.

This paper is organized as follows. In Section 2 the ROV Minerva specifications including sensors, instruments, thrusters and navigation system are presented. Section 3 gives an overview of the mathematical models used for controller design and hardware-in-the-loop (HIL) simulation testing. Section 4 is about control system architecture and control modules. Section 5 contains results from full scale testing. The conclusions are given in Section 6.

2. ROV Minerva Specifications

Minerva is powered from and communicates with a surface vessel through a 600 m umbilical. All systems needed for operation such as power supply, navigation computers and monitors are fitted inside a 15 foot container. Minerva was delivered with a joystick command console with control functions as auto depth and heading. It can be equipped with tool packages such as additional lights, water sampler, extra manipulator arm and other special purpose tools. The thruster configuration is shown in Figure 2.

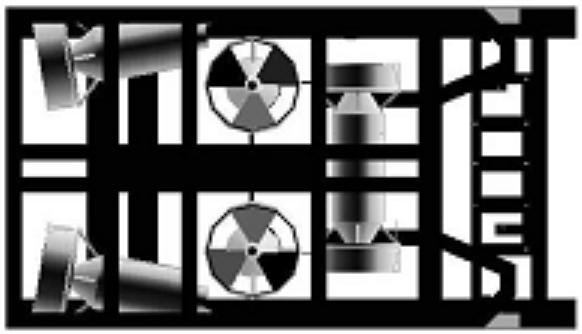

Figure 2. Minerva thruster configurations.

The starboard and port thruster are oriented towards the center line. The side thruster has two propellers, one in each end, but has the same power rating as the other thrusters. All thrusters have fixed pitch propellers. Specifications of the thrust ratings, sensors and other instruments are given in Table 1.

Table 1 ROV Minerva particulars and ratings

Dimension	L x W x H: 144 x 82 x 81 cm
Weight in air	485 kg
Payload	Approx. 20 kg
Max depth	700 m
Horizontal thrusters (2)	2 x 2000 W Bollard pull forward: 2 x 239 N Bollard pull backward: 2 x110 N
Vertical thrusters (2)	2 x 2000 W Bollard pull down: 2 x 195 N
Lateral thruster with dual propellers (1)	1 x 2000 W Bollard pull: 1 x 195 N
Speed ratings	Horizontal: 2.0 knots Vertical: 1.2 knots Lateral: 1.3 knots Turn rate: 60 deg/s
Sonar	Kongsberg Simrad MS 1000 (675 kHz) Beam Width: 1.4 deg x 22 deg Fan (nominal) Range: 0.5-100 m Scan angle: 360 deg continuous
Manipulator	5-function hydraulic arm (HLK-HD5) 1 function electric
Sensors	Pressure gage: 100 bar Flux gate compass CRS03 silicon rate sensor Teledyne RDI Workhorse Doppler Velocity Log (DVL) Kongsberg Seatex MRU6 Leakage detector
Cameras	2 x PAL color zoom 460 TV lines, 0.1 lux 1 x PAL color zoom 460 TV lines, 1 lux 1x CCD zoom high resolution PAL 530 TV lines, 15 lux

Kongsberg High Precision Acoustic Positioning and underwater navigation system (HiPAP) 500 is installed on RV Gunnerus. HiPAP is used to find the position of the ROV relative to the transducer on the surface vessel. NaviPac is an integrated navigation software by Eiva. It

calculates the North (n) and East (e) position of the ROV in UTM coordinates based on input from the HiPAP and Gunnerus's GPS and heave-roll-pitch sensor (MRU).

3. Mathematical Models

The dynamics of the underwater vehicle may be formulated in two complexity levels (Sørensen, 2011), namely a process plant model and a control plant model. The process plant model, which simulates the real physics of plant dynamics as close as possible including process disturbance, sensor outputs and control inputs, is for numerical analysis of the stability and performance of the closed-loop system. The control plant model, which is simplified from process plant model, is used for controller design and analytical stability analysis (e.g. in the sense of Lyapunov). In this section, the process plant model including the kinematics and dynamics is discussed.

Two reference frames are used in this work:

- The Earth fixed frame, called the North-East-Down frame (NED) because the x-axis points North, the y-axis points East and the z-axis points down, and the frame will be considered inertial. The position vector $\boldsymbol{\eta}$ is given relative to the NED-frame.

- The body fixed frame (body), where the x-axis points forwards along the vehicle, the y-axis points to starboard and the z-axis points down. The body fixed frame is thus always moving with the vessel. The linear and angular velocity vector $\mathbf{v}$ is given in the body frame.

The relationship between the Earth-fixed position and orientation of the underwater vehicle and its body-fixed velocities are given by the following kinematic transformation

$$\dot{\boldsymbol{\eta}} = \begin{bmatrix} \dot{\boldsymbol{\eta}}_1 \\ \dot{\boldsymbol{\eta}}_2 \end{bmatrix} = \begin{bmatrix} \mathbf{J}_1(\boldsymbol{\eta}_2) & \mathbf{0}_{3\times 3} \\ \mathbf{0}_{3\times 3} & \mathbf{J}_2(\boldsymbol{\eta}_2) \end{bmatrix} \begin{bmatrix} \mathbf{v}_1 \\ \mathbf{v}_2 \end{bmatrix} = \mathbf{J}(\boldsymbol{\eta}_2)\mathbf{v}. \tag{1}$$

The vectors defining the Earth-fixed vessel position $\boldsymbol{\eta}_1$ and orientation $\boldsymbol{\eta}_2$ using Euler angles, and the body-fixed translation $\mathbf{v}_1$ and rotation $\mathbf{v}_2$ velocities are given by

$$\begin{aligned} &\boldsymbol{\eta}_1 = \begin{bmatrix} x & y & z \end{bmatrix}^{\mathrm{T}}, \boldsymbol{\eta}_2 = \begin{bmatrix} \phi & \theta & \psi \end{bmatrix}^{\mathrm{T}}, \\ &\mathbf{v}_1 = \begin{bmatrix} u & v & w \end{bmatrix}^{\mathrm{T}}, \mathbf{v}_2 = \begin{bmatrix} p & q & r \end{bmatrix}^{\mathrm{T}}. \end{aligned} \tag{2}$$

The rotation matrices $\mathbf{J}_1(\boldsymbol{\eta}_2) \in \mathbb{R}^{3\times 3}$ and $\mathbf{J}_2(\boldsymbol{\eta}_2) \in \mathbb{R}^{3\times 3}$ are defined as in Fossen (2011).

For an underwater vehicle operating deeply submerged a simplification can be made by considering only a low-frequency (LF) model accounting predominantly for motions due to currents loads. The equations of motion for the nonlinear LF model of the underwater vehicle may be written as

$$\begin{aligned} &\dot{\boldsymbol{\eta}} = \mathbf{J}(\boldsymbol{\eta}_2)\mathbf{v}, \\ &\mathbf{M}\dot{\mathbf{v}} = -\mathbf{C}_{\mathbf{RB}}(\mathbf{v})\mathbf{v} - \mathbf{C}_{\mathbf{A}}(\mathbf{v}_{\mathbf{r}})\mathbf{v}_{\mathbf{r}} - \mathbf{D}(\mathbf{v}_{\mathbf{r}}) - \mathbf{g}(\boldsymbol{\eta}) + \boldsymbol{\tau}_{um} + \boldsymbol{\tau}_{thr}. \end{aligned} \tag{3}$$

where $\mathbf{M} \in ¡^{6\times6}$ is the system inertia matrix including added mass; $\mathbf{C_{RB}}(\nu) \in \mathbb{R}^{6\times6}$ and $\mathbf{C_A}(\nu_\mathbf{r}) \in \mathbb{R}^{6\times6}$ are the skew-symmetric Coriolis and centripetal matrices of the rigid body and the added mass; $\mathbf{g(\eta)} \in \mathbb{R}^6$ is the generalized restoring vector caused by the buoyancy and gravitation; $\boldsymbol{\tau}_{thr} \in \mathbb{R}^6$ is the control vector consisting of forces and moments produced by the thruster and fin system; $\boldsymbol{\tau}_{um} \in \mathbb{R}^6$ are the forces and moments from the umbilical (if any) acting on the underwater vehicle. Normally, the umbilical is considered for ROV only powering the vehicle in addition providing high bandwidth communication. The umbilical connecting the ROV and the mother vessel will be affected by motions of the surface vessel, motions of the ROV, current varying along the length of the cable and the amount of cable given out relative to the ROV depth. The forces from the umbilical acting on the ROV are generally of considerable size in strong currents. However, operating the ROV in moderate current and in DP mode with small velocities the effect of umbilical forces and moments can to some extend also be compensated by proper bias modeling in the observer. The umbilical on the ROV Minerva is hinged to the top of the ROV, between the vertical thrusters. It will not give any moment in yaw, as it has very little or no arm in this direction. Analysis of dynamic models of the umbilical loadings is subject for further research.

The damping vector may be divided into linear and nonlinear terms

$$\mathbf{D}(\mathbf{v}_r) = \mathbf{D}_L\mathbf{v} + \mathbf{d}_{NL}(\mathbf{v}_r, \gamma_r), \tag{4}$$

where γ_r is the relative drag angle, and $\mathbf{v}_r$ is the relative velocity vector between the current and the underwater vehicle, according to

$$\mathbf{v}_r = \begin{bmatrix} u-u_c & v-v_c & w & p & q & r \end{bmatrix}^{\mathrm{T}}, \tag{5}$$

where u_c and v_c are the x- and y- components of the current vector. The nonlinear damping is assumed to be caused by turbulent skin friction and viscous eddy-making, also denoted as vortex shedding. The strictly positive linear damping matrix $\mathbf{D}_L \in ¡^{6\times6}$ is caused by linear laminar skin friction. Notice that for increasing velocity (typical > 0.1 m/s), the linear skin friction will vanish. The flow becomes turbulent, and will be included in the nonlinear damping term. For velocities of vessel close to zero, linear damping becomes more significant than the nonlinear damping. Details of the used models including thruster models can be found in Sørensen (2011) and Kirkeby (2010).

4. Control System Architecture and Platform

4.1 Hardware and Software Platform

The selection of real time hardware (HW) and software (SW) platform is mainly motivated from flexibility, scalability and capacity for rapid control prototyping. The National Instruments (NI) CompactRIO (cRIO) programmed with Labview is used for implementation and development of the DP control system. The graphical programming language makes it quick to implement the code and deploy it on the cRIO for hardware-in-the-loop (HIL) testing

or full scale experiments with the ROV Minerva. cRIO is short for compact reconfigurable inputs and outputs (I/O). It is a programmable automation controller (PAC) which is made up by an industrial real-time processor, field programmable gate array (FPGA) and chassis with slots for hot-swappable industrial I/O modules. The cRIO used in the DP system is a NI-9074 with 400MHz industrial real-time processor and 2 million (2M) gate FPGA. A NI-9870 C-module with 4 serial ports is used for serial communication with the ROV and navigation system NaviPac. Labview is the graphical programming language that is used to program the DP control system. It is used for all programming task from the signal I/O to controller design to the graphical user interface of the DP system. The same programming environment is used whether the code is to be deployed on the host computer, real-time processor or the FPGA. A benefit with Labview in the development stage is that it is easy to modify code. Even when testing at sea with the Minerva ROV, software running on the computer or the real-time processor can be modified or new features could be added in matter of minutes. Modification of the FPGA takes longer to compile.

4.2 Signal Flow

Available outputs to the DP control system are currently 8 measurements (d, a, ψ, r, n, e, u, v) which are depth - d, altitude - a, heading - ψ, yaw rate - r, North position - n, East position - e, surge velocity - u and sway velocity - v, respectively. An overview of the main components and signals used in the DP system are seen in Figure 3.

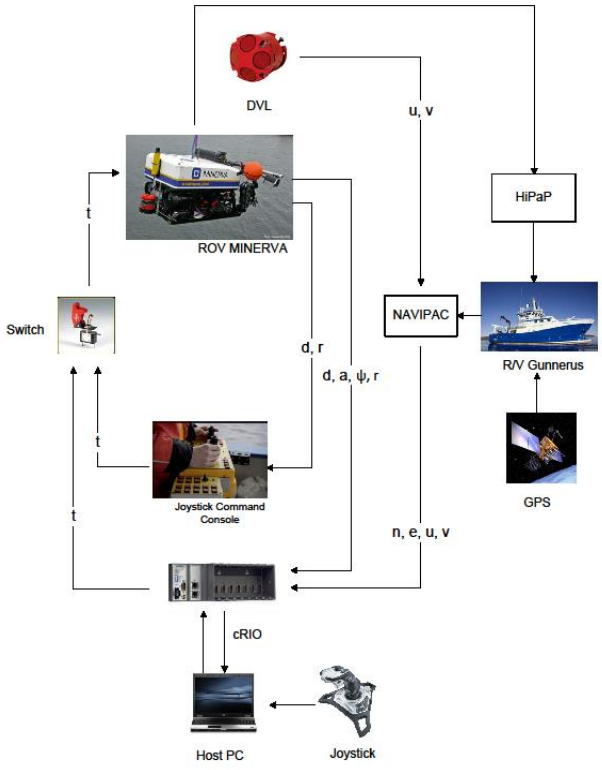

Figure 3. Overview of signal flow.

The DVL measures u and v which are the surge and sway velocity relative to the sea floor or water depending on the operating mode. The thrust vector - **t** with desired rpm of each thruster is sent from the manual command console or from the DP control system implemented on the cRIO depending on the switch position set by the pilot.

4.3 Control System Modules

The DP control system is made up by modules for *signal processing*, *guidance*, *observer* for filtering and state estimation, *controller*, *supervisor and adaption*, and *thrust allocation* as seen in Figure 4. The DP control system is interfaced to a navigation system and local thruster controllers. A graphical user interface (GUI) provides the communication and interaction with the operator.

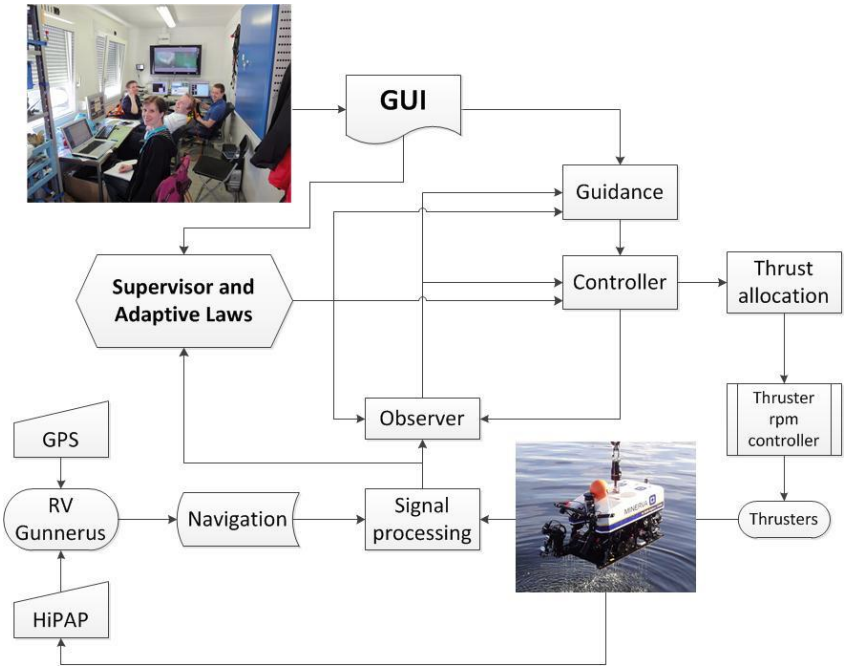

Figure 4. DP control architecture.

The output is the desired rpm for each thruster. Thruster speed control is done on an onboard processor and is not covered in this paper. Minerva is by itself stable in roll and pitch and the actuators can only cause small changes in roll and pitch angles. Therefore the working space for the ROV is reduced to the 4 degrees of freedom (4DOF) surge, sway, heave and yaw.

4.3.1 Signal Processing

The signal processing consists of two main parts, signal input and output (I/O) and signal detection. Signal I/O is the process of gathering signals from all sensors and pass them to the control system which runs at a fixed sample rate. Signal I/O is done on the FPGA where signals from the sensors and input from NaviPac are stored in a FIFO (first-in-first-out) array. When the DP control system starts a new loop, the latest available measurements are passed

for signal detection which is the first step in a control loop cycle. This makes it possible to run the control system at a specified sample rate regardless of the measurement update frequency.

All signals that enter the control system are tested. The signals must be approved as a healthy measurement before it is passed to the observer. The simplest form for signal detection implemented so far, is the bound check and velocity check. Valid bounds are given for all signals. If a signal is out of bounds, it is discarded. A max and min velocity is given for all degrees of freedom. If the next position measurement is such that the velocity must have exceeded the specified maximum, it is discarded. When a signal is discarded, a message is sent to the observer that says no measurement is available. Other additive and multiplicative signal detection methods have also been tested on the ROV Minerva. An interquartile test with dynamical bounds was also tested in station keeping. A cumulative sum (CUSUM) method was also tested (Standardi, 2011). We are currently working on improved methods for signal detection where these methods are subject for further research. The output of the signal detection block is a Boolean message vector telling which signals that passed the signal detection tests and the measurement vector $\mathbf{y} \in ¡^{7}$

$$\mathbf{y} = [x, y, z, \psi, u, v, r]^{T}. \tag{6}$$

In addition the altitude *a* is also measured, but not included in the measurement vector used in the observer.

4.3.2 Observer

Motivated by the process plant model in (3) and disregarding roll and pitch, the following nonlinear control plant model is proposed

$$\begin{aligned}
&\dot{\boldsymbol{\eta}} = \mathbf{J}(\psi)\boldsymbol{\nu}, \\
&\mathbf{M}\dot{\boldsymbol{\nu}} = -\mathbf{C}_{\mathbf{RB}}(\boldsymbol{\nu})\boldsymbol{\nu} - \mathbf{C}_{\mathbf{A}}(\boldsymbol{\nu}_{\mathbf{r}})\boldsymbol{\nu}_{\mathbf{r}} - \mathbf{D}_{\mathbf{NL}}(\boldsymbol{\nu}_{\mathbf{r}})\boldsymbol{\nu}_{\mathbf{r}} - \mathbf{D}_{\mathbf{L}}\boldsymbol{\nu} - \mathbf{g}(\boldsymbol{\eta}) + \mathbf{J}^{T}(\psi)\mathbf{b} + \boldsymbol{\tau} + \mathbf{w}_{m}, \\
&\dot{\mathbf{b}} = -\mathbf{T}_{\mathbf{b}}\mathbf{b} + \mathbf{w}_{b}.
\end{aligned} \tag{7}$$

All matrices and vectors are reduced according to the working space consisting of surge, sway, heave and yaw. $\boldsymbol{\tau} \in \mathbb{R}^{4\times 4}$ is the controller output vector. The bias term $\mathbf{b} \in \mathbb{R}^{4}$ is modeled as a Markov processes with positive semi-define diagonal matrix $\mathbf{T}_{b} \in \mathbb{R}^{4\times 4}$ of time constants and will include slowly-varying dynamics in addition to unmodeled dynamics. $\mathbf{w}_{b}$ and $\mathbf{w}_{b} \in \mathbb{R}^{4}$ are bounded disturbance vectors assumed to be zero mean Gaussian white noise processes. Eq. (7) may be written in state space form according to

$$\begin{aligned}
&\dot{\mathbf{x}} = \mathbf{f}(\mathbf{x}) + \mathbf{B}\mathbf{u} + \mathbf{E}\mathbf{w}, \\
&\mathbf{y} = \mathbf{H}\mathbf{x} + \mathbf{v},
\end{aligned} \tag{8}$$

where $\mathbf{x} = [\boldsymbol{\eta}, \boldsymbol{\nu}, \mathbf{b}]^{T} \in \mathbb{R}^{12}$, $\mathbf{u} = \boldsymbol{\tau}$ and $\mathbf{w} = [\mathbf{0}, \mathbf{w}_{m}, \mathbf{w}_{b}]^{T}$. $\mathbf{v} \in \mathbb{R}^{7}$ is the sensor noise vector assumed to be white noise, $\mathbf{H} \in \mathbb{R}^{7\times 12}$ will depend on accepted measurements from the signal processing module. The nonlinear function $\mathbf{f(x)}$ is given by

$$\mathbf{f}(\mathbf{x}) = \begin{bmatrix} \mathbf{J}(\psi)\mathbf{v} \\ \mathbf{M}^{-1}(-\mathbf{C}_{\mathbf{RB}}(\mathbf{v})\mathbf{v} - \mathbf{C}_{\mathbf{A}}(\mathbf{v}_{\mathbf{r}})\mathbf{v}_{\mathbf{r}} - \mathbf{D}_{\mathbf{NL}}(\mathbf{v}_{\mathbf{r}})\mathbf{v}_{\mathbf{r}} - \mathbf{D}_{\mathbf{L}}\mathbf{v} - \mathbf{g}(\boldsymbol{\eta}) + \mathbf{J}^{T}(\psi)\mathbf{b}) \\ -\mathbf{T}_{\mathbf{b}}\mathbf{b} \end{bmatrix}. \quad (9)$$

The dynamics of the ROV are highly nonlinear and coupled. This should be reflected in the observer as well in order to improve the state estimation.

An extended Kalman filter that takes into account nonlinear kinematics, damping, Coriolis and coupling forces are proposed. By copying the control plant model in (8), the following discrete-time (with h as the sampling period) observer with corrector and predictor is proposed

$$\begin{aligned} \hat{\mathbf{x}}(k) &= \bar{\mathbf{x}}(k) + \mathbf{K}(k)[\mathbf{y}(k) - \mathbf{H}(k)\bar{\mathbf{x}}(k)], \\ \bar{\mathbf{x}}(k+1) &= \hat{\mathbf{x}}(k) + h\mathbf{f}(\hat{\mathbf{x}}(k)) + h\mathbf{B}\mathbf{u}(k). \end{aligned} \quad (10)$$

The Kalman filter gain matrix $\mathbf{K} \in ¡^{12\times 7}$ is found to be

$$\begin{aligned} \mathbf{K}(k) &= \bar{\mathbf{P}}(k)\mathbf{H}(k)^{T}[\mathbf{H}(k)\bar{\mathbf{P}}(k)\mathbf{H}(k)^{T} + \mathbf{R}(k)]^{-1}, \\ \hat{\mathbf{P}}(k) &= [\mathbf{I} - \mathbf{K}(k)\mathbf{H}(k)]\bar{\mathbf{P}}(k)[\mathbf{I} - \mathbf{K}(k)\mathbf{H}(k)]^{T} + \mathbf{K}(k)\mathbf{R}(k)\mathbf{K}(k)^{T}, \\ \bar{\mathbf{P}}(k+1) &= \boldsymbol{\Phi}(k)\hat{\mathbf{P}}(k)\boldsymbol{\Phi}(k)^{T} + h^{2}\mathbf{E}\mathbf{Q}(k)\mathbf{E}^{T}. \end{aligned} \quad (11)$$

$\mathbf{R} = \mathbf{R}^{\mathrm{T}} \in \mathbb{R}^{7\times 7}$ and $\mathbf{Q} = \mathbf{Q}^{\mathrm{T}} \in \mathbb{R}^{12\times 12}$ are the covariance matrices. The discrete state space matrix is found by linearization according to

$$\boldsymbol{\Phi}(k) = \mathbf{I} + h\frac{\partial \mathbf{f}(\mathbf{x}(k))}{\partial \mathbf{x}(k)}\bigg|_{\mathbf{x}(k)=\hat{\mathbf{x}}(k)}. \quad (12)$$

4.3.3 Controller

The controller block consists of control algorithms for different modes of operation. A nonlinear PID position controller is developed for station keeping and a nonlinear PID speed controller for trajectory tracking. It is $\hat{\boldsymbol{\eta}}$ and $\hat{\mathbf{v}}$ from the estimated state vector $\hat{\mathbf{x}}(k)$ which is the input to the controller assuming certainty equivalence. One should notice that there is no proof of global asymptotic stability. The nonlinear PID position controller is given by (13).

$$\boldsymbol{\tau}_{PID} = -\mathbf{J}(\psi)^{T}(\mathbf{K}_{p}\tilde{\boldsymbol{\eta}} + \mathbf{K}_{d}\mathbf{J}(\psi)\hat{\mathbf{v}} + \mathbf{K}_{i}\int_{0}^{t}\tilde{\boldsymbol{\eta}}(\sigma)d\sigma) \quad (13)$$

where $\tilde{\boldsymbol{\eta}} = \hat{\boldsymbol{\eta}} - \boldsymbol{\eta}_{d}$ is the position error vector and $\mathbf{K}_{p}, \mathbf{K}_{d}$ and $\mathbf{K}_{i} \in \mathbb{R}^{4\times 4}$ are gain matrices.

In the thrust allocation algorithm the Moore-Penrose pseudo inverse in addition to the thrust characteristics for positive and negative *rpm* for each thruster are used to find the setpoint vector – $\mathbf{t}$ to the thrusters. Bollard pull tests were carried out to find proper thruster characteristics for the installed thrusters accounting for thrust losses such as thruster- hull interactions.

4.3.4 Guidance

The guidance block consists of two main modules; a reference model and path-following module. The trajectory generator includes a function for monitoring the deviation between desired and actual position of the ROV. The generated trajectory will wait for the ROV if the tracking error exceeds a threshold. A line of sight path algorithm is applied for tracking a path between waypoints. An algorithm which minimizes the cross track error of the predefined path while maintaining constant heading is also added. This is very useful for running the ROV in a grid pattern specified by the waypoints.

5. Experimental Results

Experimental results from full scale tests are presented demonstrating performance of the DP control system for station keeping and tracking operations. In the results a nonlinear output feedback controller based on extended Kalman filter and nonlinear PID is used. More results on comparison of various observers and controllers, anti-collision strategies, navigation and signal detection methods may be found in Dukan et al. (2011) and the master theses by Lysdahl (2010), Kirkeby (2010), Kørte (2011), Truong (2011), Candeloro (2011) and Standardi (2011).

An example of the performance of the DP control system in station keeping is seen to the left in Figure 5. It shows the trace of the measured and estimated positions and snap shots of the outline of the ROV, with actual dimensions, during 750 seconds of station keeping. A zoom in of the footprint trace is seen to the right. A linear Kalman filter is used with heading and yaw rate measurements from an MRU6. The maximum measured deviation from desired position was 9 cm in North and 15 cm in East direction. The estimated deviation was within 5 cm in North and 8 cm in East direction. The ROV is 72 m below the surface.

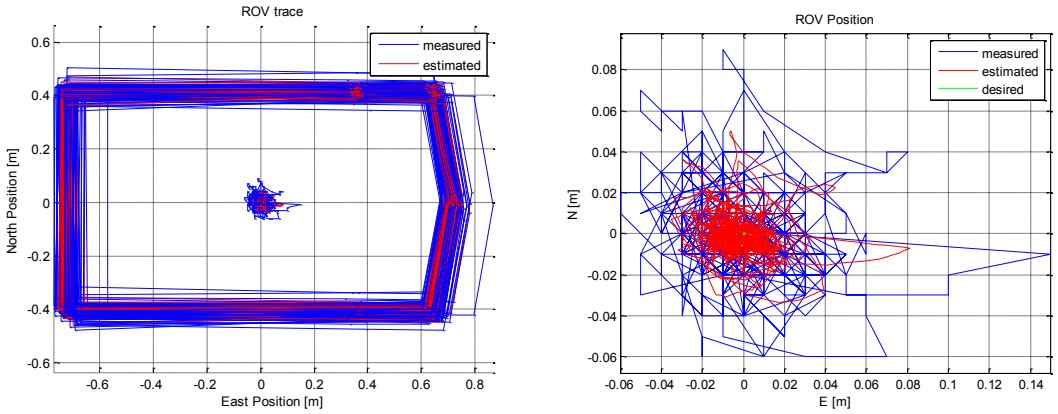

Figure 5. DP station keeping performance

North, East, depth and heading is given on top in Figure 6. Blue is measured from sensor and red is estimated from the observer. The measured depth is controlled to be within 0.1 m from desired. The resolution of the depth sensor is 0.1 m. The measured heading is controlled to be within 1 degree from desired except at two occasions at about 700 seconds where the heading error is 3 degrees. The commanded thrust forces and thruster revolution speeds in rpm are

seen at the bottom in Figure 6. Note that there are two vertical thrusters which operate at the same rpm.

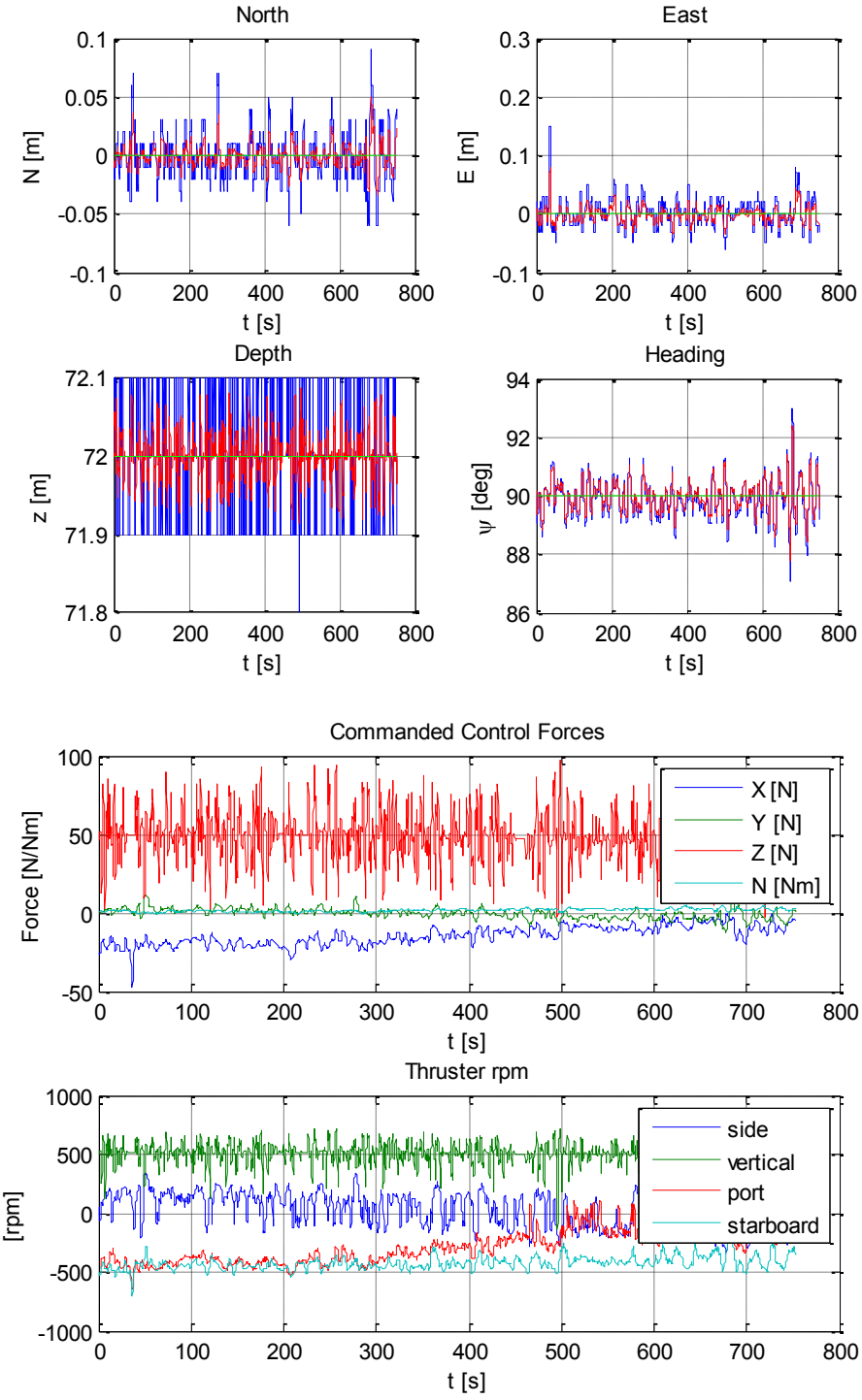

Figure 6. ROV position (top) and thrust (bottom) during station keeping.

Figure 7 shows 60 seconds of the data in Figure 6 from 140 s to 200 s.

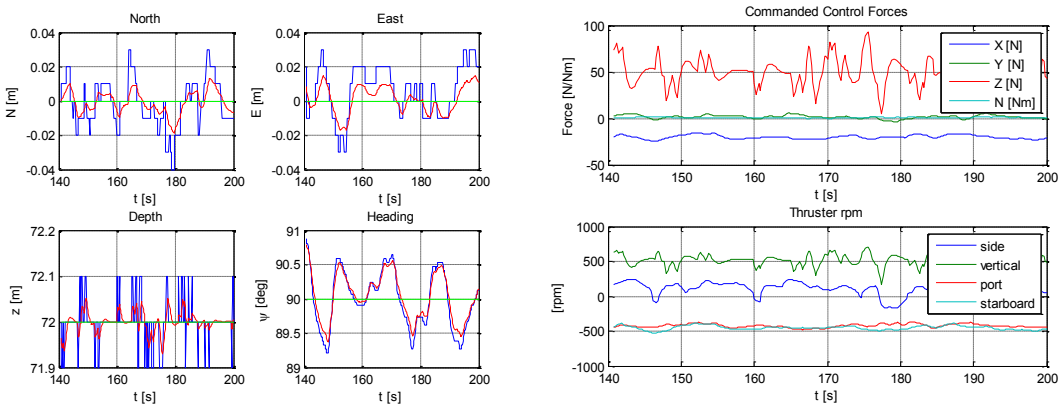

Figure 7. ROV position (left) and thrust (right) during station keeping, 60 s.

In Figure 8 a nonlinear PID speed controller is used to track a square box of 10x10m while minimizing the cross track error. Heading is towards the speed direction. Figure 8 shows the trace of the measured and estimated position in addition to snap shots the outline of the ROV with actual dimensions. The test is done with all sensors working as seen to the left in Figure 8. Results for dead reckoning, without x and y measurements, is seen to the right. The speed during tracking is 0.1 m/s and the ROV is 278 m below the surface.

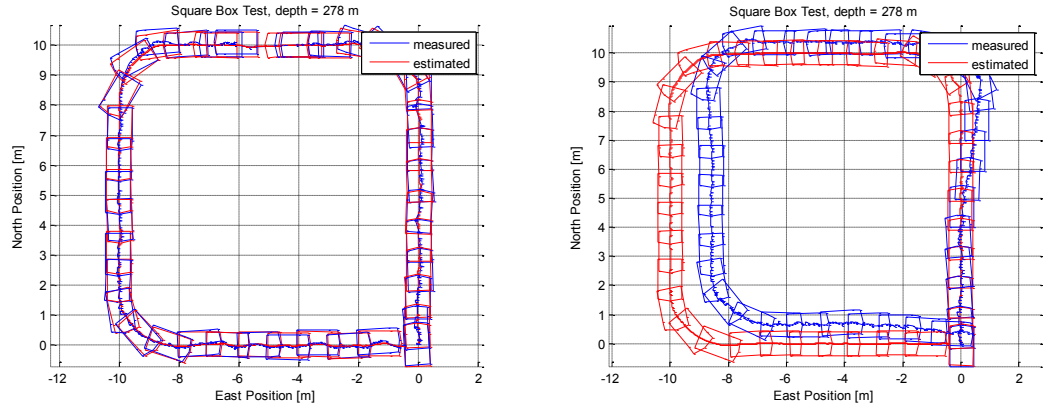

Figure 8. Square box tests, all sensors working (left) and drop out of x and y position measurements (right).

An example of trajectory tracking performance is seen in Figure 9. A nonlinear PID speed controller is used to track the desired trajectory by control of speed and cross track error. The desired trajectory is composed of line segments and half circles. The lawn mower pattern is specified by waypoints. Figure 9 shows 3 straight legs and two turns. The speed is 0.3 m/s on straight line segments and 0.1 m/s during turns. The MRU6 is used as the yaw motion sensor for the extended Kalman filter. Snap shots of the ROV outline are also given in this plot. Maximum estimated cross track error is 9 cm and measured is 20 cm. This occurs about half way into the second straight leg. The ROV is 32 m below the surface.

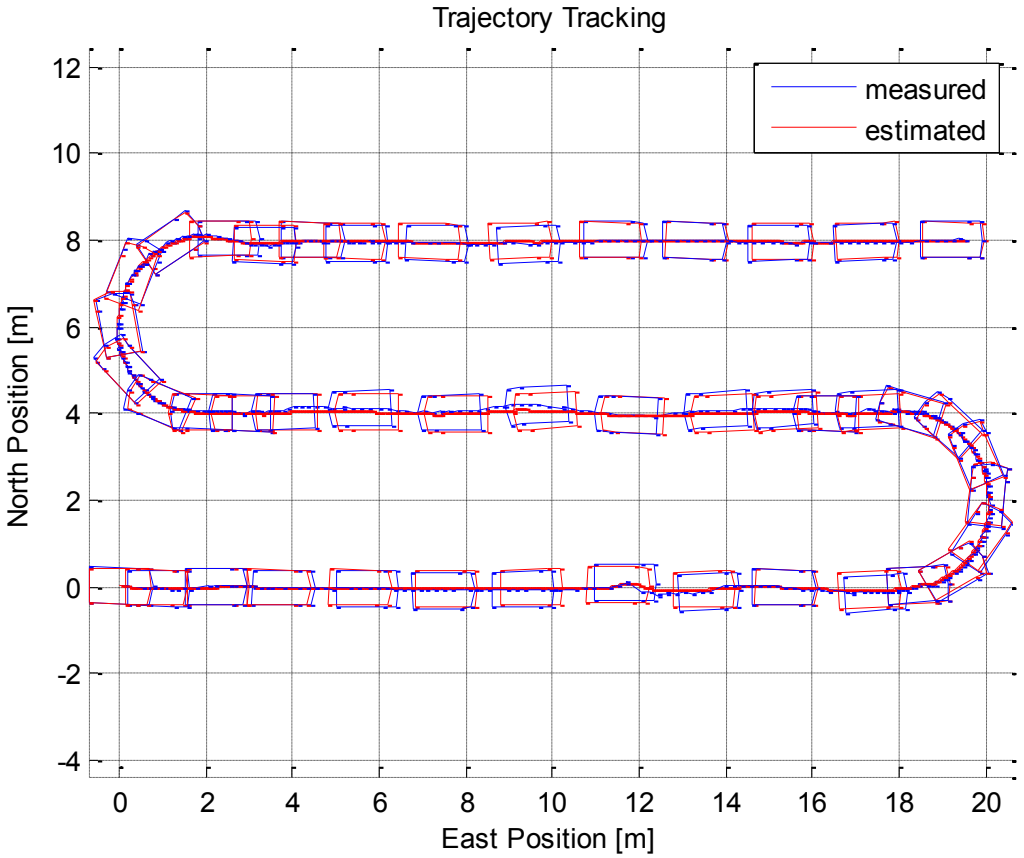

Figure 9. Path following with cross track error control.

6. Conclusions

In this paper the newly developed DP control system implemented on the ROV Minerva is presented. The selected hardware and software platforms were Labview and National Instruments cRIO. The DP control system was made up by modules for *signal processing*, *guidance*, *observer* for filtering and state estimation, *controller*, *supervisor and adaption*, and *thrust allocation*. The DP control system was interfaced to a navigation system and local thruster controllers. Experimental results with a nonlinear output feedback controller for dynamic positioning based on extended Kalman filter and nonlinear PID controller were presented. It is important to underline that the DP control system was tailor-made for rapid control prototyping used in education and research to test and verify various guidance, navigation and control strategies fulfilling various missions.

Acknowledgement

This work has been carried out at the Centre for Ships and Ocean Structures (CeSOS) and the Applied Underwater Robotics Laboratory (AUR-Lab) at NTNU. The Norwegian Research Council and the NTNU program Marine Coastal Development are acknowledged as the main sponsor of CeSOS and AUR-Lab. The authors would like to thank the crew of RV Gunnerus for the invaluable help with the full scale tests. We are also grateful to the Master students that have contributed.

References

Candeloro, M. (2011). Design of Observers for DP and Tracking of ROV Minerva with Experimental Results. MSc Thesis, Facoltà di Ingegneria, Università Politecnica Delle Marche, Ancona, Italy.

Christ, R. D. and R. L. Wernli Sr. (2007). *The ROV Manual: A User Guide to Observation-Class Remotely Operated Vehicles*. Butterworth-Heinemann, Elsevier, Oxford, UK.

Dukan, F., M. Ludvigsen, and A. J. Sørensen (2011). Dynamic Positioning System for a Small Size ROV with Experimental Results. Oceans'11, IEEE, June 6-9, Santander, Spain.

Fossen, T. I. (2011). *Handbook of Marine Craft Hydrodynamics and Motion Control*. John Wiley ltd, UK.

Kirkeby, M. (2010). Comparison of Controllers for Dynamic Positioning and Tracking of ROV Minerva. MSc Thesis, Department of Marine Technology, NTNU, Norway.

Kørte, S. Ø. (2011). Guidance & Control Strategies for UUVs. MSc Thesis, Department of Marine Technology, NTNU, Norway.

Lysdahl, C. C. (2010). Design of Dynamic Positioning System for ROV Minerva. MSc Thesis, Department of Marine Technology, NTNU, Norway.

Mair J. and I. Tena (2011). A Hover-Capable Autonomous Inspection Vehicle. Sea Technology Magazine, April. US.

Smallwood, D. A. and L. L. Whitcomb (2004). Model-Based Dynamic Positioning of Underwater Robotic Vehicles: Theory and Experiments. IEEE J. of Oceanic Engineering, 29-1, pp. 169-186.

Standardi, Laura (2011). Signal Processing and Change Detection Applied to ROV in a DP System. MSc Thesis, Facoltà di Ingegneria, Università Politecnica Delle Marche, Ancona, Italy.

Sørensen, A. J. (2011). *Marine Control Systems: Propulsion and Motion Control Systems of Ships and Ocean Structures*. UK-2011-76, Department of Marine Technology, the Norwegian University of Science and Technology, Trondheim, Norway.

Truong, P. (2011). Navigation of ROVs and Basic Signal Processing. MSc Thesis, Department of Marine Technology, NTNU, Norway.

Article B

Outlier Rejection in Underwater Acoustic Position Measurements Based on Prediction Errors

A.M. Lekkas, **M. Candeloro** and I. Schjølberg

The article has been published in the proceedings of the
4th IFAC Workshop on Navigation, Guidance and Control of Underwater Vehicles (NGCUV), IFAC-PapersOnLine
Volume 48 (2), pages 82–87. Girona, Spain, 28-30 April 2015.

Available online at www.sciencedirect.com

ScienceDirect

IFAC Papers Online
CONFERENCE PAPER ARCHIVE

IFAC-PapersOnLine 48-2 (2015) 082–087

Outlier Rejection in Underwater Acoustic Position Measurements Based on Prediction Errors

Anastasios M. Lekkas * **Mauro Candeloro** * **Ingrid Schjølberg** *

* *Centre for Autonomous Marine Operations and Systems, Norwegian University of Science and Technology, NO-7491, Trondheim, Norway (e-mail:anastasios.lekkas@ntnu.no, mauro.candeloro@ntnu.no, ingrid.schjolberg@ntnu.no)*

Abstract: Outlier detection and rejection is an important step toward more robust underwater navigation systems. More specifically, acoustic positioning measurements can be notoriously intractable by introducing spikes, or freezing for periods of time, hence driving the navigation filter state estimates to wrong values. In this paper, a simple approach for detecting and rejecting outliers for underwater operations is presented. Acoustic positioning measurements are combined with absolute velocity measurements from a DVL (Doppler Velocity Log) sensor in order to robustify the filter when the vehicle navigates in the operative range of the DVL. Simple χ^2 statistic tests are employed in order to evaluate every new measurement and result in discarding those measurements which give large residuals compared to the predicted value from the Extended Kalman Filter. Moreover, the sum of the prediction errors is computed over a fixed number of valid acoustic measurements for filter divergence monitoring purposes. The efficacy of the approach is demonstrated using experimental data acquired during ROV operations.

Keywords: underwater navigation, outlier detection, acoustic positioning, filter monitoring, ROV

1. INTRODUCTION

Over the last years significant effort has been made by the research community towards the development of underwater operations with increased level of autonomy. The ability to perform underwater tasks autonomously is invaluable not only to researchers, such as marine biologists and archaeologists, but also to the oil industry. It is indicative that, currently, a vast amount of money is spent daily on surface vessels which support time-consuming ROV (Remotely Operated Vehicle) operations for the offshore industry, many of which would require only a fraction of that time if they were performed onshore, see also Nichols (2013).

However, underwater autonomy does not come without high demands for robustness almost at all levels. This is a reasonable consequence since large deviations from the desired behavior in any of the important building blocks of the system will inevitably affect the remaining blocks. The navigation system, for instance, is responsible for fusing all available measurements in order to provide estimations of the vehicle's position, velocity and attitude. Inaccurate state estimations can lure the guidance system into generating wrong reference trajectories, which in turn leads to the control system calculating moments and forces inappropriate for the task in hand. It can be easily concluded that a low performance navigation system will most likely put both the vehicle and the operation in danger.

Underwater navigation poses great challenges, mostly due to the lack of a reliable positioning system, such as the GNSS (Global Navigation Satellite System) in the case of aerial and terrain applications. For more information on underwater vehicle navigation and relevant practical considerations the reader is referred to (Kinsey et al., 2006; Partan et al., 2007). As a result, in addition to onboard sensors such as accelerometers, gyroscopes, magnetometers, DVL (Doppler Velocity Logger), underwater vehicles rely mostly on acoustic measurements for positioning purposes. A thorough overview of acoustic positioning systems was given by Vickery (1998). One major problem with acoustic positioning systems, though, is that the measurements are affected by noise, dropouts and outliers, a phenomenon which is attributed to the presence of multiple acoustic propagation paths between the source and the receiver (Vaganay et al., 1996).

According to Hawkins (1980), an outlier is defined as "an observation which deviates so much from other observations as to arouse suspicions that it was generated by a different mechanism", and is considered to be one of the oldest problems in statistics. In addition to the book by Hawkins, other standard references targeting the statistics community are the works of Rousseeuw and Leroy (2005); Barnett and Lewis (1994), whereas the more recent book by Aggarwal (2013) is targeted to a wider audience, including the data mining and machine learning communities. A considerable amount of research work has been done in the past on outlier rejection for underwater applications.

10.1016/j.ifacol.2015.06.014

One of the first papers on the subject was by Vaganay et al. (1996), where the authors considered Long Base Line (LBL) navigation and presented two techniques (one in the time domain and one in the spatial domain) for performing outlier rejection. The same authors presented a comparison between fix computation and filtering for autonomous acoustic navigation in Vaganay et al. (1998). A nonlinear measurement feedback, instead of the conventional linear position observer gain, and a diffusion-based observer was employed by Vike and Jouffroy (2005). An offline hypothesis grid representation concept consisting of three steps was devised in (Bingham and Seering, 2006). A comparison of three outlier detection algorithms (maximum speed thresholding, a parallel Kalman filter approach, and sigma filter) for hydro-acoustic positioning was presented in (Fauske and Hallingstad, 2006). A three-dimensional underwater acoustic network time synchronization scheme with outlier detection was proposed in (Hu et al., 2008). An observer, which is robust with respect to outliers, for estimating the states of a nonlinear system was developed by Jaulin (2009) and a test case related to an underwater robot was presented. The method assumes that both the measurement errors and the number of outliers within a given time window are bounded. Morgado et al. (2013) presented a data classification algorithm based on causal median filters and provided the theoretical tools for the design of the filter parameters. In Indiveri (2013) the author presented a methodology based on the Least Entropy-Like parameter estimation technique, hence resulting in a robust and simple approach.

In this paper the goal is to investigate the efficacy of fusing acoustic positioning and DVL measurements, which are typically available onboard ROVs, for outlier detection and rejection purposes. An *Extended Kalman Filter (EKF)* is employed as the navigation filter which gives full state estimates and the main task is to detect and reject outliers *before* they enter the EKF. In order to achieve this, a number of χ^2 statistical tests are implemented every time a new measurement is available. These tests aim at evaluating the significance of the residuals which are the outcome of the predicted and measured values. The χ^2 tests are not performed on the total position prediction error but on each degree of freedom (i.e. North, East) separately. As mentioned in (Fauske and Hallingstad, 2006), such an approach could perform poorly if the estimates are inaccurate and good measurements are discarded, hence leading to *filter divergence*. Moreover, measurements from noisy sensors, such as Inertial Measurement Units (IMUs), can be deceiving since they are affected by thruster-induced vibrations that can alter the magnetic field in the neighborhood of the instrument. However we show that fusing acoustic positioning measurements with DVL absolute velocities (with respect to the sea bottom) measurements results in a satisfactory and reliable performance capable of rejecting outliers with very low computational cost. In order to avoid filter divergence, we implement a simple filter monitoring technique which calculates the sum of the prediction errors for a sliding window over a fixed sample horizon. Depending on the values of the error sum it is possible to take actions, such as commanding the ROV to enter Dynamic Positioning (DP) mode, until the values return within a certain threshold. The suggested methodology is tested using real data acquired during a recent mission in the Trondheim fjord.

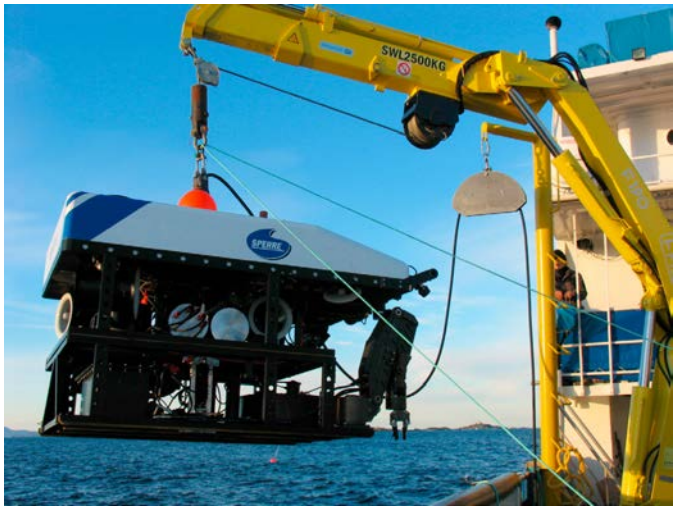

Fig. 1. ROV 30k during deployment. Courtesy of AUR-Lab, NTNU.

2. ROV CONTROL MODEL

The efficacy of the approach presented in this work will be based on experimental data acquired during a mission of the NTNU-owned ROV 30K, which is depicted in Fig. 1. When not in dynamic positioning mode, the ROV moves at a low speed, typically around 0.2 m/sec. As a consequence, for *control purposes*, the following 4DOF model is considered (more details are given by Candeloro et al. (2012), Dukan (2014) and Fossen (2011)):

$$\dot{\boldsymbol{\eta}} = \mathbf{J}(\boldsymbol{\eta})\boldsymbol{\nu}, \tag{1}$$

$$\mathbf{M}\dot{\boldsymbol{\nu}} + \mathbf{C}(\boldsymbol{\nu})\boldsymbol{\nu} + \mathbf{D}(\boldsymbol{\nu})\boldsymbol{\nu} + \mathbf{g}(\boldsymbol{\eta}) = \boldsymbol{\tau} + \mathbf{J}(\boldsymbol{\eta})^T\boldsymbol{b} + \boldsymbol{w}_m, \tag{2}$$

$$\dot{\boldsymbol{b}} = -\boldsymbol{T}_b^{-1}\boldsymbol{b} + \boldsymbol{w}_b, \tag{3}$$

where $\mathbf{M}$ is the mass and inertia matrix, $\mathbf{C}(\boldsymbol{\nu})$ the Coriolis and centripetal matrix, $\mathbf{D}(\boldsymbol{\nu})$ is the damping matrix, $\mathbf{g}(\boldsymbol{\eta})$ describes the gravitational and buoyancy forces, $\boldsymbol{\tau}$ includes the control forces and moments, and $\mathbf{b}$ is the bias vector. Moreover $\mathbf{M}, \mathbf{T}_b \in \mathbb{R}^{4\times4}$, $\boldsymbol{\tau} \in \mathbb{R}^4$, and it should be noted that the Coriolis force has a destabilizing effect on the vehicle that normally is canceled by dissipative effect due to lift effect or transom stern effects that can be included in the damping matrix.

Accordingly, the generalized position and velocity are recognized as:

$$\boldsymbol{\eta} = [x,\ y,\ z,\ \psi]^{\mathrm{T}},\ \ \boldsymbol{\nu} = [u,\ v,\ w,\ r]^{\mathrm{T}}, \tag{4}$$

where (x, y, z) is the vehicle's inertial position in Cartesian coordinates and ψ is the yaw angle. In addition, u is the surge velocity, v is the sway velocity, w is the heave velocity, and r is the yaw rate.

3. SENSORS AND NAVIGATION FILTER

3.1 Available Sensors

The vehicle is equipped with a number of sensors including:

- the HiPAP Acoustic Positioning System (APS) by Kongsberg Maritime. A transponder is installed on the vehicle and the APS outputs the x, y and z position coordinates of the transponder at a sampling rate which ranges between 1-3 Hz, dependent on water depth and user settings. The transponder on board the ROV has its own batteries and, as a consequence, the user might choose a slower ping rate in order to prolong the mission duration.
- A DVL for measuring velocity w.r.t the water or the sea floor. The DVL outputs 3-DOF velocity measurements u, v, w in the DVL frame. A typical 600 kHz DVL has bottom track range from 0.7 m to 90m with standard deviation of 0.3cm/s at 1 m/s. The ping rate is 1 Hz. There is a maximum seabed slope (assuming the instrument is level) a DVL can bottom-track. DVL can be used around offshore structures, as long as they are not vertical. Obtaining high accuracy navigation far of the sea floor, when the DVL is out of range for bottom lock, is difficult.
- A 9-DOF IMU that provides accelerations, turn rates and magnetic field measurements. An important advantage of strapdown INS is that all unknown forces acting on the vehicle are instantly felt by the accelerometers and their effect is directly included in the INS. However, mainly due to disturbances stemming from the thrusters, incorporating the IMU acceleration measurements in the integration filter can be harmful. Heading estimation is important for this phase of the operation because the prediction term relies on it to propagate the position with acceptable accuracy. The IMU is therefore used *only* for estimating the attitude of the vehicle. Magnetometer measurements are important for gyroscope bias estimation. We therefore assume that no magnetic disturbances are present, because the instrument is calibrated while on board the ROV, hence making it possible to filter out the effect of the metallic structure of the ROV.
- A pressure gauge to measure the depth. It has a maximum update rate of 8 Hz and it is way more reliable compared to the z-coordinate measurement of the APS.

3.2 Extended Kalman Filter

An Extended Kalman Filter (EKF) is responsible for fusing all the available sensor measurements in order to estimate the states of the vehicle. The measurements arrive at irregular time instants since the sensors have different sampling rates. Note that in the literature different approaches have been presented where outliers are allowed in the filter but the Kalman Filter is modified in order to deal with them, see Ting et al. (2007); Gandhi and Mili (2010). In this work, as it will be shown in the next section, the conventional EKF is employed, but the acoustic measurements are checked for outliers before they are allowed in the filter. Therefore in some cases, it is likely that only DVL measurements are allowed in the filter for a time interval. To begin with, the system (1)–(3) can be rewritten in state space form as follows:

$$\dot{\mathbf{x}} = \mathbf{f}(\mathbf{x}) + \mathbf{B}\mathbf{u} + \mathbf{E}\mathbf{w}, \tag{5}$$

$$\mathbf{y} = \mathbf{H}\mathbf{x} + \boldsymbol{\upsilon}, \tag{6}$$

where

$$\mathbf{x} = \begin{bmatrix} \boldsymbol{\eta} \\ \boldsymbol{\nu} \\ \mathbf{b} \end{bmatrix}, \quad \mathbf{u} = \boldsymbol{\tau}, \quad \mathbf{w} = \begin{bmatrix} \mathbf{0} \\ \boldsymbol{w}_m \\ \boldsymbol{w}_b \end{bmatrix}, \tag{7}$$

$\mathbf{y}$ is the measurement vector and $\mathbf{H}$ is the observation model which maps the true state space into the observed space, $\boldsymbol{\tau}$ is the control input vector and:

$$\mathbf{B} = \begin{bmatrix} \mathbf{0} \\ \boldsymbol{M}^{-1} \\ \mathbf{0} \end{bmatrix}, \quad \mathbf{E} = \begin{bmatrix} \mathbf{0} & \mathbf{0} & \mathbf{0} \\ \mathbf{0} & \boldsymbol{M}^{-1} & \mathbf{0} \\ \mathbf{0} & \mathbf{0} & \mathbf{0} \end{bmatrix}, \tag{8}$$

$$\mathbf{f}(\mathbf{x}) = \begin{bmatrix} \mathbf{J}(\boldsymbol{\eta})\boldsymbol{\nu} \\ -\mathbf{M}^{-1}\left(\mathbf{C}(\boldsymbol{\nu})\boldsymbol{\nu} + \mathbf{D}(\boldsymbol{\nu})\boldsymbol{\nu} + \mathbf{g}(\boldsymbol{\eta}) - \mathbf{J}(\boldsymbol{\eta})^T\right) \\ -\boldsymbol{T}_b^{-1}\boldsymbol{b} \end{bmatrix}, \tag{9}$$

which is linearized about the state estimates $\hat{\mathbf{x}}$ as follows:

$$\boldsymbol{\Phi}_k = \mathbf{I} + h\frac{\partial \mathbf{f}(\mathbf{x}(k), \mathbf{u}(k))}{\mathbf{x}(k)}\bigg|_{\mathbf{x}_k = \hat{\mathbf{x}}_k}, \tag{10}$$

$$\boldsymbol{\Delta} = h\boldsymbol{B}, \tag{11}$$

$$\boldsymbol{\Gamma} = h\boldsymbol{E}. \tag{12}$$

where k is the step number and h is the time step in seconds. We can therefore write the Kalman Filter measurement update as:

$$\hat{\mathbf{x}}_{k|k} = \hat{\mathbf{x}}_{k|k-1} + \mathbf{K}_k(\mathbf{y}_k - \mathbf{H}_k\hat{\mathbf{x}}_{k|k-1}), \tag{13}$$

$$\mathbf{P}_{k|k} = \mathbf{P}_{k|k-1} + \mathbf{K}_k\mathbf{H}_k\mathbf{P}_{k|k-1}, \tag{14}$$

and the time (predictor) update is:

$$\hat{\mathbf{x}}_{k+1|k} = \hat{\mathbf{x}}_{k|k} + h\mathbf{f}(\hat{\mathbf{x}}_{k|k}) + \boldsymbol{\Delta}\boldsymbol{u}(k), \tag{15}$$

$$\mathbf{P}_{k+1|k} = \boldsymbol{\Phi}_k\mathbf{P}_{k|k-1}\boldsymbol{\Phi}_k^T + \boldsymbol{\Gamma}_k\mathbf{Q}(k)\boldsymbol{\Gamma}_k^T, \tag{16}$$

where the Kalman gain K_k is defined as

$$\mathbf{K}_k = \mathbf{P}_{k|k-1}\mathbf{H}_k^T(\mathbf{H}_k^T\mathbf{P}_{k|k-1}\mathbf{H}_k + \mathbf{R}_k)^{-1}, \tag{17}$$

and $\mathbf{P}$ is the covariance matrix, $\mathbf{Q}$ is the process noise covariance, $\mathbf{R}$ is the measurement noise covariance. The next section describes the methodology used for outlier detection and rejection.

4. OUTLIER DETECTION AND REJECTION

According to Aggarwal (2013), it is important to distinguish between methods for extreme value analysis and general outlier analysis methods. In other words, it is more useful to evaluate the distance of a measurement w.r.t. a predicted value. Following Gustafsson (2010), a natural implementation of an outlier rejection algorithm is based on the normalized residual:

$$\bar{\varepsilon}_k = (\mathbf{H}_k^T\mathbf{P}_{k|k-1}\mathbf{H}_k + \mathbf{R}_k)^{-1/2}(\mathbf{y}_k - \mathbf{H}_k\hat{\mathbf{x}}_{k|k-1}) \sim \mathcal{N}(0, I). \tag{18}$$

In this way, standard hypothesis tests can be used in order to decide whether a measurement is an inlier or not. A measurement-by-measurement implementation of a χ^2 test is:

$$T(y_k^i) = (\mathbf{y}_k^i - \mathbf{H}_k^i\hat{\mathbf{x}}_{k|k-1})^T(\mathbf{H}_k^i\mathbf{P}_{k|k-1}(\mathbf{H}_k^i)^T + \mathbf{R}_k^i)^{-1} \cdot (\mathbf{y}_k^i - \mathbf{H}_k^i\hat{\mathbf{x}}_{k|k-1}) \sim x^2_{n_y^i}, \tag{19}$$

where i refers to the i_{th} sensor. This equation can be justified since the term $(\mathbf{y}_k^i - \mathbf{H}_k^i \hat{\mathbf{x}}_{k|k-1})$ is the prediction error (also innovation, or measurement residual) and $(\mathbf{H}_k^i \mathbf{P}_{k|k-1} (\mathbf{H}_k^i)^T + \mathbf{R}_k^i)^{-1}$ is the covariance of the prediction error.

A measurement is rejected as outlier if

$$T(y_k^i) > \chi^2_{\alpha, n_y^i}. \tag{20}$$

In our case the threshold is determined by first having a qualitative look of data from previous missions. This gives an idea about the behavior of the APS and the threshold is chosen so that most outliers will be detected while at the same time not too many measurements are discarded. Discarding a large number of acoustic measurements can result in dead reckoning, in the extreme case.

5. DIVERGENCE MONITORING

Although the thresholds are chosen so that mainly outliers will be rejected, this cannot be guaranteed. Moreover, if a large number of outliers appear one after the other (due to the morphology of the mission location, for instance), the vehicle will navigate based on the EKF prediction (dead reckoning), which means that sooner or later it will drift. This means that even if the APS measurements improve greatly later on, they will still be classified as outliers by (19). In order to avoid this, we implement a simple filter monitoring technique to make sure the filter has not diverged. Again, following Gustafsson (2010), a variance-based statistic is to compute the following sum of N prediction errors:

$$\begin{aligned} T(y_{1:N}) =& (\mathbf{y}_k^i - \mathbf{H}_k^i \hat{\mathbf{x}}_{k|k-1})^T (\mathbf{H}_k^i \mathbf{P}_{k|k-1} (\mathbf{H}_k^i)^T + \mathbf{R}_k^i)^{-1} \\ & \cdot (\mathbf{y}_k^i - \mathbf{H}_k^i \hat{\mathbf{x}}_{k|k-1}) \end{aligned} \tag{21}$$

$$T(y_{1:N}) \sim x^2_{n_y^i}. \tag{22}$$

However, a preferable alternative is to use a sliding window over a fixed time horizon, which can be a fixed number of acquired measurements. An exponential window for the iterated process is described by:

$$\begin{aligned} T(y_{1:k}) =& \lambda T(y_{1:k-1}) + \frac{1-\lambda}{n_y} (\mathbf{y}_k - \mathbf{H}_k \hat{\mathbf{x}}_{k|k-1})^T \\ & \cdot (\mathbf{H}_k \mathbf{P}_{k|k-1} \mathbf{H}_k^T + \mathbf{R}_k)^{-1} (\mathbf{y}_k - \mathbf{H}_k \hat{\mathbf{x}}_{k|k-1}) \end{aligned} \tag{23}$$

$$\sim \mathcal{N}(1, 2(1-\lambda)/(1+\lambda)), \tag{24}$$

where $0 \ll \lambda < 1$ is the forgetting factor in the exponential filter. It is important to note that in this case a fixed number of samples *does not* imply a fixed time window. This distinction is a natural outcome of the fact that acoustic measurements often "freeze", in which case the identical measurements are discarded. Based on the behavior of the sum (23), it can be deduced whether the filter has diverged (drifted) or not. In case of drift, actions such as dynamic positioning can be commanded in order to reset the filter.

6. EXPERIMENTAL RESULTS

The methodologies presented in the previous two sections are now implemented using real data acquired during an operation of ROV 30k. The vehicle maintained constant altitude and was commanded to follow a $2D$ lawnmower path. The algorithm checks in real time whether a measurement is an outlier or not based on the prediction error. The computation of the prediction error is performed separately for the North and the East directions because the total position norm might allow a bad East measurement to enter the filter if the corresponding North measurement is very congruent with the EKF prediction, for instance. Results using two data segments are presented, with each segment having a duration of approximately 850 sec.

Figs 2–3 depict the main results for the first data segment. It can be observed that the APS demonstrates a rather noisy behavior, including a few outliers. An interesting observation is that in the North-coordinate there are a few strong outliers between $4140 - 4170$ sec which do not appear in the East-coordinate. This justifies even further the separation of the two DOFs. In any case, if the outlier is not removed it can be seen that the estimate is affected significantly (green line) whereas outlier rejection (OR) avoids this problem (blue line). The second subplots of Figs 2–3 plot the prediction errors (residuals) as well as the filter monitoring quantity T_{div}. It is important to note that T_{div} has been normalized in order to make the plot more practical. The thresholds have to be chosen low enough so that outliers will be detected and desired accuracy will be achieved but also high enough so that not too many measurements will be discarded. The residuals exceeding the thresholds are treated as outliers. The quantity T_{div} helps detect filter convergence, in which case the filter should be reset. Divergence occurs when T_{div} exceeds the threshold (for example when a few strong outliers appear at a row) and then its value remains high even though more reliable measurements have been obtained. Regarding the time window, it was chosen $n_y = 20$ and $\lambda = 0.8$. This means that in the ideal case where the APS gave 1 measurement per second, the sliding window would be always 20 sec. It can be easily understood that this is hardly ever the case because often APS measurements freeze, a fact which leads in keeping older values from the segment (although the number of measurements used for computing T_{div} at any time instant is 20). Fig. 7 shows exactly this, i.e. how long back in time it is required to go at each time instant in order to have a window consisting of 20 accepted APS measurements. Regarding T_{div}, it can be observed for both North and East data that the value increases whenever outliers are present (as expected) but it has the tendency to drop right after, which means that no alarming situation regarding filter divergence has occurred.

A larger number of outliers is present in the second data segment, the results are shown in Figs 4–5. These are detected and rejected, hence resulting in smoother position estimates, see for instance the comparison at 5800 sec, 5850 sec and 6440 sec for the North data in Fig. 4 and several occasions of lower magnitude for the East data in Fig. 5.

Fig. 6 illustrates the efficiency of the implemented technique by plotting the ROV position estimates while the vehicle is commanded to move on a straight-line path. It is clear that allowing outliers to enter the filter (green line) can induce large estimation errors and introduce discontinuities in the estimated path. The outlier rejection algorithm (blue line), however, avoids this and gives very reliable position estimates which approximate the straight line very well.

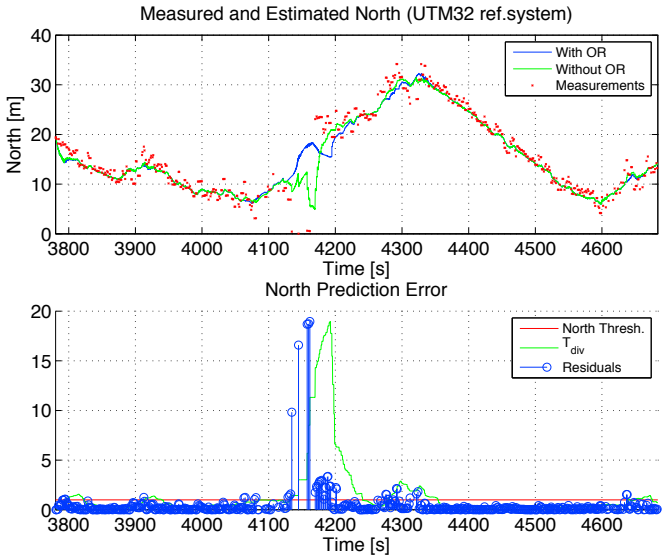

Fig. 2. Data segment 1: North

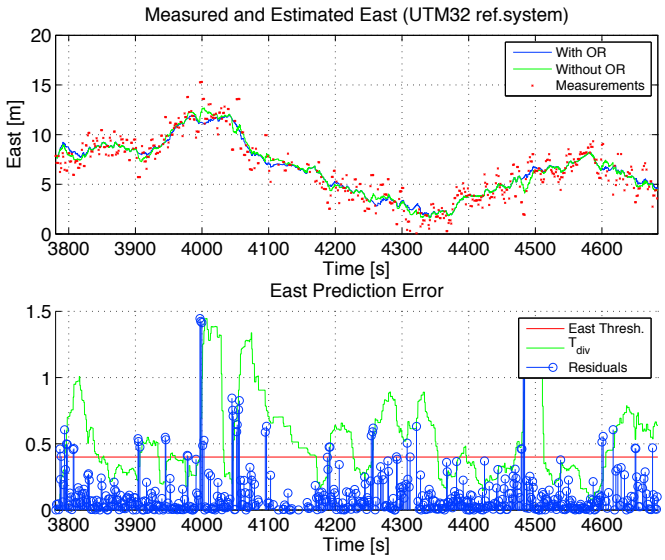

Fig. 3. Data segment 1: East

Finally, Fig. 7 is related to the filter divergence test. As mentioned earlier, the sliding window has been chosen to consider the 20 most recent *valid* acoustic measurements. Since the acoustic measurements often freeze for several seconds, in most cases the window needs to consider measurements older than 20 sec (if we assume a constant 1 Hz sampling rate) in order to achieve this. Therefore Fig. 7 shows how much back in time the window needs to go at any time instant in order to compute T_{div}. The two subplots pertains to the two data segments.

7. CONCLUSIONS

This work has dealt with the implementation of a simple technique, based on prediction errors, for outlier detection and rejection in underwater acoustic positioning measurements. The main idea was to detect outliers before they enter the Extended Kalman filter, which is employed as the navigation filter. Since IMU measurements can be very noisy and affected by vibrations stemming from the

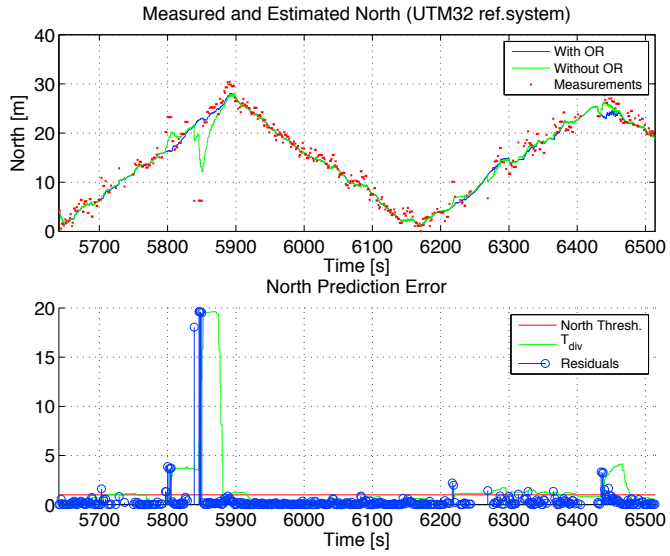

Fig. 4. Data segment 2: North

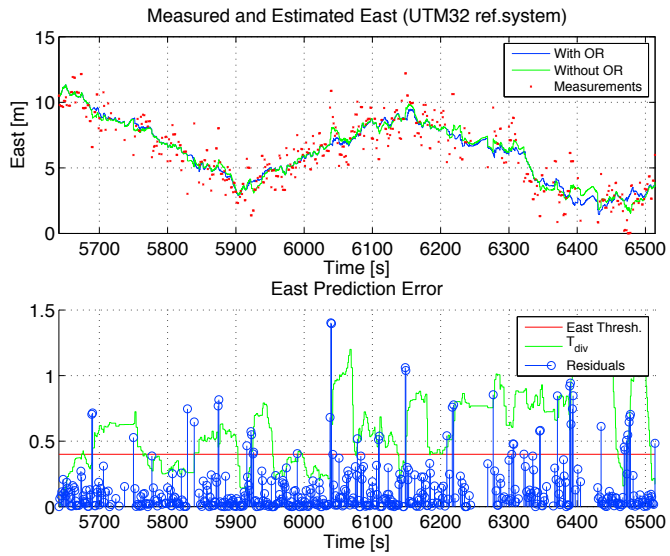

Fig. 5. Data segment 2: East

thrusters, DVL velocity measurements were used in order to improve the EKF predictions, hence resulting in satisfactory dead-reckoning navigation whenever outliers were detected. However, there is always danger that the filter will drift while operating in dead-reckoning mode, for example in case where many outliers are present for a higher time length. This could cause problems because the method is not able to distinguish the nature of the prediction error and good acoustic measurements might be classified as outliers. For that reason, a simple technique for detecting filter divergence was implemented. This first approach gave promising results when implemented on experimental data and currently work is done on robustifying it even further.

ACKNOWLEDGEMENTS

This work is supported by the Research Council of Norway, Statoil and FMC Technologies through the project Next Generation Subsea Inspection, Maintenance and Repair

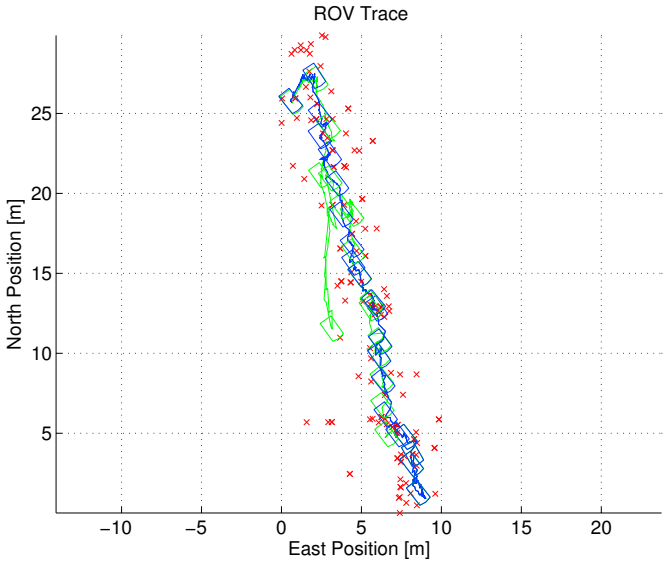

Fig. 6. State estimate comparison while moving on a straight line. Rejecting outliers (blue line) avoids the discontinuities and large errors introduced by the conventional algorithm (green line).

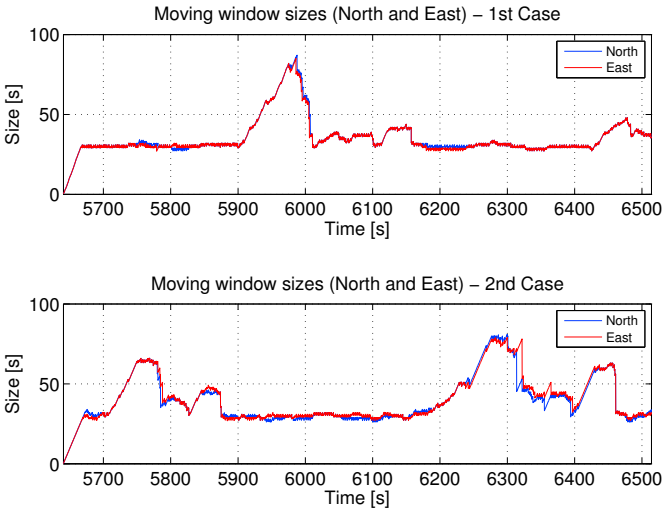

Fig. 7. Sliding time windows over fixed horizon. Although 20 samples are used in all cases, most of the times the window goes further back in time, due to the fact that a number of measurements freeze.

Operations, 234108/E30. The work is associated with CoE AMOS, 223254.

REFERENCES

Aggarwal, C.C. (2013). *Outlier analysis*. Springer.

Barnett, V. and Lewis, T. (1994). *Outliers in statistical data*. Wiley New York.

Bingham, B. and Seering, W. (2006). Hypothesis grids: Improving long baseline navigation for autonomous underwater vehicles. *IEEE Journal of Oceanic Engineering*, 31(1), 209–218.

Candeloro, M., Sørensen, A.J., Longhi, S., and Dukan, F. (2012). Observers for dynamic positioning of ROVs with experimental results. In *IFAC Conference on Manoeuvring and Control of Marine Craft*, 85–90. Arenzano, Italy.

Dukan, F. (2014). *ROV Motion Control Systems*. Ph.D. thesis, Norwegian University of Science and Technology.

Fauske, K.M. and Hallingstad, O. (2006). A comparison of outlier detection algorithms for hydro-acoustic positioning. In *OCEANS*. IEEE.

Fossen, T.I. (2011). *Handbook of Marine Craft Hydrodynamics and Motion Control*. John Wiley and Sons Ltd.

Gandhi, M.A. and Mili, L. (2010). Robust Kalman filter based on a generalized maximum-likelihood-type estimator. *IEEE Transactions on Signal Processing*, 58(5), 2509–2520.

Gustafsson, F. (2010). *Statistical sensor fusion*. Studentlitteratur.

Hawkins, D.M. (1980). *Identification of outliers*. Springer.

Hu, F., Malkawi, Y., Kumar, S., and Xiao, Y. (2008). Vertical and horizontal synchronization services with outlier detection in underwater acoustic networks. *Wireless Communications and Mobile Computing*, 8(9), 1165–1181.

Indiveri, G. (2013). An outlier robust filter for maritime robotics applications. *Paladyn, Journal of Behavioral Robotics*, 4(4), 196–203.

Jaulin, L. (2009). Robust set-membership state estimation; application to underwater robotics. *Automatica*, 45(1), 202–206.

Kinsey, J.C., Eustice, R.M., and Whitcomb, L.L. (2006). A survey of underwater vehicle navigation: Recent advances and new challenges. In *IFAC Conference of Manoeuvering and Control of Marine Craft*.

Morgado, M., Oliveira, P., and Silvestre, C. (2013). Robust outliers detection and classification for USBL underwater positioning systems. In *IFAC Intelligent Autonomous Vehicles Symposium*. Gold Coast, Australia.

Nichols, B. (2013). Surveying the field in the search for full autonomy. *Offshore Engineer*, January 2013.

Partan, J., Kurose, J., and Levine, B.N. (2007). A survey of practical issues in underwater networks. *Mobile Computing and Communications Review*, 11(4), 23–33.

Rousseeuw, P.J. and Leroy, A.M. (2005). *Robust regression and outlier detection*, volume 589. John Wiley & Sons.

Ting, J.A., Theodorou, E., and Schaal, S. (2007). A Kalman filter for robust outlier detection. In *International Conference on Intelligent Robots and Systems*, 1514–1519. IEEE.

Vaganay, J., Bellingham, J.G., and Leonard, J.J. (1998). Comparison of fix computation and filtering for autonomous acoustic navigation. *International Journal of Systems Science*, 29(10), 1111–1122.

Vaganay, J., Leonard, J.J., and Bellingham, J.G. (1996). Outlier rejection for autonomous acoustic navigation. In *IEEE International Conference on Robotics and Automation*, 2174–2181.

Vickery, K. (1998). Acoustic positioning systems. a practical overview of current systems. In *Proceedings of the IEEE Workshop on Autonomous Underwater Vehicles*, 5–17.

Vike, S. and Jouffroy, J. (2005). Diffusion-based outlier rejection for underwater navigation. In *Proceedings of MTS/IEEE OCEANS*, 1037–1042.

Article C

Observers for Dynamic Positioning of ROVs with Experimental Results

M. Candeloro, A.J. Sørensen, S. Longhi and F. Dukan

The article has been published in the proceedings of the
9th IFAC Conference on Manoeuvring and Control of Marine Craft (MCMC),
IFAC-PapersOnLine
Volume 9 (1), pages 85–90. Arenzano, Italy, 19-21 September 2012.

Observers for Dynamic Positioning of ROVs with Experimental Results ⋆

Mauro Candeloro * **Asgeir J. Sørensen** * **Sauro Longhi** ** **Fredrik Dukan** *

* *Department of Marine Technology and Centre for Ships and Ocean Structures (CeSOS), NTNU, Trondheim, Norway*
** *Department of Information Engineering, UNIVPM, Ancona, Italy*

Abstract: This paper proposes a set of model-based observers included in the DP (Dynamic Positioning) system of the ROV Minerva operated by NTNU. In particular, the observers and the other main components of the DP control system are described. A linear Kalman Filter (LKF), an Extended Kalman Filter (EKF), an adaptive Kalman Filter and a passive nonlinear observer based on the ROV Minerva mathematical models with varying fidelity are proposed. The main aim is to compare different possibilities for the implementation of the observer in a DP control system for ROVs analyzing advantages and drawbacks. Finally, experimental results obtained during DP and tracking operations performed in the Trondheim Fjord are presented.

Keywords: ROV, dynamic positioning, tracking, Kalman filter, passive observer

1. INTRODUCTION

Remotely Operated Vehicles (ROVs) are useful to accomplish missions such as sampling of biological, chemical, geological objects of interests, deep-water archeology, pipeline survey and cable and sub-sea structure inspection, maintenance and repair, and so on.

In order to accomplish those operations an automatic DP control system has been designed. It provides high precision station keeping and maneuvering in varying environmental conditions or sensor failures, leaving to the operators the high-level mission planning.

A control system for underwater vehicles is composed by several modules. Figure 1 shows the main architecture of a ROV DP control system: a *signal processing module* provides a first fault-detection and statistical filtering of the input signals, the *observer module* gives a trustworthy estimation of the system states that allows the *controller module* to produce the desired thrust to reach the reference given by the *guidance module*. The user can define, through the *Graphical User Interface* (*GUI)*, a high-level goal and receive some useful feedback. Finally, the desired control action is distributed to each thruster through the *thruster allocation module*.

In this paper four observers are designed and analyzed for the ROV Minerva. Their characteristics and performance are compared.

⋆ This work has been carried out at the Centre for Ships and Ocean Structures (CeSOS) and the Applied Underwater Robotics Laboratory (AUR-Lab) at NTNU. The Norwegian Research Council and the NTNU program Marine Coasted Development are acknowledged as the main sponsor of CeSOS and AUR-Lab. The research has been carried on for a Master's Thesis (Candeloro, 2011) work, so the extensive discussion of the theory and experiments can be found in it. The authors would like to thank the crew of RV Gunnerus for the invaluable help with the full scale tests.

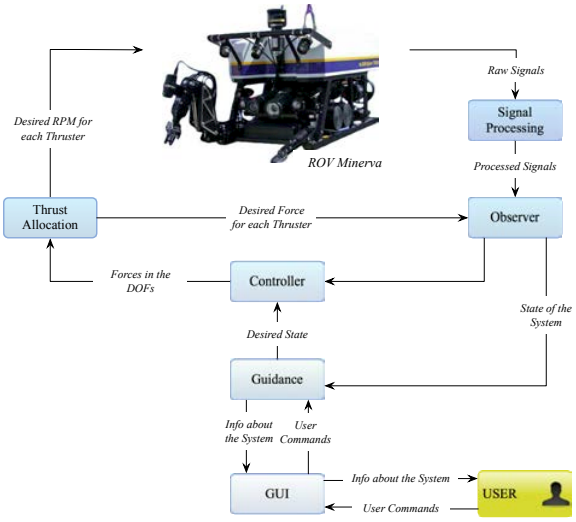

Fig. 1. Main modules of the DP Control System

The main targets of the observer module are:

- estimation of the state vector from the measurements;
- filtering of the measured signals using the additional information contained in the mathematical model;
- provide a trustworthy state prediction of the system by dead reckoning although sensors faults occur;
- estimation of the environmental disturbances;
- optimization of the thruster usage.

This paper is organized as follows: in Section 2 the ROV Minerva system is described, Section 3 introduces the used mathematical models, Section 4 presents the set of observers developed for the ROV. Section 6 reports full-scale results, evaluation and comparisons of the performance, finally Section 7 states the conclusions.

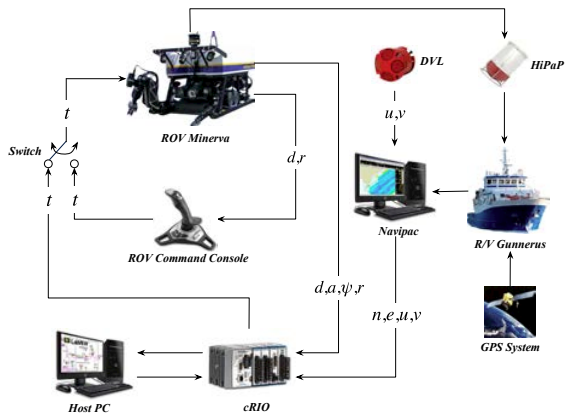

Fig. 2. Main hardware and interconnections of the system: the signal flow is represented.

2. ROV MINERVA

Minerva is a SUB-fighter 7500 ROV made by Sperre AS in 2003 for NTNU (see Sperre-AS). It weights 485Kg in air, it is powered from and communicates with a surface vessel through a 600m umbilical. Minerva is usually deployed from the NTNU Research Vessel (RV) Gunnerus. Detailed specifications of the ROV Minerva can be found in Dukan et al. (2011) or Sørensen et al. (2012).

The National Instruments (NI) CompactRIO (cRIO) programmed with Labview is used for the implementation of the control system. The graphical programming language makes the development and the implementation quick and allows HIL (Hardware-In-the-Loop) and full scale tests.

2.1 Sensors

Figure 2 shows the signal flow through the system and the sensors. The DP control system has access to the following measurements vector:

$$\boldsymbol{x} = [\, x \;\; y \;\; z \;\; \psi \;\; u \;\; v \;\; r \,]^T \tag{1}$$

where:

- (x, y) are the ROV coordinates (north and east) measured by the HiPAP (High Precision Acoustic Positioning) system mounted on the RV Gunnerus. It communicates with the transponder carried by Minerva. The (x, y) coordinates are referred to the North-East-Depth (NED) frame.
- z is the depth, measured by a 100 bar pressure gauge;
- ψ is the heading measured by a fluxgate compass;
- (u, v) are the surge and sway speed components provided by a Teledyne RDI Doppler Velocity Log (DVL); those measurements are referred to the BODY frame.
- r is the yaw rate provided by a CRS03 silicon rate sensor (gyro).

2.2 Thrusters

Minerva has five 2000W thrusters arranged as following: two vertical thrusters, one side thruster with two propellers, a starboard and a port thrusters oriented 10 degrees towards the center line. The forces that this configuration is able to wield in the forward, backward, sideways and down directions have been calculated with experimental tests (Sørensen et al., 2012). In the following the output of the control system (the forces applied to each DOF) will be indicated with the symbol $\boldsymbol{\tau} = [\, \tau_{surge} \;\; \tau_{sway} \;\; \tau_{heave} \;\; \tau_{yaw} \,]^T \in \mathbb{R}^4$.

3. MATHEMATICAL MODEL

In the following subsections the mathematical models used for simulation (Process Plant Model - PPM) and control purposes (Control Plan Model - CPM) will be presented (Sørensen, 2012). The model for ROV Minerva is based on the Newtonian approach originally proposed in Fossen (1994), then adapted for this vehicle in Kirkeby (2010).

3.1 Process Plant Model (PPM)

The PPM accurately describes the environmental effects and the ROV dynamics itself. It is used for simulations and HIL testing (Sørensen, 2012).

The simulation model of the ROV is composed by the kinematics and kinetics equations [1]:

$$\begin{aligned} \dot{\boldsymbol{\eta}} &= \boldsymbol{J}(\boldsymbol{\eta})\boldsymbol{\nu} \\ \boldsymbol{M}\dot{\boldsymbol{\nu}} &= -\boldsymbol{C}_{RB}(\boldsymbol{\nu})\boldsymbol{\nu} - \boldsymbol{C}_A(\boldsymbol{\nu}_r)\boldsymbol{\nu}_r - \boldsymbol{D}_L\boldsymbol{\nu}_r \\ &\quad - \boldsymbol{D}_{NL}(\boldsymbol{\nu}_r)\boldsymbol{\nu}_r - \boldsymbol{G}(\boldsymbol{\eta}) + \boldsymbol{\tau}_{cable} + \boldsymbol{\tau} \end{aligned} \tag{2}$$

This model considers 6 $DOFs$, where $\boldsymbol{\eta} = [\, x \;\; y \;\; z \;\; \phi \;\; \theta \;\; \psi \,]^T \in \mathbb{R}^6$ is defined in the NED frame and $\boldsymbol{\nu} = [\, u \;\; v \;\; w \;\; p \;\; q \;\; r \,]^T \in \mathbb{R}^6$ is defined in the body frame. Notice that ϕ, θ are respectively the roll and pitch angle while p, q are the correspondent rates. The kinematics relates body and NED frames through the transformation matrix $\boldsymbol{J}(\boldsymbol{\eta}) \in \mathbb{R}^{6\times6}$, see Fossen (2011). The kinetics represents the balance of the main forces acting on the ROV, i.e. the Coriolis forces, modeled by $\boldsymbol{C}_{RB}$ and $\boldsymbol{C}_A \in \mathbb{R}^{6\times6}$, that are the rigid body and the added mass components, the damping forces modeled by $\boldsymbol{D}_L$ and $\boldsymbol{D}_{NL} \in \mathbb{R}^{6\times6}$ where the latter contains the viscous drag and current loads. The relative velocity of the vehicle with respect to the fluid is $\boldsymbol{\nu}_r = \boldsymbol{\nu} - \boldsymbol{\nu}_c$, where $\boldsymbol{\nu}_c$ is the velocity vector of the fluid. $\boldsymbol{M} \in \mathbb{R}^{6\times6}$ is the mass matrix of the vehicle, $\boldsymbol{G}(\boldsymbol{\eta}) \in \mathbb{R}^6$ is the restoring force, $\boldsymbol{\tau}_{cable}$, $\boldsymbol{\tau} \in \mathbb{R}^6$ are respectively the drag force of the tether and the control forces vector. $\boldsymbol{M}$ is the sum of the added and the rigid body matrices (under the assumption of irrotational and slow-varying currents, see Kirkeby, 2010).

3.2 Control Plant Model (CPM)

The CPM is a simplified model used as a basis for model-based controllers and for analytical stability analysis such as Lyapunov stability (Sørensen, 2012). The CPM is defined in the *working space* of the vehicle in which the control objective is defined as well.

Under the hypothesis that Minerva is passively stable in pitch (ϕ) and roll (θ) it is possible to state that no actuators are needed to directly operate on those two degrees of freedom (Kirkeby, 2010 and Dukan et al., 2011). The working space of this ROV consists of surge, sway,

[1] In this paper the bold symbols indicate vectors or matrices, the dimensions are specified in the text.

heave and yaw. Moreover, the bias equation is added to handle the unmodelled effects and the slow-varying forces due to the currents (Sørensen, 2012).

$$\begin{aligned} \dot{\boldsymbol{\eta}} &= \boldsymbol{R}(\psi)\boldsymbol{\nu} \\ \boldsymbol{M}\dot{\boldsymbol{\nu}} &= -\boldsymbol{D}(\boldsymbol{\nu})\boldsymbol{\nu} - \boldsymbol{C}(\boldsymbol{\nu})\boldsymbol{\nu} - \boldsymbol{G} + \boldsymbol{R}(\psi)^{-1}\boldsymbol{b} + \boldsymbol{\tau} \\ \dot{\boldsymbol{b}} &= -\boldsymbol{T}_b^{-1}\boldsymbol{b} + \boldsymbol{E}_b\boldsymbol{w} \end{aligned} \tag{3}$$

Where $\boldsymbol{\eta} = [\, x \;\; y \;\; z \;\; \psi \,]^T \in \mathbb{R}^4$, $\boldsymbol{\nu} = [\, u \;\; v \;\; w \;\; r \,]^T \in \mathbb{R}^4$ and $\boldsymbol{b} = [\, b_{surge} \;\; b_{sway} \;\; b_{heave} \;\; b_{yaw} \,]^T \in \mathbb{R}^4$. In the following the symbols $\boldsymbol{\eta}, \boldsymbol{\nu}$ will refer to those reduced vectors. In (3) the transformation matrix $\boldsymbol{J}(\boldsymbol{\eta})$ is reduced to a pure rotational matrix on the yaw variable (Fossen, 2011). The restoring forces vector becomes $\boldsymbol{G} = [\, 0 \;\; 0 \;\; (B - W) \;\; 0 \,]^T \in \mathbb{R}^4$. Here W is the weight of the body and B is the buoyancy force. The two components of the damping and Coriolis forces are collected in one matrix: $\boldsymbol{D}(\boldsymbol{\nu}) = \boldsymbol{D}_L + \boldsymbol{D}_{NL}(\boldsymbol{\nu}) \in \mathbb{R}^{4\times4}$, $\boldsymbol{C}(\boldsymbol{\nu}) = \boldsymbol{C}_{RB}(\boldsymbol{\nu}) + \boldsymbol{C}_A(\boldsymbol{\nu}) \in \mathbb{R}^{4\times4}$. Moreover $\boldsymbol{M}, \boldsymbol{T}_b \in \mathbb{R}^{4\times4}, \boldsymbol{\tau} \in \mathbb{R}^4$ (Kirkeby 2010, Fossen and Fjellstad 1996). Notice that Coriolis has a destabilizing effect on the vehicle that normally is canceled by dissipative effect due to lift effect or transom stern effects that can be included in the damping matrix.

3.3 Simplified Control Plant Model

Assuming low speed, an even more simplified CPM can be obtained by eliminating the nonlinearities in (3).

From (2) the following simplified CPM can be derived:

$$\begin{aligned} \dot{\boldsymbol{\eta}} &= \boldsymbol{R}(\psi)\boldsymbol{\nu} \\ \boldsymbol{M}\dot{\boldsymbol{\nu}} &= -\boldsymbol{D}_L\boldsymbol{\nu} - \boldsymbol{G} + \boldsymbol{R}(\psi)^{-1}\boldsymbol{b} + \boldsymbol{\tau} \\ \dot{\boldsymbol{b}} &= -\boldsymbol{T}_b^{-1}\boldsymbol{b} + \boldsymbol{E}_b w \end{aligned} \tag{4}$$

Where all the symbols meaning was explained above.

4. OBSERVER DESIGN

In the following subsections the design of a Linear (LKF), an Extended (EKF), an adaptive Kalman Filter and a nonlinear passive observer are presented.

4.1 Observer Objective

The main target of the observer module is to reconstruct the state vector. Finally the estimated state vector is defined as following:

$$\hat{\boldsymbol{x}} = \left[\, \hat{x} \;\; \hat{y} \;\; \hat{z} \;\; \hat{\psi} \;\; \hat{u} \;\; \hat{v} \;\; \hat{w} \;\; \hat{r} \,\right]^T \tag{5}$$

that represents the state estimation under the assumption that the system is passively stable in pitch and roll (that means that is assumed $\hat{\theta} \approx \hat{\phi} \approx \hat{p} \approx \hat{q} \approx 0$). $\tilde{\boldsymbol{x}} = \hat{\boldsymbol{x}} - \boldsymbol{x}$ is defined as the estimation error.

4.2 Linear Kalman Filter

This observer is based on the CPM in (4) that can be written, in a general form:

$$\begin{aligned} \dot{\boldsymbol{x}} &= \boldsymbol{A}\boldsymbol{x} + \boldsymbol{B}\boldsymbol{u} + \boldsymbol{E}\boldsymbol{w} \\ \boldsymbol{y} &= \boldsymbol{H}\boldsymbol{x} + \boldsymbol{v} \end{aligned} \tag{6}$$

with:

$$\begin{aligned} \boldsymbol{A} &= \begin{bmatrix} \boldsymbol{0} & \boldsymbol{R}(\psi) & \boldsymbol{0} \\ \boldsymbol{0} & -\boldsymbol{M}^{-1}\boldsymbol{D} & \boldsymbol{M}^{-1}\boldsymbol{R}^T(\psi) \\ \boldsymbol{0} & \boldsymbol{0} & -\boldsymbol{T}_b^{-1} \end{bmatrix}, \quad \boldsymbol{B} = \begin{bmatrix} \boldsymbol{0} \\ \boldsymbol{M}^{-1} \\ \boldsymbol{0} \end{bmatrix} \\ \boldsymbol{E} &= \begin{bmatrix} \boldsymbol{0} & \boldsymbol{0} & \boldsymbol{0} \\ \boldsymbol{0} & \boldsymbol{M}^{-1} & \boldsymbol{0} \\ \boldsymbol{0} & \boldsymbol{0} & \boldsymbol{E}_b \end{bmatrix} \end{aligned} \tag{7}$$

$\boldsymbol{A}, \boldsymbol{E} \in \mathbb{R}^{12\times12}$, $\boldsymbol{B} \in \mathbb{R}^{12\times4}$, $\boldsymbol{H} \in \mathbb{R}^{7\times12}$. $\boldsymbol{w}$, $\boldsymbol{v}$ are white noise vectors of appropriate dimension. Although Coriolis forces and nonlinear damping are not considered, the model contains the nonlinear kinematics relationship due to the heading rotation.

In order to linearize the kinematics the heading domain is divided into 36 sectors, and the dynamic matrix $\boldsymbol{A}(\psi)$ is calculated off-line for each sector and stored in memory. Then the model is discretized and linearized for each sector in order to use the discrete LKF. Notice that it is possible to pre-calculate the solution of the Riccati equations for each sector. By monitoring the heading angle the corresponding model and set of gains are selected by proper switching strategy (some techniques are described in Sørensen, 2012).

The linearized time-discrete state-space model has the following general shape:

$$\begin{aligned} \boldsymbol{x}(k+1) &= \boldsymbol{\Phi}(\psi, k)\boldsymbol{x}(k) + \boldsymbol{\Delta}(\psi, k)\boldsymbol{u}(k) \\ &\quad + \boldsymbol{\Gamma}(\psi, k)\boldsymbol{w}(k) \\ \boldsymbol{y}(k) &= \boldsymbol{H}(k)\boldsymbol{x}(k) + \boldsymbol{v}(k) \end{aligned} \tag{8}$$

The discretization is done with the Euler method, while the linearization is the result of the first-order Taylor expansion calculated on the mean value of each sector:

$$\begin{aligned} \boldsymbol{\Phi}(\psi, k) &= e^{\boldsymbol{A}(t)h} \cong (\boldsymbol{I} + \boldsymbol{A}(t)h) \\ \boldsymbol{\Delta}(\psi, k) &= \int_0^h e^{\boldsymbol{A}(t)h} d\sigma \cong \left(\boldsymbol{I}h + \frac{1}{2}\boldsymbol{A}(t)h^2\right)\boldsymbol{B} \\ \boldsymbol{\Gamma}(\psi, k) &= \int_0^h e^{\boldsymbol{E}(t)h} d\sigma \cong \left(\boldsymbol{I}h + \frac{1}{2}\boldsymbol{A}(t)h^2\right)\boldsymbol{E} \\ \boldsymbol{H}(k) &= \boldsymbol{H}(t) \end{aligned} \tag{9}$$

Where $\boldsymbol{A}, \boldsymbol{B}, \boldsymbol{C}$ are defined in (7) and $h = 0.2s$ is the sampling time used for full-scale tests configuration.

4.3 Extended Kalman Filter

An Extended Kalman Filter is implemented to account for the nonlinearities modeled in the CPM defined in (3).

The included nonlinearities in addition to the kinematic, both dependent by the ROV velocity components, are:

- the *nonlinear damping*;
- the *Coriolis forces*.

The resulting CPM written in state space formulation is:

$$\begin{aligned} \dot{\boldsymbol{x}} &= \boldsymbol{F}(\boldsymbol{x}) + \boldsymbol{B}\boldsymbol{u} + \boldsymbol{E}\boldsymbol{w} \\ \boldsymbol{y} &= \boldsymbol{H}\boldsymbol{x} + \boldsymbol{v} \end{aligned} \tag{10}$$

where the dynamic matrix is a function of the components of the state vector $\boldsymbol{x}$:

$$\boldsymbol{F}(\boldsymbol{x}) = \begin{bmatrix} \boldsymbol{R}(\psi)\boldsymbol{\nu} \\ \boldsymbol{M}^{-1}\begin{bmatrix} \boldsymbol{R}^T(\psi)\boldsymbol{b} - \boldsymbol{G} \\ -\boldsymbol{D}(\boldsymbol{\nu})\boldsymbol{\nu} - \boldsymbol{C}(\boldsymbol{\nu})\boldsymbol{\nu} \end{bmatrix} \\ -\boldsymbol{T}_b^{-1}\boldsymbol{b} \end{bmatrix} \tag{11}$$

Both the linearization and the discretization have to be done at each time step and cannot be calculated off-line; in this case there are no proofs of global asymptotic stability (Sørensen, 2012). The Extended Kalman Filter (see, for instance, Simon (2006) for the complete set of equations) can be used on the state-space model in (10), where (11) is linearized on the estimated state for each time step:

$$\boldsymbol{\Phi}(k) = \boldsymbol{I} + h \left. \frac{\partial \boldsymbol{f}(\boldsymbol{x}(k), \boldsymbol{u}(k))}{\partial \boldsymbol{x}(k)} \right|_{\boldsymbol{x}(k)=\hat{\boldsymbol{x}}(k)} \tag{12}$$

4.4 Adaptive Kalman Filter

An adaptive algorithm is added to the Kalman Filters in order to automatically update the gains of the algorithm by monitoring the estimation error. The following is an application of the adaptive Kalman Filter proposed in Jetto et al. (1999).

The model and sensors error covariance collected into the matrices $\boldsymbol{R}$ and $\boldsymbol{Q}$ are corrected by monitoring the gap between the measured innovation term and its analytical predictions. The shapes of the two covariance matrices are arbitrarily chosen as:

$$\begin{aligned} \boldsymbol{R} &= \sigma_r^2 \cdot diag\left[r_1 \;\; r_2 \;\; \dots \;\; r_7\right] = \sigma_r^2 \cdot \boldsymbol{R}' \in \mathbb{R}^{7\times 7} \\ \boldsymbol{Q} &= \sigma_q^2 \cdot diag\left[q_1 \;\; q_2 \;\; \dots \;\; q_{12}\right] = \sigma_q^2 \cdot \boldsymbol{Q}' \in \mathbb{R}^{12\times 12} \end{aligned} \tag{13}$$

Where $\boldsymbol{R}'$ and $\boldsymbol{Q}'$ are arbitrarily chosen and fixed. The main covariance information used by the Kalman filter is summarized by the ratio of the covariance terms $\frac{r_i}{q_i}$ that can be tuned by changing one term and keeping the other one fixed. So, assuming the covariance characteristics of the sensors to be known (it can be experimentally calculated), it is possible to calculate the covariance matrix of the model (in general very difficult to estimate) as the result of the adaptive algorithm. This algorithm gives the estimation $\hat{\sigma}_q^2$ of the factor σ_q^2 in (13) for each time step, regulating in this way the ratio of the covariance gains. The complete recursive algorithm can be found in Jetto et al. (1999).

4.5 Nonlinear Passive Observer

A nonlinear passive observer for Autonomous Unmanned Vehicles (AUVs) that is able to use all the information contained in the PPM in (2) was proposed in Refsnes (2007). This work is here adapted for ROV applications. Moreover a proportional velocity feedback that avoid to waste accessible information is added (Fossen, 2011).

The following observer is composed by two CPMs working together (Refsnes, 2007). The first CPM is called *Current Induced Vehicle Model* (CIVM) and is defined in (14): it does not include nonlinear terms, it only considers the surge, sway and yaw DOFs [1], and it works together with the *nominal model* defined in (15) in order to give a current estimation (velocity and direction). In particular the nominal model is composed by the Kinematic equation in (4): without considering any injection term it gives information about the vehicle behavior *"in the case of absence of currents"*. By subtracting the velocities given

[1] This assumption can be done if the currents are assumed to be irrotational. In this case they will influence just the motion in the first two degrees of freedom (north and east).

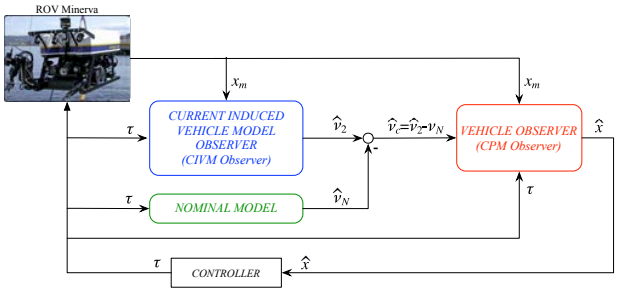

Fig. 3. Main connections between the CIVM, the nominal model and the Vehicle Observer.

by the nominal model from the estimations given by the CIVM it is possible to have a current estimation, as stated in (16).

$$\begin{aligned} \dot{\hat{\boldsymbol{\eta}}}_2 &= \boldsymbol{J}(\psi_2)\hat{\boldsymbol{\nu}}_2 + \boldsymbol{K}_{1p}\tilde{\boldsymbol{\eta}}_2 \\ \boldsymbol{M}\dot{\hat{\boldsymbol{\nu}}}_2 &= -\boldsymbol{D}_L\hat{\boldsymbol{\nu}}_2 + \boldsymbol{\tau} + \boldsymbol{J}^T(\psi)\hat{\boldsymbol{b}}_2 + \boldsymbol{K}_{2p}\tilde{\boldsymbol{\eta}}_2 \\ \dot{\hat{\boldsymbol{b}}}_2 &= -\boldsymbol{T}^{-1}\hat{\boldsymbol{b}}_2 + \boldsymbol{J}^T(\psi_2)\boldsymbol{K}_{3p}\tilde{\boldsymbol{\eta}}_2 \end{aligned} \tag{14}$$

$$\boldsymbol{M}\dot{\boldsymbol{\nu}}_N = -\boldsymbol{D}_L\boldsymbol{\nu}_N + \boldsymbol{\tau} \tag{15}$$

$$\hat{\boldsymbol{\nu}}_c = \left[\hat{u}_2 - u_N \;\; \hat{v}_2 - v_N \;\; \hat{w}_2 - v_N \;\; 0 \;\; 0 \;\; 0\right]^T \tag{16}$$

The second CPM, called *Vehicle Observer* takes in account all the modeled terms defined in the PPM in (2):

$$\begin{aligned} \dot{\hat{\boldsymbol{\eta}}} &= \boldsymbol{J}(\psi)\hat{\boldsymbol{\nu}} + \boldsymbol{K}_{4p}\tilde{\boldsymbol{\eta}} + \boldsymbol{K}_{1v}\tilde{\boldsymbol{\nu}} \\ \boldsymbol{M}\dot{\hat{\boldsymbol{\nu}}} &= -\boldsymbol{D}_L\hat{\boldsymbol{\nu}}_r - \boldsymbol{D}_{NL}(\boldsymbol{\nu}_r)\hat{\boldsymbol{\nu}}_r - \boldsymbol{C}_{RB}(\boldsymbol{\nu})\boldsymbol{\nu} \\ &\quad -\boldsymbol{C}_A(\boldsymbol{\nu}_r)\boldsymbol{\nu}_r + \boldsymbol{\tau} + \boldsymbol{J}^T(\psi)\hat{\boldsymbol{b}} + \boldsymbol{K}_{5p}\tilde{\boldsymbol{\eta}} + \boldsymbol{K}_{2v}\tilde{\boldsymbol{\nu}} \\ \dot{\hat{\boldsymbol{b}}} &= -\boldsymbol{T}^{-1}\hat{\boldsymbol{b}} + \boldsymbol{J}^T(\psi)\boldsymbol{K}_{6p}\tilde{\boldsymbol{\eta}} + \boldsymbol{K}_{3v}\tilde{\boldsymbol{\nu}} \end{aligned} \tag{17}$$

where, in this case, the nonlinear terms are properly estimated by using the current estimation obtained before and the relative velocity, that is given by $\boldsymbol{\nu}_r = \boldsymbol{\nu} - \boldsymbol{\nu}_2$.

The overview of this algorithm is represented in Figure 3.

5. PARAMETERS TUNING PHASE

The main parameters of the Kalman filters are collected in the covariance matrices of the model ($\boldsymbol{Q}$) and sensors errors ($\boldsymbol{R}$). The $\boldsymbol{R}$ is usually known (from the data-sheets of the sensors or calculated with experimental tests), while it is almost impossible to know precisely the $\boldsymbol{Q}$ matrix. Some methods to estimate it are described in literature, or adaptive methods like the one presented in Subsection 4.4 can be used. In this work a trial-error phase was useful to set up the $\boldsymbol{Q}$ matrix given the known $\boldsymbol{R}$. In this phase filtering, transient and dead reckoning properties have been taken in consideration.

The gains used for the passive observer need to be chosen in order to satisfy the required stability and passivity properties. The stability proofs and the relative gains constrains are given in Refsnes (2007) while the stability proof that includes velocity feedback is provided in Candeloro et al. (2012). When all the stability constrains are satisfied an experimental trial-error phase on the real system is required to obtain the desired steady-state and transient behaviors.

Notice that a trial-error tuning phase has to be repeated in full-scale, since the real system can differ substantially from the simulated one.

6. FULL-SCALE RESULTS

Full-scale tests have been performed from autumn 2010 to spring 2011 in the Trondheim fjord, those results are presented and evaluated qualitatively in the following subsections, discussing the reported figures. Notice that, in general, performance indexes are useful to quantify the performance of the algorithms. For the simulations and the full-scale results the IAE, ISE, ITAE indexes and the L^∞ norm [2] have been evaluated and compared. In this paper just some final considerations are reported. Refer to the full thesis work (Candeloro, 2011) for an extensive quantitatively analysis done through performance indexes.

6.1 Squared-Shape Path Test

In this first test the ROV Minerva follows a square-shaped path of $5m$ side, counter-clock wise direction, with fixed heading at $0°$. The starting point is $(n, e) = (0, 0)$. A nonlinear PID controller is used (Kirkeby, 2010). Figure 4 reports both the results for the LKF and the EKF. The estimation errors for x and y are kept under $0.2m$ for the LKF, under $0.25m$ for the EKF. Simulating a HiPAP fault (for a semi-dead reckoning test) the position control error reached peaks of 2m at the end of the path for all the observers. An interesting fact is underlined by the first plot in the second row of Figure 4: with a simulated drop out of the position measurement the estimated path seems rotated of a certain angle if compared with the measured one, revealing a possible misalignment of the DVL sensor.

6.2 Squared-Shape Path Test with Guidance

In this test the ROV is controlled by a guidance system and a PID controller that corrects the velocities in order to follow the path while minimizing the cross-track error. Figures 5(a), 5(b) and 6 show the results that were obtained with the LKF and EKF and the passive observer. The cross track errors is always kept under $0.2m$ in all the cases. The EKF has the best performances all over the path. The estimation error is under the $0.2m$ for both North and East coordinates for the Kalman filters. It reaches $0.25m$ with the nonlinear passive observer.

The same test described above was repeated simulating a dead-reckoning mission, caused by a HiPAP drop out. The position sensors have been excluded from the feedback and only the DVL is used to reconstruct the positions. Right plot in Figure 5(b) shows the results obtained with the EKF; similar results are obtained with the LKF (left plot in Figure 5(b)) with the exception of a bigger drift. Control errors reach $1.8m$ at the end of the path. Worse results have been obtained with the nonlinear observer.

6.3 Adaptive Kalman Filter

In Figure 7(a) the EKF was used with the adaptive modification explained in Subsection 4.4. The system is perturbed with a velocity step in the reference model

[2] Those indexes are respectively the "Integral of the Absolute Error", the "Integral of the Squared Error" and the "Integral of the Time times Absolute Error", their mathematical formulation and properties are explained in Candeloro (2011) and references therein.

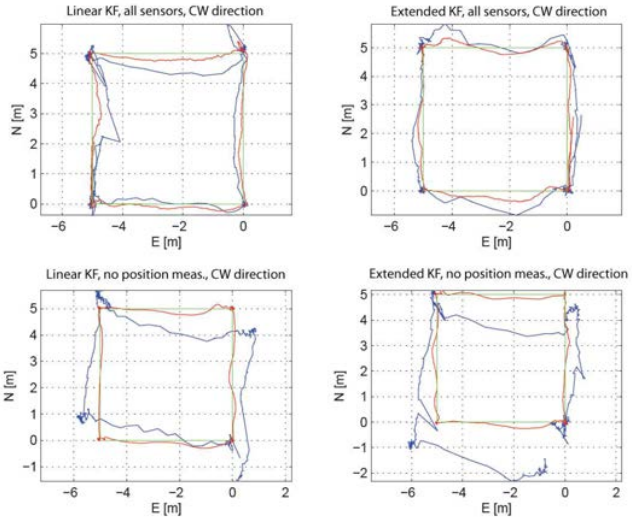

Fig. 4. Squared-shape path test, the ROV keeps its heading fixed at zero degrees. Green, red and blue lines are respectively desired, estimated and measured positions.

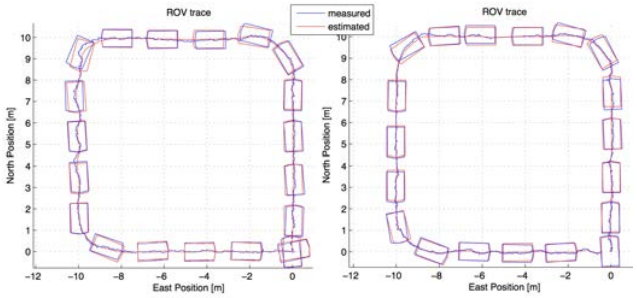

(a) Full sensors configurations.

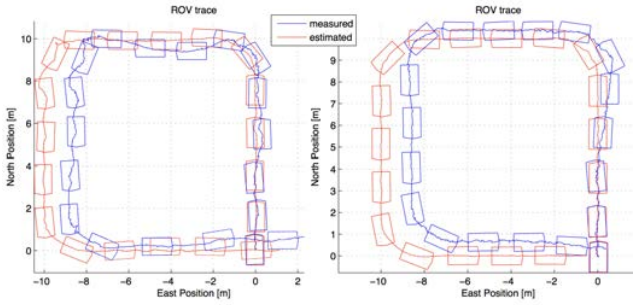

(b) Position sensors excluded.

Fig. 5. Square test with guidance for the LKF (left) and EKF (right) with different sensors configurations.

(*marker "A"* in the Figure): this creates oscillations (during the third side of the square, from the *marker "B"* to the *marker "C"*). From Figure 7(b) it is possible to see how the evolution of the gains calculated by the adaptive algorithm is able to bring the ROV in position again. The performance are comparable with the ones obtained after a long trial-and-error tuning phase, the usage of this algorithm can make the design phase significantly shorter.

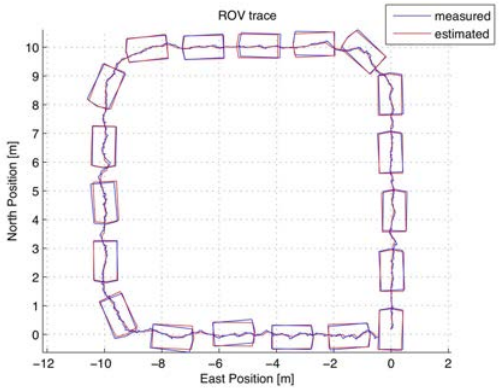

Fig. 6. Square test with guidance for the passive observer.

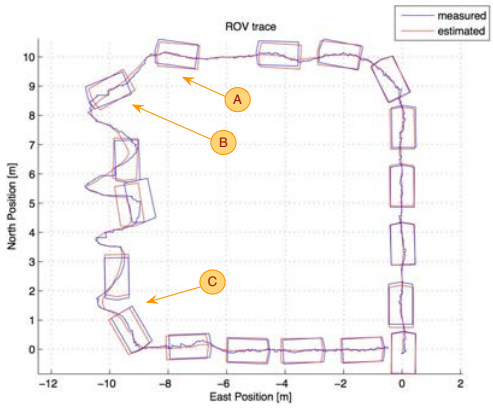

(a) System behavior.

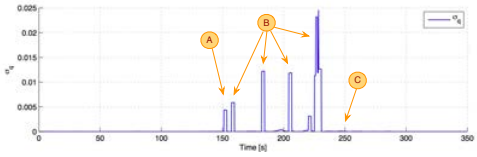

(b) Dynamic of the covariance values ratio $\frac{q_i}{r_i}$.

Fig. 7. Square test with guidance for the EKF with the adaptive modification.

6.4 "S" Path with Guidance

A result obtained with the EKF, the nonlinear PID and the guidance system is reported in Figure 8. The path is challenging and covers a longer distance. This configuration, that gave the best results, kept the estimation error under $0.2m$ with a steady state controlled velocity of $0.3\frac{m}{s}$.

7. CONCLUSIONS

In this paper a set of observer for the ROV Minerva was designed, tested and compared with full-scale tests. In particular the EKF gave the best performance in terms of estimation and control error while the passive filter resulted to be highly sensible on the parameters settings and less accurate. Moreover a LKF and an adaptive tuning algorithm were tested and evaluated. The adaptive algorithm was able to keep high performance by avoiding a long tuning phase. A quantitative comparison of the performance indexes that confirm those statements is in Candeloro (2011).

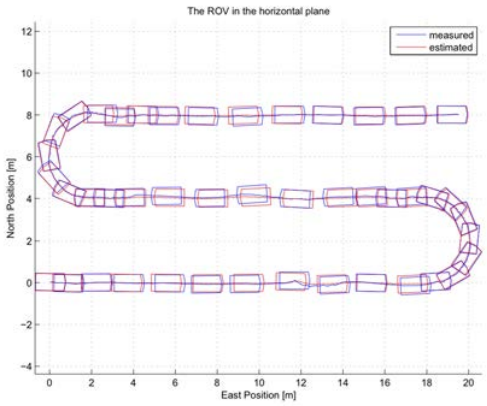

Fig. 8. "S" shape test with guidance, the estimation is provided with the EKF.

REFERENCES

Candeloro, M. (2011). *Design of Observers for DP and Tracking of ROV Minerva with experimental results.* Master's thesis, UNIVPM.

Candeloro, M., F.Dezi, A.J.Sørensen, and S.Longhi (2012). Analysis of a multi-objective observer for uuvs. In *NGCUV, 2012 IEEE - Portugal.*

Dukan, F., M.Ludvigsen, and A.J.Sørensen (2011). Dynamic positioning system for a small size rov with experimental results. In *OCEANS, 2011 IEEE - Spain.*

Fossen, T.I. (1994). *Guidance and Control of Ocean Vehicles.* John Wiley and Sons Ltd, UK.

Fossen, T.I. (2011). *Handbook of Marine Craft Hydrodynamics and Motion Control.* John Wiley and Sons Ltd.

Fossen, T.I. and Fjellstad, O. (1996). Robust adaptive control of underwater vehicles: a comparative study. *Modeling, Identification and Control*, 17(1), 47–61.

Jetto, L., S.Longhi, and G.Venturini (1999). Development and experimental validation of an adaptive extended kalman filter for the localization of mobile robots. *Robotics and Automation, IEEE Transactions on.*

Kirkeby, M. (2010). *Comparison of Controllers for Dynamic Positioning and Tracking of ROV Minerva.* Master's thesis, NTNU.

Refsnes, J.E.G. (2007). *Nonlinear Model-Based Control of Slender Body AUVs.* Ph.D. thesis, Norwegian University of Science and Technology (NTNU).

Simon, D. (2006). *Optimal State Estimation.* Wiley.

Sørensen, A.J. (2012). *Marine Control Systems - Propulsion and Motion Control of Ships and Ocean Structures. Lecture Notes, UK-2012-76.* NTNU.

Sørensen, A.J., F.Dukan, M.Ludvigsen, D.A.Fernandez, and M.Candeloro (2012). *Development of Dynamic Positioning and Tracking System for the ROV Minerva. In Recent Advances in Unmanned Marine Vehicles. G. Roberts and B. Sutton.* Department of Marine Technology, to be published.

Sperre-AS (2012). Subsea technology specialist company. URL `http://ww.sperre-as.com/en/`.

Article D

Analysis of a Multi-Objective Observer for UUVs

M. Candeloro, F. Dezi, A.J. Sørensen and S. Longhi

The article has been published in the proceedings of the
3rd IFAC Workshop on Navigation, Guidance and Control of Underwater Vehicles (NGCUV), IFAC-PapersOnLine
Volume 3 (1), pages 343–348. Porto, Portugal, 10-12 April 2012.

Analysis of a Multi-Objective Observer for UUVs ⋆

Mauro Candeloro * **Fabio Dezi** ** **Asgeir J. Sørensen** *
Sauro Longhi **

* *Department of Marine Technology and Centre for Ships and Ocean Structures (CeSOS), NTNU, Trondheim, Norway*
** *Department of Information Engineering, UNIVPM, Ancona, Italy*

Abstract: UUVs (Unmanned Underwater Vehicles) were introduced in the past to perform various operations in the ocean environment such as marine biology mapping and monitoring, archaeology and oil and gas inspections and interventions. In this paper the operatively range of the UUVs is explored and the possibility of using it in the wave zone is analysed. Then a multi-objective control system that is able to operate into different model regimes could be designed. This aspect moves the main interest to the observer module, that should be able to produce good estimations of the system state regardless from the environment conditions or the mission characteristics. This paper addressed a switching observer for a multi-objective controller where simulation results based on a medium-sized ROV model are reported and discussed.

Keywords: ROV, dynamic positioning, tracking, passive observer, wave zone, currents estimation, multi-objective observer.

1. INTRODUCTION

UUVs such as Remotely Operated Vehicles (ROVs) and Autonomous Underwater Vehicles (AUVs) are useful to accomplish missions such as sampling of biological, chemical, geological objects of interests, deep-water archaeology, pipeline survey and cable inspection, sub-sea structures inspection, maintenance and repair, and so on. The main target of UUVs is to reduce the employment of divers in order to increase the safety and the range of the underwater missions in space and time.

The increased number of operations leads to the necessity of extending the range of environmental conditions and speed regime under which vehicles perform their task with adequate performance and safety (Sørensen et al., 2005). For those kind of challenges a large number of hybrid control systems and adaptive algorithms have been used. For instance hybrid control systems have been widely used in the control of aeroplanes and other land-based vehicles, moreover extensive work on the theory of supervisory switching control has been presented by Hespanha (2001) and Hespanha et al. (2003) and many switching strategies have been proposed in the latest years. Nguyen et al. (2007) introduced and solved this problem for ships, where an hybrid controller solved the problem of the dynamic positioning from calm to extreme sea conditions. In this work those concepts have been used to design a basic structure of a multi-objective observer and a switching logic. It is important to mention that the same issues are often solved using the concept of adaptive control. In a multi-objective observer the supervisory control allows the switching among bank of observers that are *structurally different*; this is needed if the observer needs to handle structural changes in the hydrodynamics (i.e. strong vs low currents) maintaining high performance (Hespanha, 2001) and cannot be done with an adaptive observer, for instance using a gain scheduling algorithm.

In particular a ROV Dynamic Positioning (DP) control system operating both deeply submerged and in the wave zone is considered in this context. The range of the wave zone is dependent on the current sea state and is typical effective down to water depth equal to half of the wave lengths. In this case it is useful not to compensate for the high-frequency wave induced motions resulting in useless waste of energy or inaccurate control due to thrusters saturation.

A general discussion regarding the possibility of usage of a ROV despite high depth, currents forces, wave entity and mission target is reported. Then, using a reduced ROV model, a switching observer module capable to fit different working and environmental conditions is designed. In particular the single components are analysed and the main focus will be on currents estimation and waves filtering. Simulation results based on a Newtonian ROV model are presented and discussed.

The work is organized as following: in Section 2 operational and environmental conditions are discussed. Section 3 presents the ROV mathematical model. In Section 4 the simulation models for the environmental effects are presented. In Section 5 the passive observers (a DP observer, a tracking observer, an observer for the wave filtering and a current observer) are described and designed. Section

⋆ This work has been carried out at the Centre for Ships and Ocean Structures (CeSOS) and the Applied Underwater Robotics Laboratory (AUR-Lab) at NTNU. The Norwegian Research Council and the NTNU program Marine Coasted Development are acknowledged as the main sponsor of CeSOS and AUR-Lab.

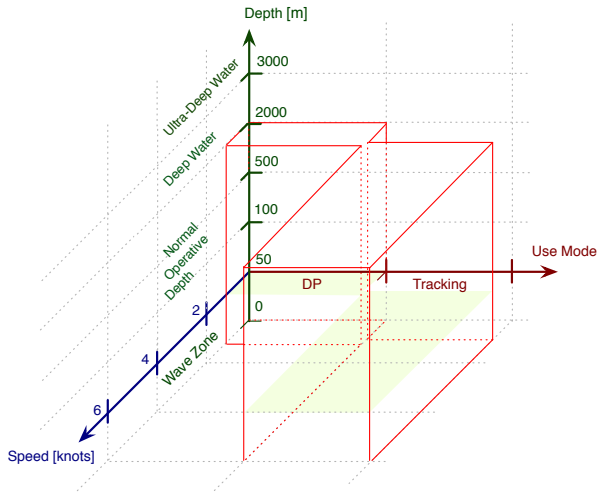

Fig. 1. Relations between use modes, speeds of the ROV and environmental conditions.

6 discusses briefly about gain tuning. Switching logic of the supervisor is briefly discussed in Section 7. Section 8 presents some simulation results. Conclusions and ideas for further work are reported in Section 9. Appendix A presents a mathematical analysis of the passivity and stability properties.

2. ROV WORKSPACE

Figure 1 briefly compares three main aspects that influence the marine control systems design:

- Use mode;
- Sea state;
- Depth.

The figure is inspired by Sørensen et al. (2005) where the authors proposed a hybrid control for ships. The image has been slightly modified in order to introduce the possibility of operating on the wave-zone, that have not been explored widely for this class of vehicles yet.

An UUV could be used for inspection or exploration missions in tracking mode up to 6 knots and manipulations and sea-bed sampling operations with velocity close to zero (DP operation). Finally, it could surmount an obstacle or perform inspection operations in low water depth through the wave zone respectively in tracking and DP mode.

The estimation of the environmental condition is crucial. Its variation from calm to extreme loadings can result in changes of the disturbance characteristics, as well as the control objective and the vehicle desired trajectory. An example may be large variations in current speed and directions, and operation in-and-out the wave zone. Moreover, other aspects that influence the dynamic of the system could be included in Figure 1: the tether will add a strong drag effect especially for deep water and with higher currents, the nonlinear dynamic effects due to Coriolis will be pronounced with higher speed and so on.

3. ROV MATHEMATICAL MODEL

Using the classical Newtonian approach the Process Plant Model (PPM) of an underwater vehicle operating below the wave zone can be written as following (Fossen, 2011):

$$\begin{aligned} \dot{\boldsymbol{\eta}} &= \boldsymbol{J}(\boldsymbol{\eta})\boldsymbol{\nu} \\ \boldsymbol{M}\dot{\boldsymbol{\nu}} &= -\boldsymbol{C}_{RB}(\boldsymbol{\nu})\boldsymbol{\nu} - \boldsymbol{C}_A(\boldsymbol{\nu}_r)\boldsymbol{\nu}_r + \boldsymbol{D}_L\boldsymbol{\nu}_r \\ &\quad + \boldsymbol{D}_{NL}(\boldsymbol{\nu}_r)\boldsymbol{\nu}_r + \boldsymbol{G}(\boldsymbol{\eta}) + \boldsymbol{\tau}_{cable} + \boldsymbol{\tau} \end{aligned} \tag{1}$$

This model is a $6DOFs$ model, where $\boldsymbol{\eta} = [\, x \;\; y \;\; z \;\; \phi \;\; \theta \;\; \psi \,]^T \in \mathbb{R}^6$ is defined in the NED (North-East-Down) frame and $\boldsymbol{\nu} = [\, u \;\; v \;\; w \;\; p \;\; q \;\; r \,]^T \in \mathbb{R}^6$ is defined in the body frame. The kinematics associates the velocities to the positions through the transformation matrix $\boldsymbol{J}(\boldsymbol{\eta}) \in \mathbb{R}^{6\times6}$. This matrix maps the body fixed frame to the NED frame. Kinetics represents the balance of the main forces acting on the ROV that are: Coriolis forces, modelled by $\boldsymbol{C}_{RB}$ and $\boldsymbol{C}_A \in \mathbb{R}^{6\times6}$ (respectively the rigid body and the added mass components), the damping forces modelled by $\boldsymbol{D}_L$ and $\boldsymbol{D}_{NL} \in \mathbb{R}^{6\times6}$ (where the latter contains the viscous drag and current loads). The relative velocity of the vehicle with respect to the fluid is $\boldsymbol{\nu}_r = \boldsymbol{\nu} - \boldsymbol{\nu}_c$, where $\boldsymbol{\nu}$ is the velocity vector of the vehicle and $\boldsymbol{\nu}_c$ is the velocity vector of the fluid. $\boldsymbol{M} \in \mathbb{R}^{6\times6}$ is the mass matrix of the vehicle (including added mass), $\boldsymbol{G}(\boldsymbol{\eta}) \in \mathbb{R}^6$ is the restoring vector force, $\boldsymbol{\tau}_{cable}$ and $\boldsymbol{\tau} \in \mathbb{R}^{6\times1}$ are respectively the force of the tether and the control forces vector.

4. ENVIRONMENTAL MODEL

The proposed observers are able to estimate the responses due to currents and wave loads. The environmental models used in the simulations are explained in the following subsections.

4.1 Current Loads

In this work it is assumed that the current is irrotational (yaw, pitch and roll components are negligible) and it has slow varying speed ($\dot{v}_c \cong 0$), so it can be modelled as a 2-D current with slowly varying speed v_c and direction β_c. v_c is generated as a random walk process $\dot{v}_c = w_1$, where w_1 is the zero-mean white noise. The same dynamics generates the variation of the direction. Finally the current can be defined in the NED frame as following:

$$\boldsymbol{v}_c^{NED} = [\, v_c\cos(\beta_c) \;\; v_c\sin(\beta_c) \;\; 0 \;\; 0 \;\; 0 \;\; 0 \,]^T \tag{2}$$

The current in the body frame is given by:

$$\boldsymbol{v}_c^{BODY} = \boldsymbol{J}(\psi)^{-1}\boldsymbol{v}_c^{NED} \tag{3}$$

4.2 Wave Response

Wave responses are often modelled either with RAO (*Response Amplitude Operators*) based model or linear state-space models (WF models). In this work the wave induced motions is modelled (for each degree of freedom) with the following second-order wave transfer function:

$$h(s) = \frac{K_w s}{s^2 + 2\lambda\omega_0 s + \omega_o^2} \tag{4}$$

The corresponding wave induced motions is given by:

$$\begin{aligned}\begin{bmatrix}\dot{x}_{\omega 1}\\ \dot{x}_{\omega 2}\end{bmatrix} &= \begin{bmatrix}0 & 1\\ -\omega_0^2 & -2\lambda\omega_0\end{bmatrix}\begin{bmatrix}x_{\omega 1}\\ x_{\omega 2}\end{bmatrix} + \begin{bmatrix}0\\ K_\omega\end{bmatrix} w\\ y_\omega &= [0\ 1]\begin{bmatrix}x_{\omega 1}\\ x_{\omega 2}\end{bmatrix}\end{aligned} \tag{5}$$

Here $x_{\omega 2}$ is the amplitude of the wave induced motion, K_ω is defined as $K_\omega = \lambda\omega_0\sigma$, where λ is the damping coefficient, ω_0 is the dominating wave frequency, and σ describes the wave intensity, the model is driven by white noise (w). Those parameters depend by the dominating wave frequency (Fossen, 2011) and were chosen in order to have a realistic behaviour in simulation tests.

As proposed in Sørensen (2012) a linear superposition is assumed, so the resulting motion of (5) is added to the motion in (1). This gives the total motion of the LF (Low Frequency) and WF (Wave Frequency).

5. PASSIVE OBSERVER

A control algorithm needs to have reliable and smooth input signals in every working and environmental condition. A multi-objective observer is proposed in order to handle the various operations and environmental characteristics represented in Figure 1 and summarized in Section 2.

The presented observers are based on a reduced $4DOFs$ model derived from the most general $6DOFs$ model of the ROV described in the previous section. The estimated positions and velocities state vectors become $\hat{\boldsymbol{\eta}} = \begin{bmatrix}\hat{x} & \hat{y} & \hat{z} & \hat{\phi}\end{bmatrix}^T \in \mathbb{R}^4$ and $\hat{\boldsymbol{\nu}} = \begin{bmatrix}\hat{u} & \hat{v} & \hat{w} & \hat{r}\end{bmatrix}^T \in \mathbb{R}^4$.

In the following different observers based on different Control Plant Models (CPMs) are presented. It is convenient to define reduced models based on the *working space* of the system for control purposes if the control system cannot operate on all the DOFs. The simulations are based on the model of the ROV Minerva (operated by NTNU) where no thrusters are able to control the roll and pitch. Moreover it has been shown that ROV Minerva is passively stable in pitch and roll (Dukan et al., 2011).

The passive filter was chosen to solve the estimation problem. This kind of observers has been widely developed, used and commercialized for ships (Fossen, 2011). A passive observer does not require high computational performances as the nonlinear kinematics is handled without any need for linearisation. Kalman filters have been used for decades for those purposes especially in the *extended* version. Note however that there are no proofs of GES (Globally Exponential Stability) for it and that its implementation for complex systems could require the computation of more than one hundred Riccati equations at each step (see, for instance, Candeloro et al., 2012). Although the technology is powerful and easily accessible nowadays it is still an interesting challenge to design a light observer module that is part of a cheap, embedded, fast and performing control system.

5.1 Passive Observer for DP

For DP operations the velocity of the vehicle is close to zero. Moreover, assuming low current velocity it is possible to approximate $\boldsymbol{\nu}_r \simeq \boldsymbol{\nu} \simeq \mathbf{0}$. In general, with low relative velocities, nonlinear effects are negligible (Sørensen and J.Refsnes, 2009), because both Coriolis forces and the nonlinear damping depend by the square of the velocities. Hence, the DP observer (assuming that both positions and velocities measurements are available) becomes:

$$\begin{aligned}\dot{\hat{\boldsymbol{\zeta}}} &= \boldsymbol{A}_\omega + \boldsymbol{K}_\omega\tilde{\boldsymbol{\eta}}_f\\ \dot{\hat{\boldsymbol{\eta}}} &= \boldsymbol{J}(\psi)\hat{\boldsymbol{\nu}} + \boldsymbol{K}_{1p}\tilde{\boldsymbol{\eta}} + \boldsymbol{K}_{1v}\tilde{\boldsymbol{\nu}}\\ \boldsymbol{M}\dot{\hat{\boldsymbol{\nu}}} &= -\boldsymbol{D}_L\hat{\boldsymbol{\nu}} + \boldsymbol{\tau} + \boldsymbol{J}^T(\psi)\hat{\boldsymbol{b}} + \boldsymbol{K}_{2p}\tilde{\boldsymbol{\eta}} + \boldsymbol{K}_{2v}\tilde{\boldsymbol{\nu}}\\ \dot{\hat{\boldsymbol{b}}} &= -\boldsymbol{T}^{-1}\hat{\boldsymbol{b}} + \boldsymbol{J}^T(\psi)\boldsymbol{K}_{3p}\tilde{\boldsymbol{\eta}} + \boldsymbol{K}_{3v}\tilde{\boldsymbol{\nu}}\end{aligned} \tag{6}$$

In this model the nonlinearity is given only by the reduced kinematics matrix $\boldsymbol{J}(\psi) \in \mathbb{R}^{4\times 4}$. The gain matrices $\boldsymbol{K}_{ip}, \boldsymbol{K}_{iv} \in \mathbb{R}^{4\times 4}$ are supposed to be diagonal, positive definite. The unmodelled effects and the slowly varying disturbances are modeled with the *bias* term $\hat{\boldsymbol{b}} \in \mathbb{R}^4$, where the time constants matrix $\boldsymbol{T} \in \mathbb{R}^{4\times 4}$ describes how fast is the model. The "tilde" symbol defines the estimation error: $\tilde{\boldsymbol{x}} = \boldsymbol{y} - \boldsymbol{C}\hat{\boldsymbol{x}}$, where $\boldsymbol{y}$ is the measurements vector. The first equation in (6) acts as a wave load estimator, used to filter out the high frequency motion from the state estimations.

A sketch of the passivity proof with velocity feedback is reported in Appendix A. It recalls the extensive stability proof reported in Fossen (2011).

5.2 Passive Observer for Tracking

For higher relative velocities (tracking operations or with not-negligible current speed) the approximation done in the previous subsection is not valid any more. The main nonlinear effect due to the nonlinear damping is included in the model in (7) while the Coriolis forces are still not included. Notice that Coriolis is having a destabilizing effect on the vehicle that normally will be canceled by dissipative effect due to transom stern effects to be included properly in D_L and D_{NL} (Sørensen and J.Refsnes, 2009).

$$\begin{aligned}\dot{\hat{\boldsymbol{\zeta}}} &= \boldsymbol{A}_\omega\hat{\boldsymbol{\zeta}} + \boldsymbol{K}_\omega\tilde{\boldsymbol{\eta}}_f\\ \dot{\hat{\boldsymbol{\eta}}} &= \boldsymbol{J}(\psi)\hat{\boldsymbol{\nu}} + \boldsymbol{K}_{1p}\tilde{\boldsymbol{\eta}} + \boldsymbol{K}_{1v}\tilde{\boldsymbol{\nu}}\\ \boldsymbol{M}\dot{\hat{\boldsymbol{\nu}}} &= -\boldsymbol{D}_L\hat{\boldsymbol{\nu}}_r - \boldsymbol{D}_{NL}(\boldsymbol{\nu}_r)\hat{\boldsymbol{\nu}}_r + \boldsymbol{\tau} + \boldsymbol{J}^T(\psi)\hat{\boldsymbol{b}} +\\ &\quad \boldsymbol{K}_{2p}\tilde{\boldsymbol{\eta}} + \boldsymbol{K}_{2v}\tilde{\boldsymbol{\nu}}\\ \dot{\hat{\boldsymbol{b}}} &= -\boldsymbol{T}^{-1}\hat{\boldsymbol{b}} + \boldsymbol{J}^T(\psi)\boldsymbol{K}_{3p}\tilde{\boldsymbol{\eta}} + \boldsymbol{K}_{3v}\tilde{\boldsymbol{\nu}}\end{aligned} \tag{7}$$

$\boldsymbol{D}_{NL}$ is the nonlinear damping matrix that will depend by the relative velocity $\boldsymbol{\nu}_r$. As before, $\boldsymbol{K}_{ip}, \boldsymbol{K}_{iv} \in \mathbb{R}^{4\times 4}$ are proposed to be diagonal, positive definite.

5.3 Wave Filtering

The wave load estimator is represented by the first equation in (6) and (7). It is used to filter out the main effect of the waves, in order not to let the thrusters compensate for it (Fossen 2011). Its effect is represented in Figure 2, where it is clear that the notch effect centred in ω_0 should filter out the main components of the wave spectra.

The key of the performance of this filter is the estimation of the dominant wave frequency ω_0: the more accurate the main frequency estimation the better the spectrum compensation. The estimation of this value is not treated here; some techniques can be found in literature: in Nguyen et al. (2007) an on-line spectral analysis of the measurements is used in order to extract its main frequency, Sørensen (2012), proposes an adaptive algorithm. In this

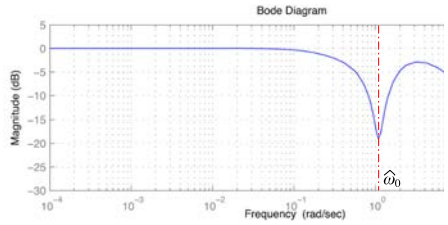

Fig. 2. Transfer function between $\boldsymbol{\eta}$ and $\hat{\boldsymbol{\eta}}$.

work the main frequency is approximated of an analysis of the spectra of the measured then used in the observer.

Notice that the proportional correction in wave filter uses the high-pass filtered position ticular the following equation will hold (Sør

$$\tilde{y}_f^{(i)}(s) = \frac{T_{fi}s}{1+T_{fi}}\tilde{y}^{(i)}(s)$$

Where T_{fi} is the filter time constant. This out, at this stage, other important effect varying currents motion.

Notice that the waves hydrodynamics introd *switch* of the filtering effect. This is due to th waves load decreases exponentially with dep 1990). So, the estimations of the waves lo (7) will converge to zero for high depths depths higher than half of the wave length, the wave is considered negligible) and autonomously exponer increase for decreasing depths. Notice however tha wave filter cannot handle properly this exponential for fast depth changes because of its own dynamic in order to increase its velocity, it is possible to *force* the wave filtering to include the exponential effect. A factor that reproduces the waves dynamics is then introduced:

$$\hat{\boldsymbol{\eta}}_{WF_d} = e^{-k\hat{z}}\hat{\boldsymbol{\eta}}_{WF_0} \tag{9}$$

where $k = \frac{\omega_0^2}{g} = \frac{2\pi}{\lambda}$ is the wave number and depends by the sea state. $\hat{\boldsymbol{\eta}}_{WF_d}$ is the waves frequency estimation on the position state vector at depth d, $\hat{\boldsymbol{\eta}}_{WF_0}$ is the waves frequency estimation on the position state vector at depth $d = 0$ and $\hat{z}$ is the depth estimation, typically found by filtering the measurement of a pressure gauge.

5.4 Current Estimation

A current observer can be crucial for the performance of a control system. In this work its importance is that it can be used to get an estimation of the relative velocity. The following scheme is inspired by the work for AUVs of Refsnes (2007), and it is summarized in Figure 3.

The DP observer (6) receives as inputs the measured state of the system and the thrusters forces on the DOFs. This model asymptotically converges to the real state (Appendix A and Refsnes 2007), that means $\hat{\boldsymbol{\eta}} \to \boldsymbol{\eta}$, $\hat{\boldsymbol{\nu}} \to \boldsymbol{\nu}$ and $\hat{\boldsymbol{b}} \to \boldsymbol{b}$, where $\boldsymbol{b}$ mainly contains the nonlinear unmodelled terms, the parameters uncertainties, the cable drag and the current effects. On the other side, a *nominal model* (that reproduces the ROV dynamics and receives as input just the control forces) produces the estimation of the velocities *as they would be if no current would*

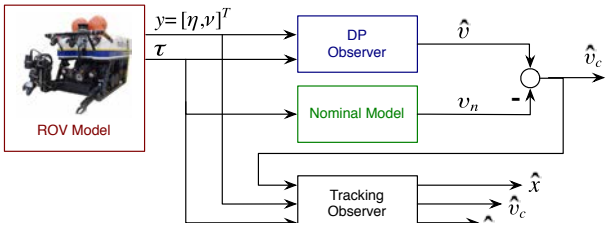

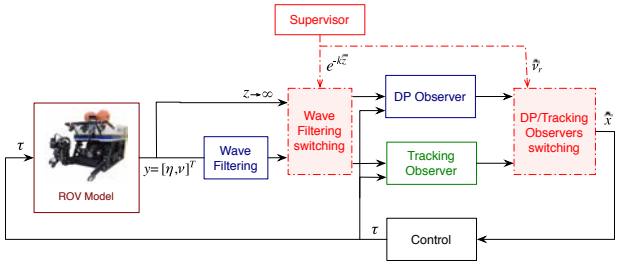

Fig. 4. Overview of the multi-objective observer.

affect the system. Moreover, the nominal model is affected by the same modelling uncertainties of the DP observer. Finally, an estimation of the current can be obtained by subtracting the velocities estimation provided by the nominal model from the ones given by the DP observer.

The measured state, its estimation provided by the first observer, the current estimation and the thrusters forces are then given as inputs to the tracking observer (7) that produces a reliable estimation of the state (by modelling the nonlinear terms using the current estimation).

6. GAIN TUNING

The gains used for the observers in (6) and in (7) need to assure the required stability and passivity properties. It is possible to prove the Globally Exponential Stability (GES) for the basic passive observer and for the passive observer with wave filtering (Fossen, 2011). Moreover a sketch of the proof with velocity feedback is reported in Appendix A. If an adaptive rule is used to tune the wave filter in the passive observer it is possible to avoid the manual tuning of the $\boldsymbol{K}_\omega$ (Sørensen, 2012). When all the stability constrains are satisfied (for instance the Lyapunov stability proofs includes the KYP, Kalman-Yakubovich-Popov lemma that gives those constrains) a trial-error phase is required to improve the performances of the transient and obtain the desired behaviour.

7. SWITCHING CRITERIA

The proposed multi-objective observer, as any hybrid control system, presents a hierarchical structure which relies on two main components:

- A high-level supervisory system that selects the appropriate observer for the particular operation;
- A set of observers that target the different operations and conditions;

Table 1. Simulated wave amplitudes.

Depth [m]	0	2	5	10
Wave Amplitude [m]	0.4521	0.3996	0.3123	0.1686

In the estimator-based supervision, the supervisor com pares the behaviours of some admissible models with th actual process, and then decides which model is the bes to describe the ongoing process. More about the stat of art about the hybrid control for UUVs can be foun in Sørensen and J.Refsnes (2009), Sørensen et al. (2005 Nguyen et al. (2007) and references therein.

In particular two main concepts are used to select th observer during the ROV operation. The wave filters in cluded in (6) and (7) are *naturally switched* because the hydrodynamics of the waves, as explained above. Th exponential weight that simulate this effect is also include to change the dynamics of the wave filtering during fas depth changes. In general this term will act as an auto- matic and smooth switch. Moreover the tracking observer (7) is more accurate with higher relative velocities, while the DP observer (6) can approximate well the behaviour only if the relative velocity is low. So the supervisor can switch between those two whenever the estimated relati velocity over/under-goes a fixed threshold. The chang from the DP to the tracking observer can be implemente by using a low-pass filter, an hysteresis method and weighting function α_c (as described in Nguyen et al., 2007

$$\hat{\boldsymbol{\eta}}_{DP\to track} = \alpha_c(t-t_0)\hat{\boldsymbol{\eta}}_{track} + (1-\alpha_c(t-t_0))\hat{\boldsymbol{\eta}}_{DP}; \quad (1$$

In other words the switching logic aims to detect where Figure 1 the system is to select the proper algorithm b monitoring the estimation of some *key variables* (dept and relative velocity), see Figure 4.

8. SIMULATION RESULTS

Figure 5 shows a DP application: the ROV is kept position while a slowly varying current with $|\nu_c| \approx 0.2\frac{m}{s}$ pushes the ROV mainly along the north direction. The estimation of the current is then made with (7) and the procedure explained in Subsection 5.4. In this case the tracking observer is used, in fact although the ROV is keeping its position, the relative velocity is still high: $|\nu_r| = |\nu| - |\nu_c| \approx |\nu_c| \approx 0.2\frac{m}{s}$. We can see that the current estimation is stable and accurate although the headi changes in fast steps. Notice that the current estimati is referred to the NED frame.

In Figure 6 the ROV is in DP on the wave zone. The dep is gradually decreased until the ROV reaches $z = 2m$. It possible to see how the waves load increases its magnitu while the ROV is reaching the surface. In this case current was included in the simulations ($\boldsymbol{\nu}_r = \boldsymbol{\nu} \approx \mathbf{0}$), the DP observer in (6) is selected. It is possible to see th the wave load is highly filtered out and the x, y coordinat are kept constant while changing depths. An importa advantage in wave filtering is the reduction of the thruste usage (bottom plot in Figure 6) that increases the contr performance, avoids the saturation of the thrusters a saves energy. The simulated waves at the sea surface h wave length $\lambda = 8.1074m$, period $T = 5.712s$, dominati frequency $\omega_0 = 1.1\frac{rad}{s}$. Moreover their impact on the RO for the various depths is summarized in Table 1.

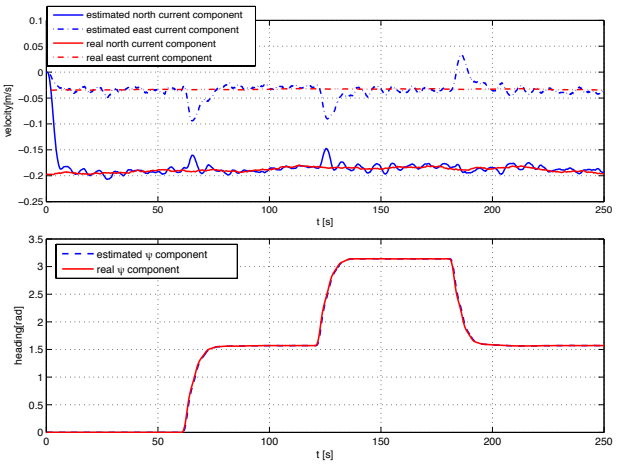

Fig. 5. DP operation with current below the wave zone. The top plot compares $\boldsymbol{\nu}$ and $\boldsymbol{\nu}_c$. The ROV is keeping its north and east coordinates while changing heading.

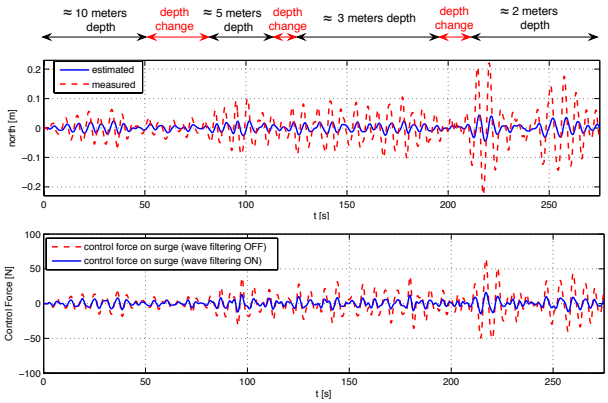

Fig. 6. DP simulation in the wave zone, the depth is changed fast to test various wave loads. Top plot compares x and $\hat{x}$, bottom plot shows the thruster action with and without the wave filtering.

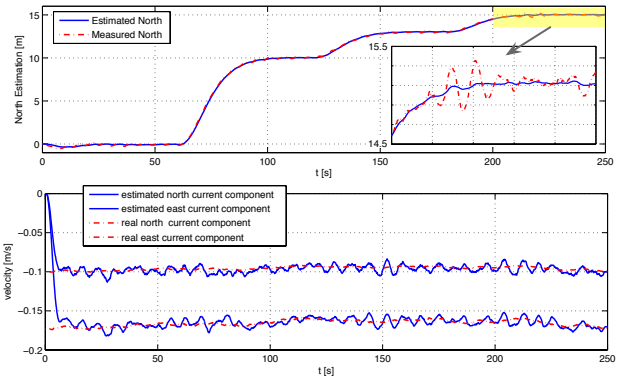

Fig. 7. A tracking operation shows the current observer and the wave filter working together. Top plot compares x and $\hat{x}$, the bottom one compares $\boldsymbol{\nu}$ and $\boldsymbol{\nu}_c$.

Finally a tracking operation was done with both currents and wave effect in constant depth. The ROV makes some steps along the north direction. From figure 7 both the current estimation and the wave filtering run together. The current is slowly varying and its direction is mainly along the north direction. In the top picture the effect of the wave filtering is also clear from the zoom window.

9. CONCLUSIONS

This paper addressed design considerations towards model-based multi-objective observers of underwater vehicles conducting a diversity of missions. Challenges related both to the environment and to the kind of operation were discussed. In particular waves and currents loads and DP and tracking operations were considered. A switching algorithm has been developed to switch between the DP and tracking observers and include/exclude the exponential effect in the wave filtering. Finally the observers have been simulated with a ROV Process Plant Model, in order to show the concepts and the performance. The presented concepts are in an early stage and will be extended with further work. In particular more characteristics of the dynamic of the underwater vehicles will be addressed and considered in the designing stage, an on-line algorithm to estimate the main wave frequency will be developed. The most general $6DOFs$ will be implemented so that full-scale data can be collected both from ROVs and AUVs.

REFERENCES

Candeloro, M., A.J.Sørensen, S.Longhi, and F.Dukan (2012). Observers for dynamic positioning of rovs with experimental results, submitted. In *Submitted to MCMC, 2012 Arenzano, Italy*.

Dukan, F., M.Ludvigsen, and A.J.Sørensen (2011). Dynamic positioning system for a small size rov with experimental results. In *OCEANS, 2011 IEEE - Spain*, 1 –10. doi:10.1109/Oceans-Spain.2011.6003399.

Faltinsen, O. (1990). *Sea Loads on Ships and Offshore Structures*. Cambridge University Press.

Fossen, T. (2011). *Handbook of Marine Craft Hydrodynamics and Motion Control*. John Wiley and Sons, UK.

Hespanha, J. (2001). Tutorial on supervisory control. *Lecture notes for the workshop control using logic and switching for the 40th conference on decision and control, Orlando, Florida*.

Hespanha, J., D.Liberzon, and A.S.Morse (2003). Hysteresis-based switching algorithms for supervisory control of uncertain system. *Automatica*, 39(2).

Khalil, H. (2002). *Nonlinear Systems*. Pearson Education.

Nguyen, T., A.J.Sørensen, and S.T.Quek (2007). Design of hybrid controller for dynamic positioning from calm to extreme sea conditions. *Automatica*, 43, 768–785.

Refsnes, J. (2007). *Nonlinear Model-Based Control of Slender Body AUVs*. Ph.D. thesis, Norwegian University of Science and Technology (NTNU).

Sørensen, A. (2012). *Marine Control Systems - Propulsion and Motion Control of Ships and Ocean Structures. Lecture Notes, UK-2011-76*. Department of Marine Technology, NTNU.

Sørensen, A. and J.Refsnes (2009). Towards supervisory-switched control of hybrid underwater vehicle. *International Journal of the Society for Underwater Technology*, 28, 141–150.

Sørensen, A., S.T.Quek, and T.D.Nguyen (2005). Improved operability and safety of dp vessels using hybrid control concept. In *OSV, 2005 Singapore*.

Appendix A. SKETCH OF THE PASSIVITY PROOF

The inclusion of the proportional correction of the velocity does not compromise the stability proof of the observer, that can be found, for instance, in Fossen (2011) or Sørensen (2012). In particular the proof in Fossen (2011) can be slightly modified as following. Considering the mathematical model in (1) as the unknown process it is possible to show the passivity by studying the error system given by the comparison between the CPM model in (A.1) and (5.1).

$$\begin{aligned} \dot{\hat{\boldsymbol{\zeta}}} &= \boldsymbol{A}_\omega \\ \dot{\hat{\boldsymbol{\eta}}} &= \boldsymbol{J}(\psi)\hat{\boldsymbol{\nu}} \\ \boldsymbol{M}\dot{\hat{\boldsymbol{\nu}}} &= -\boldsymbol{D}_L\hat{\boldsymbol{\nu}} + \boldsymbol{\tau} + \boldsymbol{J}^T(\psi)\hat{\boldsymbol{b}} \\ \dot{\hat{\boldsymbol{b}}} &= -\boldsymbol{T}^{-1}\hat{\boldsymbol{b}} \end{aligned} \tag{A.1}$$

Subtracting the (A.1) from the (5.1) the error system can be found:

$$\begin{aligned} \begin{bmatrix} \dot{\tilde{\boldsymbol{\zeta}}} \\ \dot{\tilde{\boldsymbol{\eta}}} \end{bmatrix} &= \left[\begin{bmatrix} \boldsymbol{A}_\omega & \boldsymbol{0} \\ \boldsymbol{0} & \boldsymbol{0} \end{bmatrix} - \begin{bmatrix} \boldsymbol{K}_\omega \\ \boldsymbol{K}_{1p} \end{bmatrix} \begin{bmatrix} \boldsymbol{C}_\omega & \boldsymbol{I} \end{bmatrix} \right] \begin{bmatrix} \tilde{\boldsymbol{\zeta}} \\ \tilde{\boldsymbol{\eta}} \end{bmatrix} + \begin{bmatrix} \boldsymbol{0} \\ -\boldsymbol{K}_{1v} \end{bmatrix} \boldsymbol{J}(\psi)\tilde{\boldsymbol{\nu}} = \\ &= \left[\boldsymbol{A}_0 - \boldsymbol{K}_0\boldsymbol{C}_0 \right] \tilde{\boldsymbol{\eta}}_0 + \boldsymbol{B}_0\boldsymbol{J}(\psi)\tilde{\boldsymbol{\nu}} \\ \boldsymbol{M}\dot{\tilde{\boldsymbol{\nu}}} &= -\boldsymbol{D}\tilde{\boldsymbol{\nu}} + \boldsymbol{J}(\psi)^T\tilde{\boldsymbol{b}} - \boldsymbol{J}(\psi)^T\boldsymbol{K}_{2p} - \boldsymbol{K}_{2v}\tilde{\boldsymbol{\nu}} = \\ &= -(\boldsymbol{D} + \boldsymbol{K}_{2v})\tilde{\boldsymbol{\nu}} - \boldsymbol{J}(\psi)^T\tilde{\boldsymbol{z}} \\ \dot{\tilde{\boldsymbol{b}}} &= -\boldsymbol{T}^{-1}\tilde{\boldsymbol{b}} - \boldsymbol{K}_{3p}\tilde{\boldsymbol{\eta}} - \boldsymbol{J}(\psi)\boldsymbol{K}_{3v}\tilde{\boldsymbol{\nu}} \end{aligned} \tag{A.2}$$

that can be rewritten as a cascade of two dynamical systems in the following way:

$$\begin{aligned} \boldsymbol{H}_2 &\begin{cases} \dot{\tilde{\boldsymbol{x}}} = \begin{bmatrix} \tilde{\boldsymbol{\eta}}_0 \\ \tilde{\boldsymbol{b}} \end{bmatrix} = \boldsymbol{A}\tilde{\boldsymbol{x}} + \boldsymbol{B}\boldsymbol{J}(\psi)\tilde{\boldsymbol{\nu}} \\ \tilde{\boldsymbol{z}} = \boldsymbol{C}\tilde{\boldsymbol{x}} \end{cases} \\ \boldsymbol{H}_1 &\left\{ \boldsymbol{M}\dot{\tilde{\nu}} = -(\boldsymbol{D} + \boldsymbol{K}_{2v})\tilde{\boldsymbol{\nu}} + \boldsymbol{\epsilon}_z \right. \end{aligned} \tag{A.3}$$

That is the feedback connection of two dynamical systems as represented in Fossen, 2011. A feedback system as the one composed by $\boldsymbol{H}_1$ and $\boldsymbol{H}_2$ is passive if one of the subsystems is strictly passive and the other one is passive (Khalil, 2002).

Taking $S_1 = \frac{1}{2}\tilde{\boldsymbol{\nu}}^T\boldsymbol{M}\tilde{\boldsymbol{\nu}}$ as Lyapunov function it is possible to see that $\boldsymbol{H}_1$ is state strictly passive: the modification due to the $\boldsymbol{K}_{2v}$ matrix increase the damping in (A.3), and so the passivity of the system. Moreover the system $\boldsymbol{H}_2$ is passive if the gain matrices $\boldsymbol{K}_{ip}, i = 1 \dots 3$ and $\boldsymbol{K}_{iv}, i = 1 \dots 3$ are chosen such that the Kalman-Yakubovich-Popov lemma holds (Khalil, 2002). In this case the presence of adjunctive gain matrices gives more freedom to find the values to respect the lemma.

Article E

HMD as a new Tool for Telepresence in Underwater Operations and Closed-Loop Control of ROVs

M. Candeloro, E. Valle, M.R. Miyazaki, R. Skjetne, M. Ludvigsen, A.J. Sørensen

The article has been published in the proceedings of the
MTS/IEEE OCEANS 2015.
Washington DC, USA, 19-22 October 2015.

HMD as a new Tool for Telepresence in Underwater Operations and Closed-Loop Control of ROVs

Mauro Candeloro, Eirik Valle, Michel R. Miyazaki, Roger Skjetne, Martin Ludvigsen, Asgeir J. Sørensen
Centre for Autonomous Marine Operations and Structures (AMOS),
Norwegian University of Science and Technology (NTNU)
Otto Nielsens veg 10, NO-7491 Trondheim, Norway
Email: mauro.candeloro@ntnu.no, eirik.valle@gmail.com, michel.r.miyazaki@ntnu.no,
roger.skjetne@ntnu.no, martin.ludvigsen@ntnu.no, asgeir.sorensen@ntnu.no

***Abstract*—With the recent development of computer graphics and video-gaming, 360° cameras and related technologies, Head Mounted Displays (HMDs) are becoming a popular tool to improve the users experience and efficiency. This trend is also connected to the computer technology improvements of the latest years and its price decrease: HMDs are now more performing and, at the same time, commercially accessible to the masses.**

In this paper a HMD is used to improve the telepresence experience, to increase the situational awareness during underwater operations, and to actively control a Remotely Operated Vehicle (ROV). Although HMDs are already used to actively control the *point of view* of the operator by moving the camera system of vehicles, in this paper they are used to control the vehicle itself, providing a hand-free Human-Machine Interface (HMI). In this way the operator has the possibility of controlling other devices (e.g. a manipulator attached to the ROV) *while* moving the ROV, highly increasing the efficiency of the underwater operations.

Three control methods inspired by previous work developed for the classical joystick interface are presented, full-scale experiments and conclusions on the usability of the proposed solution for real off-shore operations are discussed.

I. Introduction

A Head (or Helmet) Mounted Display (HMD) is, as the name implies, a device containing one or more displays that is attached to the head (or the helmet) of an operator. Depending by its configuration it can display the same image or different views to the eyes, providing, in the latter case, a stereoscopic view. With the decrease of price of inertial sensors and Micro-Electro-Mechanical Systems (MEMS), most of the HMDs available in the market have integrated inertial sensors to track the user's head attitude in its Degrees Of Freedom (DOFs): roll, pitch and yaw.

Although some prototypes of those devices have their roots back in the 60s, and even if the research on those devices never stopped since, they became highly popular in the commercial market only in the latest years, in connection with the development of the computer technology and of related products: for example HMDs offer a completely new approach to video-gaming, since the user can feel *inside* a virtual world, instead of an external viewer. The HMD sensors allows the user to move his visual perspective inside that virtual world, giving a fully immersive experience. Some producers of flying drones provides the possibility of viewing the cameras on supported HMDs, providing to the user a first-person perspective of the flight. The recently introduced 360° cameras, in connection with HMDs, can also provide the possibility of get different views of the vehicle surroundings by moving the head towards the point of interest.

As described in the previous examples, those devices can accomplish different goals depending by the application. In this context it is important to define the following terms [22]:

- **Virtual Reality** (VR): a computer-generated simulation of a three-dimensional image or environment that can be interacted with in a seemingly real or physical way by a person (e.g. video-gaming applications);
- **Augmented Reality** (AR): a technology that superimposes a computer-generated image on a user's view of the real world (e.g. drones control applications);
- **Telepresence**: the use of virtual reality technology for remote control of machinery or for apparent participation in distant events (e.g. remote vehicles control).

In this paper the telepresence aspect is mainly treated, although augmented reality could have a great impact for the further development of this technology. A recent overview of the aspects of virtual reality in connection with the usage of HMDs is provided in [15].

Notice that, as briefly mentioned above, the idea of using stereoscopy and HMDs to increase the effectiveness of certain teleoperations is not a novel idea. The first related reference can be found, to the knowledge of the authors, in [13], where the feasibility of monocular HMDs for aerospace applications was studied. In this paper is in fact mentioned:

"The exact nature of the visual displays utilized in a space ship will depend on precisely what operations man is expected to perform [during] a given mission [...]. Nonlinear displays and other relatively novel display characteristics should not be overlooked or neglected in attempting to find an adequate solution to... [such problems]."

Since then, many others have used such technology for different applications: [14] proposes a first approach to use HMDs for telemanipulation, where the effectiveness of such approach is investigated. The head motion is linked to the motion of cameras on the area where the manipulator is operating, freeing the operator's hands from the need of controlling the cameras orientation. [2] lists possible applications of the HMD technology, spanning between military, space exploration,

978-0-933957-43-5 ©2015 MTS

aviation, industrial and medicine applications. [24] and [7] suggest some HMDs prototypes for medical applications. [3] proposes a telepresence system to visit museums, [16] uses a HMD to better operate excavation field robot. Some research is also focused on understanding the problems of motion sickness and nausea given by the prolonged used of HMDs, that can highly impact on the effectiveness and that is one of the main obstacles to a wider employment of this technology, see for example [19], [18] or [4]. [18] is also a good review of the HMD technology in connection with teleoperation. Moreover comparative results with standard interfaces are presented.

In this paper the usage of HMDs is explored with the objective of increasing the telepresence experience and the situational awareness while operating a Remotely Operated Vehicle (ROV); moreover the motion of the vehicle is controlled by the operator (by moving his head) through a HMD.

Notice that a similar work has been done in [18] for land robots, while there exist no similar work published for underwater vehicles, to the best knowledge of the authors. [27] approached this vision from an industrial design point of view, suggesting the possibility of employing HMDs for underwater operations.

In this paper the interest is mainly focused in knowing if this could actually replace the classical joystick control for underwater operations in the future, especially for operations where the employment of the classical joysticks means the need of two operators at the same time. This is relevant because the usage of the HMDs would leave the operator with both the hands free to operate other tools than the vehicle itself; in particular would be possible to control manipulator(s) mounted on the vehicle *while* controlling the vehicle motion. Nowadays those two operations (control of the vehicle and of the manipulator) can only be done by two operators. This results in a challenging situation due to the necessary tasks synchronization: the inputs that one operator give to one system (e.g. the ROV) cannot disregard (and will influence) the inputs that the other operator is giving to the system he is controlling (e.g. the manipulator). This will necessarily cause many small corrections that can make the operations imprecise or slow. A more efficient operation is expected if one operator could control the whole system.

This paper is organizes as following: Section II briefly presents the ROV used for the experiments and its applications, Section III presents the used HMD, Section IV presents the cameras and the stereo-rig mounted on the vehicle. Section V describes the software used to process the HMD images and the interface to the ROV control software. Section VI presents the algorithms that use the HMD attitude output to control the vehicle motion. Section VII shows the experimental results obtained in May 2015 in Trondheimsfjorden, Norway. Finally, Section VIII states the conclusions, possibilities and limitations of this technology and possible further work.

II. The 30k ROV

A. Vehicle Description

The 30K ROV is a work class ROV that is powered from and communicates with a surface vessel through a $1000m$ umbilical (Figure 1). All systems needed for operation such as power supply, navigation computers and monitors are fitted inside a control container carried by the aforementioned vessel. It weights $1800\mathrm{Kg}$, and its dimensions are respectively $260, 150, 160\mathrm{cm}$ for length, width and height. Maximum depth rating is $1000\mathrm{m}$. It is propelled by six $3000\mathrm{W}$ thrusters, two horizontal, three vertical and one lateral.

30k is equipped with a 7DOFs hydraulically-powered Raptor manipulator from Kraft Telerobotics connected with a joystick that reproduces its kinematics, provides force feedback and allows for master/slave control of the device.

The sensors payload includes an X-Sens100 IMU, a transponder that communicates with a Kongsber High-Precision Acoustic Positioning (HiPAP) system, a Teledyne RDI Workhorse Doppler Velocity Log (DVL), a Valeport mini Pressure Sensor. For a detailed list of specifications, refer to [26], [9] and [5]. Figure 2 shows the vehicle, the sensors payload and the connections with the control devices.

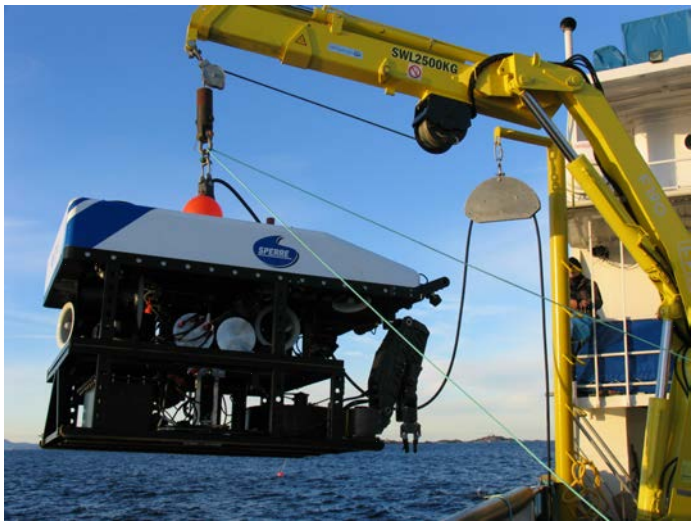

Fig. 1. Sperre 30k work-class ROV in the launch phase.

B. Standard Operations

The Applied Underwater Robotics Laboratory (AUR-Lab) of NTNU, Norway, operates the vehicle mainly in two different ways depending by the operations needs: for manipulation work, picking operations, sensor deployment operations (and so on) two operators are needed: one controls the vehicle by using the ROV control console provided by the vendor (Figure 2), and the other one controls the manipulator with its joystick. For survey, mapping and exploration missions the automatic DP control system developed at NTNU is preferred, since accuracy and precision of positioning is to be prioritized (refer to [25] for information concerning the control system, to [17] for the AUR-Lab operations).

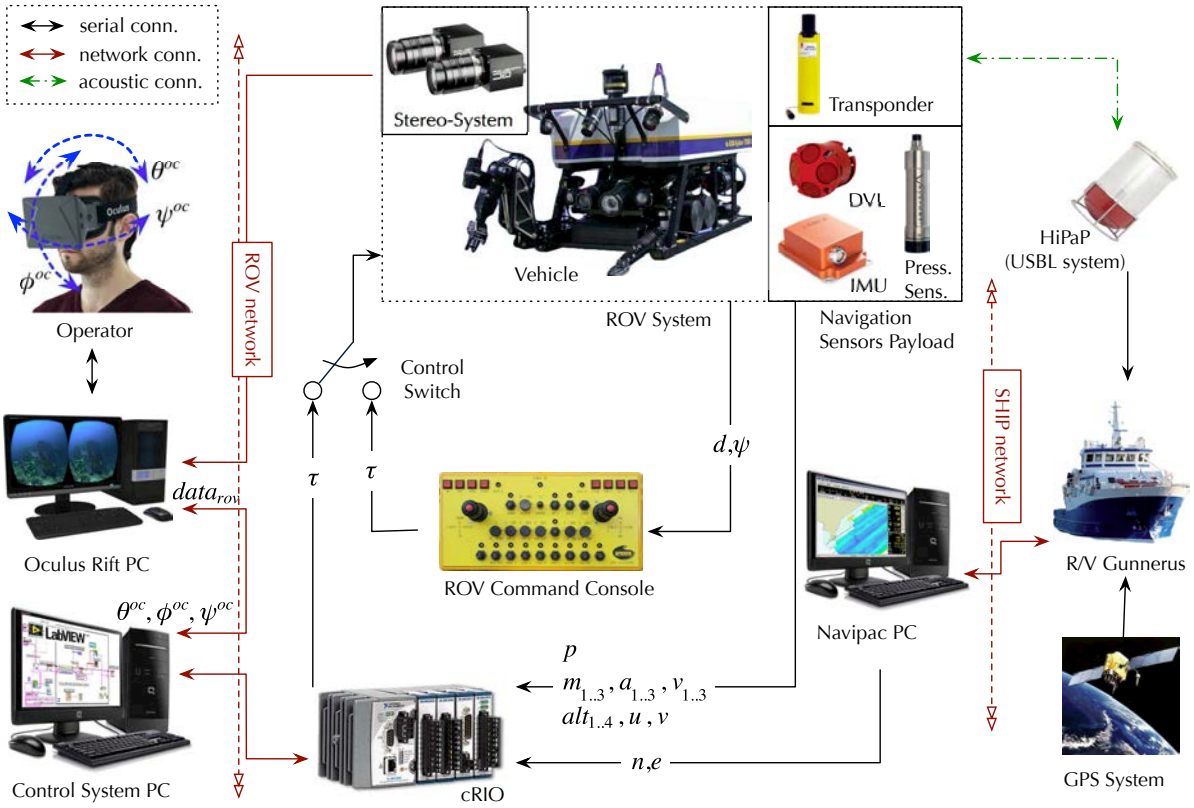

Fig. 2. Main hardware components and connections. Black, red and green lines represent respectively serial, network and acoustic connections. The main sensors payload and signal flow is represented. In the left part the connection between the OR, the OR PC and the DP Control System PC is shown, together with the exchanged information.

III. Oculus Rift

The HMD used in this work is the Oculus Rift (OR) DK2, shown in Figure 3. It is one of the most known HMD systems, but it is still only available as a developer kit. The consumer edition is believed to be released in 2016. The Oculus Rift has a magnetometer, accelerometer and gyroscope for tracking head attitude at a high refresh rate since its mainly designed for VR applications, where the ability to look around in a virtual world is essential. In addition to the attitude information, it is possible to measure the relative position of the device in space through an external infrared tracker that also increases the accuracy of the attitude measurements. More information about the hardware can be found in [1].

Although this device has been considered to increase the telepresence with vehicles like aerial drones, or to simulate the presence in fictional 3D scenarios (for videogames purposes), to the knowledge of the authors it has never been used for the active control of ROVs before.

Fig. 3. The Oculus Rift is the HMD chosen for increasing the telepresence experience and to actively control the ROV 30k.

IV. Stereo-Vision System

The ROV is equipped with two Allied Vision GC1380C that provide images at a resolution of 1360×1024 pixels at a frame rate of 20.2fps; higher frame rate could be achieved by reducing the resolution of the cameras [29]. In this experiment reduced the resolution to obtain 30fps. Those cameras are fitted in underwater camera casings and mounted on a stereo-rig. The images are sent to the OR to provide a stereoscopic view of the underwater environment. Although this settings was experimental, from the first tests the operator got a much more *immersive* experience, given the real 3D view feeling. In further work more work should be done to find the optimal camera positioning to get the best view experience. Notice that this stereo-rig has been used by AUR-Lab also for the construction of underwater photogrammetry models [20].

V. Software

Two computers are used to run all the softwares needed for the operations. One computer is focused on the user interface, OR image rendering and camera processing. The second computer is used for the real-time control of the ROV [25]. The system architecture is shown in Figure 2.

A. Oculus Rift computer

The software developed for stereoscopic capture and visualization consists of three independent threads, which runs in parallel after the initialization process. The main reason for the parallel processing is due to different time frames for each independent process. Two external libraries were used, OpenCV and PvAPI, [21] and [23] respectively.

One thread is responsible to queue and capture the frames for both cameras using the PvAPI library. The cameras were sampled in 30Hz to avoid performance issues. Both images where queued as soon as the most recent frame was captured, increasing efficiency.

The second thread is responsible for the communication with the OR. The OR is instantiated in a singleton, while data such as readings for the accelerometers were stored on a shared memory. In this thread the last images captured by the cameras are rendered directly in the OR, with the corresponding camera for each eye. It is a common practice to have the rendering thread running between 60Hz and 75Hz to avoid motion sickness. The software was based on the examples presented in [8].

Finally, the communication with the control computer is held by the last thread. The OR attitude is sent to the control computer trough a UDP protocol, at 5Hz , which is interpreted according to the selected control algorithm (speed control, position control, etc). Also, the bidirectional communication enables the possibility to display critical data on the headset (such as depth, distance to target, heading, etc). This introduces a certain level of *Augmented Reality* to the user experience; in the authors opinion improving the impact of the Augmented Reality experience with more complex and elaborated information can increase widely the situational awareness. This would increase widely, in turn, the efficiency of the mission.

B. Control computer

The second computer is responsible for the DP control system. It runs on an independent PC in order to increase the reliability as well as ensuring that no HMI-related thread would interrupt the communication with the ROV.

The DP system is developed using LabView, on its Graphical User Interface (GUI) it is possible to enable, disable the HMD control, and chose the different HMD control methods. If the communication with HMD is lost, the operator can take control of the vehicle using the joystick.

The DP system runs a Kalman Filter for sensor fusion and state estimation, a nonlinear PID controller, signal processing, thrust allocation algorithms and so on. Details can be found in [25], [9], [11], [6] and references therein.

VI. Oculus Rift Control Methods

The Oculus Rift IMU output is given as an input to a guidance system, which goal is to produce a feasible desired state for the control system. In particular the goal is to associate the three possible rotations of the head with the changes of three DOFs of the vehicle. Recalling that an ROV can freely move in space through its 6 DOFs: $\boldsymbol{\eta} = [\ x \quad y \quad z \quad \phi \quad \theta \quad \psi\ ]$, the goals is to control x (surge) with a forward and backward motion of the head, y (sway) with a sideways motion of the head and ψ (way) rotating the head left and right. It is here necessary to say that ϕ and θ are passively stable [25], hence don't require active control, and z is controlled independently by an altitude or depth controller, dependently by the requirements of the specific mission [9]. Consequently, the control of ϕ, θ and z will not be treated in the following.

A. Oculus Rift Variables

The selected guidance system is based on the one developed for the joystick interface in [10] and produces a direct thrust or a *oculus rift* velocity reference $\boldsymbol{\nu}^{oc}$ from which desired *vehicle* position and speed $\boldsymbol{\eta}_d$ and $\boldsymbol{\nu}_d$ are calculated, depending by the selected control method.

The normalized head angle measured by the OR attitude sensors are (see the link between the variable and the head rotation in the top left corner of Figure 2):

$$\overline{\boldsymbol{\Theta}^{oc}} = [\ \overline{\phi^{oc}} \quad \overline{\theta^{oc}} \quad \overline{\psi^{oc}}\ ] \tag{1}$$

where $\overline{\phi^{oc}}, \overline{\theta^{oc}}, \overline{\psi^{oc}} \in [-1, 1]$ are respectively the OR roll, pitch and yaw. The normalization is done to have common and defined limits for the angle ranges.

Experimental tests suggested that is beneficial to introduce a saturation and a dead zone when considering the OR output vector $\boldsymbol{\Theta}^{oc}$. The saturation helps the operator not to bend his head over the comfort limit, while the dead zone allows the operator to rapidly find the zero head position without inducing oscillations in the process. The OR roll and pitch angles are saturated at $30°$, while yaw is saturated at $45°$. The dead zone is constrained to $5°$ around the zero position.

B. Direct Thrust Control

The simplest OR control is a feed-forward force control. This turns operators head movements directly into thrust commands and involves no feedback terms, the following control law is employed:

$$\boldsymbol{\tau} = \boldsymbol{K}^{\tau}_{oc} \boldsymbol{T}^{b}_{oc} \overline{\boldsymbol{\Theta}^{oc}} \tag{2}$$

where $\boldsymbol{K}^{\tau}_{oc}$ is defined so that the maximum output will correspond to the maximum available thrust:

$$\boldsymbol{K}^{\tau}_{oc} = \text{diag}\ \begin{bmatrix} X_{\max} & Y_{\max} & 0 & 0 & 0 & N_{\max} \end{bmatrix} \tag{3}$$

where $X_{\max}$, $Y_{\max}$ and $N_{\max}$ are respectively the maximum available thrust in surge, sway and yaw. $\boldsymbol{T}^{b}_{oc}$ is the transformation matrix that links the OR reference frame to the ROV body frame:

$$\boldsymbol{T}^{b}_{oc} = \begin{bmatrix} 0 & -1 & 0 \\ -1 & 0 & 0 \\ 0 & 0 & -1 \end{bmatrix} \tag{4}$$

Notice that the minus sign in the transformation matrix is necessary to obtain the expected ROV motion given a certain head rotation. For example it is expected for the ROV to move forward when the head is bended forward. In the following tests the $\boldsymbol{T}_{oc}^{b} = \boldsymbol{I}$, where $\boldsymbol{I}$ is the identity matrix. Finally $\boldsymbol{\tau}$ is the 4 elements thrust vector, that specifies a thrust value for every *controllable* DOF.

C. Speed Reference

In this case, the change of the OR variables is mapped to a desired OR velocity $\boldsymbol{\nu}^{oc}$ that is the input to a reference model. A mapping is needed to associate the DOFs in the OR reference system to the body frame DOFs of the vehicle:

$$\boldsymbol{\nu}^{oc} = \boldsymbol{K}_{oc}^{\nu} \boldsymbol{T}_{oc}^{b} \overline{\boldsymbol{\Theta}^{oc}} \tag{5}$$

where $\boldsymbol{K}_{oc}^{\nu}$ is a diagonal scaling matrix for velocity:

$$\boldsymbol{K}_{oc}^{\nu} = \text{diag} \begin{bmatrix} K_u & K_v & 0 & 0 & 0 & K_r \end{bmatrix} \tag{6}$$

The implemented reference model is a second-order low-pass filter (see, for instance, [12] for an in-depth description of the model):

$$\begin{aligned} \dot{\boldsymbol{\eta}}_d &= \boldsymbol{J}(\psi_d)\boldsymbol{\nu}_d \\ \ddot{\boldsymbol{\nu}}_d + 2\boldsymbol{\Delta}\boldsymbol{\Omega}\dot{\boldsymbol{\nu}}_d + \boldsymbol{\Omega}\boldsymbol{\nu}_d &= \boldsymbol{\Omega}^2\boldsymbol{\nu}^{oc} \end{aligned} \tag{7}$$

$\boldsymbol{\Delta}$ and $\boldsymbol{\Omega}$ represents the damping and natural frequency parameters for every DOF and should be set so that the reference model would produce a feasible output for the vehicle. In [28] the values used for those parameters are extensively reported. Notice that the $\boldsymbol{\nu}^{oc}$ produced by (5) is given to the second equation in (7) to produce a *vehicle* desired velocity $\boldsymbol{\nu}_d$. This is then transformed in the desired position with the first equation of (7), that is a coordinate transformation to the NED frame described by the matrix $\boldsymbol{J}(\psi_d)$.

D. Position and Velocity control

For the closed loop control of the ROV, a nonlinear PID control law is implemented. This algorithm can work in two modes: position and velocity reference control. For the position control the following algorithm is used:

$$\boldsymbol{\tau} = -\boldsymbol{J}^{T}(\hat{\boldsymbol{\eta}}) \left(\boldsymbol{K}_p \tilde{\boldsymbol{\eta}} + \boldsymbol{K}_i \int_0^t \tilde{\boldsymbol{\eta}} d\boldsymbol{\tau} \right) + \boldsymbol{K}_d \tilde{\boldsymbol{\nu}} \tag{8}$$

where $\tilde{\boldsymbol{\eta}} = \boldsymbol{\eta}_d - \hat{\boldsymbol{\eta}}$ is the control error defined as the difference between the desired and estimated state vector. $\boldsymbol{K}_p$, $\boldsymbol{K}_i$, $\boldsymbol{K}_d$ are proper tuning matrices to be chosen dependently by the vehicles characteristics and the expected convergence performance. If the velocity control is chosen, the force elements corresponding to surge and sway are changed into:

$$\begin{aligned} X &= -K_{p,u}(u - u_d) - K_{i,u} \textstyle\int_0^t (u - u_d) d\tau \\ Y &= -K_{p,v}(v - v_d) - K_{i,v} \textstyle\int_0^t (v - v_d) d\tau \end{aligned} \tag{9}$$

where u and v are the surge and sway speeds. For the integral effect of both controllers, an anti wind-up algorithm is implemented in the following way:

$$\boldsymbol{\tau}_i = \left(\boldsymbol{K}_i - \boldsymbol{K}_{\text{anti},i} (\text{sat}(\boldsymbol{\tau}_i) - \boldsymbol{\tau}_i) \right) \int_0^T \bar{\boldsymbol{\eta}}(t) d\boldsymbol{\tau} \tag{10}$$

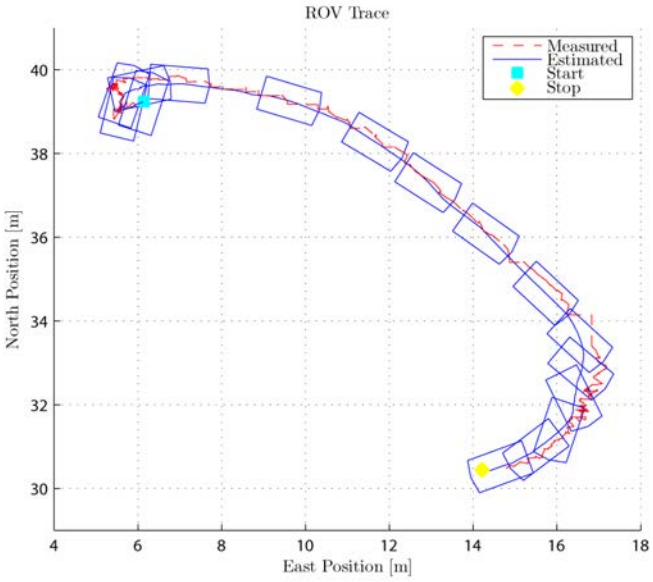

Fig. 4. Force control is used to push 30k on a straight line, ending with a turn. Although this method is more responsible, it is more challenging to obtain a smooth response.

$\boldsymbol{K}_{\text{anti}}$ is the anti-windup tuning matrix. All the numerical values for the tuning matrices that have been used in the experiments reported here can be found in [28]. Notice that with those control methods external forces or disturbances (like the tether drag and current forces) are automatically taken care by the DP system [10], this leaves the operator with the only duty of controlling the vehicle motion.

VII. Experimental Results

The experiments aimed to test the OR control methods. The ROV has been steered with the OR providing the inputs to the three algorithms and the state of the ROV has been logged. Some results are showed and commented in the following. It is difficult to quantitatively compare the performance of the algorithms, since the experiments have been done in full scale in a unstructured environment. The main objective, at this stage, is to evaluate the usability of the methods and the operator feedback while controlling the ROV with them.

A. Motion Tests

Three results concerning the three control methods are shown: Figure 4, 5 and 6 show respectively the results for tests related to force, velocity and position control. Force control is used to move the vehicle on a line, ending with a right turn. Velocity control is used to move the vehicle forward on a straight line. Position control is used to move the ROV on a square path, notice that the heading is easily kept stable and constant nevertheless the change in the other DOFs.

Although force control is more responsive, due to the absence of a reference model, the operator reported an higher difficulty of controlling the motion of the vehicle in a smooth way. Following a straight line has been easier with the other

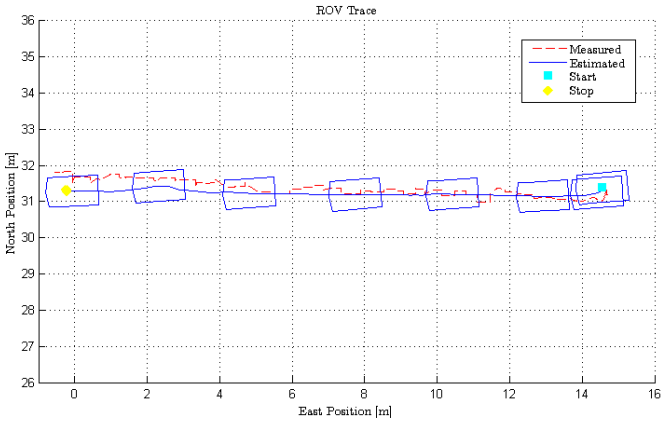

Fig. 5. Velocity control is used to run a straight line. Here the velocity is successfully kept constant along the line.

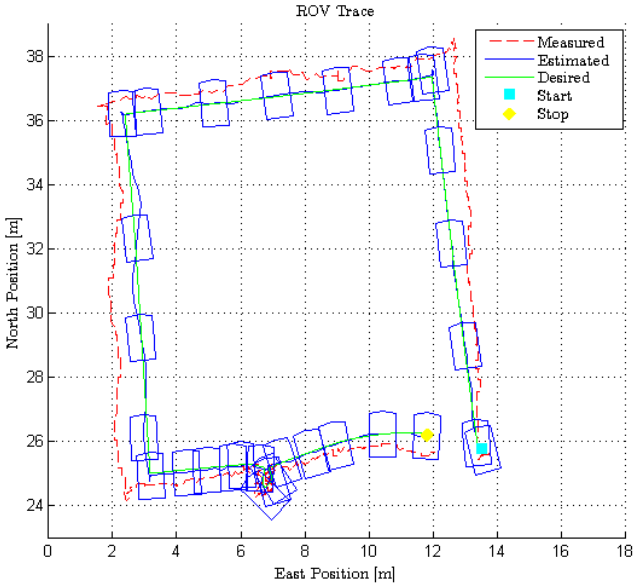

Fig. 6. In this result the operator is moving the vehicle in position control. It is possible to notice that, although the operator does not have a full map representation superimposed on the OR screen, he is able to perform a square with quite high precision, keeping constant heading along all the path.

control functions. In particular it is possible to see how accurate was the motion along the square path, using the position control.

B. Inspection Tests

In the authors opinion, HMDs are definitely suitable for inspection works, in particular it allows to move around an Object Of Interest (OOI) keeping the focus on the object by slightly changing the heading and moving sideways at the same time. In Figure 7 a small object is inspected by the operator, while the ROV is moved in a small circle around it.

Another test has been done with the purpose of inspecting a bigger object of interest, i.e. Hercules wreck, a tugboat

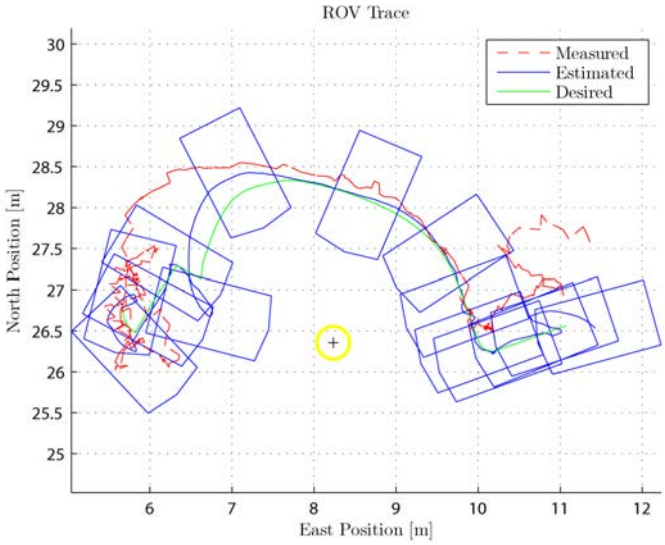

Fig. 7. Position control is used to inspect an object (a bottle on the sea bottom). It is clear that the operator manages to slowly tilt his head in such a way that the OOI is always kept in the field of view of the cameras.

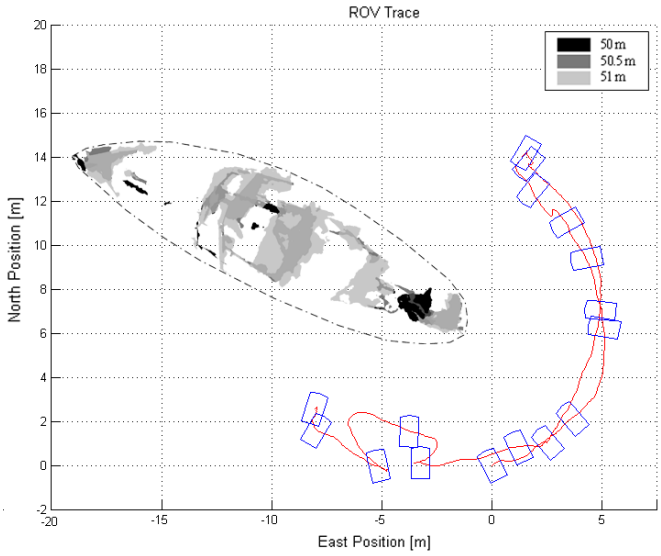

Fig. 8. 30k is inspecting the stern of the Hercules wreck. 3 layers of the photogrammetry model of the wreck are also drawn. The full photogrammetry model is presented in [20]. The ROV is kept stable at 50m depth

that sank in the Trondheimsfjorden in 1957. It is possible to see from Figure 8 how the position control allows smooth inspection maneuvers, making it easy to constantly look at the object of interest. In this case the ROV has been moved sideways while the operator was inspecting the stern of the boat. The stereoscopic view allows to have a great immersive feeling for the operator.

C. Manipulation Tests

Having the possibility of controlling the vehicle with his head, the operator can use his hands to operate the manipulator (Figure 9). This gives him control over the whole system. In

Fig. 9. The HMD allows the operator to have full control over the whole system, without having to rely on a second operator.

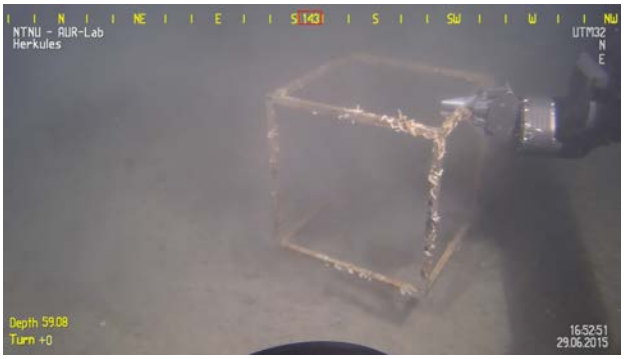

Fig. 10. Here the moment when the box is grabbed is shown: the ROV is kept stable with the HMD and the manipulator is actuated using the joystick depicted in Figure 9.

the reported test a box frame (Figure 10) have been grabbed by the operator, while the ROV was kept stable through the OR. In further work comparative examples will be presented to quantitatively show the effectiveness of this method over the classical joystick method with two operators [14]. Here it is possible to qualitatively report that the operation has been executed with high efficiency: the operator was able to slowly approach the object, adjust the position of the vehicle so that the manipulator could easily grab it, extend the manipulator while repositioning the vehicle so that the object could have been actually reached, grab the object and move to another position to replace it.

VIII. Conclusion and Further Work

In this paper a HMD system is proposed in order to increase the efficiency of Remotely Operated Vehicles teleoperations and telepresence by augmenting the situational awareness. Moreover the HMD has been used as an interface device for closed-loop control of the ROV, providing to the operator the possibility of having full control on the whole underwater system. The HMD interface gave satisfactory results, showed by the experimental results discussed above. Those suggest that there is space for further improvements that could let this HMI become highly beneficial for real offshore operations, improving their efficiency. In particular the augmented reality is a key to improve the situational awareness of the operator even more. A systematic set of tests that would involve more operators and comparative results against standard control interfaces will be presented in further work. Introduction of more advanced guidance methods is also considered.

Acknowledgment

This work has been carried out at the Centre for Autonomous Marine Operations and Systems (AMOS). The Norwegian Research Council is acknowledged as the main sponsor of AMOS through the Centres of Excellence funding scheme, Project number 223254. Stein Nornes is acknowledged also for the photogrammetry model of Hercules and the valuable help during the experiments.

References

[1] Oculus rift developer forum. https://developer.oculus.com/. Accessed: 2015-07-20.

[2] Head-mounted electronic device permits viewing of two images at once. *Electrical Engineering*, 81(6):483–484, June 1962.

[3] A. Agah, R. Walker, and R. Ziemer. A mobile camera robotic system controlled via a head mounted display for telepresence. In *Systems, Man, and Cybernetics, 1998. 1998 IEEE International Conference on*, volume 4, pages 3526–3531 vol.4, Oct 1998.

[4] H.L. Alexander. Experiments in teleoperator and autonomous control of space robotic vehicles. In *American Control Conference, 1991*, pages 1474–1477, June 1991.

[5] V. Berg. Development and commisioning of a dp system for rov sf 30k. Master's thesis, Department of Marine Technology, Norwegian University of Science and Technology, Trondheim, Norway, 2012.

[6] M. Candeloro, A.J. Sørensen, S. Longhi, and F. Dukan. Observers for dynamic positioning of rovs with experimental results. In *9th IFAC Conference on Manoeuvring and Control of Marine Craft (MCMC)*, volume 1, pages 85–90, September 19-21 2012.

[7] I.S. Cardenas and J.H. Kim. Advanced technique for tele-operated surgery using an intelligent head-mount display system. In *Biomedical Engineering Conference (SBEC), 2013 29th Southern*, pages 143–144, May 2013.

[8] B.A. Davis, K. Bryla, and P.A. Benton. *Oculus Rift in Action*. Manning Publications Co., 2015.

[9] F. Dukan. *ROV Motion Control Systems*. PhD thesis, Department of Marine Technology, Norwegian University of Science and Technology, Trondheim, Norway, 2014.

[10] F. Dukan and A.J. Sørensen. Joystick in closed-loop control of rovs with experimental results. *3rd IFAC Workshop on Navigation, Guidance and Control of Underwater Vehicles (NGCUV)*, pages 293–300, 2012.

[11] D. Fernandes. *An Output Feedback Motion Control System for ROVs*. PhD thesis, Department of Marine Technology, Norwegian University of Science and Technology, Trondheim, Norway, 2015.

[12] T.I. Fossen. *Handbook of Marine Craft Hydrodynamics and Motion Control*. John Wiley and Sons, UK, 2011.

[13] R.J. Hall and J.W. Miller. Feasibility study for a monocular head-mounted display. *Hughes Aircraft Company, Special Technical Document SD 60-70*, 1960.

[14] W.S. Kim, A. Liu, K. Matsunaga, and L. Stark. A helmet mounted display for telerobotics. In *Compcon Spring '88. Thirty-Third IEEE Computer Society International Conference, Digest of Papers*, pages 543–547, Feb 1988.

[15] K. Kiyokawa. Trends and vision of head mounted display in augmented reality. In *Ubiquitous Virtual Reality (ISUVR), 2012 International Symposium on*, pages 14–17, Aug 2012.

[16] Q.H. Le, K.T. Park, Y.M. Jeong, and S.Y. Yang. A study on remote control system integrated intuitive vision system for field robot using head tracker system. In *Control, Automation and Systems (ICCAS), 2014 14th International Conference on*, pages 326–330, Oct 2014.

[17] M. Ludvigsen, P. Lågstad, T. Thorsnes, Ø. Ødegård, R.E. Hansen, M. Candeloro, A.J. Sørensen, S.M. Nornes, G. Johnsen, and C. Malmquist. Underwater vehicles for environmental management in coastal areas. In *Oceans15 MTS/IEEE Genova*, May 18-21 2015.

[18] H. Martins, I. Oakley, and R. Ventura. Design and evaluation of a head-mounted display for immersive 3d teleoperation of field robots. *Robotica*, FirstView:1–20, 5 2014.

[19] M.E. Morphew, J.R. Shively, and D. Case. Proceedings of spie - the international society for optical engineering. In *American Control Conference, 1991*, September 2004.

[20] S. M. Nornes, M. Ludvigsen, Ø. Ødegård, and A.J. Sørensen. Underwater photogrammetric mapping of an intact standing steel wreck with rov. In *4th IFAC Workshop on Navigation, Guidance and Control of Underwater Vehicles (NGCUV)*, April 28-30 2015.

[21] OpenCV. Opencv library refefrence. http://docs.opencv.org, June 2015.

[22] Oxford University Press. Oxford dictionaries. http://www.oxforddictionaries.com/definition/english/, August 2015.

[23] PvAPI. Pvapi legacy software from allied vision. http://www.alliedvision.com/en/support/software-downloads.html, June 2015.

[24] E. Schneider, K. Bartl, T. Dera, S. Bardins, G. Boning, P. Wagner, and T. Brandt. Gaze-aligned head-mounted camera with pan, tilt, and roll motion control for medical documentation and teaching applications. In *Systems, Man and Cybernetics, 2006. SMC '06. IEEE International Conference on*, volume 1, pages 327–331, Oct 2006.

[25] A.J. Sørensen, F. Dukan, M. Ludvigsen, D. Fernandes, and M. Candeloro. Development of dynamic positioning and tracking system for the rov minerva, 2012.

[26] Sperre. 30k specifications. http://sperre-as.com/produkter/rov/systemer/sub-fighter-30k, August 2015.

[27] S. Surn. Interaction design in a 4d sea map. Master's thesis, Department of Production Design, Norwegian University of Science and Technology, Trondheim, Norway, June, 2015.

[28] E. Valle. Marine telepresence system. Master's thesis, Department of Marine Technology, Norwegian University of Science and Technology, Trondheim, Norway, 2015.

[29] Allied Vision. Prosilica gc1380. http://www.alliedvision.com/en/products/cameras/detail/1380.html, August 2015.

Article F

Photomosaic camera as simultaneous data collector and navigation aid on Unmanned Underwater Vehicles

S.M. Nornes, **M. Candeloro**, Ø. Ødegård, G. Johnsen, and A.J. Sørensen

The article has been presented at
Ocean Optics XXII.
Portland, Maine, 26-31 October 2014.

Photomosaic camera as simultaneous data collector and navigation aid on Unmanned Underwater Vehicles*

Stein M. Nornes†[1], Mauro Candeloro[1], Øyvind Ødegård[1], Geir Johnsen[2], and Asgeir J. Sørensen[1]

[1] *Centre for Autonomous Marine Operations and Systems (AMOS), Department of Marine Technology, Norwegian University of Science and Technology (NTNU), Norway*
[2] *Department of Biology, Norwegian University of Science and Technology(NTNU), Norway*

October 20, 2014

Abstract

When collecting environmental data with a UUV such as a Remotely Operated Vehicle (ROV) or an Autonomous Underwater Vehicle (AUV), the typical end user is not concerned with how accurate the navigation system is, as long as it is "good enough" not to distort the data. How accurate the localization needs to be to accomplish this, depends highly on the spatial and temporal resolution of the measured parameters. For sensors such as a CTD with a grid size measured in meters this is quite easily achievable, whereas a photomosaic camera with pixels measured in millimetres puts higher demands on the navigation accuracy. Simultaneously, the photomosaic camera also provides highly accurate measurements which can be utilized by the navigation system. If a distinct feature on the sea floor is detected in two separate images taken some time apart, the navigation system can accurately calculate the difference in the localization of the platform between the two points in time. This payload aided navigation technique is known as Simultaneous Localization and Mapping (SLaM). While a global position offset may still be present in the data, this is now shared by the entire set, and the all-important relative position accuracy between the data measurements improves.

1 Introduction

When operating on land with frequently updated high-resolution maps and increasingly accurate and reliable GPS readings, navigation is rapidly becoming a trivial task. In areas where none of these utilities are available, like for instance underwater operations

*This work was partly supported by the Research Council of Norway through its Centres of Excellence funding scheme, project number 223254/F50

†Email: stein.nornes@ntnu.no

using unmanned underwater vehicles such as ROVs and AUVs, it is still a major obstacle that needs to be resolved in order to approach high precision control and true autonomy. At NTNU, a lot of research is done on the development on motion control systems and dynamic positioning systems for ROVs, see Dukan and Sørensen [2014], Caharija et al. [2013], and Sørensen et al. [2012].

Several end users, such as industry, environmental agencies and the scientific community desire an accurate visual maps of objects and areas of interest. When an area is too deep to be mapped by aerial photos or divers (>20m), this can be done using an ROV or an AUV equipped with a photomosaic camera.

In 2003 a historic shipwreck was discovered close to one of the planned Ormen Lange (Norwegian offshore natural gas field) pipeline routes at close to 200 meters depth[Søreide and Jasinski, 2005]. During a revisit of the wreck site in 2012 an attempt was made at creating a photomosaic map of the site using the NTNU ROV Minerva (see section 4). The results from this mapping highlight the importance of accurate positioning to achieve satisfactory coverage of the area of interest.

Figure 2 shows how a lawn-mower pattern with inaccurate positioning data causes large gaps to appear in the finished mosaic. Figure 1 shows a mosaic of another wreck with a site drawing from the original excavation superimposed. After postprocessing, the gaps and shortcomings of the mosaics become quite obvious. Unfortunately this postprocessing was carried out several months after the cruise, as is often the case. This necessitated organizing a second cruise in order to fill the gaps.

A simple, intuitive solution to avoid these gaps would of course be to increase the degree of image overlap between the lines in the pattern. While this will probably eliminate the gaps, it comes at the cost of having to do a larger number of lines to map the same area. This would mean having to increase the time of the survey or reducing the spatial coverage. In the ROV-case, increasing the mission time might be possible even if it will be costly. In the AUV-case however, the mission time will likely be limited to the battery capacity of the vehicle, meaning spatial coverage will have to be reduced.

A more optimal solution would be to have an adaptive system capable to automatically detecting the degree of image overlap. This would allow the system to detect gaps online and fill them, as well as automatically adjusting the linespacing to achieve the highest possible spatial coverage with the available time.

The main objectives of this work is to develop a strategy for image-aided guidance, navigation and control of UUVs, determine the strategy's demands for inertial sensor accuracy, develop a system utilizing real-time mosaicking to automatically detect gaps/degree of overlap and optimize time use and spatial coverage. The combination of these objectives will lead to an increase in the level of autonomy for UUVs.

2 Increasing Autonomy

Operations such as the attempted photomosaic of the Ormen Lange wreck site highlight the potentail value of being able to process data in (approximately) real-time and correct such issues while still on site. Being able to solve such issues without the need for human

intervention will give a more autonomous system that can reduce the workload (and correspondingly fatigue and faulty decisions) of human operators. Because of this, many different fields of research are collaborating in the strive for true autonomy.

There are many different definitions of autonomy and the gradual transition from direct human control to complete autonomy. One of the more concise definitions of levels of autonomy is the following from the Committee on Autonomous Vehicles in Support of Naval Operations [2005]:

Level 1 (Manual Operation)

- The human operator directs and controls all mission functions, while the vehicle still flies autonomously.

Level 2 (Management by Consent)

- The system automatically recommends actions for selected functions and prompts the operator at key points for information or decisions.

Level 3 (Management by Exception)

- The system automatically executes mission-related functions. The operator is alerted to function progress and exceptions, and may override or alter parameters and cancel or redirect actions within defined time lines.

Level 4 (Fully Autonomous)

- The operator is alerted to function progress, while the system automatically executes mission-related functions when response times are too short for operator intervention.

Due to the work of Dukan et al. [2011], NTNUs ROV Minerva (see section 4) has a Dynamic Positioning and Tracking System that qualifies it for level 1 autonomy. By implementing the real-time mosaic algorithm in section 3 and using this to detect the spatial coverage of the collected data, we aim to approach level 2 autonomy: Detecting the degree of image overlap and spatial coverage will allow the system to optimize the linespacing of the lawnmower pattern and suggest changes to the operator.

Figure 3 displays the overall architecture of the photomosaic recording system. The Guidance module calculates a smooth trajectory for the vehicle based on waypoints either supplied by the operator or the Online planning module. The Control system then calculates the thruster forces needed to achieve this trajectory. In this architecture, the real-time photomosaic is implemented in the lower level "Photo analysis"-block, while the time and spatial coverage optimization will be implemented in the higher level "Online re-/planning"-block. The two-way connection between Photo analysis and State estimation is explained in section 3.

2.1 Simultaneous Localization and Mapping

SLaM addresses the problem of acquiring a spatial map of a mobile robot environment while simultaneously localizing the robot relative to this model [Siciliano and Khatib, 2008]. The SLaM problem is generally regarded as one of the most important problems in the pursuit of building truly autonomous mobile robots. SLaM methods have now reached a state of considerable maturity [Durrant-Whyte and Bailey, 2006].

Future challenges will centre on methods enabling large-scale implementations in increasingly unstructured environments and especially in underwater environments. This project will be focussing on increasing the autonomy of unmanned underwater vehicles, which will allow us to explore hitherto inaccessible areas, like under the arctic icecap or very deep waters. Also in shallow water with multilayer waters, close to vertical obstacles/walls or near surface navigation using known methods such as acoustics is a challenge.

3 Method for real-time photomosaic

The algorithm is implemented using Object Oriented Labview, and it is designed on a framework that allows its real time execution in parallel with the execution of the ROV Control System software.

In this architecture the information produced by the two systems can be interchanged, in order to improve the performance of both systems. In this work the mosaic techniques is used both as a mapping tool for end users, such as archeologists or biologist, but also to improve the navigation of underwater vehicles in the vicinity of the sea bottom. Many applications require the ROV to be close to the sea bottom (2-3 meters). At these altitudes the ROV light can be reflected off the ground and reach the camera sensors without significant dissipation, enabling the use of visual feedback in the Control System.

This possibility is of high relevance, especially for missions that aim to reduce the operator intervention and increase the vehicle autonomy. Following a pipeline or inspecting a wreck site, for instance, can be done in an autonomous mode only if the standard navigation system of the ROV includes systems able to sense and provide some information of what surrounds the vehicle.

Figure 4 describes the architecture of the photomosaic pipeline. H represents the Homography matrix between two following pictures, that is the information that links two images taken with a monovision system. This Matrix includes rotation and translation information. Distances to the features depicted in the image are unavailable information, unless the images are obtained using a stereovision system. The homography matrix information can be fused together with measurements provided by Inertial Measurement Systems to provide better estimates of the attitude and position of the vehicle.

Moreover the navigation data of the vehicle can be used to improve the feature detection and feature matching both in terms of speed and quality performance. For instance the features can be searched only in the area of the picture that is supposed to

overlap.

The mosaic software itself is quite standard, using a Scale-Invariant Feature Transform (SIFT) approach for the feature description and a RANSAC algorithm to remove outliers. The contribution here is related to the construction of a real time mosaic for underwater application, and the cooperation of the two software systems. Moreover an estimate of the sea bottom is used together with the ROV navigation data to improve the mosaic.

4 Experiments in Trondheim Harbour

Minerva is a SUB-fighter 7500 ROV made by Sperre AS in 2003 for NTNU. It is a medium sized ROV (144x82x81 cm, 485 kg), and is a frequently used test platform for navigation and control research. Usually deployed from the NTNU research vessel (RV) Gunnerus, it is powered from and communicates with the surface vessel through a 600 m umbilical. All systems needed for operation such as power supply, navigation computers and monitors are fitted inside a 15 foot container. The ROV can be piloted manually using a joystick console, or automated using a Dynamic Positioning system (DP) developed and continuously expanded at NTNU. For more details on Minerva and the DP system, the reader is referred to Dukan et al. [2011].

Currently, the software is being prepared for initial testing on Minerva in Trondheim Harbour. Figure 6 shows a photomosaic constructed using this software on a set of images captured from the same site on a previous cruise.

5 Conclusion

In this work we have explained the motivation for using a photomosaic camera not only as a payload sensor, but also as a navigation aid for UUVs. A Labview implementation of a real-time photomosaic software for the NTNU ROV Minerva has been presented, along with the overall architecture of the planned autonomous system. Field trials of this software are planned to be cunducted in Trondheim Harbour in the end of October 2014, and once they are finished the project will move into performance analysis and work on implementation of the planning/replanning layer of the system.

Bibliography

W. Caharija, K. Y. Pettersen, A. J. Sørensen, M. Candeloro, and J. T. Gravdahl. Relative velocity control and integral line of sight for path following of autonomous surface vessels: Merging intuition with theory. *Proceedings of the Institution of Mechanical Engineers, Part M: Journal of Engineering for the Maritime Environment*, pages 1475090213512293–, 2013. ISSN 1475-0902. doi: 10.1177/1475090213512293. URL `http://pim.sagepub.com/content/early/2013/12/18/1475090213512293.abstract`.

Committee on Autonomous Vehicles in Support of Naval Operations. *Autonomous Vehicles in Support of Naval Operations*. National Research Council, 2005. ISBN 9780309096768.

F. Dukan and A. J. Sørensen. Sea floor geometry approximation and altitude control of ROVs. *Control Engineering Practice*, 29:135–146, 2014. ISSN 09670661. doi: 10.1016/j.conengprac.2014.04.006.

F. Dukan, M. Ludvigsen, and A. J. Sørensen. Dynamic positioning system for a small size ROV with experimental results. In *OCEANS 2011 IEEE - Spain*, 2011. ISBN 9781457700866. doi: 10.1109/Oceans-Spain.2011.6003399.

H. Durrant-Whyte and T. Bailey. Simultaneous localization and mapping: Part I & II. *IEEE Robot Autom Mag*, 13(2):99–117, 2006. doi: 10.1109/MRA.2006.1638022. URL `http://ieeexplore.ieee.org/stamp/stamp.jsp?arnumber=1638022`.

B Siciliano and O Khatib. *Springer Handbook of Robotics*. Springer-Verlag, 2008.

F. Søreide and M.E. Jasinski. Ormen Lange: investigation and excavation of a shipwreck in 170m depth. In *OCEANS, 2005. Proceedings of MTS/IEEE*, pages 2334–2338 Vol. 3, 2005. doi: 10.1109/OCEANS.2005.1640113.

A. J. Sørensen, F. Dukan, M. Ludvigsen, D. A. Fernandez, and M. Candeloro. *Further Advances in Unmanned Marine Vehicles*, chapter 6: Development of Dynamic Positioning and Tracking System for the ROV Minerva, pages 113–128. IET, UK, 2012. ISBN 978-1-84919-479-2.

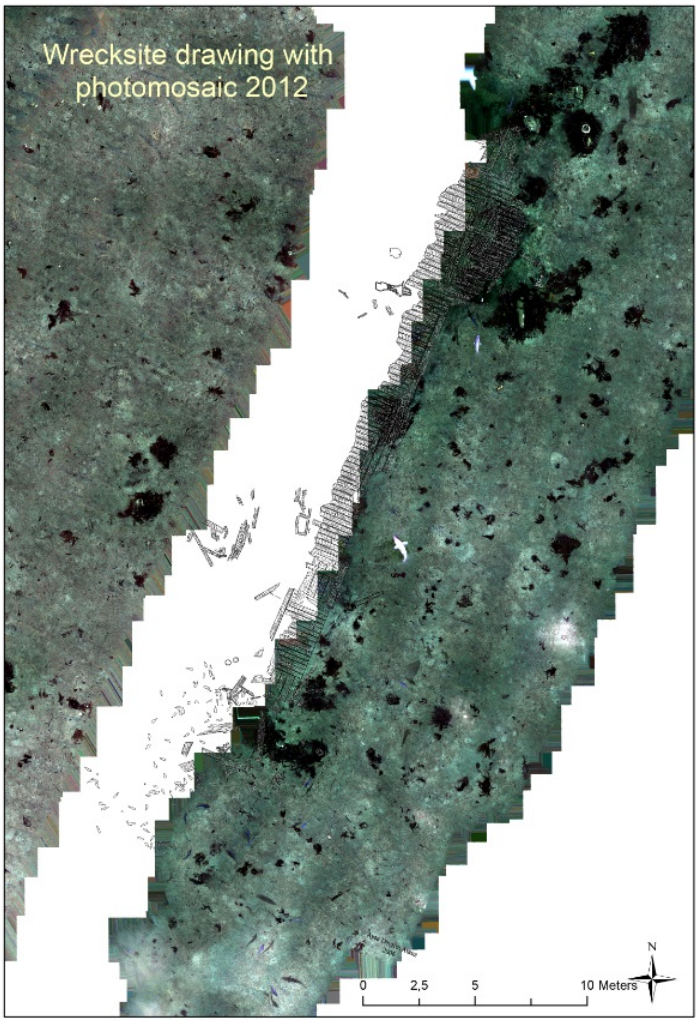

Figure 1: Wrecksite drawing of the main Ormen Lange wreck. Note how only half of the wreck is covered by the mosaic, due to inaccurate positioning data

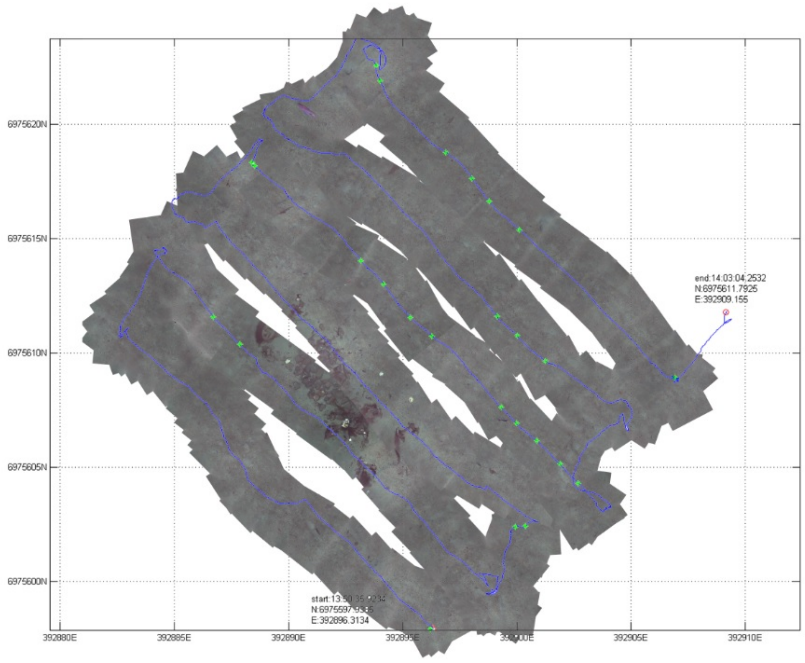

Figure 2: Lawn-mower pattern mosaic of the secondary Ormen Lange wreck demonstrating how inaccurate positioning data causes large gaps to appear in the finished mosaic

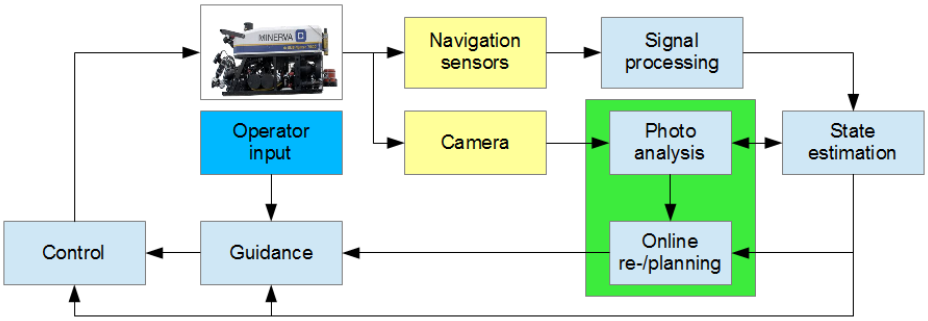

Figure 3: Flow chart describing the overall architecture of the system. The Guidance module calculates a smooth trajectory for the vehicle based on waypoints either supplied by the operator or the Online planning module. The Control system then calculates the thruster forces needed to achieve this trajectory. The green block represents the scope of this project. The two-way connection between Photo analysis and State estimation is further expanded in Figure 4

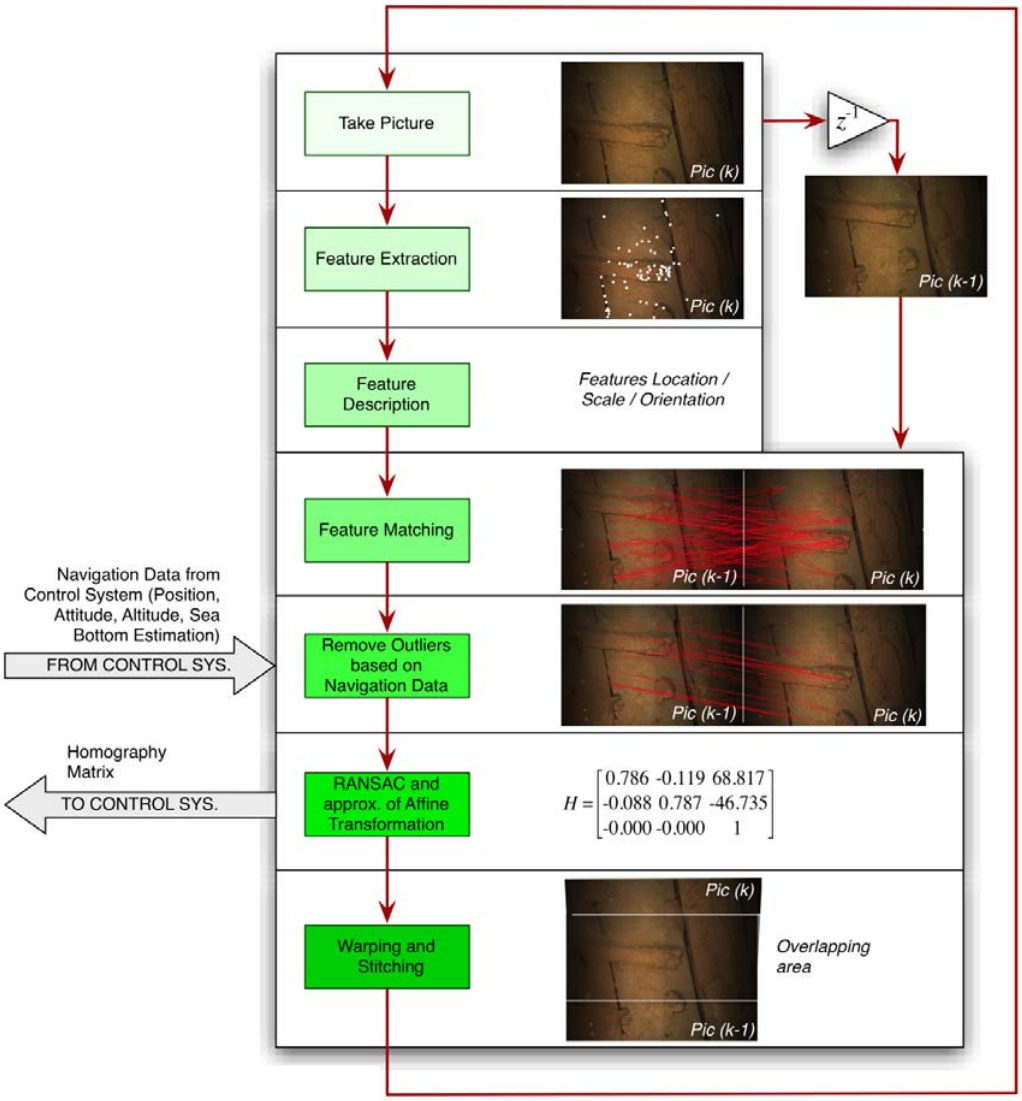

Figure 4: The pipeline of the real-time photomosaic software. State estimates from the State estimation block in Figure 3 are used to remove false feature matches. The resulting homography matrix is then returned, enabling further refining of the state estimates.

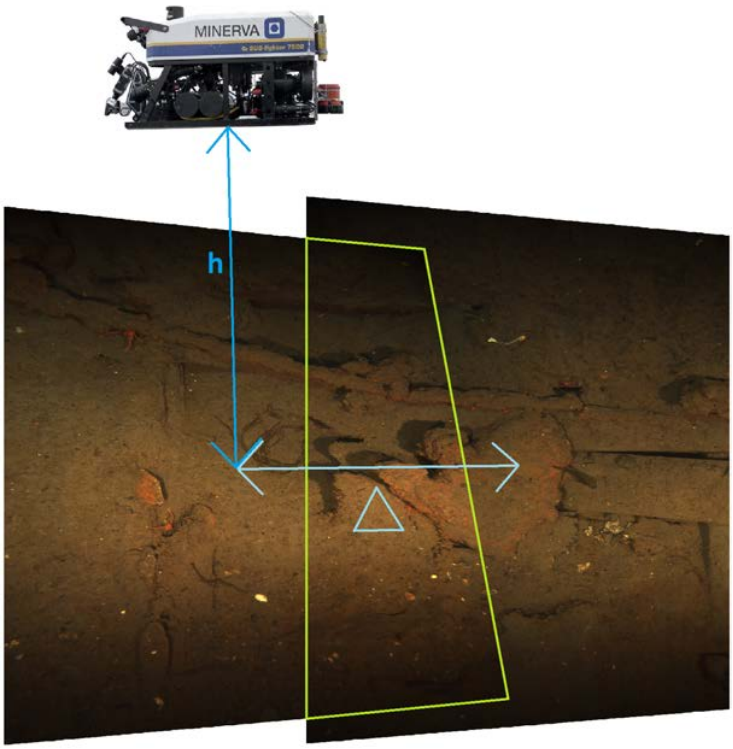

Figure 5: By determining the shift Δ between the recorded images, we can calculate a more accurate estimate of the relative position change of the vehicle in the time passed between recordings

Figure 6: First testmosaic using the software on previously recorded images from a wreck in Trondheim Harbour

Article G

Sensor-based Autonomous Path-Planner for Sea-Bottom Exploration and Mosaicking

M. Candeloro, F. Mosciaro, A.J.Sørensen, G. Ippoliti and M. Ludvigsen

The article has been published in the proceedings of the
10th IFAC Conference on Manoeuvring and Control of Marine Craft (MCMC),
IFAC-PapersOnLine
Volume 48 (16), pages 31–36. Copenhagen, Denmark, 24-26 August 2015.

Available online at www.sciencedirect.com

ScienceDirect

IFAC Papers Online CONFERENCE PAPER ARCHIVE

IFAC-PapersOnLine 48-16 (2015) 031–036

Sensor-based Autonomous Path-Planner for Sea-Bottom Exploration and Mosaicking ⋆

Mauro Candeloro * **Fernando Mosciaro** ** **Asgeir J.Sørensen** *
Gianluca Ippoliti ** **Martin Ludvigsen** *

* *Centre for Autonomous Marine Operations and Structures (AMOS), NTNU, Trondheim, Norway*
** *Dipartimento di Ingegneria dell'Informazione, UNIVPM, Ancona, Italy*

Abstract: A typical mission for an underwater vehicle is to research and map OOIs (Objects Of Interest). Objects Of Interest are specified in connection with the mission purposes, relevant examples span from biological species (e.g. seagrass or coral colonies) to artifacts (e.g. ship wrecks). For their research and mapping the deployment of Autonomous and Remotely Operated Vehicles is becoming the state-of-art, due to their ease of performing difficult operations in a safe way. Moreover, photo-mosaicking tools can be used to provide a complete map of the explored area. In order to achieve this aim, the navigation usually relies on simple lawn-mower or zig-zag patterns, where an area is scanned extensively to collect the pictures, that would be analyzed, processed and stitched after the mission. This paper aims to increase the autonomy of underwater vehicles that are equipped with a still-picture camera by using a *deliberative*, *sensor-driven* planning strategy. By *sensing* the environment extracting its information from the pictures, the path can be defined *on-the-fly*, in order to *increase the collected data*.

Keywords: UUVs, Sea-bed Mapping, Sensor-Based Path-Planning, Autonomy, Photomosaic.

1. INTRODUCTION

A typical mission for an underwater vehicle is to research and map OOIs (Objects Of Interest) in an unstructured and often poorly known environment. The collected data varies from the applications and the end-users needs, but acoustic and optical data are the standard for underwater mapping purposes. This work is focused on proposing steering strategies aimed to the collection of still-camera pictures for sea-bottom mapping and the creation of seamless maps of the sea bottom (i.e. *photo-mosaics*).

This work will focus on Unmanned Underwater Vehicles (UUVs), that mainly include Autonomous Underwater Vehicles (AUVs) and Remotely Operated Vehicles (ROVs) but can be referred to any underwater vehicle that would require a higher autonomy level during the mission. Notice that the degree of autonomy for an untethered vehicle becomes extremely important, due to the battery constraints and the lack of real-time feedback of high level data (e.g. video or sonar data), given by the bandwidth limitations of the acoustic link. For those reasons the mission planning becomes the main factor for the operations success.

A standard approach to a sea-bed mapping mission is described in Fig. 1: the first step is to define off-line a Lawn-Mower Pattern (LMP) to cover a certain area of dimensions depending by the energy or time constraints of the vehicle. Data from the sea bottom will be collected and stored by the vehicle during the mission, in order to be analyzed off-line after its recovery. This means that the information about the environment that is collected along the mission are not actively used *during* the mission. This may imply a mission re-planning and a refined attempt (for example if the area occupied by the OOIs has not be completely covered).

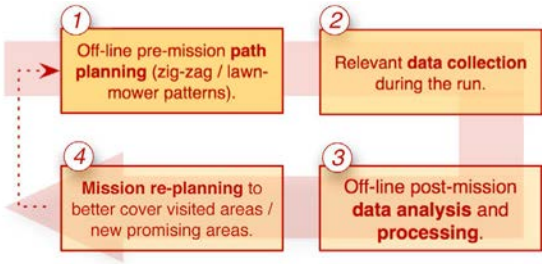

Fig. 1. High-level steps for researching and mapping OOIs. The off-line path planning is a crucial step.

A wide literature concerning general theory and description of off-line path-planning can be found, for example, in Tsourdos et al. (2010) (mainly about aerial applications). Methods and examples of strategies aimed to underwater land demining can be found in Acar et al. (2003), where comparisons between the most common techniques (e.g. random search, LMPs, probabilistic search) are presented. Seto (2013) offers a review of the state-of-art of the autonomy for underwater vehicles.

In this paper we will propose a strategy to automate the research and photo-mosaicking missions, by using a sensor-

⋆ This work has been carried out at the Centre for Autonomous Marine Operations and Systems (AMOS). The Norwegian Research Council is acknowledged as the main sponsor of AMOS through the Centres of Excellence funding scheme, Project number 223254.

10.1016/j.ifacol.2015.10.254

based on-line path-planner based on still-picture camera data feedback, in order to improve the mission outcome by increasing the quantity and quality of acquired data.

The online path planner proposed here is inspired from the work of Paull et al. (2012), extended in Paull et al. (2013). This work is, in turn, inspired by Cai and Ferrari (2009). Those works describe an on-line path planner that aims to have full coverage of an area, where the processed information coming from a Side Scan Sonar are used to update the objective function that, when optimized, gives new reference to the vehicle guidance system.

The proposed planner proposes the following contributions:

- it provides waypoints, instead of a continuous heading reference. This allows to obtain a LMP-behavior useful for mosaicking applications;
- it is based on feedback from still-camera pictures;
- does not aim on optimizing the coverage of an area. On the other hand, it tries to cover the highest amount of OOIs that can sense.

The paper is organized as following: Section 2 presents the motivation and the modeling of the individuated objects, Section 3 gives information on the mosaicking mission needs. Section 4 formulates the path-planning algorithm, and the components of the target function. Section 5 presents the simulations set-up and Section 6 shows the results of the simulation and performance comparisons with the standard low-mower patterns. Conclusions and further work are described in Section 7.

2. CAMERA DATA ANALYSIS

The nature of the sensors that is employed to sense the environment will deeply influence the methodology used to automatically re-plan the mission or the path. This is due to two characteristics: the different working frequency of the sensors (where the data processing time should be also considered), and the covered area at every sample. Paull et al. (2012, 2013) uses a SSS (Side Scan Sonar), which provides high frequency data, spanning an area that is tens of meters wide towards both the sides of the vehicle.

2.1 Still-Picture Camera

In this work a still-picture camera is used to sense the environment. Cameras provide the following benefits:

- they are cheap sensors that are often part of the standard payload of underwater vehicles;
- they provide a complete and intuitive representation of the pictured area and can produce data for mosaicking;
- they don't require continuous illumination (strobes could be used) reducing power consumption.

On the other hand, the image processing requires time and puts limitations on the working frequency of the planner. Moreover the pictured area is of few square meters ($< 25\text{m}^2$, depending by the vehicle altitude, light field and water characteristics), giving only a small overview of the area at every shoot, making the planning-ahead more challenging.

This work does not focus on the image processing part (that is OOIs detection and recognition, Fig. 2, n.2), so the image dataset is supposed to be already processed (Fig. 2, n.3). Some works in literature proposes methods to automatically recognize and classify biological OOIs: Purser et al. (2009), for instance, detects the coverage of corals and sponges in the pictures.

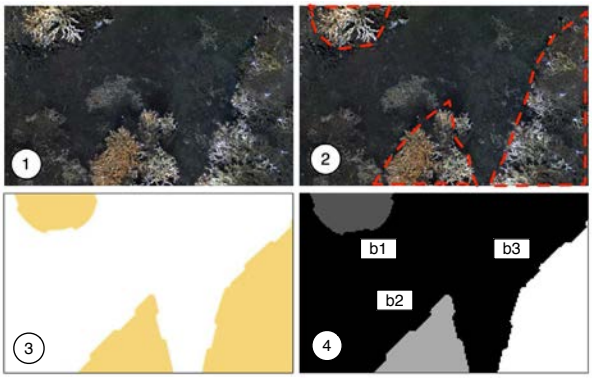

Fig. 2. The considered OOIs are corals colonies. Image processing algorithms could recognize their main features in the images. (1) is the original picture, in (2) the corals features are extracted. We suppose that the processed data (3) is already available (pictures have been manually processed off-line). in (4) the different pixels blobs are recognized. The dataset used in this paper is based on a photo mosaic created from real pictures collected at the Tautra coral reef, Norway, with Minerva ROV, see Fig. 5.

A standard 50 mm camera gives a field of view with vertical angle of 27.0° and horizontal angle of 39.6°. Those angles should then be reduced of a factor due the refraction characteristics of water, that can be approximated with a factor of $n_w = 1.339$ for sea water (Wozniak and Dera, 2007). The new camera angle of view (α') becomes:

$$\alpha' = 2 \arcsin \left[\frac{\sin(\alpha/2)}{n_w} \right] \tag{1}$$

Given the relative position of the vehicle to the respect of the sea bottom (that is considered to be flat), and the relative position of the camera with the vehicle, it is possible to determine the projection of the image (as in Fig. 4) with simple geometry calculations.

2.2 OOIs Modeling

The binary image (Fig. 2, n.3) is analyzed to find the connected components (named *blobs*, Fig. 2, n.4) that can be described as the connected and homogeneous groups of pixels with similar characteristics. Since the images, as stated above, give only a limited spatial information about the sea bottom, some assumptions about the neighborhood of the analyzed picture have to be done in order to know where to direct the vehicle: an estimation of how the blob could possibly extend in the neighborhood of the picture is then needed. Key factors here are the knowledge of its *main orientation* and the assumption that the blobs representing the OOIs have *continuous distribution*.

A1. The OOIs are ***homogeneously distributed***, that means that they occupy the space in colonies, covering dense areas. This is a realistic assumption for coral colonies, seagrass forests or human artifacts, such as pipelines or ship wrecks.

Assumption 2.2 it's important since the information read from a single picture could not be extended to the surrounding area otherwise.

To extract the characteristics of the blobs the concept of moment of an area is used (Hu, 1962). This allows to calculate their center and main orientation. The raw moments of an area are defined as:

$$M_{pq} = \sum_x \sum_y x^p y^q f(x,y);\ (x,y) \in I \tag{2}$$

where x, y are the pictures pixels coordinates and $f(x,y)$ is either 1 or 0 respectively if the pixel is part of the blob or not. p, q determines the orders of the moment. The considered pixels are the ones contained in the image I. The *centroid* is given by $\left[\bar{x} = \frac{M_{10}}{M_{00}}, \bar{y} = \frac{M_{01}}{M_{00}}\right]$ and represents an approximated center point for the blob. Information about the orientation of the object can be obtained by the second order central moments:

$$\mu_{pq} = \sum_x \sum_y (x-\bar{x})^p (y-\bar{y})^q f(x,y);\ (x,y) \in I \tag{3}$$

By choosing $\{p,q\} = \{2,0\}, \{0,2\}, \{1,1\}$, it is possible to calculate the following matrix:

$$\Sigma = \begin{bmatrix} \mu'_{20} & \mu'_{11} \\ \mu'_{11} & \mu'_{02} \end{bmatrix} \tag{4}$$

where the apex represents the normalization of the values with the zero order moment μ_{00}. The eigenvalues and eigenvectors of this matrix are equals, respectively, to the modules and directions of the axis of the ellipse that has the same second order moments as the related blob. This extension of this ellipse outside the current picture can give some estimation on where it could be more interesting to navigate. Assumption **A1** is crucial in this context, since the ellipses (the considered models of the OOIs) represent a compact and homogeneously distributed area and, from this moment on, will be considered as the model of the blob and, indirectly, the model of the OOI.

3. MOSAICKING APPLICATION

The planning of the path aims to cover the highest amount of OOIs to provide the chance of building a mosaic of the explored area. The interval between the pictures should be long enough to allow image processing to individuate the blobs, on the other hand following pictures should contain a certain overlap to allow the mosaicking process (Ludvigsen et al., 2007). The vehicle speed, altitude and the pictures frequency have then to be chosen given the aforementioned factors. Notice that the pictures dedicated to the mosaic process could be taken at higher frequency than the ones dedicated to the navigation (since no specific overlapping constraints are needed in the latter case).

In this work a lawn-mower-like pattern behavior is prioritized, since it allows to collect data on neighbors area. The data collected along a LMP is easier to interpret for an end-user (since the shooting points are along a known-shaped path), and also makes the process of mosaicking easier and faster.

Table 1. Maximum velocities and transect spacing for a LMP with required picture overlapping of 30%. Angle of view defined in (1).

Pic.Freq. [Hz] \ Alt. [m]	2	3	4	5
2	2.26 $[\frac{m}{s}]$	3.38 $[\frac{m}{s}]$	4.50 $[\frac{m}{s}]$	5.62 $[\frac{m}{s}]$
1	1.13 $[\frac{m}{s}]$	1.69 $[\frac{m}{s}]$	2.25 $[\frac{m}{s}]$	2.81 $[\frac{m}{s}]$
0.5	0.56 $[\frac{m}{s}]$	0.85 $[\frac{m}{s}]$	1.13 $[\frac{m}{s}]$	1.40 $[\frac{m}{s}]$
Trans. Spacing [m]	1.84	2.76	3.68	4.59
Covered Area [m^2]	4.1	9.2	16.4	25.63

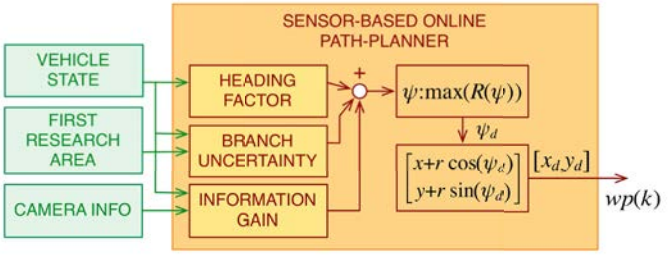

Fig. 3. Main blocks of the planner. Given the vehicle state, the user defined FRA and the pictures information (green blocks in the Figure), the sensor-based online path-planner calculates the components of the objective function (described in Section 4). The maximization of the objective function, together with the vehicle kinematics define the following waypoint. The functional elements of the planner are grouped in the orange block in the Figure.

In Table 1 maximum speeds of the vehicle as a function of altitudes and pictures shooting frequencies is shown. The values are calculated considering the need of at least 30% of pictures overlapping. Notice that lateral overlap is also needed, so the *maximum transects spacing* (distance between parallel lines) is shown as well.

4. AUTOMATIC PATH PLANNER

Inspired by Paull et al. (2013), the objective function is composed by three main components:

- the ***heading factor*** $J(\psi)$, related to the heading changes (prioritizes the choice of a new waypoint along the current direction, to decrease the heading changes. In this context this terms tries also to prioritize heading changes that would make a lawn-mower-like pattern);
- the ***information gain*** $B(\psi)$, given by the sensor feedback of the pictured area (prioritizes the exploration of the area containing the OOIs);
- the ***branch uncertainty*** $G(\psi)$, related to the unvisited area (prioritizes the unexplored parts of the pre-selected area).

Those three terms will compose the total utility $R(\psi)$, a function that depends by the vehicle heading and that, maximized, will provide the desired heading and, consequently, the next waypoint.

In the planning phase the following aspects will be taken in account:

A2. Underwater operations have to deal with ***limited resources***. In particular the energy and time limits decides the maximum length of the mission;
A3. the sea bottom is supposed to be ***highly unknown***. Otherwise the mission could be optimally pre-planned off-line. A basic knowledge of the area is supposed to be known, to define a *First Research Area* (FRA) and an approximation of the coral coverage on it;
A4. the vehicle can leave the FRA if estimates the presence of OOIs outside it, in other words ***the sensor information is prioritized*** over the coverage FRA.

A general scheme of the planner is shown in Fig. 3.

4.1 Cells division

The sea-bottom is divided into a squared cells grid:

$$W = \bigcup_{i=1}^{N_c} c_i \tag{5}$$

where c_i represents a cell, W represents the considered map of the sea bottom. Waypoints are chosen along the lines connecting the centers of the cells, diagonal movement are not allowed.

The cell dimension is calculated depending on the approximated coverage surface at the given vehicle altitude, in particular the distance between the centers of neighbors cells will be chosen to guarantee the necessary overlap between pictures taken from parallel transects (Table 1).

The cells division is useful for two main reasons: allows to easily account for visited areas and for the probability of presence of an OOI. Moreover provides a grid where waypoints could be easily chosen.

4.2 Lawn-Mower Pattern

Chosen a starting area of interest, the mission starts following a pre-defined LMP designed inside the aforementioned FRA. This path will be run at constant speed taking regular pictures at a frequency depending by its speed and altitude (Table 1) until any OOI is found in the field of view of the camera. As soon as something is detected the sensor-based on-line path-planner is triggered, starting to select the following waypoints (Fig. 3).

4.3 Target Function

The desired waypoints will be the one that correspond to the heading that maximizes the objective function $R(\psi)$:

$$R(\psi) = \omega_G G(\psi) + \omega_B B(\psi) + \omega_J J(\psi) \tag{6}$$

where $G(\psi), B(\psi), J(\psi) \in [0,1]$ and $\omega_G, \omega_B, \omega_J \in \mathbb{R}$ are gains useful to tune the behavior of the planner.

Notice that in this context the heading will be chosen in a finite discrete set that will include three alternatives:

$$\psi_d = argmax\big\{R(\psi)\big\}, \quad \psi \in \{0, 90, -90, 180\} \tag{7}$$

The choice of having those three possible alternatives is motivated by the fact that a LMP-behavior is favorable.

4.4 $J(\psi)$: Heading Factor

A gain is associated with the heading changes. Notice that $\psi_d = 0$ means that the desired heading (measured in the vehicle frame) is required not to be changed. A constant gain is assigned to the possible desired headings:

$$\begin{aligned} J(0) &= \omega_0; \\ J(90) &= J(-90) = \omega_{90}; \\ J(180) &= \omega_{180}. \end{aligned} \tag{8}$$

where $\omega_0 > \omega_{90} \in [0 \dots 1]$, $\omega_{180} = 0$. The higher the gain, the higher the chance of that desired heading to be chosen. The direction that allows to keep the heading constant assumes a higher gain than any change. Notice that, although an immediate inversion of direction is not allowed, the angle $\psi = 180$ is still considered, since it may give indications that an inversion of direction may be needed, and this could be achieved with two following turns. A penalty is set to the heading that would set the new waypoint to be outside the FRA:

$$J(\psi) = 0 \text{ if } \{x_d \notin [x_{\min}, x_{\max}] \vee y_d \notin [y_{\min}, y_{\max}]\} \tag{9}$$

where $[x_{\min}, x_{\max}]$ and $[y_{\min}, y_{\max}]$ represents respectively the x and y limits of the area.

Notice that some exceptions are added to the algorithm in order to force a LMP-like trajectory. For instance:

- $J(0)$ and $J(90)$ are increased at step $(k+1)$ if 90 degrees was the chosen direction at step k (symmetric condition holds as well);
- $J(0)$ is increased at step $(k+1)$ if 0 degrees was the chosen direction at step k and $B(0) > 0.1$;
- $J(90)$ is increased if $B(180) > 0.8$ and $J(90) > J(-90)$ (symmetric condition holds as well).

The magnitude of the gains increase is constant along the path, and it is set up in the tuning phase.

4.5 $B(\psi)$: Information Gain

The probability of OOIs presence associated to every cell is estimated through a simple application of the Bayes formula, that results in the probability of the *OOIs presence* (A) conditioned by the *picture and blobs analysis* (B) result:

$$P(A|B) = \frac{P(B|A)P(A)}{P(B)} \tag{10}$$

where:

$$\begin{aligned} P(B|A) &= k \cdot c_{bd} \frac{\sum_i |a_b|}{|c|} \cdot \sum_i \iint_c b(x,y)_i \, dxdy \\ P(A) &= c_0 \\ P(B) &= P(B|A)P(A) + P(\bar{A})P(B|\bar{A}) \\ P(\bar{A}) &= 1 - P(A) = 1 - c_0 \\ P(B/\bar{A}) &= 1 - c_{bd}. \end{aligned} \tag{11}$$

where $0 \le k \le 1$, $0 \le c_{bd} \le 1$ is the confidence of the chosen blob-detection algorithm (e.g. the 15-point automatic algorithm, see Purser et al., 2009), $|a_b|$ is the area of the ellipse that overlaps to the considered cell, $|c|$ is the area of the cell, $b(x,y)$ is either 1 if the pixel (x,y) of the cell is covered by the ellipse, otherwise zero. $0 \le c_0 \le 1$ is an a-priori estimation of the presence of the OOIs in the FRA. The index i counts the number of ellipses in a certain cell. The overlapping area, if present, is not considered and it is evaluated only for one of the ellipses. To translate the

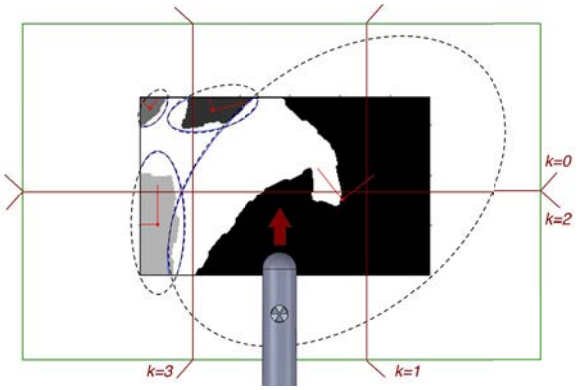

Fig. 4. The vehicle, the pictured area (the rectangle with the blobs) and the OOIs (the blobs) are represented. The ellipses that model the blobs (with the axis directions) give information on how they could possibly extend outside the pictured area. The cells are also represented (squares with red and green borders). The *branches* are represented with the index k.

cells probabilities to a single value for every direction, the same branch approach explained in Subsection 4.6 is used. Notice that if a new probability value is associated to the same cell in a further step, only the maximum value is kept in memory. Fig. 4 shows the picture taken from the vehicle, the blobs and their model.

4.6 G(ψ): Branch Uncertainty

The branch uncertainty attracts the vehicle towards the most unexplored part of the FRA (i.e. the cells where the vehicle has not been traveling yet, independently by the foreseen presence of some OOIs on them), so that this area is prioritized over the rest of the seabed. It is allowed for the vehicle to leave it temporarily if some OOIs are found out of it. This term is slightly different from the one in Paull et al. (2012, 2013) since for every possible branch only the number of unvisited cells is considered:

$$G_k = \frac{\sum_{l=1}^{L} (L-l+1) \sum_{i=1}^{m_{lk}} \frac{\hat{H}_i}{m_{lk}}}{\sum_{i=1}^{L-1} l} \qquad (12)$$

where $k = 0, 1, 2, 3$ represent the possible branches (corresponding to the area that the vehicle would approach if one direction is chosen, as shown in Fig. 4), l is the *level* of every cell (the number of cells that is necessary to travel from the current location to reach it), L is the total number of levels, m_{lk} is the number of cells in level l of the branch k. $\hat{H}_i$ is the entropy value of the cell i, that can be either 0, if the cell has not been visited, or 1, if the cell has been visited. Notice that $G(90 \cdot k) = G_k$.

5. SCENARIO DESCRIPTION

The chosen scenario is based on a black and white map, where the OOIs, represented as black spots, are estimated off-line from the analysis of a real mosaic of a coral reef. This mosaic, of dimensions 20m × 10m and centimeter resolution, is replicated to create a bigger area of dimensions 80m × 40m (see Fig. 5), giving a realistic seabed map to be used for simulations. The simulations are

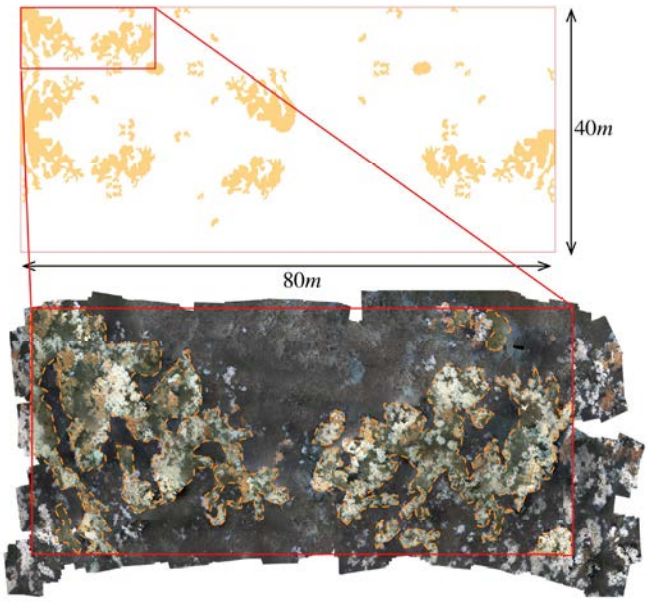

Fig. 5. The photomosaic has been created using the images taken from the ROV Minerva at the Tautra coral reef, Norway, in April 2012. The main corals distribution has been detected and underlined. In order to make the map bigger (to extend the simulated mission time) and to keep the realistic distribution of the coral, the final map (orange map above the mosaic) has been composed in a modular way, using the original photomosaic as the main module. Notice that the *modules* have not been only stitched together but also mirrored, rotated, and slightly modified in order to increase the variability of the map.

initialized choosing random starting points and FRAs in this map, to verify that the performance of the algorithm are not strictly related with the initial conditions. Notice that the coral-mapping application is only a choice for this work. Any other OOIs respecting the aforementioned assumptions could be treated.

6. SIMULATIONS

Fig. 6 and Fig. 7 show two simulation results. In the first one a simple map is considered to illustrate the algorithm behavior: the vehicle starts in a straight line until some object is seen, then a LMP (light blue section) tries to cover the OOIs distribution. The remaining part is covered by the second LMP (violet section), then the vehicle goes back to the FRA and starts a LMP to search for new objects (blue section). When new OOIs are found the vehicle starts mapping them (brown and light blue sections). In this simulation the LMP would have visited 74 cells with OOIs, while the proposed planner visits 109 cells with OOIs (+83%).

The second case is based on the real map of Fig. 5. Here is also possible to see how the vehicle follows the same logic, designing LMPs on top of the OOIs that sees along its way. In this example the LMP designed on the FRA would have found 48 cells with OOIs, while the planner visits 155 cells with OOIs (+223%). Notice that both the simulations are

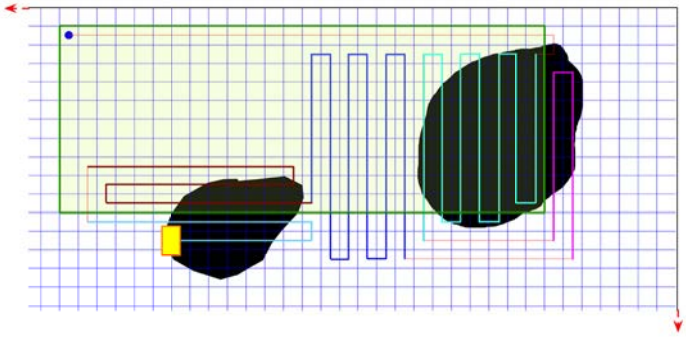

Fig. 6. Simulation case 1. The vehicle starts from the blue dot in the top left part of the FRA (green box). Five LMPs are designed to map the OOIs. The yellow box shows the last pictured area of the vehicle. The red arrows on the borders of the maps indicates that the map extends in those directions.

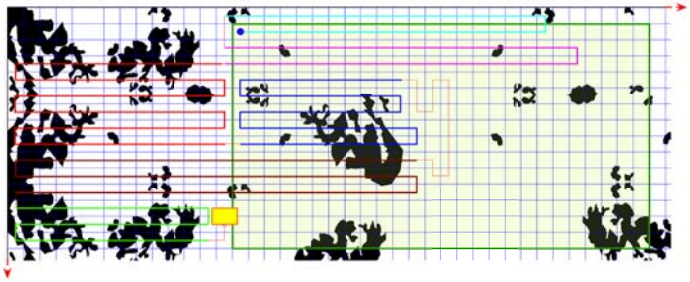

Fig. 7. Simulation case 2. The vehicle starts from the blue dot in the top left part of the FRA (green box). Five LMPs are designed to map the OOIs that are found along the way. It is clear how the vehicle seeks for the OOis, avoiding empty areas.

Table 2. Comparison between the predefined LMP and the proposed planner for 30 different simulations (random initial point, direction and FRA) based on the map of Fig. 5.

	LMP	ON-LINE PLANNER
Cells w/OOI	84.95	105.45
Cells w/OOIs (comp.)	-	+24.13%
Turns	23.4	83.05
Turns/100m	5.28	14.88
Turns (comp.)	-	+254.91%

aborted when the vehicle ends its autonomy, that means that, from the next step, the vehicle will have to go back to the starting point to be retrieved.

A broader set of tests is presented in Table 2. 30 simulations have been launched on the map, randomly choosing the initial waypoint and the dimension of the FRA. The number of OOIs seen by the proposed planner and by a classic LMP defined on the FRA is compared, together with the number of turns. It is possible to notice that in any case the proposed planner increases the number of visited OOIs; on the other hand the number of turns increases as well. The gains are kept constant for the whole set of simulations: $\omega_G = 10$, $\omega_B = 20$, $\omega_J = 12$.

7. CONCLUSIONS

This paper proposed a sensor-based on-line path-planner. This planner uses the information provided by cameras mounted on an underwater vehicle to guide it towards the area with the highest probability of presence of OOIs. This methodology is focused on creating a path that can be used to perform photo-mosaicking of the sea-bottom while navigating. Simulations are proposed to show its advantages over a standard LMP, often used for this kind of missions.

Further work will include the AUVs/ROVs dynamics in the simulations (this will also imply the necessity of foresee more than one waypoint at every step), in order to verify the feasibility of the path following also in presence of currents or waves disturbance. For instance, currents could be considered to orient the generated path in such a way that the energy consumption is optimized. The picture analysis part should be treated as well, offering a practical example of the quality of the information that can be extracted from real underwater pictures for this purpose. Sea-trials should also be run to validate the algorithm.

REFERENCES

Acar, E.U., Choset, H., Zhang, Y., and Schervish, M. (2003). Path planning for robotic demining: Robust sensor-based coverage of unstructured environments and probabilistic methods. *The International Journal of Robotics Research*, 22(7 - 8), 441 – 466.

Cai, C. and Ferrari, S. (2009). Information-driven sensor path planning by approximate cell decomposition. *Systems, Man, and Cybernetics, Part B: Cybernetics, IEEE Transactions on*, 39(3), 672–689. doi: 10.1109/TSMCB.2008.2008561.

Hu, M.K. (1962). Visual pattern recognition by moment invariants. *Information Theory, IRE Transactions on*, 8(2), 179–187. doi:10.1109/TIT.1962.1057692.

Ludvigsen, M., Sortland, B., Johnsen, G., and Singh, H. (2007). Applications of geo-referenced underwater photo mosaics in marine biology and archaeology. *Oceanography*, 20(4), 140–149.

Paull, L., Saeedi, S., Seto, M., and Li, H. (2013). Sensor-driven online coverage planning for autonomous underwater vehicles. *Mechatronics, IEEE/ASME Transactions on*, 18(6), 1827–1838. doi:10.1109/TMECH.2012.2213607.

Paull, L., SaeediGharahbolagh, S., Seto, M., and Li, H. (2012). Sensor driven online coverage planning for autonomous underwater vehicles. In *Intelligent Robots and Systems (IROS), 2012 IEEE/RSJ International Conference on*, 2875–2880. doi:10.1109/IROS.2012.6385838.

Purser, A., Bergmann, M., Lundälv, T., Ontrup, J., and Nattkemper, T. (2009). Use of machine-learning algorithms for the automated detection of cold-water corals habitats: a pilot study. *Marine Ecology Progress Series*, 397, 241–251.

Seto, M. (2013). *Marine Robot Autonomy*. Springer.

Tsourdos, A., White, B., and Shanmugavel, M. (2010). *Path Planning for Multiple UAVs, in Cooperative Path Planning of Unmanned Aerial Vehicles*. John Wiley & Sons, Ltd, Chichester, UK.

Wozniak, B. and Dera, J. (2007). *Light Absorption in Sea Water*. Springer.

Article H

Continuous Curvature Path Planning using Voronoi diagrams and Fermat's spirals

M. Candeloro, A.M. Lekkas, A.J. Sørensen and T.I. Fossen

The article has been published in the proceedings of the
9th IFAC Conference on Control Applications in Marine Systems (CAMS),
IFAC-PapersOnLine
Volume 9 (1), pages 132–137. Osaka, Japan, 17-20 September 2013.

9th IFAC Conference on Control Applications in Marine Systems
The International Federation of Automatic Control
September 17-20, 2013. Osaka, Japan

Continuous Curvature Path Planning using Voronoi diagrams and Fermat's spirals

Mauro Candeloro [*,**] **Anastasios M. Lekkas** [***]
Asgeir J. Sørensen [*,**] **Thor I. Fossen** [**,***]

[*] *Department of Marine Technology, NTNU, Trondheim, Norway*
[**] *Centre for Autonomous Marine Operations and Systems (AMOS), NTNU, Norway*
[***] *Department of Engineering Cybernetics, NTNU, Trondheim, Norway*

Abstract: This paper presents a two-dimensional curvature-continuous path planning algorithm based on Voronoi diagrams and Fermat's spiral segments. The map and the obstacles position are assumed to be known *a-priori* and static. Despite the disposition of the obstacles, the Voronoi diagram always presents at least one collision-free path, maximally distant from all the obstacles. If more than one *flyable* path is available, the shortest one is selected. The result is further refined to obtain a more practical path that is piecewise linear with discontinuous curvature and velocity. Fermat's spirals are used to smooth the path and provide curvature-continuity. A maximum threshold for the curvature is set so that the result of the algorithm respects kinematics and dynamics constraints of the vehicle. Moreover a minimum clearance from the obstacles can be chosen to respect additional safety constraints. The final result of the algorithm is a simple and intuitive path composed only by straight lines and spiral segments.

Keywords: Path Planning, Fermat's Spiral, Voronoi Diagram, Obstacle Avoidance.

1. INTRODUCTION

Guidance systems and path planning algorithms are crucial for the motion control system performance of an autonomous or semi-autonomous vehicle (LaValle, 2006, Breivik and Fossen, 2009). This is true regardless on the kind of vehicle (such as ships, planes, AUVs: Autonomous Underwater Vehicles , ASVs: Autonomous Surface Vehicles, UAVs: Unmanned Aerial Vehicles) and it assumes a critical level of importance for operations in cluttered environment. In this case, in fact, the performance depends upon the ability of the vehicle to meet the path characteristics. Many algorithms have been proposed to produce a path that would allow good tracking performance. It is possible to mention, for instance, the potential field method, the *FM** algorithm and its variations, genetic algorithms, grid-based methods, quadratic programming and so on (LaValle, 2006, Pêtrès et al., 2007, Tsourdos et al., 2011).

As the name indicates, path planning pertains to the procedure of determining which route to take when moving from one location to another, given a certain number of waypoints to reach along the path. Often only an endpoint is specified, while the intermediate waypoints are used for the geometrical construction of the path in such a way that the performance requirements can be assured (Figure 1).

The most critical performance requirement is safety: the vehicle should not collide or even go too close (hence putting itself in a risky situation) to any obstacle located in the navigation space. A *clearance factor*, i.e. the minimum vehicle-obstacles distance is defined to achieve this purpose. The path planning should also consider the vehicle kinematics and dynamics characteristics (Tsourdos et al., 2011) so that the resulting path can be *flyable* from the target vehicle. This *flyability* property is mainly due to the curvature characteristics of the path, that has to be a *continuous* function not exceeding a certain (maximum) threshold (corresponding to the maximum turning radius of the vehicle). The continuity requirement is important because it avoids, for instance, discontinuities in the cross-track error, i.e. deviations from the desired path that can decrease the control performance (Nelson, 1989, Pêtrès et al., 2007). Finally, if more routes are able to reach the endpoint by respecting the requirements, the *shortest-length* path is selected and further refined.

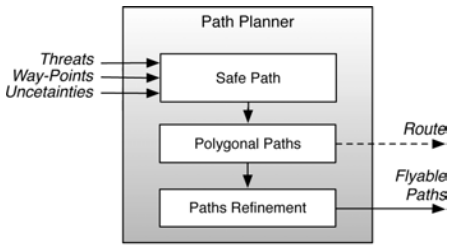

Fig. 1. Approach to path planning (Tsourdos et al., 2011).

We can summarize the goal of this paper as following: a path $\boldsymbol{r}(q)$, $q \in \mathbb{R}$ that connects the final position (target) $\boldsymbol{P}_{fi}$ from the starting position $\boldsymbol{P}_{si}$; respecting the aforementioned constraints has to be defined:

$$\boldsymbol{P}_{si}(x_{si}, y_{si}) \xrightarrow{\coprod_{safe}, \coprod_{\kappa}, \coprod_{length}, \boldsymbol{r}(q)} \boldsymbol{P}_{fi}(x_{fi}, y_{fi}) \quad (1)$$

Where (x_{si}, y_{si}) and (x_{fi}, y_{fi}) are respectively the initial and final coordinates, and $\coprod_{safe}$, $\coprod_{\kappa}$ and $\coprod_{length}$ are the *safety*, the *curvature* and the *length* constraints.

In this paper the two dimensional case with static obstacles will be considered, giving the fundamentals to generalize the approach to three dimensions in future work. Despite this simplification the presented results are not trivial and can be used in many applications: ships and ASVs are underactuated vehicles that require only two-dimensional path planners, while special AUVs applications can require to define obstacle-free waypoints at the surface to perform localization updates through GPS signals by emerging from time to time. In this case the generated path can be seen as the surface-projection of a three-dimensional underwater path.

The main contributions proposed in this paper concern the employment of Voronoi diagrams in path planning for marine applications (they have been mainly used for terrestrial robots) to design an algorithm that produces a simple path (only composed by straight lines connected by spirals) that gives a more natural and intuitive result than the widely used Bezier curve (used in Ho and Liu, 2009b, Ho and Liu, 2009a). The final result still provides curvature continuity respecting maximum turning radius of the vehicle.

This paper is organized as following: Section 2 describes the obstacles generation and Voronoi diagrams, Section 3 describes Fermat's curve and curvature continuity properties, Section 4 lists the main steps of the path planning algorithm and path refinement steps, Section 5 presents simulation results. Finally, Section 6 states the conclusions and introduce further work and possibilities. The paper structure follows the classical approach to path planning, also represented in Figure 1.

2. VORONOI DIAGRAMS FOR PATH PLANNING

Voronoi diagrams have been used for many applications since the beginning of the 20th century, and many possibilities have been found in the path planning problems for mobile robots autonomous environment exploration. This is due to three main aspects: **a)** The Voronoi diagram is a strong geometrical tool that divides the geometrical space in a way such that the borders of the regions are maximally distant from all the obstacles in the cluttered environment, **b)** it is an algorithm that has $\boldsymbol{O}(n)$ complexity, while the majority of other mathematical tools can solve the same problem with quadratic complexity and **c)** mobile robots kinematics allows them to change heading without affecting the other DOF (degrees of freedom), so they can easily run a path composed only by a sequence of straight lines. Some examples in this field are Matsumoto et al. (2007), Bhattacharya and Gavrilova (2007), Zhou et al. (2011), Ho and Liu (2009a,b); Bortoff (2000), Chandler et al. (2000) are examples of path planning for underactuated vehicles.

An in-depth description of Voronoi diagrams and their possible applications can be found in Aurenhammer (1991).

2.1 Mathematical Formulation

The basic idea behind Voronoi diagrams is explained in the following: a finite set of points $\boldsymbol{P} = \{p_1, ..., p_2\}$, called *generator points*, are contained in a space $\boldsymbol{X}$ (in this work $\boldsymbol{X} \subset \mathbb{R}^2$) where a metric function $d(\cdot)$ is defined. The procedure associates to each point $p_i \in \boldsymbol{P} \subset \boldsymbol{X}$ a *Voronoi region* $\boldsymbol{R}_i$ defined as the set of points $x_i \in \boldsymbol{X}$ such that their distance to p_i is lower than the distance from x_i to any other point of $\boldsymbol{P}$. In mathematical terms, if:

$$d(x, p) = \inf\{d(x, p) | p \in \boldsymbol{P}\} \tag{2}$$

the Voronoi region is defined as:

$$\boldsymbol{R}_k = \{x \in X | d(x, \boldsymbol{P}_{\mathrm{k}}) \leq d(x, \boldsymbol{P}_{\mathrm{j}}) \forall j \neq k\} \tag{3}$$

The final Voronoi diagram $\boldsymbol{V}(p_i)$ will consist in the set of the Voronoi regions borders, that is the intersection of the tuple of cells $(\boldsymbol{R}_k)_{k \in \boldsymbol{K}}$:$\boldsymbol{V}(p_i) = \bigcap_i \boldsymbol{R}_i$, where $\boldsymbol{K}$ is a set of indexes. It is obvious that the shape and the properties of the final diagram will depend on the definition of the metric used in the process (for instance curved Voronoi diagrams are presented in Boissonnat et al., 2006): this freedom justifies the versatility of this tool.

2.2 Obstacles and Metric Definition

Using Voronoi diagrams for path planning and obstacle avoidance it is straightforward if the obstacles are considered to be the generator points p_i. In this case the borders of the Voronoi regions $\boldsymbol{R}_i$ are composed by the points that are maximally distant from the obstacles or, in other words, the points that can be harmlessly navigated. Some implementations of the Voronoi scheme also imply the definition of a *clearance factor* (Bhattacharya and Gavrilova, 2007) to reduce the distance path-obstacles (where possible) reducing the length of the final path, i.e. the fuel consumption of the vehicle.

In this work we will consider complex polygons as obstacles; they are generated as simple geometrical representation of the obstacles (islands and mainland) of a real map. The objects vertexes have been chosen to be the generator points of the Voronoi diagram.

The L_2-distance function (the Euclidean distance) has been considered as the metric function $d(\cdot)$:

$$d\{(x_1, y_1), (x_2, y_2)\} = \sqrt{(x_2 - x_1)^2 + (y_2 - y_1)^2} \tag{4}$$

this metric will generate Voronoi regions with straight borders. A possible path can then be a sequence of straight lines (regions borders) connected at their endpoints that links the starting with the final waypoints. Such a path can be a starting result to be further refined in order to achieve the performance constraints.

3. FERMAT SPIRALS: THEORY AND ADVANTAGES

As previously mentioned, the construction of the path should reflect the dynamics and kinematics properties of the vehicle. For mobile robots it is possible to design discontinuous paths: they can easily stop, direct the heading to a new waypoint and then start moving again towards it. This is not possible, in general, for every vehicle. In particular for underactuated vehicles the motion of some DOFs can influence the others (coupled dynamics); consequently the path needs to be modified in order to become *flyable*: this can be achieved providing continuous curvature.

In this work this issue is faced by connecting straight segments with spiral segments that are able to *smooth* the

discontinuity of the Voronoi diagrams at the edges of the Voronoi regions. The curvature of the resulting path will be zero along the straight segments, it will continuously increase at most at the maximum feasible curvature of the vehicle and finally decrease continuously to zero to join a new straight line. Usually this procedure is done by using spirals segments (Tsourdos et al. 2011) that provide, unlike circular arcs, curvature continuity joints. Clothoids are the most widely used curves for those kind of applications, however their design depends on Fresnel integrals that do not have an explicit solution. Pythagorean hodographs are also common for such applications, their weak aspect is that their final shape is often difficult to model, and the flexibility can only be guaranteed by increasing the order of the polynomials and so the complexity.

In this paper Fermat spirals, a special case of Archimedean spirals, have been used. The main reasons for choosing the Fermat's spiral are two: **a)** it can be connected with a straight line because the curvature is zero at its starting point, **b)** it is extremely easy to implement and fast in term of computational requirements (Dahl, 2013).

3.1 Mathematical basis

The following theoretical analysis is based on Dahl (2013). If a straight line is rotating with constant angular velocity around a fixed point (the center of the spiral), the Archimedean spiral can be drawn by a point starting from a center point and moving away from it along the rotating line. In polar coordinates this is expressed by:

$$r = b + a\theta^{1/x} \tag{5}$$

where (r, θ) are the polar coordinates and b and a are designing parameters that define the turning of the spirals and the distance between successive turnings. By setting $x = 2$ and $b = 0$ we get the Fermat's spiral, that is the geometrical curve we used in this work; in this case:

$$r = a\sqrt{\theta} \tag{6}$$

that is, in Cartesian coordinates:

$$\begin{bmatrix} x \\ y \end{bmatrix} = \begin{bmatrix} x_0 + a\sqrt{\theta}\cos(\rho\theta + \chi_0) \\ y_0 + a\sqrt{\theta}\sin(\rho\theta + \chi_0) \end{bmatrix} \tag{7}$$

Where we generalized the expression for any initial position $\boldsymbol{r}_0 = [x_0, y_0]$, both turning direction $\rho = \{1, -1\}$ and any different initial tangent angles χ_0. Notice that the parameter a is a scaling factor.

3.2 Curvature

By changing the Fermat's spiral parameters it is possible to achieve any curvature; its mathematical formulation is:

$$\kappa(\theta) = \frac{2\sqrt{\theta}(3 + 4\theta^2)}{a(1 + 4\theta^2)^{3/2}} \tag{8}$$

notice that the curvature depends only on the polar coordinates and on the scaling factor a. Moreover it is important to underline the inverse proportional relationship between the scaling factor and the curvature. Differentiating this expression and imposing it to be equals to zero we can find the value of θ that defines the maximum curvature:

$$\theta_{max} = \sqrt{\frac{\sqrt{7}}{2} - \frac{5}{4}} \tag{9}$$

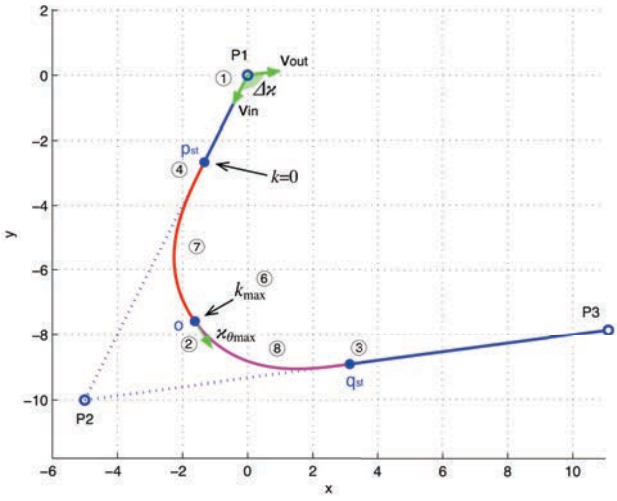

Fig. 2. Construction of Fermat's spiral link as explained in Subsection (3.3).

The curvature is important when it comes to the definition of a certain Fermat's spiral arc: this parameter should be monitored to be sure that the vehicle constraints are respected. Along the Fermat's spiral the curvature will continuously increase from zero to $\theta_{endpoint}$, that is the curvature of the last point of the spiral. θ_{max} is the maximum curvature that the spiral can mathematically reach. So for a spiral segment:

$$\theta_{\kappa_{max}} = \min\left(\theta_{endpoint}, \theta_{max}\right) \tag{10}$$

By setting a fixed maximum desired curvature it is possible to calculate the desired scaling factor:

$$a = \frac{1}{\kappa_{max}} \frac{2\sqrt{\theta_{\kappa_{max}}}(3 + 4\theta^2_{\kappa_{max}})}{\left(1 + 4\theta^2_{\kappa_{\max}}\right)^{3/2}} \tag{11}$$

Notice that the tangents of the curve for a certain θ can be found with the following expression:

$$\chi(\theta) = \arctan\left(\frac{\sin(\theta) + 2\theta\cos(\theta)}{\cos(\theta) - 2\theta\sin(\theta)}\right); \tag{12}$$

that is useful to provide smooth curvature transitions by imposing the same tangents in the connection points and to find the intersection points between the Fermat spirals and the straight lines.

3.3 Fermat's spiral joints algorithm

The implementation algorithm needs to receive as input the two straight segment that should be connected with the Fermat spiral. Notice that in this work the Fermat spiral is built such that the intersection point will correspond to the middle point of the shortest segment, this assures the continuity of the path in the case of two Fermat spirals that needs to be connected without a straight line in the middle. In general this technique provides the lowest curvature possible, that, from another point of view, requires the softest possible heading control.

The algorithm will follow the next steps (the steps numbers and symbols refer to Figure 2):

1. Find the initial and final tangents $\boldsymbol{v}_{in}$ and $\boldsymbol{v}_{out}$, and course change magnitude $\Delta\chi = \chi_{endpoint} - \chi_{startpoint}$;

2. Find endpoint tangent $\chi_{\theta_{max}} = \frac{\Delta\chi}{2}$ and the related θ (numerically) by solving (12);
3. Find intersection point with the shortest segment, that will be its mean point;
4. Find the intersection point $\boldsymbol{q}_{st}$ with the other segment by using (13) or (14) respectively if the first or the second segment is the shortest (Figure 2):

$$\begin{cases} l = \dfrac{-\boldsymbol{p}_{st} + \boldsymbol{P}_2}{\boldsymbol{v}_{in}} \\ \boldsymbol{q}_{st} = \boldsymbol{P}_2 + l \cdot \boldsymbol{v}_{out} \end{cases} \tag{13}$$

$$\begin{cases} l = \dfrac{-\boldsymbol{q}_{st} - \boldsymbol{P}_2}{\boldsymbol{v}_{out}} \\ \boldsymbol{q}_{st} = \boldsymbol{P}_2 - l \cdot \boldsymbol{v}_{in} \end{cases} \tag{14}$$

5. Find scaling factor corresponding to the desired curvature with (11);
6. Find maximum curvature with (10);
7. Calculate a sufficient number of points to approximate the curve from zero curvature to maximum curvature using (7);
8. Calculate the curve from maximum curvature back again to zero curvature (the last part of the link) by mirroring the formula used in step 6.

4. PATH PLANNING SOFTWARE

The path planning software is mainly based on 5 subroutines (Figure 3):

System parameters setting: defines obstacles, vehicle constraints, clearance factor and so on;
Obstacles definition: generates the obstacles map and the obstacles edges;
Path generation: defined the path connecting the starting and ending point;
Fermat's spirals design: smooths the path edges assuring curvature continuity;
Plotting: plots the result.

As mentioned above, the Voronoi diagram gives a first obstacle-free path defined by a set of waypoints, smoothed by the *Fermat's spiral design* module, that implements the algorithm of Subsection 3.3. The steps to achieve this goal are contained in the *Path generation* module. Figure 3 shows and enumerates the main functions of this module. The Voronoi diagram gives a raw obstacle-free roadmap (3.a), the paths that goes out the borders of the map are removed (3.b). Given a feasible path, its (almost)-collinear waypoints are removed (3.f) since having fewer waypoints reduces the length of the path, fuel consumption and heading changes. The clearance constraints is checked and an alternative path is chosen if the safety constraints are not met (3.g). Finally, unnecessary waypoints are removed (3.h). Steps (3.b), (3.f) and (3.h) are briefly explained in the following subsections. Notice that the clearance check should be repeated after step (3) since the spirals could violate the clearance constraints. In this case those should be re-drawn with a higher curvature, until the clearance constraints are met again. If this is not possible than other waypoints should be selected from the Voronoi diagram and the procedure repeated. This step is not included in Figue 3 for space reasons.

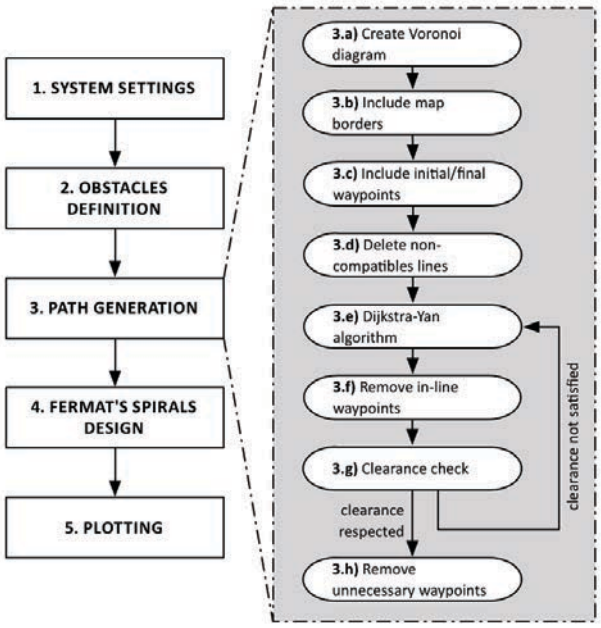

Fig. 3. Main modules of the path planning software. *Path generation* module steps are also represented.

4.1 Map borders constraint

The map borders that are obstacle-free are defined in the system parameters settings phase, and modeled as obstacles, not to be crossed. In this way any possible path going outside the map is avoided.

4.2 Remove in-line waypoints

The Voronoi diagram creates a high number of vertexes, proportional to the number of points that model the obstacles in the map. If all the vertexes defining a path would be considered we would have two negative effects: the first one is geometrical and it can bring to the necessity of defining spiral links with high curvature that could not be accomplished by the vehicle, the second one is practical, and it is connected to the fact that there is no meaning to perform the path $A - B - C$ if A and C can be connected with a straight line without decreasing the quality of the path. This means that, if A, B and C are almost collinear (a certain threshold defines the word "almost") then B can be eliminated. A similar approach can be found in Zhou et al. (2011).

4.3 Suppression of waypoints in excess

For the same reasons defined in Subsection 4.2 the final path can still be refined by eliminating all those waypoints that do not influence the quality of the path in terms of safety and clearance to the obstacles. The procedure can be summarized with the following pseudo-code:

```
1 function removeExcess(wayPoints)
2     for each waypoint do
3         Q1=waypoint(i);
4         Q2=waypoint(i+2);
5         P =waypoint(i+1);
```

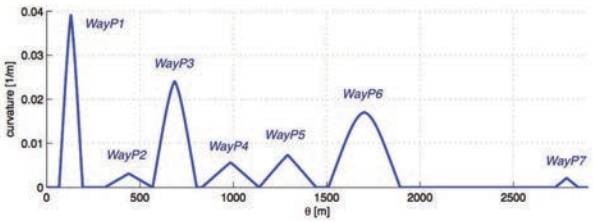

Fig. 4. Curvature as a function of distance from the starting point. Continuity of the function is clear. Peaks corresponds to waypoints.

```
6         if {clearance of ((Q1,Q2),Obst.)>thres.}
7             remove P from the list;
8         else
9             i=i+1;
10        end if;
11    end for;
12 end function.
```

5. SIMULATIONS

Figures 5 and 6 report the result of a simulation based on a real map of the Norwegian coastline, in particular part of Fensfjorden, 50Km north of Bergen is represented. The vehicle, that can be a fishing boat, a research vessel or a ferry operating in the fjord, needs to reach the *final point* from the *starting point* keeping a certain clearance from the obstacles and avoiding unnecessary turns or excessively long paths. The main results of the algorithm steps and the final results are reported in the figures. It is possible to see how the performance requirements are reached, providing a practical and intuitive path. Figure 4 provides the final path curvature; it is possible to see that the curvature is continuous and that the highest value of the curvature ($0.04m^{-1}$, corresponding to a turning radius of $25m$) can be feasible for the aforementioned vessels.

6. CONCLUSIONS

This paper presented the path planning problem with obstacle avoidance given a real map of the area of interest, the position of the obstacles, the initial and final waypoints and the vehicle kinematics and dynamics constraints. The Voronoi diagram has been used to obtain a set of feasible paths, the Dijkstra algorithm to select the shortest path in the set of the feasible ones (shortest in terms of distance) and Fermat's spirals to provide curvature continuity. Ad-hoc modifications of the algorithms provided also the ability of defining a path with a certain clearance to the obstacles to respect adjunctive safety constraints. Practical aspects are also considered in a final path refinement step and, to this direction, only the necessary waypoins are kept in order to reduce the required maximum curvature, and avoid unnecessary heading changes or longer paths (and, consequently, fuel consumption). Finally simulation results based on a real map of the Norwegian coastline have been presented. Further work will consider dynamic obstacles (such as ships) and the extension to three dimensions, providing a path planner algorithms suitable for any underwater or aerial application. As mentioned in Bortoff (2000), the main problem with Voronoi-based methods is that the effects of uncertainties of the map information are not considered. Consequently a local planner that considers the area surrounding the vehicle will be added to modify the path if new information about the obstacles in the navigation area makes unsafe the planned path. Finally, clearance constraints related to sea depth will be added to increase the operation safety.

ACKNOWLEDGEMENTS

This work has been supported by the Department of Marine Technology and the Centre for Autonomous Marine Operations and Systems (AMOS), both of the Norwegian University of Science and Technology (NTNU). The Norwegian Research Council is acknowledged as the main sponsor of AMOS.

REFERENCES

Aurenhammer, F. (1991). Voronoi diagrams - a survey of a fundamental geometric data structure. *ACM Computing Surveys*, 3, 345–404.

Bhattacharya, B. and Gavrilova, M. (2007). Voronoi diagram in optimal path planning. *4th Int. Symposium on Voronoi Diagrams in Science and Engineering*.

Boissonnat, J., Wormser, C., and Yvinec, M. (2006). Curved voronoi diagrams. *Effective Computational Geometry for Curves and Surfaces*.

Bortoff, S. (2000). Path planning for uavs. *In Proc. of the American Control Conference, Chicago, IL.*, 364368.

Breivik, M. and Fossen, T. (2009). Guidance laws for autonomous underwater vehicles. *Underwater Robots*.

Chandler, P.R., Rasmussen, S., and Pachter, M. (2000). Uav cooperative path planning. *In Proc. of AIAA Guidance, Navigation and Control Conference*.

Dahl, A. (2013). *Path Planning and Guidance for Marine Surface Vessels*. Master's thesis, NTNU, Norway.

Ho, Y. and Liu, J. (2009a). Collision-free curvature-bounded smooth path planning using composite bezier curve based on voronoi diagram. *Computational Intelligence in Robotics and Automation (CIRA), 2009 IEEE International Symposium on*.

Ho, Y. and Liu, J. (2009b). Smoothing voronoi-based obstacle-avoiding path by length-minimizing composite bezier curve. *International Conference on Service and Interactive Robotics, Taipei, Taiwan*.

LaValle, S. (2006). Planning algorithm. *Cambridge University Press*.

Matsumoto, Y., Imai, K., and Suzuki, H. (2007). Curved voronoi diagrams consisting of influence areas with differentiable boundaries. *4th International Symposium on Voronoi Diagrams in Science and Engineering*.

Nelson, W. (1989). Continuous-curvature paths for autonomous vehicles. *Robotics and Automation, 1989. Proceedings., 1989 IEEE International Conference on*.

Pêtrès, C., Pailhas, Y., Patrón, P., Petillot, Y., Evans, J., and Lane, D. (2007). Path planning for autonomous underwater vehicles. *IEEE Transactions on Robotics*, 23.

Tsourdos, A., White, B., and Shanmugavel, M. (2011). *Cooperative Path Planning of Unmanned Aerial Vehicles*. Wiley.

Zhou, F., Song, B., and Tian, G. (2011). Bezier curve based smooth path planning for mobile robot. *Journal of Information & Computational Science*, 8, 2441–2445.

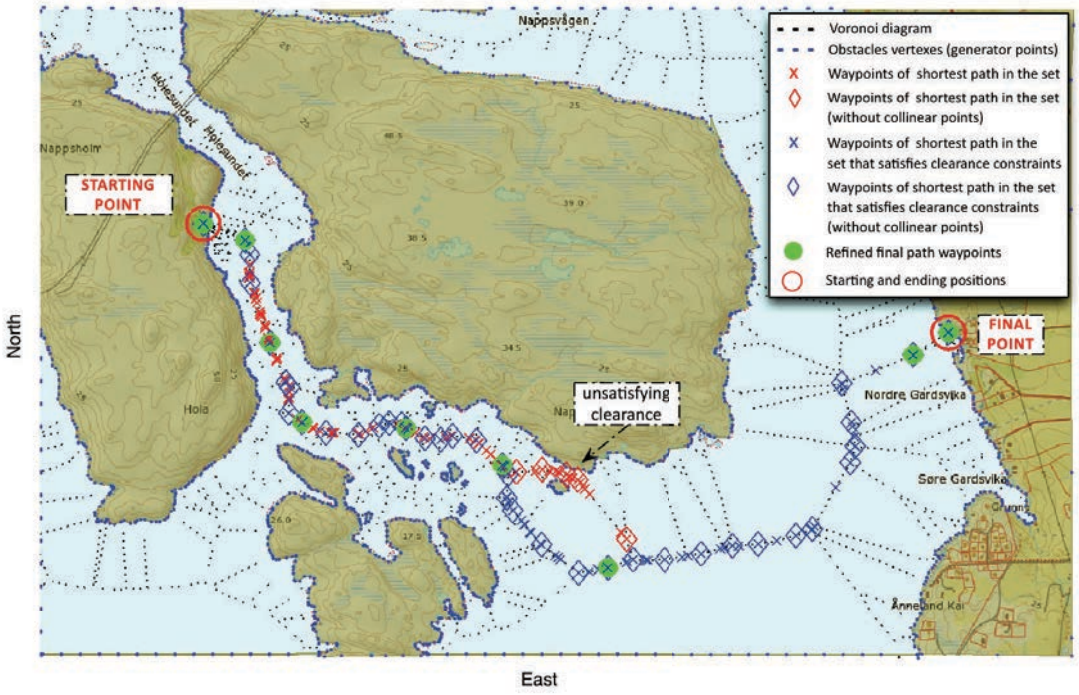

Fig. 5. The result of the main steps of Figure 3 are reported here: Dijkstra algorithm selects the shortest path in the set (red-crossed waypoints), collinear waypoints are removed (red-diamond waypoints). Clearance check is not satisfied for this path, so Dijkstra algorithm is used again to find the second shortest path that satisfies clearance constraints (blue-crossed waypoints), collinear waypoints are then removed (blue-diamond waypoints). The resulting refined path (green waypoints) is obtained by removing those waypoints that are not improving the quality of the path.

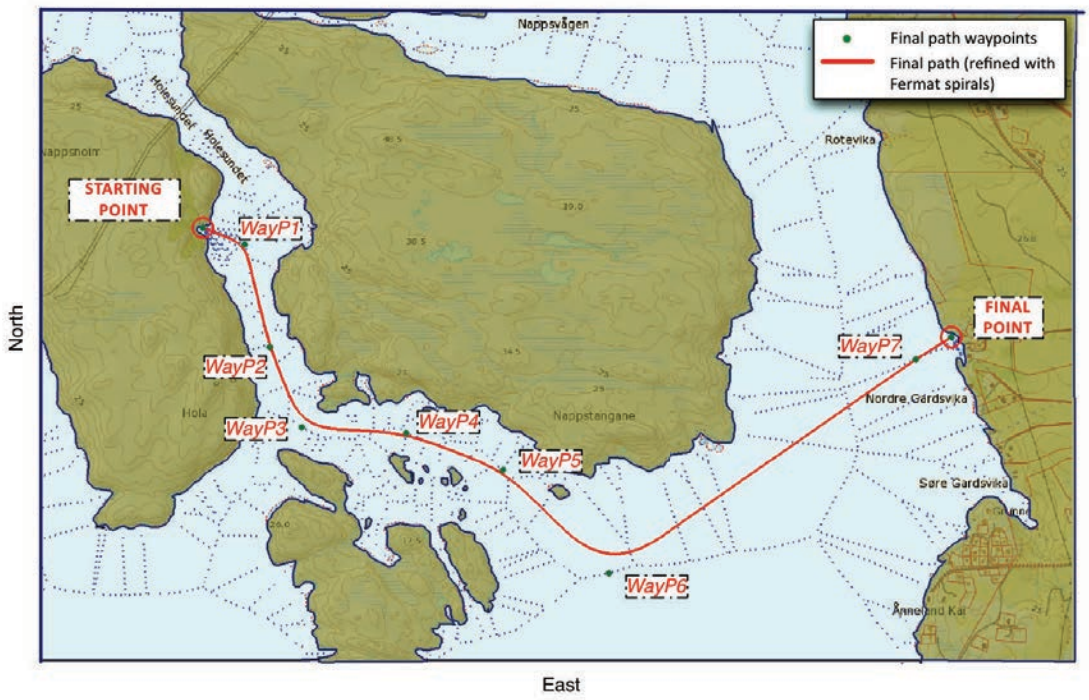

Fig. 6. The waypoints of the refined path define a discontinuous-curvature path. Fermat's spirals are then added providing continuous curvature. The resulting path is practical, safe and defined by a few waypoints that makes unnecessary the presence of high-curvature turns.

Article I

A Voronoi-Diagram-Based Dynamic Path-Planning System for Underactuated Marine Vessels

M. Candeloro, A.M. Lekkas, A.J. Sørensen

The article has been submitted for the second review to the *IFAC Control Engineering Practice*, 2016.

A Voronoi-Diagram-Based Dynamic Path-Planning System for Underactuated Marine Vessels☆

Mauro Candeloro[a,b,*], Anastasios M. Lekkas[a], Asgeir J. Sørensen[a,b]

[a] *Department of Marine Technology, NTNU, Trondheim, Norway.*
[b] *Centre for Autonomous Marine Operations and Systems, NTNU, Trondheim, Norway.*

Abstract

The main contribution of this paper is the development of a rapid, dynamic path-planning system for 3-DOF marine surface vessels navigating in environments where other marine vehicles might be operating too. The method is based on the Voronoi diagram and generates the initial path while ensuring that clearance constraints are satisfied with respect to both land and shallow waters. Fermat's Spiral (FS) segments are used to connect successive straight lines, hence, resulting in curvature-continuous paths that are rapidly computed. When a ship is detected, the range of its position during a given time frame is estimated, and the path-planning system produces in real time a new safe and smooth path. The International Regulations for Preventing Collisions at Sea (COLREG) are taken into account in the replanning procedure. An indirect adaptive Line-Of-Sight (LOS) guidance algorithm from the existing literature is implemented to ensure the underactuated vessel will counteract the effects of unknown environmental forces, such as ocean currents, while converging to the safe path. Simulations show the effectiveness of the proposed approach.

Keywords: Path-Planning, Underactuated Vessels, Replanning, Navigation Support Systems

☆A rudimentary version of this paper was presented at the 9th IFAC Conference on Control Applications in Marine Systems, which was held in Osaka, Japan, during September 2013. This paper was recommended for publication in revised and extended form by Associate Editor "Kazuhiko Hasegawa".

*Corresponding author:
E-mail address: mauro.candeloro@ntnu.no (M. Candeloro).
URL: http://www.ntnu.edu/employees/mauro.candeloro

1. Introduction

Considerable progress has been achieved over the last years in the field of autonomous marine vehicles and systems, with unquestionably visible positive results for a large number of applications within the ocean sector. The works by Seto (2013), Ludvigsen and Sørensen (2016), and Marino et al. (2015) present an overview of advances of autonomy for marine applications, a new autonomous architecture for marine vehicles, and autonomous strategies for coordinated operations of marine robots, respectively. Increased autonomy can provide great added value in several contexts, with two of the most important ones being increased efficiency and safety of operations. Despite the efforts to increase the autonomy level of marine operations, many open issues are still to be addressed in order to make the current systems safe and efficient enough for their actual employment, especially when interaction with humans or other assets is expected. In the case of motion planning for marine vessels, route planning and replanning (as response to unexpected changes in the environment) are two important challenges that need to be tackled. These tasks become rather complex when there are dynamic elements in the environment, uncertainties in the sensors data, and safety requirements to satisfy. Planning of operations is underlined by many authors as a substantial limitation that prevents systems from reaching a higher autonomous level. According to Watson and Scheidt (2005) "*automation of planning processes has been a central problem in the field of artificial intelligence for more than 30 years [...]*". As a matter of fact, autonomous surface vessels navigating on sea, or autonomous passenger flights are still not allowed. However, new initiatives on autonomous ships are currently being taken forward, with the establishment of a part of the Trondheim Fjord, Norway, as test site for new systems, Kongsberg (2016).

Extensive research pertaining to path-planning and obstacle avoidance has been conducted in the last years. The work by Tsourdos et al. (2010) focuses on the particular challenges of cooperative path planning for UAVs, whereas LaValle (2006) and Choset et al. (2005) present a wider and more generic scope from the computer science perspective. The work by Zeng et al. (2015) gives a literature review w.r.t. to Autonomous Underwater Vehicles (AUVs), Caiti (2014) presents a complete and recent review of motion planning algorithms for marine control systems, and Antonelli et al. (2001)

present a practical application of dynamic path planning and obstacle avoidance for an AUV. One classification of path-planning methods distinguishes between *global* and *local* path-planning algorithms. Global path-planning algorithms evaluate the whole information available on a certain area in order to generate an obstacle- free path between the departure location, or initial waypoint, and the destination, or final waypoint. The generated path must satisfy certain constraints, such as the dynamic constraints of the vehicle and environment-related constraints (weather conditions, and minimum allowed distance from obstacles, for instance). A large number of methods and tools addressing these challenges have been developed in the path planning literature. A few notable examples are the rapidly-exploring random trees (Lavalle, 1998), the Voronoi Diagram (VD) (Aurenhammer, 1991), the visibility (Lozano-Pérez and Wesley, 1979), the potential field method (Khatib, 1985, Lee et al., 2004), the occupancy grid methods (Elfes, 1987), and optimization methods, such as Semi-Lagrangian methods (Falcone and Ferretti, 2013), pseudospectral optimal control (Lekkas et al., 2016) and the A* algorithm (Hart et al., 1968, Dolgov et al., 2010 Larson et al., 2006, 2007, Naeem et al., 2012). Local path-planning algorithms, on the other hand, take into account the surrounding space of the vehicle and are able to respond to unpredicted factors, such as unmapped obstacles etc. A few examples of local methods are the dynamic window (Fox et al., 1997), the virtual force field (Borenstein and Koren, 1991) and its extension, the modified virtual force field (Lee et al., 2004), and the velocity obstacle method (Fiorini and Shiller, 1993). Global and local algorithms often complement each other.

Dynamic collision avoidance (CA) for marine vehicles has been widely investigated in literature. Statheros et al. (2008) presents a state-of-art report describing the mathematical methods utilized to model marine vehicles, the most common CA algorithms, and the navigation systems employed in CA scenarios. Campbell et al. (2012) present a review of intelligent USV collision avoidance research in terms of control, path planning and collision avoidance architecture with regards to COLREGs incorporation. Other examples of recent works on CA are the following: Naeem et al. (2012), uses the Velocity Obstacle methods to provide a CA system which respects the COLREGS (IMO, 1977). Perera et al. (2015) presents a fuzzy-based CA system with experimental results on a scaled ship model. Woerner (2016) considers the problem of collision avoidance for marine vehicles by extending the traditional obstacle velocity into a multi-threshold based approach in order to represent and evaluate human ship driving practices more realistically. The current

paper develops a VD-based dynamic path-planning and CA system, which incorporates the benefits of local and global approaches, as in van den Berg et al. (2006).

Due to its simplicity and low computational cost, the Voronoi diagram has been used consistently for path-planning purposes, including aerial operations Bortoff (2000); Chandler et al. (2000); Bellingham et al. (2002) and marine operations. More specifically, Christopher Gold and co-workers have advocated the use of VDs (static and dynamic) for collision avoidance in marine applications (Gold, 1998; Gold et al., 2005; Goralski and Gold, 2007; Gold, 2016). However, none of the aforementioned works give any details regarding the technical aspects of such an approach. In Marino et al. (2012), the authors addressed a harbour-patrolling problem and exploited the advantages of Voronoi tessellations to automatically distribute a number of marine vehicles over the environment. A similar application was considered by Antonelli et al. (2012). In these works, the VD edges were not used to assist generate the path of a vehicle, but to determine the locations of the marine vehicles so as to achieve full coverage of an area.

In Candeloro et al. (2013) we considered a static environment and the first step was to generate a roadmap using the VD. Then a number of heuristic techniques was used in order to produce a set of successive waypoints in between the initial and final waypoints. All the successive waypoints were then connected using paths consisting of straight lines and Fermats Spiral (FS) segments. The final path was curvature-continuous and the whole process had a low computational cost, thus making it a good candidate for online implementation.

In this paper, we consider a dynamic 2-D environment and the Voronoi diagram is used in both the path-planning and replanning phase, where additional heuristics allow to speed up the process and create flyable and intuitive paths. In the first phase a map is supposed to be known, while in the second phase the path is replanned locally on the basis of real-time sensor information. This paper extends the work by Candeloro et al. (2013) through the following contributions:

- Depth constraints are taken into account in order to avoid the problem of grounding during operations in shallow (for a given vehicle) waters[1].

[1]In this article the term "*grounding*" refers to the collision of the vessel with the sea-bottom, that may occur in shallow-water operations, if proper precautions are not

This makes it possible to exploit in a more useful manner the information included in the nautical charts and adjust the method to a wide number of marine vehicles.

- A novel methodology for path following of paths with FS segments is developed to test the path-planning and replanning algorithms in the dynamic case, thus adding the time variable to the simulated case. In addition, the influence of unknown ocean currents is taken into account.
- A fast, VD-based replanning strategy, which is based on the same principles and procedure of the initial path-planning algorithm, is implemented in a modular way.
- The replanning algorithm generates alternative local paths which are compliant with the COLREGs. When an obstacle is detected, it is treated as a local disturbance and a deviation from the original path is computed. The new local path takes into account the COLREGS and the current dynamic constraints (vehicle velocity and estimated motion of the dynamic obstacle) so as to ensure collision avoidance and reconnection to the original path.

In Candeloro et al. (2016), this work is further extended for the underwater domain, thus demonstrating the ability of our approach to tackle planning and replanning in the three-dimensional case. Due to the complexity of the problem though, Candeloro et al. (2016) considered only the geometrical aspects of the problem without taking into account temporal constraints, an aspect which is addressed in detail in the current paper.

The paper is structured as follows: Section 2 describes the maps and the preprocessing of the environmental data. Section 3 describes the path-planning algorithm. In Section 4, the path following algorithm is developed. Section 5 presents the motion control objective. Section 6 presents the simulated vessel model. Section 7 focuses on the LOS guidance algorithm. 8 defines the characteristics on the unknown obstacles and describes the obstacle tracking algorithm. 9 presents the on-line path replanning system and the actions that are taken when an obstacle is encountered. Section 10 presents the case study and simulation results. Finally, Section 11 states the conclusions and further work.

---

taken.

2. Geographical Data Sources

The data used in this paper is obtained from *Global Administrative Areas, GADM* (which is developed by the Universities of California, Berkeley and Davis and the International Rice Research Institute)[2]. These maps come in vectorial and raster file formats. The *shapefile* (.shp) is a popular geospatial vector data format used by many Geographic Information System (GIS) program packages. These data need to be manipulated in a certain way to be used into the proposed planning software. In particular:

1. A rectangular portion of the map (ROI, i.e. Region Of Interest) containing the starting and ending point of the route is chosen (AOI_1 in Fig. 1, where start and final points are marked as $\mathrm{WP_s}$ and $\mathrm{WP_f}$);
2. Only the map data in the ROI is loaded in memory;
3. Many land portions that are close to the borders of the ROI are naturally cut. These areas should be closed, so that a closed convex polygon is generated again (for example by connecting the segments $\overline{\mathrm{DE}}$, $\overline{\mathrm{EF}}$ and $\overline{\mathrm{FA}}$ to the segments $\overline{\mathrm{AB}}$ and $\overline{\mathrm{CD}}$);
4. It is observed that lines that should represent the same pieces of land are often segmented. Moreover these structures are often missing some connection points. This should be corrected by unifying the structures and including the missing data (for example one contour lines in Fig. 1 is divided in 4 segments: $\overline{\mathrm{GH}}$, $\overline{\mathrm{IL}}$, $\overline{\mathrm{MN}}$, $\overline{\mathrm{OP}}$. By adding the segments $\overline{\mathrm{NO}}$, $\overline{\mathrm{PG}}$, $\overline{\mathrm{HI}}$, $\overline{\mathrm{LM}}$ it is possible to obtain a correctly defined polygon).

If the map is too big to be processed in a reasonable time, it can be partitioned into sub-areas, solutions for every partition can be found and subsequently merged (Fig. 1).

3. Path-Planning System: Initial Path Generation

In this section the main steps of the path-planning system are presented. Both land, water depth, and clearance constraints will be explained and considered in the following.

[2]The database from GADM can be found at http://www.gadm.org/

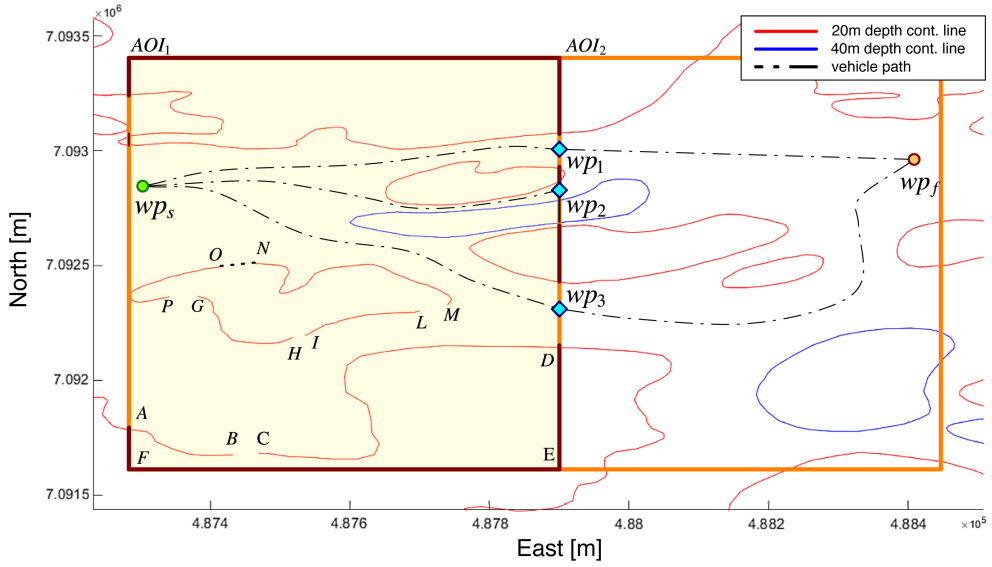

Figure 1: Red and blue full lines represent depth contour lines. WP_s and WP_f are *starting* and *final* waypoints of the path. The AOI is partitioned in two parts to simplify the calculations. The waypoints WP_1, WP_2 and WP_3, need to be added to connect the two sub-paths defined in the two AOIs. Finally, the path passing through WP_1 is selected because is the shortest in the set.

3.1. Land and Depth Constraints

The most important performance requirement that a path should satisfy is safety. The vessel must not collide with, or get too close (hence putting itself closer to a possible risky situation) to any obstacle located in the navigation space. A *minimum clearance*, i.e. the minimum vessel-obstacles distance, is defined to achieve this purpose. Moreover, surface vessels may have navigation constraints due to shallow water depths depending on their dimensions and operations. Some operations may have to be carried along the coastline, and the vessel should not encounter the risk of grounding. In this work, the obstacles (e.g. the coastlines, the depth contours or other vehicles) are represented as polygons. This allows to represent complex environments as simple geometrical structures. The number of vertexes defines the detail level and depends by the scaling and the size of the map.

3.2. Path-Planning System Steps

The path-planning module aims to generate the waypoints on which the path should be built upon. This algorithm provides a safe path that connects

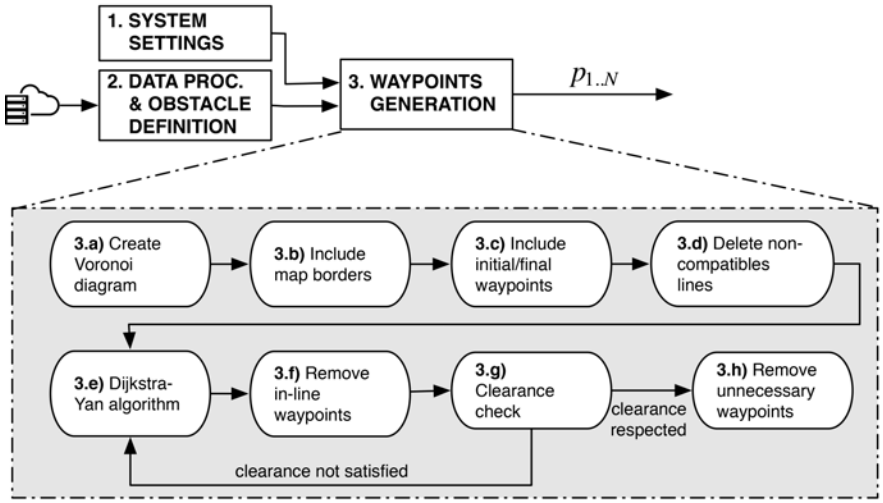

Figure 2: Block diagram representing the *Waypoints Generation* module of the path-planning system. From the map data a series of waypoints that respect the constraints and connect the starting waypoint with the final one, is produced.

a starting with a final waypoint that respects the kinematics and dynamics constraints of the vessel. Notice that this stage is performed before the vessel starts its navigation, and provide an initial path that can be modified at any time if an obstacle or some unexpected event happens on the way. Once the map data is loaded and the obstacles are acquired as polygons, the *waypoints generation* module can be activated. Fig. 2 shows the main steps of this algorithm: the Voronoi diagram gives a raw obstacle-free roadmap (3.a), and the paths that are outside the AOI are removed (3.b). The shortest path among the feasible ones is chosen, and its (almost)-collinear waypoints are removed (3.f) since having fewer waypoints reduces the length of the path, heading changes and, consequently, the fuel consumption. The clearance constraints is checked, and an alternative path is chosen if the safety constraints are not met (3.g). Finally, *unnecessary* waypoints (these which are not almost-collinear and could be removed without breaking the clearance constraints) are removed (3.h). This module produces a series of waypoints which need to be connected in a smooth way to produce a *flyable* path for an underactuated vessel, see also Candeloro et al. (2013).

An important property for the path is its curvature continuity. This requirement is important to avoid unwanted phenomena, such as discontinuities in the cross-track error. This is dealt with in the *path smoothing* module,

that produces a path that is formed by straight and FS segments. A new clearance check is performed also with the final, smoothed, path.

3.3. The Voronoi Diagram and Resulting Waypoints

A Voronoi diagram is a tool to divide a geometrical space in a number of regions determined by the distribution of the objects present in that space. This general approach allowed many scientists to use this tool in a wide number of fields and applications Aurenhammer (1991). In applications such as path planning (and specifically path planning for marine vehicles), the Voronoi diagram can be useful for its property of producing a roadmap with edges that are maximally distant to the generator points Candeloro et al. (2013, 2016).

The vertexes $V_{o,i}$ of the obstacles' (modeled as polygons, as in Section 2) are selected as the generator vertexes of the Voronoi diagram. The resulting Voronoi diagram edges, are shown as black lines in Fig. 3. Notice that, in order to limit the Voronoi diagram to the area of interest (corresponding surroundings of the production factory), a number of random vertexes are generated in the obstacle-free edges of the scenario.

Given the Voronoi diagram's edges, the candidate waypoints can be identified in the edges extreme points (Voronoi diagram vertexes). The waypoints which represent the shortest path among the ones provided by the roadmap, are selected through the Yen modification Yen (1970) of the Dijkstra optimization algorithm Dijkstra (1959). This algorithm is able to find the *k-shortest* paths. In this way, suboptimal solutions can be found if the optimal solution do not respect the preassigned clearance constraints. Notice that the Voronoi edges and vertexes which are too close to the obstacles, i.e. do not respect the predefined clearance constraints, are eliminated, originating the modified diagram which is possible to see in Fig. 4-A.

The implementation detail to obtain the Voronoi diagram are not given, since they are extensively treated in the literature, see Ledoux (2007), or Candeloro et al. (2016) for a general procedure.

4. Path Generation Using Fermat's Spiral

The idea of using FS segments for path-planning purposes was introduced and developed in Dahl (2013) and Lekkas et al. (2013). In this paper it is presented the whole methodology necessary for a vessel to follow a path, despite to the presence of ocean currents. In this context, it is convenient to

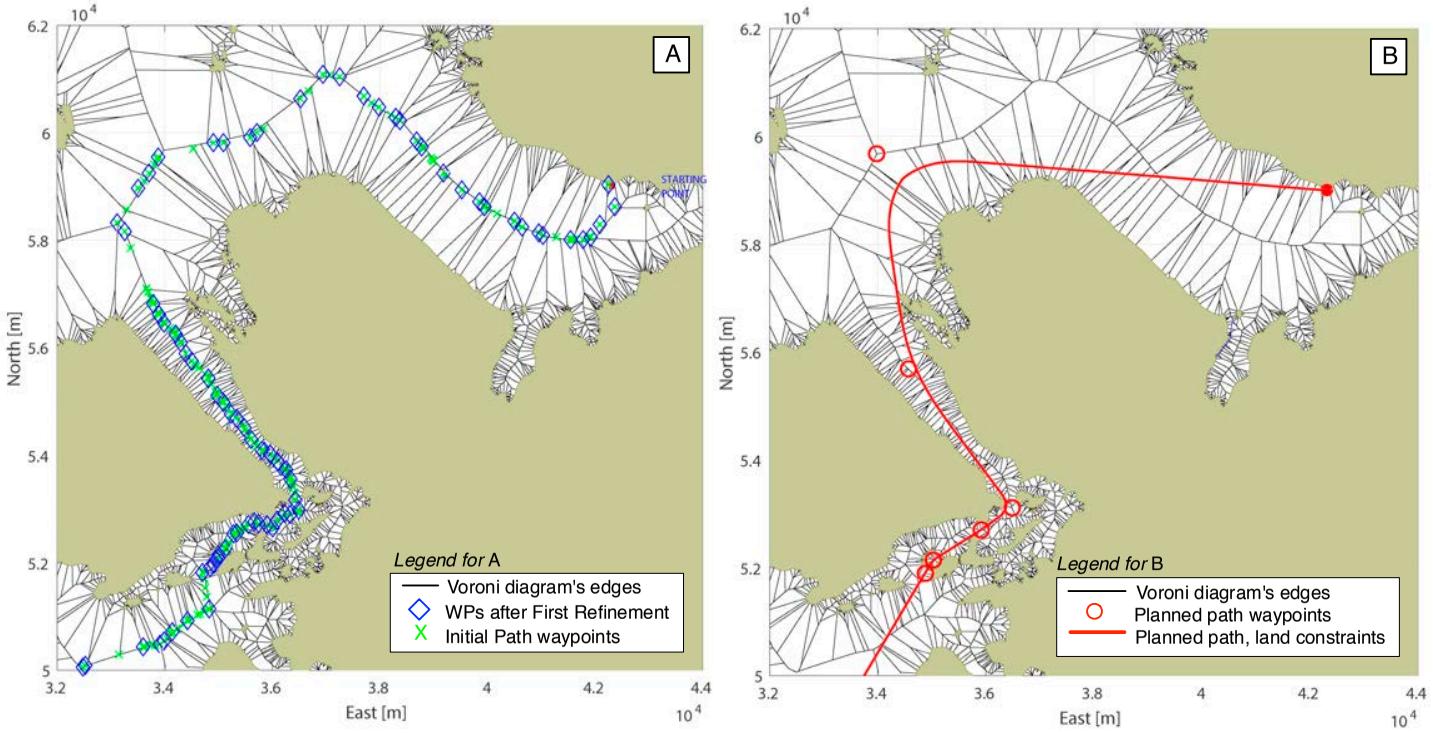

Figure 3: (A) shows the land obstacles, modeled as polygons. Their vertexes are used as a generator points for the Voronoi diagram (black lines). The waypoints and Voronoi edges too close to the obstacles (i.e. not respecting the clearance constraints) will be eliminated producing the diagram as in Fig. 4-A (in this figure the diagram is kept in its original form for clarity). The Yen-Dijkstra algorithm is able to find the shortest available path in the roadmap, and further simplification steps allows to find the minimum number of waypoints which can connect starting and final waypoints respecting the clearance constraints. In (B) a final, curvature-continuous path (constituted by straight segments and Fermat spirals) is obtained from the final waypoints.

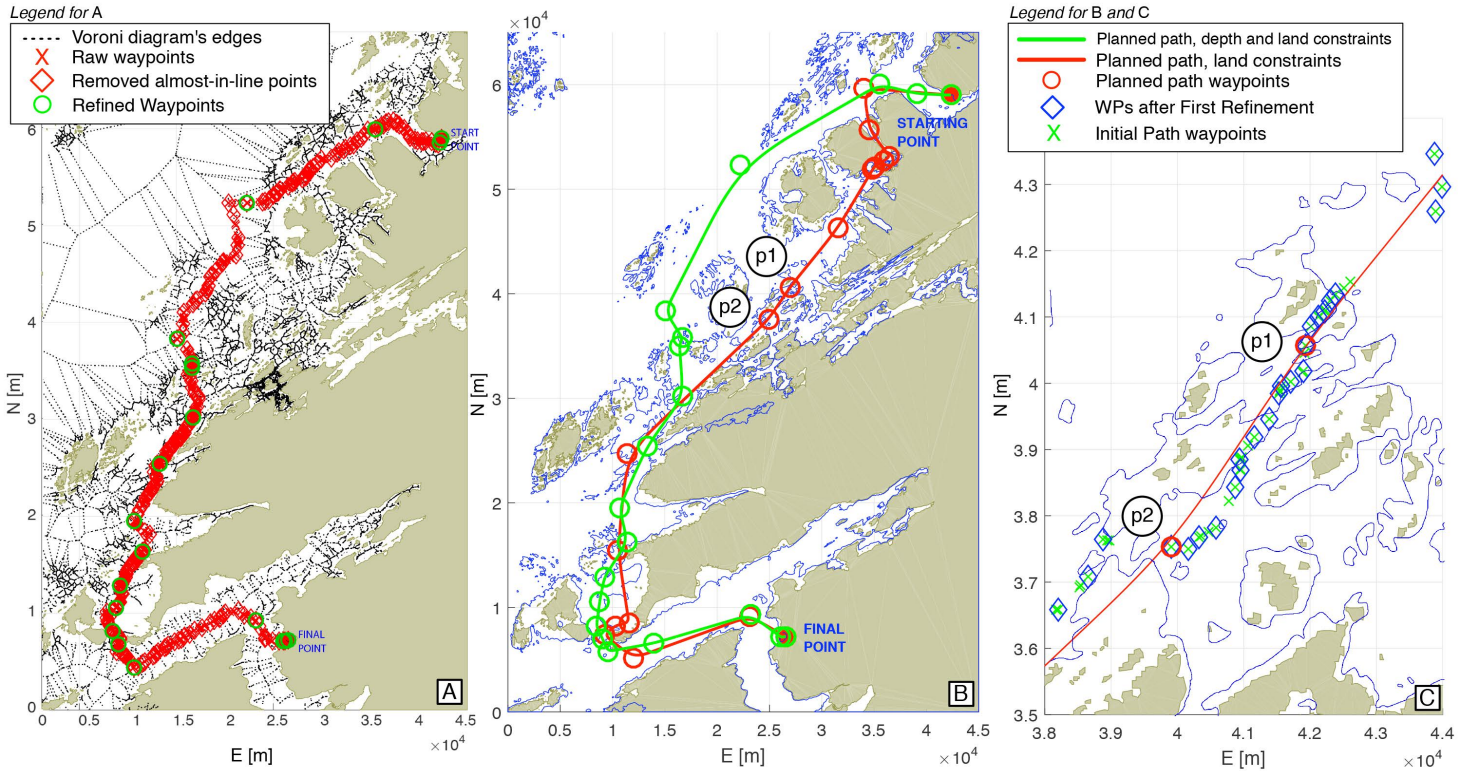

Figure 4: Path-planning algorithm running on a real map. The area covers $45000\,\mathrm{x}\,65000\mathrm{m}^2$ in the region of Sør Trondelag, Norway. The (n, e) coordinates have centered in $(x_0, y_0) = (515000, 7050000)$. The map data was processed as shown in Section 2. **A** shows the Vononoi diagram's edges and the waypoints (WPs) that connect starting with final points respecting land and ocean depths constraints (depth contour lines are reported in **B**). The intermediate WPs are also shown, to illustrate how the implemented heuristic can simplify the problem. **B** shows the paths produced by the path-planning algorithm: the red and green paths shows respectively the one obtained considering land constraints and land plus depth constraints. Blue lines represent the contour ocean depth lines corresponding to the constraint's value. these paths have been calculated as shown in Section 3. **C** presents the detailed path between the WPs P_1 and P_2. Green crosses and blue diamonds are, respectively, the WPs after the steps 3.e) and 3.f) of Fig. 2. Red circles are the WPs after step 3.h). Red path is produced after step 4.g).

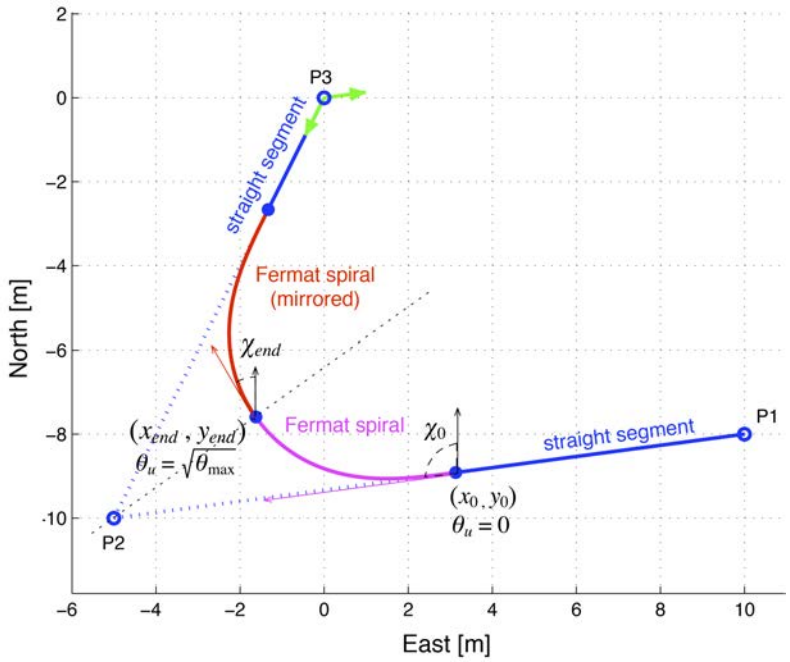

Figure 5: Initial and mirrored Fermat's spiral segments connecting two straight lines. The resulting path is curvature-continuous. The parameter on which the mathematical formulation of the FS is based, θ, is reported, together with the course angle χ.

parametrize the FS segments as a bijective function of θ, so that any point on the path $\mathrm{P} = (\mathrm{x}, \mathrm{y}) = \mathrm{f}(\theta)$. Therefore, given a vessel position $\mathrm{P} = (\mathrm{x}, \mathrm{y})$, there are two possible cases: P *is* on the desired path, in which case the goal is to continue moving on the path, or P *is not* on the desired path (i.e. nonzero cross-track error), in which case the closest point on the path must be determined and fed to the guidance algorithm to lead the vessel back on the path. If external disturbances, as ocean currents, or wind, are present, it is necessary to compute the heading angle correction that will counteract them and minimize the cross-track error. An example of FS is illustrated in Fig. 6, together with some of the variables introduced in the next subsections.

Similarly to clothoids, connecting two lines using FS requires two segments: the first one starts at the end of the first line (where the curvature is zero) and reaches up to the middle of the total turn. The second segment is the mirrored version of the former one, starts where the initial segment ended, and goes all the way to the second line. The advantage of using FS instead of clothoids is that it requires much less computational time, due to

the fact that FS can be described by simple parametric equations, whereas clothoids require the numerical solution of Fresnel integrals. In Dahl (2013) and Lekkas et al. (2013), FS equations in Cartesian coordinates were proposed, which introduce singularities when differentiated with respect to θ. By substituting $\theta_{\mathrm{u}} = \sqrt{\theta}$ it is possible to obtain a singularity-free formulation:

$$\mathbf{p}_{\mathrm{FS}}\left(\theta_{\mathrm{u}}\right) = \begin{bmatrix} \mathrm{x}_0 + \mathrm{k_s}\theta_{\mathrm{u}} \cos\left(\rho\theta_{\mathrm{u}}^2 + \chi_0\right) \\ \mathrm{y}_0 + \mathrm{k_s k}\theta_{\mathrm{u}} \sin\left(\rho\theta_{\mathrm{u}}^2 + \chi_0\right) \end{bmatrix}, \quad \text{for } 0 < \theta_{\mathrm{u}} < \sqrt{\theta_{\max}}, \tag{1}$$

where $\mathbf{p}_0 = [\mathrm{x}_0, \mathrm{y}_0]^{\mathrm{T}}$ is the starting position of the segment, $\mathrm{k_s}$ denotes the scaling factor, χ_0 the initial tangent angle, and

$$\rho = \begin{cases} 1 & \text{for an anti-clockwise turn} \\ -1 & \text{for a clockwise turn.} \end{cases} \tag{2}$$

Regarding the parameter θ, it holds $\theta = 0$ at the starting point of the *initial* segment where the spiral is connected to a straight line and the curvature is zero, and $\theta = \theta_{\max}$ at the *end point of the initial segment*, which is located midway the end of the total turn.

The formulation in (5) gives the singularity-free expression for the velocity and acceleration:

$$\frac{\mathrm{d}}{\mathrm{d}\theta_{\mathrm{u}}}\mathbf{p}_{\mathrm{FS}}\left(\theta_{\mathrm{u}}\right) = \mathrm{k_s}\begin{bmatrix} \cos\left(\rho\theta_{\mathrm{u}}^2 + \chi_0\right) - 2\rho\theta_{\mathrm{u}}^2 \sin\left(\rho\theta_{\mathrm{u}}^2 + \chi_0\right) \\ \sin\left(\rho\theta_{\mathrm{u}}^2 + \chi_0\right) + 2\rho\theta_{\mathrm{u}}^2 \cos\left(\rho\theta_{\mathrm{u}}^2 + \chi_0\right) \end{bmatrix}, \tag{3}$$

$$\frac{\mathrm{d}^2}{\mathrm{d}\theta_{\mathrm{u}}^2}\mathbf{p}_{\mathrm{FS}}\left(\theta_{\mathrm{u}}\right) = \mathrm{k_s}\begin{bmatrix} -6\rho\mathrm{u} \sin\left(\rho\theta_{\mathrm{u}}^2 + \chi_0\right) - 4\rho^2\mathrm{u}^3 \cos\left(\rho\theta_{\mathrm{u}}^2 + \chi_0\right) \\ 6\rho\mathrm{u} \cos\left(\rho\theta_{\mathrm{u}}^2 + \chi_0\right) - 4\rho^2\mathrm{u}^3 \sin\left(\rho\theta_{\mathrm{u}}^2 + \chi_0\right) \end{bmatrix}. \tag{4}$$

Similarly, for the mirrored segment will hold:

$$\mathbf{p}_{\overline{\mathrm{FS}}}\left(\theta_{\mathrm{u}}\right) = \begin{bmatrix} \mathrm{x}_{\mathrm{end}} - \mathrm{k_s}\theta_{\mathrm{u}} \cos\left(\rho\theta_{\mathrm{u}}^2 - \chi_{\mathrm{end}}\right) \\ \mathrm{y}_{\mathrm{end}} + \mathrm{k_s}\theta_{\mathrm{u}} \sin\left(\rho\theta_{\mathrm{u}}^2 - \chi_{\mathrm{end}}\right) \end{bmatrix}, \quad \text{for } 0 < \theta_{\mathrm{u}} < \sqrt{\theta_{\max}} \tag{5}$$

where $\mathbf{p}_{\mathrm{end}} = [\mathrm{x}_{\mathrm{end}}, \mathrm{y}_{\mathrm{end}}]^{\mathrm{T}}$ is the position at the end of the curve, i.e. $\mathbf{p}_{\mathrm{end}} = \mathbf{p}_{\overline{\mathrm{FS}}}\left(\theta_{\mathrm{end}}\right)$, and χ_{end} is the course angle at that point. Fig. 6 depicts an illustration of how the initial and mirrored segment connect two straight lines. Equations related to the mirrored segment are not reported here for space issue. Section 5 explains why the first and second derivatives are needed when implementing a path-following scenario where no temporal constraints are present.

5. Motion Control Objective

For each vessel position $(\mathrm{x(t)}, \mathrm{y(t)})$ it is necessary to determine the closest corresponding point on the path, $(\mathrm{x_d}(\theta^*), \mathrm{y_d}(\theta^*))$, which corresponds to a unique parameter value θ^*, see also Fig. 6. The minimum distance between the vessel and the monotonic curve between two active waypoints will be defined as the cross-track error (Lekkas and Fossen, 2014a). The tangent and normal lines through the point $(\mathrm{x_d}(\theta), \mathrm{y_d}(\theta))$ are given by:[3]

$$\mathrm{y_t} - \mathrm{y_d}(\theta) = \frac{\mathrm{y_d'}(\theta)}{\mathrm{x_d'}(\theta)}(\mathrm{x_t} - \mathrm{x_d}(\theta)), \tag{6}$$

$$\mathrm{y_n} - \mathrm{y_d}(\theta) = -\frac{1}{\frac{\mathrm{y_d'}(\theta)}{\mathrm{x_d'}(\theta)}}(\mathrm{x_n} - \mathrm{x_d}(\theta)). \tag{7}$$

The θ value corresponding to the path-normal that intersects the vessel is found by requiring that $(\mathrm{x_n}, \mathrm{y_n}) = (\mathrm{x}, \mathrm{y})$. Moreover, from (7) it follows that:

$$\mathrm{y_d'}(\theta^*)(\mathrm{y} - \mathrm{y_d}(\theta^*)) + \mathrm{x_d'}(\theta^*)(\mathrm{x} - \mathrm{x_d}(\theta^*)) = 0. \tag{8}$$

This involves solving the roots of the third-order cubic function for θ^*. Instead of using an analytical solution a numerical solution based on Newton-Raphson method will converge quite fast. For instance,

$$\theta_{\mathrm{j}+1}^* = \theta_{\mathrm{j}}^* - \frac{\mathrm{f}(\theta_{\mathrm{j}}^*)}{\mathrm{f'}(\theta_{\mathrm{j}}^*)}, \tag{9}$$

where:

$$\mathrm{f}(\theta_{\mathrm{j}}^*) = \mathrm{y_d'}(\theta_{\mathrm{j}}^*)(\mathrm{y} - \mathrm{y_d}(\theta_{\mathrm{j}}^*)) + \mathrm{x_d'}(\theta_{\mathrm{j}}^*)(\mathrm{x} - \mathrm{x_d}(\theta_{\mathrm{j}}^*)), \tag{10}$$

$$\mathrm{f'}(\theta_{\mathrm{j}}^*) = \mathrm{y_d''}(\theta_{\mathrm{j}}^*)(\mathrm{y} - \mathrm{y_d}(\theta_{\mathrm{j}}^*)) + \mathrm{x_d''}(\theta_{\mathrm{j}}^*)(\mathrm{x} - \mathrm{x_d}(\theta_{\mathrm{j}}^*)) - \mathrm{x_d'}(\theta_{\mathrm{j}}^*)^2 - \mathrm{y_d'}(\theta_{\mathrm{j}}^*)^2, \tag{11}$$

will converge in a few iterations if the the initial path variable θ_0^* is taken as the last θ_{i} value when moving along the path between two waypoints parametrized on the interval $[\theta_1, \theta_{\mathrm{n}}]$.

[3] The syntax $\mathrm{x'}(\theta)$, represents the derivative of the variable with respect of its parameter θ: $\mathrm{x'}(\theta) = \frac{\mathrm{dx}}{\mathrm{d}\theta}$.

The normal line from the point $(\mathrm{x_d}(\theta^*), \mathrm{y_d}(\theta^*))$ on the path through the point (x, y) on the vessel defines the along-track and cross-track errors $(\mathrm{x_e}, \mathrm{y_e})$. Moreover:

$$\begin{bmatrix} \mathrm{x_e} \\ \mathrm{y_e} \end{bmatrix} = \mathbf{R}^{\mathrm{T}}(\gamma_\mathrm{p}) \begin{bmatrix} \mathrm{x} - \mathrm{x_d}(\theta^*) \\ \mathrm{y} - \mathrm{y_d}(\theta^*) \end{bmatrix}, \tag{12}$$

where $\mathbf{R}(\gamma_\mathrm{p}) \in \mathrm{SO}(2)$ is the rotation matrix in yaw (Fossen, 2011). In algebraic form, the equations of the along-track and the cross-track error for a given vessel position (x, y) become:

$$\mathrm{x_e} = (\mathrm{x} - \mathrm{x_d}(\theta^*)) \cos(\gamma_\mathrm{p}) + (\mathrm{y} - \mathrm{y_d}(\theta^*)) \sin(\gamma_\mathrm{p}), \tag{13}$$

$$\mathrm{y_e} = -(\mathrm{x} - \mathrm{x_d}(\theta^*)) \sin(\gamma_\mathrm{p}) + (\mathrm{y} - \mathrm{y_d}(\theta^*)) \cos(\gamma_\mathrm{p}), \tag{14}$$

where γ_p is the path-tangential angle:

$$\gamma_\mathrm{p} = \mathrm{atan2}(\mathrm{y}'_\mathrm{d}(\theta^*), \mathrm{x}'_\mathrm{d}(\theta^*)). \tag{15}$$

For a path-following scenario $\mathrm{x_e} = 0$, which leads to the following control objective for curved path-following (Lekkas and Fossen, 2014a):

$$\lim_{\mathrm{t} \to +\infty} \mathrm{y_e}(\mathrm{t}) = 0. \tag{16}$$

6. Vessel Model and Control System

Consider a surface vessel at the position (x, y) moving with the ground speed:

$$\mathrm{U} = \sqrt{\mathrm{u}^2 + \mathrm{v}^2}, \tag{17}$$

where u and v are the velocities in surge and sway respectively. The speed U is assumed to be positive and bounded:

$$\mathrm{U_{min}} \leq \mathrm{U} \leq \mathrm{U_{max}}, \;\; 0 < \mathrm{U_{min}}. \tag{18}$$

In the following, however, the relative surge and sway velocities will be mostly considered, $\mathrm{u_r} = \mathrm{u} - \mathrm{u_c}$ and $\mathrm{v_r} = \mathrm{v} - \mathrm{v_c}$, where $\mathrm{u_c}$ and $\mathrm{v_c}$ will be defined below. In this way, the three DOFs horizontal dynamics of the surface vessel can be represented by three differential equations Fossen (2011):

$$\dot{\mathrm{u}} = \mathrm{f_{u_r}}(\mathrm{u_r}, \mathrm{v_r}, \mathrm{r}, \tau), \tag{19a}$$

$$\dot{\mathrm{v}} = \mathrm{f_{v_r}}(\mathrm{u_r}, \mathrm{v_r}, \mathrm{r}, \tau), \tag{19b}$$

$$\dot{\mathrm{r}} = \mathrm{f_r}(\mathrm{u_r}, \mathrm{v_r}, \mathrm{r}, \tau), \tag{19c}$$

The vessel kinematic equations for horizontal plane motion can be expressed in terms of the relative surge and sway velocities according to Fossen (2011):

$$\dot{\mathrm{x}} = \mathrm{u_r}\cos(\psi) - \mathrm{v_r}\sin(\psi) + \mathrm{V_x} \tag{20a}$$

$$\dot{\mathrm{y}} = \mathrm{u_r}\sin(\psi) + \mathrm{v_r}\cos(\psi) + \mathrm{V_y} \tag{20b}$$

$$\dot{\psi} = \mathrm{r} \tag{20c}$$

where ψ and r are the yaw angle and rate, respectively. The body-fixed ocean current velocities $(\mathrm{u_c}, \mathrm{v_c})$ and North-East current velocities $(\mathrm{V_x}, \mathrm{V_y})$ satisfy:

$$[\mathrm{u_c}, \mathrm{v_c}]^\top = \mathbf{R}^\top(\psi)[\mathrm{V_x}, \mathrm{V_y}]^\top \tag{21}$$

Notice that the pair $(\mathrm{V_x}, \mathrm{V_y})$ is constant in NED, while the body-fixed current velocities $(\mathrm{u_c}, \mathrm{v_c})$ depend on the heading angle ψ.

7. Guidance System and Ocean Current Compensation

The LOS guidance method is widely used to generate reference trajectories for the heading angle, so that the vessel's trajectory will converge on the desired path. Consequently, a wide literature is available, see, for instance, Caharija et al. (2014) and the references therein. In this work, an adaptive version of the LOS algorithm is used in order to compensate for environmental disturbances.

7.1. Indirect Adaptive LOS for Ocean Current Compensation

An additional term, α_y is added to the classic LOS algorithm with the purpose of disturbance rejection (Lekkas and Fossen, 2014b):

$$\psi_\mathrm{d} = \gamma_\mathrm{p} - \beta_\mathrm{r} + \arctan\left(-\frac{\mathrm{y_e} + \alpha_\mathrm{y}}{\Delta}\right), \tag{22}$$

which gives the desired heading angles ψ_d. $\Delta > 0$ is the user specified lookahead distance and $\beta_\mathrm{r} = \mathrm{atan2}(\mathrm{v_r}, \mathrm{u_r})$. The (22), results in the following cross-track error dynamics:

$$\dot{\mathrm{y}}_\mathrm{e} = -\frac{\mathrm{U_r}(\mathrm{y_e} + \alpha_\mathrm{y})}{\sqrt{\Delta^2 + (\mathrm{y_e} + \alpha_\mathrm{y})^2}} + \theta_\mathrm{y}, \tag{23}$$

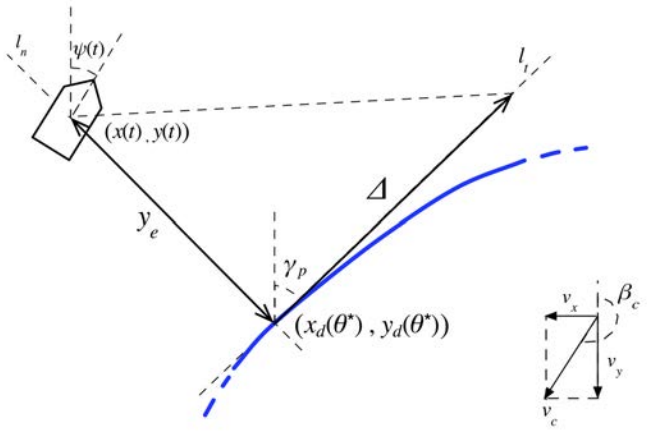

Figure 6: Main variables concerning the LOS algorithm are reported in this figure: the *lookahead distance* Δ is directing the vessel over a point along the path tangent, oriented at an angle γ_{p}. The control objective tries to reduce the *cross track error* $\mathrm{y_e}$.

with θ_{y} denoting the effect of the unknown current that needs to be compensated for, and the relative speed is recognized as $\mathrm{U_r} = \sqrt{\mathrm{u_r^2} + \mathrm{v_r^2}}$. In the same work the following adaptive observers providing estimates for $\mathrm{y_e}, \theta_{\mathrm{y}}$ were proposed (Fossen and Lekkas, 2015):

$$\dot{\hat{\mathrm{y}}}_{\mathrm{e}} = -\frac{\mathrm{U_r}(\hat{\mathrm{y}}_{\mathrm{e}} + \alpha_{\mathrm{y}})}{\sqrt{\Delta^2 + (\mathrm{y_e} + \alpha_{\mathrm{y}})^2}} + \hat{\theta}_{\mathrm{y}} + \mathrm{k_1}(\mathrm{y_e} - \hat{\mathrm{y}}_{\mathrm{e}}), \tag{24}$$

$$\dot{\hat{\theta}}_{\mathrm{y}} = \mathrm{k_2}(\mathrm{y_e} - \hat{\mathrm{y}}_{\mathrm{e}}), \tag{25}$$

where $\mathrm{k_1}$ and $\mathrm{k_2}$ are tuning constants, $\mathrm{U_r}$ is the relative speed, and Δ is the user specified lookahead distance. Choosing α_{y} as:

$$\alpha_{\mathrm{y}} = \Delta \frac{\hat{\theta}_{\mathrm{y}}/\mathrm{U_r}}{\sqrt{1 - (\hat{\theta}_{\mathrm{y}}/\mathrm{U_r})^2}} \tag{26}$$

minimizes the cross-track error dynamics, i.e. $\mathrm{y_e(t)} \to \infty$, Fossen and Lekkas (2015). This indirect adaptive LOS is implemented by computing the desired heading angles according to (22) with α_{y} given by (26).

8. Obstacles Classification and Tracking

In this paper, an obstacle tracking algorithm is utilized to detect and estimate the state of the encountered obstacles. This approach introduces

uncertainties in the knowledge of the obstacles state, and in the time utilized for the detection itself, allowing to create a more realistic and challenging scenario. An approach similar to the one in Karoui et al. (2015) is utilized, and briefly presented in the following. Notice that two assumptions holds:

Assumption 1 *Obstacles are supposed to be defined by a nearly-constant velocity vector, where changes in magnitude and direction are bounded.*

Assumption 2 *Moving obstacles are assumed to follow the COLREG.*

Assumption 1 allows the replanning algorithm to plan a proper anti-collision maneuver based on a predictable behavior of the obstacle, while Assumption 2 gives indications on *how to* safely replan, i.e., following the COLREG.

Given Assumption 1 it is possible to use the constant velocity dynamical model described in Lerro and Bar-Shalom (1993). Karoui et al. (2015) propose an obstacle detection and identification method that could be implemented in synergy with the obstacle tracking and planning techniques here proposed. The considered model is composed by the following dynamic and measurement equations[4]:

$$\mathbf{x}_{\mathrm{o}}^{\mathrm{n}}(\mathrm{k}) = \mathbf{F}\mathbf{x}_{\mathrm{o}}^{\mathrm{n}}(\mathrm{k}-1) + \mathbf{G}\mathbf{w}_1(\mathrm{k}), \tag{27a}$$

$$\mathbf{y}^{\mathrm{n}}(\mathrm{k}) = \mathbf{H}\mathbf{x}_{\mathrm{o}}^{\mathrm{n}}(\mathrm{k}) + \mathbf{w}_2(\mathrm{k}), \tag{27b}$$

where $\mathrm{k} > 0 \in \mathbb{I}$ is the discrete time index, $\mathbf{x}_{\mathrm{o}}^{\mathrm{n}}(\mathrm{k}) = [\mathbf{p}_{\mathrm{o}}^{\mathrm{n}}(\mathrm{k}),\ \mathbf{v}_{\mathrm{o}}^{\mathrm{n}}(\mathrm{k})]^{\mathrm{T}} \in \mathbb{R}^{4\times 1}$ is the state of the moving obstacle (position and velocity) at sensor ping k in the NED frame. $\boldsymbol{\xi} = \mathbf{G}\mathbf{w}_1(\mathrm{k}) \in \mathbb{R}^{4\times 1}$ is the process noise modeled by the covariance matrix $\mathbf{Q} \in \mathbb{R}^{4\times 4} : \boldsymbol{\xi} \sim \mathcal{N}(0, \mathbf{Q})$, $\mathbf{w}_1 \in \mathbb{R}^{4\times 1}$ is the Gaussian measurement noise modeled by the covariance matrix $\mathbf{R} \in \mathbb{R}^{2\times 2} : \mathbf{w}_2 \in \mathbb{R}^{2\times 1} \sim \mathcal{N}(0, \mathbf{R})$.

A linear Kalman Filter, which includes a bias correction is implemented to obtain an estimation of the state of the obstacle and of the related error covariance, as discussed in Lerro and Bar-Shalom (1993). The resulting filter is known as de-biased converted Kalman Filter. More details can be found in Karoui et al. (2015). Assuming a Gaussian behavior of the sensor noise is a standard practice in literature. Although in reality the sensor noise

[4]In the following, the superscript x^{n} represents the NED (North-East-Down) frame, the superscript x^{s} represents the sensor frame. For more information, refer to Fossen, 2011

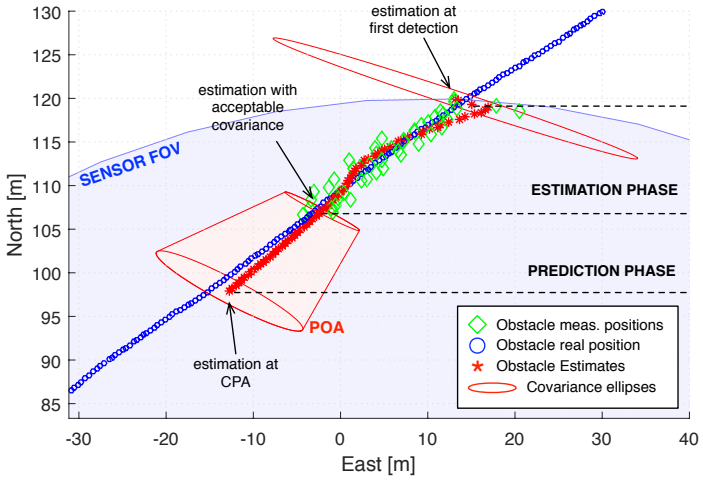

Figure 7: An obstacle is first detected when it enters the sensor's FOV, but the tracking commences when the covariance is sufficiently low. The POA is the convex hull containing the two covariance ellipses corresponding to the first acceptable estimation and the estimation at CPA.

might follow a different behavior, the practical application has shown that the Kalman filter is a reliable estimator. This approach is also utilized in Quidu et al. (2012); Karoui et al. (2015).

The obstacle detection and identification module is out of the scope of this paper, so the position measurements are available as soon as the obstacle enters the sensor's field of view (FOV). Notice that, in this work, the obstacle is estimated as a point. In Subsection 9.4 a certain, predefined shape will be associated to it. The process that has been used in this work to originate the simulated measurements is described in Section 10.

Fig. 7 shows an example of obstacle tracking. The covariance of the estimation error (provided by the de-biased converted Kalman filter) is used to generate the confidence ellipse around the estimated position of the obstacle which, in turns, are used to generate the Projected Obstacle Area (POA).

9. Path-Planning System: Replanning Phase

In order to safely avoid the obstacles identified by the tracker, the replanning procedure adds extra waypoints and produces a flyable deviation from the original path. The algorithm also guarantees smooth re-convergence to the original path.

9.1. Timing

Safe path replanning requires accuracy in both obstacle tracking and the timing of the sequential steps. The following time variables and periods are defined (see Fig. 8):

- *Tracking time* (t_t): the obstacle enters the sensor area and it is identified. From this moment the *obstacle tracking* runs for a period T_t, until the state of the obstacle is estimated with a certain precision;
- *Replanning time* (t_r): the path replanning system starts to re-calculate the route. The replanning period T_r lasts until the algorithm produces a result;
- *Action time* (t_a): the vessel changes its course to follow the new segment.

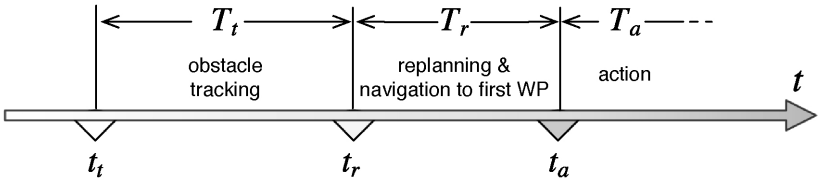

Figure 8: Time variables and periods involved in path replanning.

9.2. Closest Point of Approach

The *Closest Point of Approach* (CPA) is a way to evaluate the hazard due to the minimum potential distance between the target vessel and the obstacle (Kuwata et al., 2014). In this work, the CPA is used to determine whether a replan is necessary or not, and to build the Projected Obstacle Area (POA) in Section 9.4. The CPA is described by d_{CPA}, t_{CPA}, the minimum distance and the time instant when the target vessel and the obstacle reach it, respectively:

$$t_{CPA} = \frac{(\mathbf{p}_v - \mathbf{p}_o) \cdot (\mathbf{v}_v - \mathbf{v}_o)}{||\mathbf{v}_v - \mathbf{v}_o||}, \tag{28}$$

$$d_{CPA} = ||(\mathbf{p}_v + \mathbf{v}_v t_{CPA}) - (\mathbf{p}_o + \mathbf{v}_o t_{CPA})||, \tag{29}$$

where $\mathbf{p}$ and $\mathbf{v}$ are he position and velocity vectors of the target vessel and the obstacle. It is clear that if $||\mathbf{v}_v - \mathbf{v}_o|| \to 0$ then $t_{CPA} \to \infty$ it is implied that the obstacle and target vessel are on the same course with equal speed. The replanning procedure starts if the target vessel is in a collision risk:

Definition 1 *The target vessel is in a collision risk if:*

$$(0 < \mathrm{t_{CPA}} \leq \mathrm{t_{risk}}) \quad \wedge \quad (\mathrm{d_{CPA}} \leq \mathrm{d_{risk}}). \tag{30}$$

9.3. Compliance to COLREG Guidelines

The International Maritime Organization (IMO) established the COLREGs in (IMO, 1977). For the replanning phase we consider the rules found in Section II of the COLREG (*Conduct of Vessels in Sight of One Another*) and mainly refer to Rules 14-15 (*head-on situation* and *crossing situation*), both illustrated in Fig. 9. Another relevant rule, although not considered in this work, is Rule 13 (*overtaking situation*). In general, the target vessel should always leave the moving obstacle on its port side. In the case of a crossing situation, the target vessel may keep its course if the vehicle comes from his starboard side, but leave the obstacle on his port side otherwise (as in Fig. 9-A). To determine the situation, the relative course α_r can be calculated in the following way:

$$\alpha_\mathrm{r} = \mathrm{atan2}(\mathrm{y_v} - \mathrm{y_o}, \mathrm{x_v} - \mathrm{x_o}) - \psi_\mathrm{o}, \tag{31}$$

where x and y are the Cartesian coordinates of the target vehicle/obstacle, and ψ_o is the obstacle heading angle. The angle α_r determines the situation as defined in Fig. 9-A.

9.4. Projected Obstacle Area

When a dynamic obstacle is detected, it is possible to predict its near-future positions, thus generating the Projected Obstacle Area (POA) (Larson et al., 2006, 2007). The size of the POA is a function of the uncertainty in tracking the obstacle (high uncertainty will result in a higher number of probable near-future positions) and the speed of the obstacle. In this paper, the KF obstacle position estimates are used to compute the POA. In particular, the covariance is used for: a) assessing whether the obstacle tracking is reliable enough to be used in the replanning phase, and b) building the POA. As soon as the tracking accuracy is acceptable, i.e. the estimation covariance is low enough, the prediction of the obstacle's future states starts. The last considered prediction is the one corresponding to the CPA. The convex hull containing the first and last obstacle state estimations' covariance ellipses obtained during this procedure defines the POA, as shown in Fig. 7. If $\mathbf{v}_\mathrm{o} \approx 0$, the POA is approximated as a circle with a certain radius (Fig.

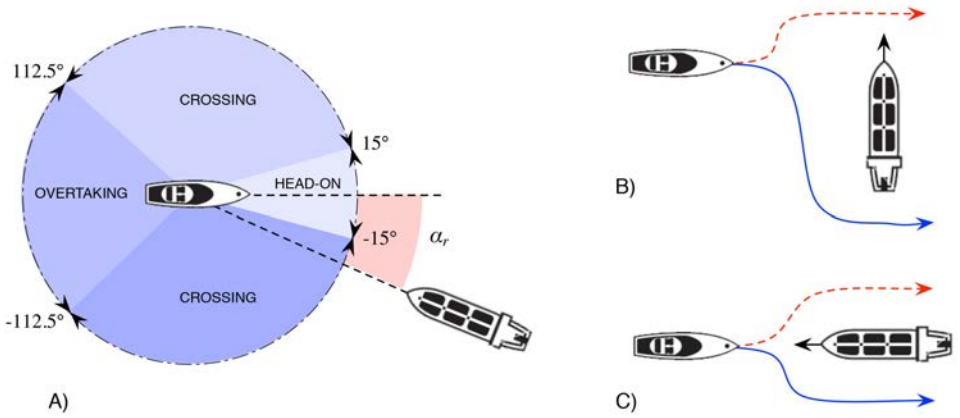

Figure 9: The possible mutual situations between the *target vehicle* and *moving obstacle* are showed in (A). A crossing and a head-on situation are depicted in (B) and (C), respectively. Solid blue lines indicate the approved maneuver from the *target vehicle* perspective, whereas red dashed lines are maneuvers to avoid.

14). The POA is then further refined so as to exclude the paths that do not satisfy the COLREG. This is illustrated in Fig. 13, where the POA is extended towards the border of the replanning area to exclude the routes that would take the obstacle on the port side.

9.5. Path Replanning System Steps

In the case where replanning is needed, the same algorithm that generated the initial path is now applied to a restricted area centered on the current position of the target vessel. The size of that area is determined based on a compromise between the need for a fast solution and the need to consider a large enough area that can give valid replanning alternatives. When an obstacle is detected and tracking commences, the replanning module follows the routine below:

1. Define the replanning area (local map);
2. Compute and add the POA to the local map;
3. Compute the first WP of the replanned segment;
4. Compute the last WP of the replanned segment;
5. Generate the VD on the local map;
6. Connect fhe first and last WPs to the VD;
7. Compute the shortest path;
8. Simplify and smooth the path.

If no solution is found, the process is repeated after increasing the dimension of the replanning area. During the replanning period T_r, the CPA is continuously monitored and an emergency stop can be executed, should the need arise. The procedure to calculate the POA (Step 2) was given in Section 9.4 and Steps 5–8 are identical with those presented in Section 3. The procedure that follows explains in detail how the replanning area (Step 1), as well as the first and last WPs, are computed (see also Figs 8 and 10):

1. The first waypoint WP_s of the replanned segment is obtained calculating the position of the target vessel at the time $T^* > t_c + T_r$, where T^* is a conservative estimation of the time that the replanning algorithm takes to give a solution for the selected area, and t_c is the current time;
2. $\overrightarrow{d}_{wp}$ (the versor representing the direction of the line connecting the waypoints WP_k and WP_{k+1}) is calculated. This direction defines the orientation of the replanning frame $\{r\}$. The x and y axis of this frame are respectively perpendicular and parallel to $\overrightarrow{d}_{wp}$. Its center is located on the target vessel COG. All the following variables are defined in this frame;
3. The following values are calculated: $ox = \min(o_x)$, $oX = \max(o_x)$, $oy = \min(o_y)$ and $oY = \max(o, y)$ that are the minimum and maximum coordinates of the POA. Notice that $\mathbf{p}_o^r = (o_x, o_y) \in POA$;
4. The replanning area $\overline{ABCD}$ is defined from the intersections of four lines parallel to the axis of the frame $\{r\}$: l1, l2, s1, s2;
5. The following values are calculated: $l1_y = v_y$, $l2_y = oY + \Delta y_{l2}$;
6. The intersection of l2 with the original path $r(\theta)$ gives WP_f, that is the final waypoint of the replanned segment;
7. The following values are calculated: $s1_x = \min\{p_{v,x}, ox, wp_{f,x}\} - \Delta x_{s1}$, $s2_x = \max\{p_{v,x}, oX, wp_{f,x}\} + \Delta x_{s2}$ define the side lines. Notice that $WP_f = (WP_{f,x}, WP_{f,y})$ and $p_v = (p_{v,x}, p_{v,y})$;
8. The following values are calculated: $\Delta x_{s1} = 100$, $\Delta x_{s2} = 2000 - |oX|$, $\Delta x_{l2} = 2000 - oY$
9. In case of moving obstacle, the *forbidden navigation area* (see Fig. 10) limited by the coordinates o_y, o_Y and $s1_x$ and $WP_{f,x}$ is added as an additional obstacle.

The values of Δ_{s1}, Δ_{s2} and Δ_{l2} are defined arbitrarily to have a replanning area of around 2000x2000 square meters, that extends in both directions for an extension of around 4 times the range of the sensor. This area can be

successfully replanned in less than $T_r = 0.6$s, so it is possible to define $T^* = 2$s. If a solution cannot be found, the replanning area is increased and the procedure repeated again. If during this process the CPA becomes critical, the navigation is stopped. Moreover, this paper considers dynamic obstacles with realistic dynamics. In this sense it is supposed that changes in their speed or direction cannot occur instantly, and can be identified by the obstacle tracking algorithm. If the new conditions do not allow a replanning in the safety time margins, the system would notify the captain that an emergency stop may be needed.

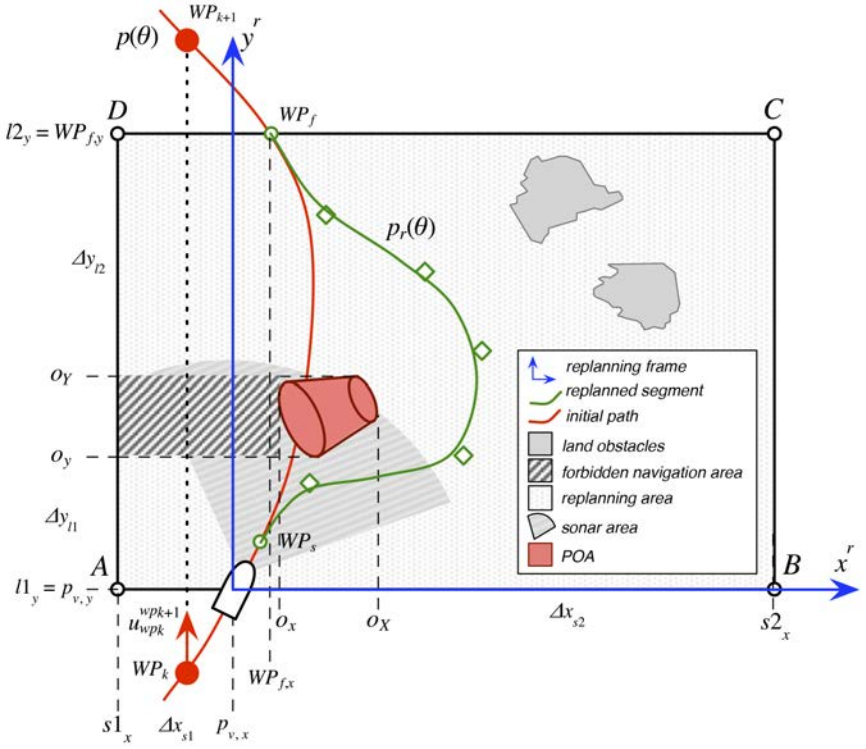

Figure 10: Illustration of the replanning area. The replanning frame (blue axes) is oriented towards the line connecting the WP_k to WP_{k+1}.

10. Case Study and Simulation Results

In this section, we present information related to setting-up and running the simulations. A block diagram illustrating the logic flow of the whole

path-planning system and the sections within the paper that describe its elements can be seen in Fig. 11.

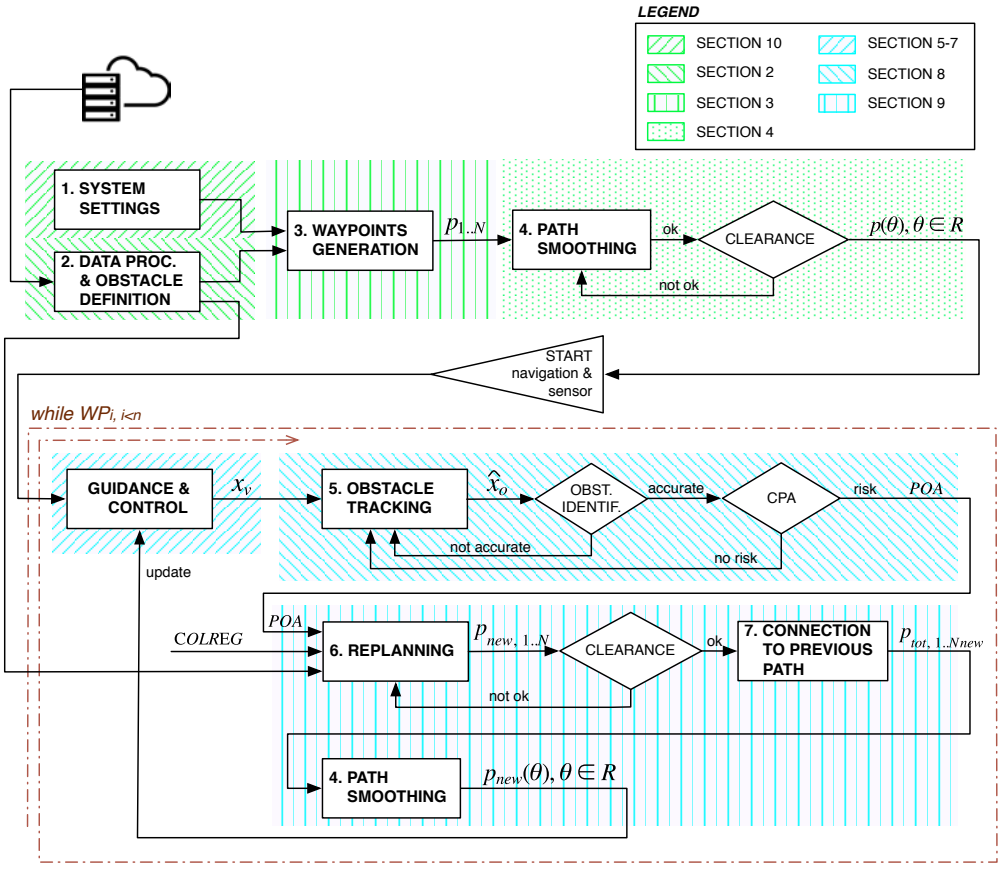

Figure 11: Illustration of the algorithm's block elements and their correspondence with the sections of this paper. The upper part is executed offline, while the red dashed line contains the online processes.

10.1. Map and Environmental Conditions

The simulations are carried out on real map data, representing a region of around 3000 Km^2 in the Sør-Trøndelag region of Norway. The data have been obtained from the sources reported in Section 2. We considered a constant (w.r.t. the inertial frame) ocean current of magnitude $\mathrm{U_c} = 2\mathrm{m/s}$ and direction $\beta_c = 90°$ (from West to East).

10.2. Obstacles Motion

As mentioned in Section 8, we consider *dynamic obstacles* with unknown velocity, which is estimated online along with the obstacle's position. In particular, the obstacle speed is modified by adding a Gaussian noise around its average speed:

$$|\mathrm{u_o}| \sim \mathcal{N}\left(|\bar{\mathrm{u}}_\mathrm{o}|, \frac{|\bar{\mathrm{u}}_\mathrm{o}|}{3}\right) \tag{32}$$

Where u is the surge speed, that is the first element of the $\mathbf{v}_\mathrm{o}$ obstacle velocity vector. The course angle evolves following a random walking process, where at every step the probabilities of changing direction is set at 0.4, giving as a result a motion with a certain variability in the course. The heading varies with steps of $\Delta_\psi = 1^\circ$, where the period that is used for generating the moving obstacle motion is set to 0.01s. The random walking process that generates the heading can then be defined by the following discrete probability function:

$$\mathrm{P}\left[\psi_\mathrm{o}(\mathrm{k}+1) = \psi_\mathrm{o}(\mathrm{k}) + \Delta_\psi\right] = 0.2; \tag{33}$$

$$\mathrm{P}\left[\psi_\mathrm{o}(\mathrm{k}+1) = \psi_\mathrm{o}(\mathrm{k})\right] = 0.6; \tag{34}$$

$$\mathrm{P}\left[\psi_\mathrm{o}(\mathrm{k}+1) = \psi_\mathrm{o}(\mathrm{k}) - \Delta_\psi\right] = 0.2; \tag{35}$$

This adds a certain level of unpredictability to the simulated obstacle motion, that is useful to test and challenge the assumptions stated in Section 8.

10.3. Simulations Parameters

The simulations were implemented using the model for *Cybership II*, a *1:70* replica of a supply ship (the model parameters can be found in Skjetne, 2005). The target vessel is moving with a relative total speed of $\mathrm{U_r} = 5\mathrm{m/s}$. The LOS tuning constants from (24)–(25) were chosen as: $\mathrm{K}_1 = 10$, $\mathrm{K}_2 = 0.8$. Moreover, the lookahead distance of (22) and following is set to $\Delta = 20\mathrm{m}$.

10.4. Sensor Characteristics

A variety of sensors can be used for obstacle detection, from passive-ranging cameras (in monocular and stereo configurations) to active-ranging radars, sonars and lidars. Configurations that fuse data from radars and cameras, or range finders and cameras are the most widely utilized ones (Almeida et al., 2009, Heidarsson and Sukhatme, 2011, Larson et al., 2006, 2007). This paper does not treat the sensing module itself nor the data

interpretation, in fact the obstacle is detected as soon as it enters the sensor's FOV. The interested reader is referred to Quidu et al. (2012); Karoui et al. (2015) instead, since the solution therein can be used to detect and avoid both above and sub-surface obstacles in the middle-short range by using only one sensor (sonar). A similar solution is also utilized in Heidarsson and Sukhatme (2011). In our case, the following values define the accuracy and other characteristics of the simulated sensor:

$$\sigma_{\mathrm{d}} = 0.05\mathrm{m}, \tag{36}$$

$$\sigma_{\delta} = 1.5^{\circ}, \tag{37}$$

$$\sigma_{\mathrm{v}} = 10^{-3}\mathrm{m/s}^2. \tag{38}$$

where $\sigma_{\mathrm{d}}, \sigma_{\delta}$ are the standard deviations of the measurement errors' range and bearing, respectively, and σ_{v} the standard deviation of the model error. These variables are used to tune the obstacle tracking algorithms, as in Karoui et al. (2015). Moreover, the sensor is supposed to have a range of 500m, and to span an angle $\delta \in [-60^{\circ},\ 60^{\circ}]$.

10.5. Simulation Results

This section presents a simulation study where two consecutive replanning sessions are needed to avoid two obstacles. The simulation is based on the map area from Fig. 4. However, in this case study we do not consider depth constraints because the resulting paths are safer by keeping the vehicle further away from small islands, hence making the replanning phase easier to execute successfully. On the contrary, we choose to perform the dynamic replanning algorithm at a crammed area with small islands and two additional obstacles (one static and one dynamic).

The selected path segment is between WP_{22}–WP_{23}, see Fig. 12. The vehicle encounters the dynamic obstacle first and starts following the first replanned segment (or deviation). Before returning to the original path, the vehicle encounters the static obstacle and needs to perform a second replanning. Notice that, after travelling on the second replanned segment (green curve), the vehicle converges initially back to the first replanned segment (blue curve) and then to the original path (red curve), that is, it does not go directly from the green to the red path. The FOVs of the sensor in the two moments in which the obstacles are first identified are also shown. Notice that an unknown ocean current is flowing from West to East.

Figures 13–15 represent zoomed areas of Fig. 12. They show respectively:

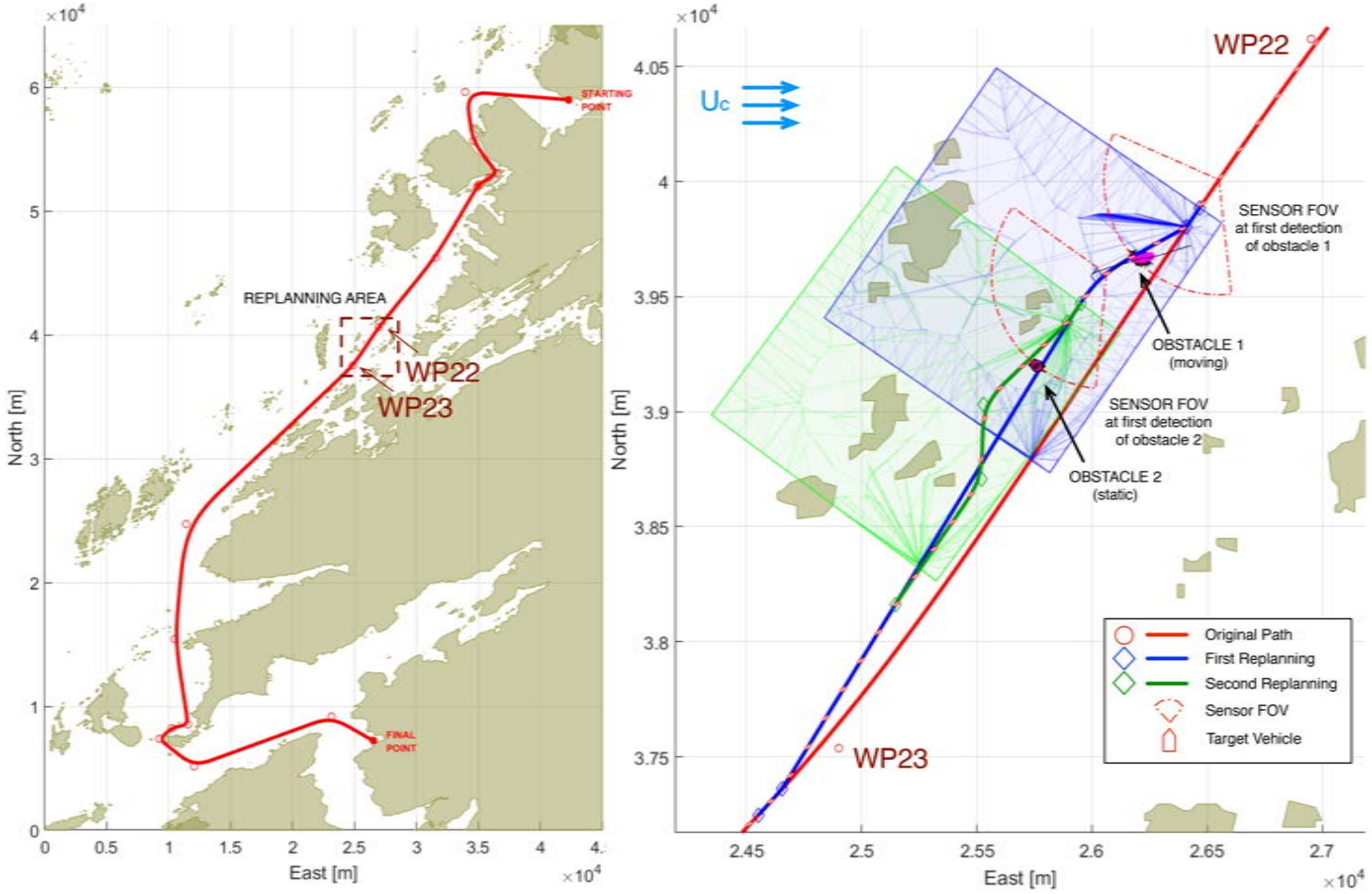

Figure 12: Demonstration of consecutive replanning involving a dynamic obstacle followed by a static obstacle. The initial path (left plot) is generated based on land constraints. The second plot focuses on the area between WP_{22} and WP_{23}, where the two obstacles are detected and evaded. The two resulting replanning areas are highlighted with blue and green colors. The Voronoi diagram edges used for determining the replanned segments waypoints are also visible.

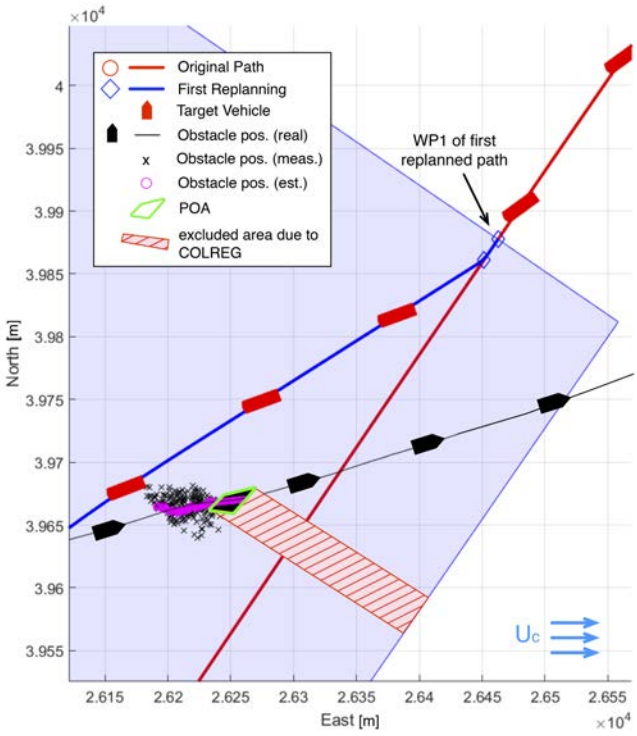

Figure 13: Detail of the first replanning and of the tracking of *Obstacle 1*. Black crosses are the measured position of the obstacle, violet dots the estimated positions. The POA is also indicated, together with the artifact obstacle added due to the COLREG constraints.

- The first deviation from the original path is due to the moving *obstacle 1* (black vehicle). Notice that this case falls in the *crossing situation* of the COLREGs (from Subsection 9.3). The moving obstacle is at the starboard side of the target vehicle when it enters the field of view of the sensor, consequently the target vehicle should change its course in order to leave the obstacle on its port side. For this purpose a virtual obstacle is added to the replanning area, excluding alternative paths that do not satisfy the COLREGS (light green box in Fig. 13).
- The deviation from the blue path due to the static obstacle (approximated as a circle of standard dimension, as explained in Subsection 9.4). Notice that in this case the POA is not modified, since the COLREGs do not apply.
- The moments when the target vessel joins again the first replanned path (blue), and the initial path (red).

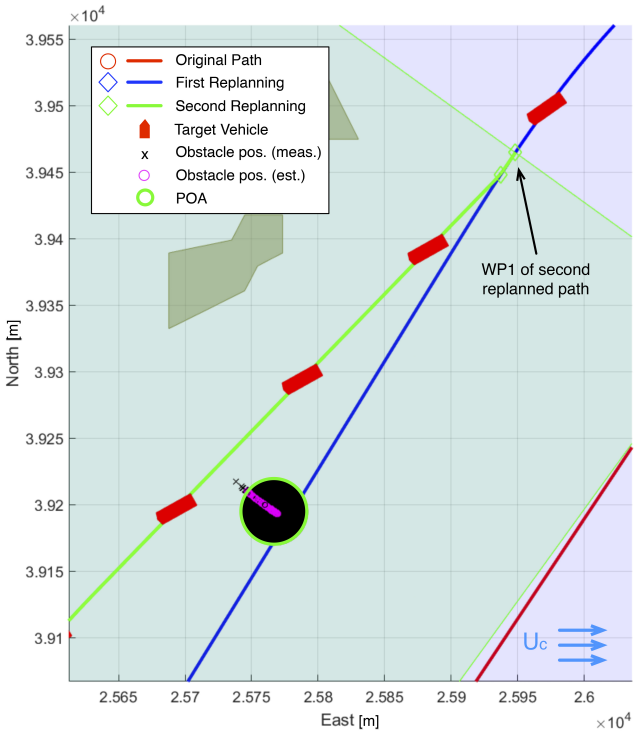

Figure 14: Detail of the second replanning and of the tracking of the second obstacle. Black crosses are the measured position of the obstacle, violet dots the estimated positions. In this case the POA is approximated as a disc of standard dimensions, and COLREGs do not need to be included.

In the aforementioned figure the measures positions of the obstacles (black crosses) and their estimated positions (violet circles), are also depicted. It can be seen how smoothly the vessel is deviated from the original path and joins it again after the escaped risk. The following plots show the details of the control performance along the path.

Fig. 16 shows the CTE for the simulated example. t = 252s corresponds to the *time of action* t_a, introduced in Subsection 9.1 and Fig. 8. The end of the plot corresponds to the moment when the vessel reach WP_{24} of the original path. Small oscillations in the CTE due to the replanning can be noticed: in these points the vessel changes its course rapidly, and the controller must adjust for the new current estimation. Despite of these aspects, the CTE is kept under 0.4m along the whole replanned segment. The initial oscillations are due to the fact that the starting vessel's heading is not aligned with the path direction at the starting waypoint (WP_{22}).

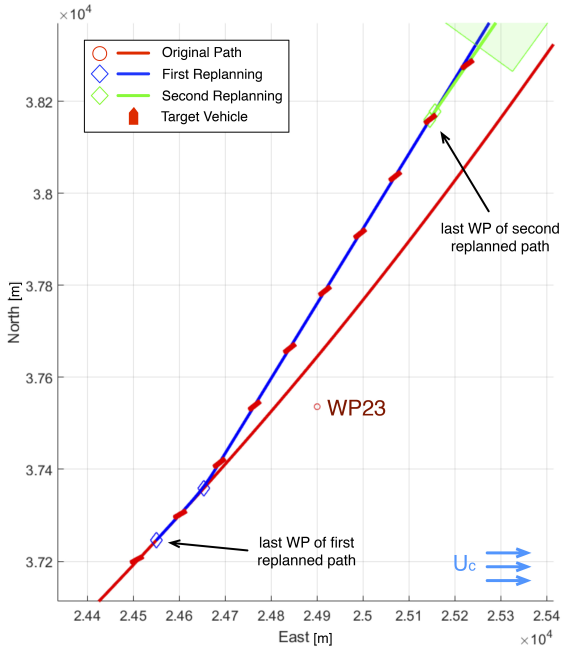

Figure 15: Detail of path convergence: the second replanned path (green) converges smoothly on the first replanned one (blue), the first replanned path, finally, converges smoothly to the original one (red).

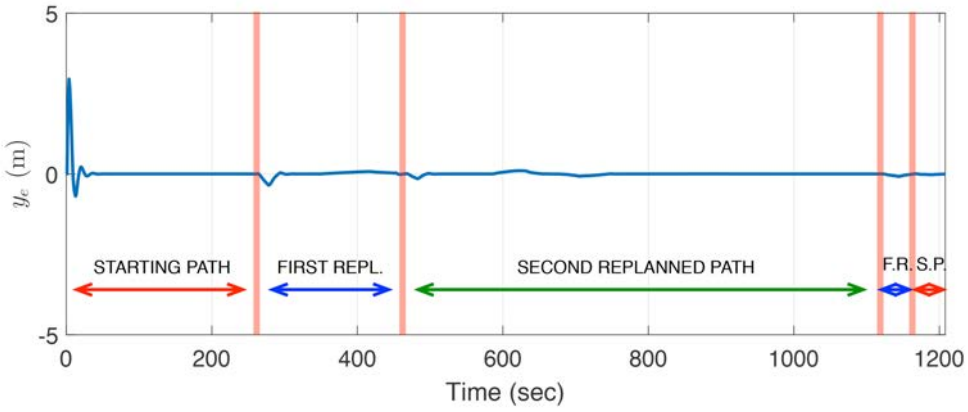

Figure 16: Cross-track error along the path. Small disturbances (always below 0.4 m) can be observed whenever a replanning process takes place. The initial oscillations are due to the vessel's initial heading, which is not aligned with the path direction at WP_{22}.

11. Conclusions

We presented a dynamic path-planning system for underactuated marine surface vehicles based on the Voronoi Diagram (VD). Given a departure and a destination location, the algorithm first plans an initial path at *global* level (that is, considering the whole available map) by refining significantly the original VD roadmap through a number of heuristics. One more new element is that, in addition to land constraints, the sea depth data available in nautical charts are exploited in order to avoid navigating in shallow waters. Successive straight-line segments are connected using Fermat's Spiral (FS) segments, which ensures low computational cost and results in practical and intuitive paths that satisfy the dynamic constraints (curvature continuity and maximum value) of the underactuated vehicle. A methodology for FS path following was also developed and presented for the first time here.

When an obstacle (static or dynamic) is detected and its motion is tracked using the onboard sonar, the algorithm enters a *replanning phase* and generates a path deviation at *local* level that ensures collision avoidance while respecting the COLREGs. Apart from the predicted future trajectory of the obstacle itself, the replanning phase also takes into account the time intervals needed for the algorithm to replan and the vehicle to change its course, so as to produce a useful deviation. The process is very similar to the initial planning phase, but additional heuristics are developed so as to select a sensible map area size wherein to seek path deviations, and to connect this local deviation to the original path smoothly after a collision has been avoided.

The simulated case study focused on a crammed area with many small islands and two (a priori unknown) obstacles, one dynamic and one static. The locations of the obstacles resulted in consecutive double replanning of the local path. The marine vehicle avoided both obstacles and then continued smoothly onto the original path. Without any special effort to optimize the algorithm running time in Matlab, the replanning time never overcame the threshold of 0.6 s. This concerned a map area of approximatively $2000 \times 2000\,\mathrm{m}^2$, hence making this solution very promising for real applications.

Acknowledgments

This work has been carried out at the Centre for Autonomous Marine Operations and Systems (AMOS). The Norwegian Research Council (RCN) is acknowledged as the main sponsor of NTNU AMOS through the Centres

of Excellence funding scheme, Project number 223254. Christian Malmquist from Kartverket is acknowledged for sharing his great knowledge about maps. The second author was supported by RCN through the project *Next Generation Subsea IMR Operations*, Project number 234108.

References

Almeida, C., Franco, T., Ferreira, H., Martins, A., Santos, R., Almeida, J. M., Carvalho, J., Silva, E., May 2009. Radar based collision detection developments on USV ROAZ II. In: Proceedings of MTS/IEEE OCEANS.

Antonelli, G., Chiaverini, S., Finotello, R., Schiavon, R., Apr 2001. Real-time path planning and obstacle avoidance for RAIS: an autonomous underwater vehicle. IEEE Journal of Oceanic Engineering 26 (2), 216–227.

Antonelli, G., Chiaverini, S., Marino, A., May 2012. A coordination strategy for multi-robot sampling of dynamic fields. In: Proceedings of the Proceedings of the IEEE International Conference on Robotics and Automation (ICRA). pp. 1113–1118.

Aurenhammer, F., 1991. Voronoi diagrams - a survey of a fundamental geometric data structure. ACM Computing Surveys 3, 345–404.

Bellingham, J. S., Tillerson, M., Alighanbari, M., How, J. P., Dec 2002. Cooperative path planning for multiple UAVs in dynamic and uncertain environments. In: Proceedings of the 41st IEEE Conference on Decision and Control (CDC). Vol. 3. pp. 2816–2822.

Borenstein, J., Koren, Y., June 1991. The vector field histogram-fast obstacle avoidance for mobile robots. IEEE Transactions on Robotics and Automation 7 (3), 278–288.

Bortoff, S. A., Sept 2000. Path planning for uavs. In: Proceedings of the American Control Conference (ACC). Vol. 1. pp. 364–368.

Caharija, W., Pettersen, K. Y., Sørensen, A. J., Candeloro, M., Gravdahl, J. T., Mar 2014. Relative velocity control and integral line of sight for path following of autonomous surface vessels: Merging intuition with theory. Journal of Engineering for the Maritime Environment 228 (2), 180–191.

Caiti, A., 2014. Motion Planning for Marine Control Systems. Springer London, London.

Campbell, S., Naeem, W., Irwin, G., 2012. A review on improving the autonomy of unmanned surface vehicles through intelligent collision avoidance manoeuvres. Annual Reviews in Control 36 (2), 267 – 283.

Candeloro, M., Lekkas, M. A., Hegde, J., Sørensen, A. J., May 2016. A 3d dynamic voronoi diagram-based path-planning system for uuvs. In: Proceedings of MTS/IEEE OCEANS.

Candeloro, M., Lekkas, M. A., Sørensen, A. J., Fossen, T. I., 2013. Continuous curvature path planning using voronoi diagrams and fermat's spirals. 9th IFAC Conference on Control Applications in Marine Systems 9 (1), 132–137.

Chandler, P., Rasmussen, S., Pachter, M., Aug 2000. Uav cooperative path planning. In: of Aeronautics, A. I., Astronautics (Eds.), Proceedings of the AIAA Guidance, Navigation, and Control Conference and Exhibit.

Choset, H., Lynch, K. M., Hutchinson, S., Kantor, G. A., Burgard, W., Kavraki, L. E., Thrun, S., June 2005. Principles of Robot Motion: Theory, Algorithms, and Implementations. MIT Press, Cambridge, MA.

Dahl, A. R., 2013. Path Planning and Guidance for Marine Surface Vessels. Master's thesis, Department of Engineering Cybernetics, Norwegian University of Science and Technology, Trondheim, Norway.

Dijkstra, E. W., 1959. A note on two problems in connexion with graphs. Numerische Mathematik 1, 269–271.

Dolgov, D., Thrun, S., M., M., J., D., Jan 2010. Path Planning for Autonomous Vehicles in Unknown Semi-structured Environments. The International Journal of Robotics 29 (5), 485–501.

Elfes, A., June 1987. Sonar-based real-world mapping and navigation. IEEE Journal on Robotics and Automation 3 (3), 249–265.

Falcone, M., Ferretti, R., 2013. Semi-Lagrangian Approximation Schemes for Linear and Hamilton-Jacobi Equations. Society for Industrial and Applied Mathematics, Philadelphia, PA.

Fiorini, P., Shiller, Z., May 1993. Motion planning in dynamic environments using the relative velocity paradigm. In: Proceedings of the Proceedings of the IEEE International Conference on Robotics and Automation (ICRA). Vol. 1. pp. 560–565.

Fossen, T. I., 2011. Handbook of Marine Craft Hydrodynamics and Motion Control. John Wiley and Sons Ltd.

Fossen, T. I., Lekkas, A. M., Mar 2015. Direct and indirect adaptive integral line-of-sight path-following controllers for marine craft exposed to ocean currents. International Journal of Adaptive Control and Signal Processing.

Fox, D., Burgard, W., Thrun, S., Mar 1997. The dynamic window approach to collision avoidance. IEEE Robotics Automation Magazine 4 (1), 23–33.

Gold, C., 2016. Tessellations in GIS: Part IImaking changes. Geo-spatial Information Science 19 (2), 157–167.

Gold, C., Chau, M., Dzieszko, M., Goralski, R., 2005. 3D Geographic Visualization: The Marine GIS. Springer Berlin Heidelberg, pp. 17–28.

Gold, C. M., 1998. The use of the dynamic Voronoi data structure in autonomous marine navigation. pp. 217–220.

Goralski, I. R., Gold, C. M., July 2007. Maintaining the Spatial Relationships of Marine Vessels Using the Kinetic Voronoi Diagram. In: Proceedings of the 4th International Symposium on Voronoi Diagrams in Science and Engineering (ISVD). pp. 84–90.

Hart, P. E., Nilsson, N. J., Raphael, B., July 1968. A Formal Basis for the Heuristic Determination of Minimum Cost Paths. IEEE Transactions on Systems Science and Cybernetics 4 (2), 100–107.

Heidarsson, H. K., Sukhatme, G. S., May 2011. Obstacle detection and avoidance for an autonomous surface vehicle using a profiling sonar. In: Proceedings of the IEEE International Conference on Robotics and Automation (ICRA). pp. 731–736.

IMO, 1977. International Maritime Organization - The International Regulations for Preventing Collisions at Sea. `https://goo.gl/7mPxS7`, accessed in Nov, 2016.

Karoui, I., Quidu, I., Legris, M., Aug 2015. Automatic Sea-Surface Obstacle Detection and Tracking in Forward-Looking Sonar Image Sequences. IEEE Transactions on Geoscience and Remote Sensing 53 (8), 4661–4669.

Khatib, O., Mar 1985. Real-time obstacle avoidance for manipulators and mobile robots. In: Proceedings of the IEEE International Conference on Robotics and Automation (ICRA). Vol. 2. pp. 500–505.

Kongsberg, Oct 2016. World's First Official Test Bed for Autonomous Shipping Opens in Norway. `https://goo.gl/oEdLk2`, accessed in Nov, 2016.

Kuwata, Y., Wolf, M. T., Zarzhitsky, D., Huntsberger, T. L., Jan 2014. Safe Maritime Autonomous Navigation With COLREGS, Using Velocity Obstacles. IEEE Journal of Oceanic Engineering 39 (1), 110–119.

Larson, J., Bruch, M., Ebken, J., May 2006. Autonomous navigation and obstacle avoidance for unmanned surface vehicles. Society of Photo-Optical Instrumentation Engineers (SPIE) Conference Series 6230, 623007.

Larson, J., Bruch, M., Ebken, J., Rogers, J., Webster, R., 2007. Advances in autonomous obstacle avoidance for unmanned surface vehicles.

Lavalle, S. M., Nov 1998. Rapidly-Exploring Random Trees: A New Tool for Path Planning. Tech. rep., Computer Science Dept., Iowa State University.

LaValle, S. M., 2006. Planning Algorithms. Cambridge University Press, New York, NY, USA.

Ledoux, H., July 2007. Computing the 3D Voronoi Diagram Robustly: An Easy Explanation. In: Proceedings of the 4th International Symposium on Voronoi Diagrams in Science and Engineering (ISVD). pp. 117–129.

Lee, S. M., Kwon, K. Y., Joh, J., June 2004. A fuzzy logic for autonomous navigation of marine vehicles satisfying COLREG guidelines. International Journal of Control Automation and Systems 2 (2), 171–181.

Lekkas, A. M., Dahl, A. R., Breivik, M., Fossen, T. I., 2013. Continuous-Curvature Path Generation Using Fermat's Spiral. Modeling, Identification and Control (MIC) 34 (4), 183–198.

Lekkas, A. M., Fossen, T. I., 2014a. Integral LOS path following for curved paths based on a monotone cubic Hermite spline parametrization. IEEE Transactions on Control Systems Technology 22 (6), 2287–2301.

Lekkas, A. M., Fossen, T. I., Oct 2014b. Trajectory tracking and ocean current estimation for marine underactuated vehicles. In: IEEE Conference on Control Applications (CCA). pp. 905–910.

Lekkas, A. M., Roald, A. L., Breivik, M., 2016. Online Path Planning for Surface Vehicles Exposed to Unknown Ocean Currents Using Pseudospectral Optimal Control. Vol. 49. pp. 1 – 7, 10th {IFAC} Conference on Control Applications in Marine Systems (CAMS).

Lerro, D., Bar-Shalom, Y., July 1993. Tracking with debiased consistent converted measurements versus EKF. IEEE Transactions on Aerospace and Electronic Systems 29 (3), 1015–1022.

Lozano-Pérez, T., Wesley, M. A., Oct 1979. An algorithm for planning collision-free paths among polyhedral obstacles. Communications of the ACM (CAMC) 22 (10), 560–570.

Ludvigsen, M., Sørensen, A. J., 2016. Towards integrated autonomous underwater operations for ocean mapping and monitoring. Annual Reviews in Control.

Marino, A., Antonelli, G., Aguiar, A. P., Pascoal, A., Oct 2012. A new approach to multi-robot harbour patrolling: Theory and experiments. In: 2012 IEEE/RSJ International Conference on Intelligent Robots and Systems. pp. 1760–1765.

Marino, A., Antonelli, G., Aguiar, A. P., Pascoal, A., Chiaverini, S., Jan 2015. A Decentralized Strategy for Multirobot Sampling/Patrolling: Theory and Experiments. IEEE Transactions on Control Systems Technology 23 (1), 313–322.

Naeem, W., Irwin, G. W., Yang, A., Sept 2012. COLREGs-based collision avoidance strategies for unmanned surface vehicles. Special Issue on Intelligent Mechatronics 22 (6), 669–678.

Perera, L. P., Ferrari, V., Santos, F. P., Hinostroza, M. A., Soares, C. G., April 2015. Experimental evaluations on ship autonomous navigation and

collision avoidance by intelligent guidance. IEEE Journal of Oceanic Engineering 40 (2), 374–387.

Quidu, I., Jaulin, L., Bertholom, A., Dupas, Y., July 2012. Robust Multitarget Tracking in Forward-Looking Sonar Image Sequences Using Navigational Data. IEEE Journal of Oceanic Engineering 37 (3), 417–430.

Seto, M., 2013. Marine Robot Autonomy. Springer.

Skjetne, R., 2005. The maneuvering problem. Ph.D. thesis, Department of Marine Technology, Norwegian University of Science and Technology, Trondheim, Norway.

Statheros, T., Howells, G., Maier, K. M., Jan 2008. Autonomous ship collision avoidance navigation concepts, technologies and techniques. Journal of Navigation 61 (1), 129142.

Tsourdos, A., White, B., Shanmugavel, M., 2010. Cooperative Path Planning of Unmanned Aerial Vehicles. Wiley.

van den Berg, J., Ferguson, D., Kuffner, J., May 2006. Anytime Path Planning and Replanning in Dynamic Environments. In: Proceedings of the Proceedings of the IEEE International Conference on Robotics and Automation (ICRA). pp. 2366 – 2371.

Watson, D. P., Scheidt, D. H., 2005. Autonomous systems. Johns Hopkins APL Technical Digest 26 (4).

Woerner, K., 2016. Multi-contact protocol-constrained collision: avoidance for autonomous marine vehicles. Ph.D. thesis, Massachusetts Institute of Technology.

Yen, J. Y., 1970. An algorithm for finding shortest routes from all source nodes to a given destination in general networks. Quarterly of Applied Mathematics 27, 526–530.

Zeng, Z., Liana, L., Sammut, K., He, F., Tang, Y., Lammas, A., Dec 2015. A survey on path planning for persistent autonomy of autonomous underwater vehicles. Ocean Engineering 110 (A), 303–313.

Article J

A 3D Dynamic Voronoi Diagram-Based Path-Planning System for UUVs

M. Candeloro, A.M. Lekkas, J. Hegde, A.J. Sørensen

The article has been published in the proceedings of the
MTS/IEEE OCEANS 2016,
Monterey, California. 19-23 September 2016.

A 3D Dynamic Voronoi Diagram-Based Path-Planning System for UUVs

Mauro Candeloro, Anastasios M. Lekkas, Jeevith Hegde, Asgeir J. Sørensen
Norwegian University of Science and Technology (NTNU)
Centre for Autonomous Marine Operations and Structures (AMOS)
Otto Nielsens veg 10, NO-7491 Trondheim, Norway
Email: {mauro.candeloro, anastasios.lekkas, jeevith.hegde, asgeir.sorensen}@ntnu.no

***Abstract*—This paper proposes a rapid path-planning and replanning system for Unmanned Underwater Vehicles (UUVs) that navigate in environments where subsea structures and other vehicles may be present. The proposed method is based on the Voronoi diagram, which is used to generate an initial set of connected waypoints (a *roadmap*) in the three-dimensional (3D) space, ensuring a certain clearance to avoid collisions with obstacles or grounding (e.g. collision with the ground). A 3D continuous path, composed by straight segments and circumference arcs, connects the aforementioned waypoints. If the vehicle encounters any moving or static obstacle and a collision risk is detected, the path is replanned online. In this context, an evaluation of the risk must be performed, and a list of traffic rules inspired by the International Regulations for Preventing Collisions at Sea (COLREGs, which are adopted for surface vessels), and by the Traffic and Collision Avoidance System (TCAS, which is adopted for aerial vehicles), is proposed for underwater vehicles. Those rules define the replanning procedure, so that an effective and safe collision avoidance maneuver can be performed whenever necessary. Simulations are performed on an subsea factory scenario, and results are presented to show the effectiveness of the proposed method.**

I. Introduction

Considerable progress has been achieved in the latest years with respect to autonomous operations for UUVs, including dedicated operations for Autonomous Underwater Vehicles (AUVs) and Remotely Operated Vehicles (ROVs). This concerns also the development of new control architectures, which are able to integrate the autonomous aspect *in-the-loop* [2], [3]. In particular, there is a stronger trend that aims to merge the characteristics of both the technologies to obtain an untethered vehicle that could navigate efficiently and perform manipulation work on underwater structures [4], also in very challenging conditions [5]. Moreover, the undergoing research on underwater docking stations would allow to have battery-recharging possibility on-the-spot and have permanently hovering vehicles on the sea bottom [6], [7], [8], [9]. In such a scenario, it is possible to foresee a number of vehicles operating around underwater structures, moving from one to another depending on the operational needs. In [10], the term *AROV* (Autonomous ROV), which underlines the merging of the AUV and ROV technology for subsea intervention operations, is introduced. The same paper addresses also safety aspects of autonomous subsea operations, reviewing and underlining the need for guidelines regulating subsea IMR operations [10], [11]. In the following, the general category of UUVs will be considered, including all those underwater vehicles with extended autonomy characteristics, intervention and docking abilities, the latter giving permanent hovering possibilities. It is clear how, in the depicted context, how crucial the path-planning and replanning phases become. The UUV should be able to plan its travel based on a-priori information concerning its mission and the surrounding environment, and to replan it if any obstacle comes on its way, representing a real collision risk. In [12], a survey concerning path-planning in relation to persistent underwater autonomous operations is presented.

Path-planning and obstacle avoidance are widely addressed among the automatic control community working with marine applications. It is common to decompose the path-planning in two sub-problems: the first concerns the design of an initial path prior to the mission start, and the second concerns the ability of handling unexpected events by locally modifying it. *Global* and *local* path-planning algorithms are respectively used to solve those two problems [13], [14]. Specific applications of path-planning and obstacle-avoidance for marine applications can be found in [15], [16], [11].

This paper extends the idea proposed in [17] and [18] by moving the scenario of interest from the two-dimensional (2D) ocean surface to the three-dimensional (3D) underwater space.

A simplified representation of the environment is utilized to generate a 3D Voronoi diagram that produces a global roadmap, in which a set of waypoints, connecting an inital to a final position, is selected. Some examples that use the Voronoi diagram for the purpose of path-planning, can be found in [19], [20], [17], [18]. Straight segments are smoothed by using circular arcs to provide continuity and meet the kinematic requirements of underactuated vehicles [14], [21]. The path is locally modified if the vehicle identifies in the surroundings an obstacle which represents a potential risk, re-converging to the initial one after the local deviation. The replanning is performed respecting a set of traffic rules, which are inspired by the regulations currently followed by surface vessels and aerial vehicles. For aerial vehicles, the *Threat Resolution module*, part of the Traffic Alert and Collision Avoidance System (TCAS), takes care of producing path alternatives when a collision risk occurs [22]. For surface vessels, the rules 13, 14, 15, 16 and 17 of the International Regulations for

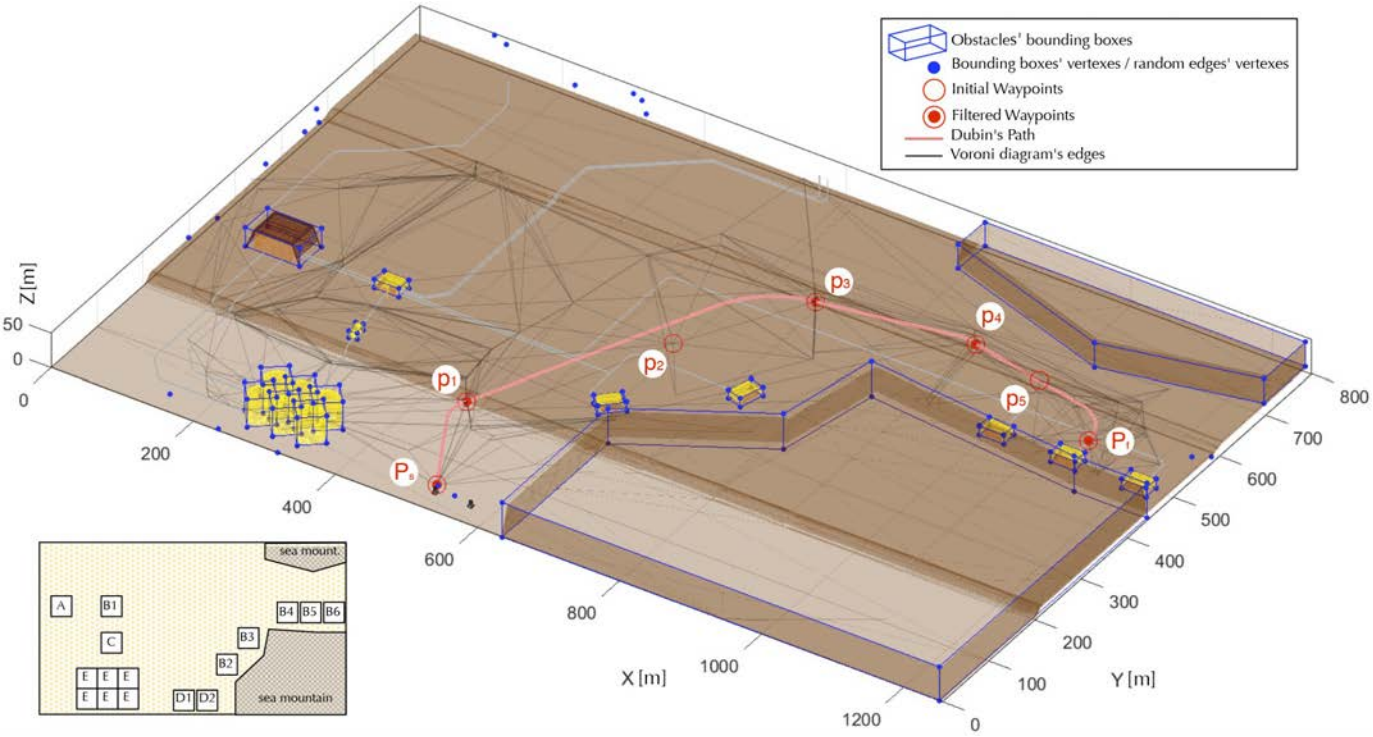

Figure 1: The scenario utilized in this paper. The topography of the Åsgard Subsea Production System (SPS) [1] is used as a basis for the scenario represented in figure, in which the simulations take place. In the bottom left corner, the topology of the field is shown; letters refer to the tags in Figure 2. The other elements in the figure are explained in Sections IV and VII.

Preventing Collisions at Sea (COLREG), regulate the behavior of the vessel when overtaking, head-on or crossing situations occur [23]. Notice that, to the best of the authors' knowledge, there are still no official traffic rules and regulations that underwater vehicles must follow during autonomous nor supervised operations.

This paper is organized as following: Section II describes the applications of the proposed systems, Section III describes how the environment and obstacles are modeled, Section IV describes the main 3D path-planning system, Section V defines a list of traffic rules that the underwater vehicles should follow to safely avoid collisions, Section VI presents the 3D path-replanning system, Section VII describes the simulation scenario and presents detailed results of a planning and replanning situation. Finally, Section VIII states the conclusions.

II. Applications

In the last few decades, numerous Subsea Production Systems (SPS) have been developed and installed on the seabed to recover hydrocarbons from subsea reservoirs. Many examples can be found, for instance, along the Norwegian coastline, such as the Gullfaks oil field and the Åsgard gas field. Here, subsea templates, wellheads and subsea trees compose the underwater infrastructure needed for the extraction and refinement processes of the resources [24], [1]. Those infrastructures require constant and periodic Inspection, Maintenance and Repair (IMR) operations, which are usually carried out with remotely operated vehicles supported by surface vessels. Nevertheless, permanent underwater solutions are being explored. Some prototype solutions are under testing, such as the Battelle UUV docking and replenishment station, which provides the possibility of having a Bluefin-12 UUV permanently docked and operative [25]. Docking solutions are also being explored at MBARI and WHOI institutions [8], [9], [26] .

In this paper, the Åsgard SPS field layout, is taken as an inspiration for the simplified scenario in which the proposed simulations take place [1]. Notice that the Åsgard gas field is the first subsea factory which can process and transport hydrocarbons directly to land without assistance of support vessels [27], which makes it an ideal case-study for such operations.

In this context, it is possible to foresee different kinds of UUVs docked and ready to perform observation and maintenance tasks, depending on the needs of the surrounding infrastructures. Notice that this work may also be applied to ROVs, AUVs, and new generation vehicles, such as snake-like robots. The latter is an interesting and promising novel kind of vehicles (also denoted as swimming manipulators) that could easily navigate into tight and confined spaces, which is impossible for classical vehicles [28]. This characteristic makes the employment of swarms of such vehicles effective for IMR operations on SPS.

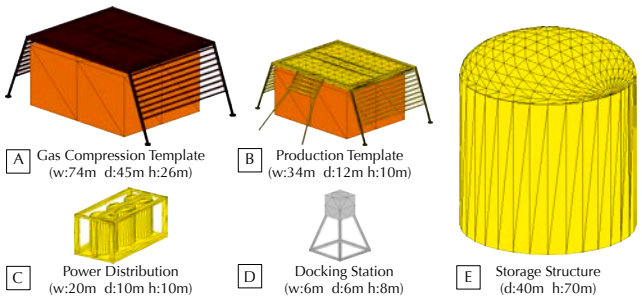

Figure 2: Some of the elements included in a SPS. Sizes vary from SPS to SPS, the ones which are used in this representation tried to report a realistic example of the proportions and sizes of such structures. Darker lines represent the mesh utilized to represent the objects.

III. Scenario and Obstacles Modeling

A simplified scenario is modeled and imported in MathWorks Matlab in order to be used as a basis for the simulations. The single elements (templates, pipelines, gas compression systems, storages, and so on) are modeled using Rhino, dimensioning them with the sizes found from the producers websites, e.g. [29], [30]. Moreover, the scenario layout is organized as the one of the Åsgard SPS [1], while some elements were added to increase its complexity (Figure 1).

In this paper, obstacles are represented as a list of vertexes $V_{o,i}$, connected by polygonal meshes which compose the 3D structure of the obstacles, as in Figure 2. For the purpose of the global path planning, it is not useful to consider the internal details of such structures since, in their proximity, the vehicle should be able to rely on a localization system which exploit vision sensors, near field acoustics, and other mechanisms which are more suitable for accurate positioning in the proximity of objects. For this reason, complex obstacles are simplified with their bounding boxes, highly reducing the number of vertexes required to model them. In Figure 1 it is possible to see the blue bounding boxes around every obstacle. Simple polyhedron-shaped envelopes bound the underwater structures and environment elements (e.g. underwater cliffs).

IV. Path-Planning System

The path-planning system is the module which takes as input a simplified representation of the environment, producing a feasible path, which connect a starting point P_s with a final point P_f in the vehicle configuration space (in Figure 1, P_s corresponds to the docking station D1, P_f corresponds to the template B5). This path is supposed to satisfy safety constraints (which require the vehicle to be at a certain minimum distance to any objects in the surroundings), and kinematic constraints (which guarantee flyability[1] of the path). The main modules of this system are represented in Figure 3.

[1]The term *flyability* defines the kinematic and dynamic ability of a vehicle to navigate along a certain path, as defined in [14].

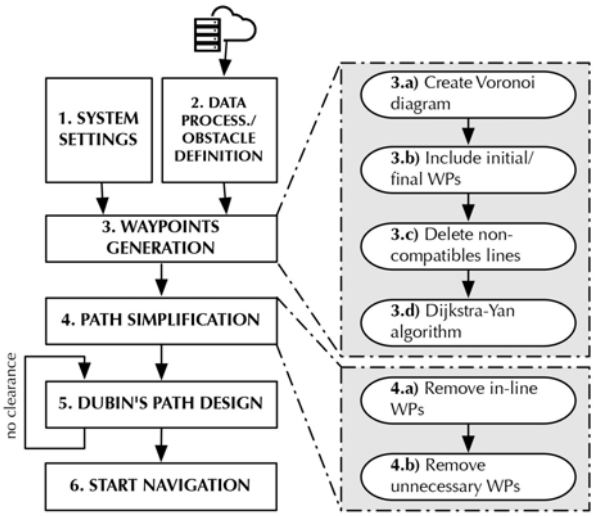

Figure 3: Main path-planning system's steps. The obstacles data is processed (Section III), the waypoints are selected from the roadmap provided by the Voronoi diagram generated on the obstacles (Subsection IV-A). Starting and final waypoints are integrated with the roadmap, the path is simplified (Subsection IV-B), and a Dubins path is used to smoothly connect the WPs (Subsection IV-C). Finally, the navigation of the vehicle starts.

A. 3D Voronoi Diagram

A Voronoi diagram is a tool to divide a geometrical space in a number of regions determined by the distribution of the objects present in that space. This general approach allowed many scientists to use this tool in a wide number of fields and applications [31]. In applications such as path planning (and specifically path planning for marine vehicles), the Voronoi diagram can be useful for its property of producing a roadmap with edges that are maximally distant to the generator points [17], [18]. In this paper, we are interested in the definition of a 3D Voronoi diagram. Below, a brief explanation of the main concepts related with Voronoi diagrams will be given, without presenting specific algorithms, which are extensively treated in the literature [32].

Voronoi diagrams can be defined as the dual structure of the Delaunay triangulation. Moreover, a n-dimensional Delaunay triangulation can be calculated from a $(n+1)$-dimensional convex-hull through a *lifting transformation* [33], [34]. The following definitions, referring to the 2D case for representation reasons, may be useful in this context (a visual representation is shown in Figure 4). Given a set of points p, q, r in the 3D space $S \in \mathbb{R}^3$, and their projection $p_0, q_0, r_0 \in S_0 : z = x^2 + y^2$ it is possible to define:

Delaunay Triangulation three points $p, q, r \in S$ form a Delaunay triangle if and only if the circumcircle of these points contains no other points of S;

Voronoi Diagram two points $o_{p_1 q_1 r_1}, o_{p_2 q_1 r_1}$ connect a Voronoi diagram's edge, if they are 2 circumsphere centers, where every one of two circumspheres is formed by the three vertexes of an adjacent Delaunay triangle;

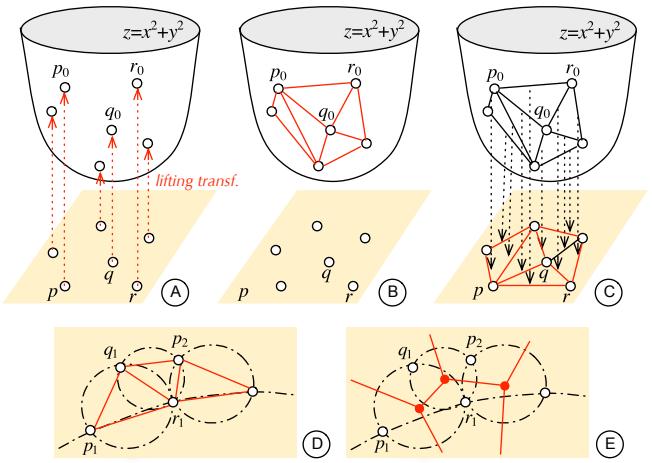

Figure 4: The convex hull method includes: the lifting transformation (A), the calculation of the related convex hull (B), and the definition of the Delaunay triangulation (lifting transformation inverse) (C). (D) shows an example of Delaunay triangulation, with related circumcircles. The Voronoi diagram will be the Delaunay triangulation dual (E).

Convex Hull three points $p_0, q_0, r_0 \in S_0$ form a face of the convex hull of S_0 if, and only if, the plane defined by those points has all the points of S_0 lying on one side.

The process which produces a Voronoi diagram in n-dimensions from the related convex hull (defined in $(n+1)$-dimensions), is called *convex-hull approach*, and has a complexity of $O(n \log n)$ (in the worst case) [34]. This is the approach which is used in this paper.

The vertexes $V_{o,i}$ of the obstacles' bounding boxes are selected as the generator vertexes of the Voronoi diagram in the selected scenario (Section III). The resulting Voronoi diagram edges are shown as black-dotted lines in Figure 1. Notice that, in order to limit the Voronoi diagram to the area of interest (corresponding surroundings of the production factory), a number of random vertexes are generated in the obstacle-free edges of the scenario (many of those vertexes can be noticed in Figure 1, on the yz planes, at $x = 0$m and $x = 1230$m, and on the xz planes, at $y = 0$m and $y = 800$m). The latter is a heuristic which proved to be effective, despite of its simplicity.

Given the Voronoi diagram's edges, the candidate waypoints can be identified in the edges extreme points (Voronoi diagram vertexes). The waypoints which represent the optimal path (in the sense of path with minimum distance among the ones provided by the roadmap) are selected through the Yen modification [35] of the Dijkstra optimization algorithm [36]. This algorithm is able to find the *k-shortest* paths, (shortest, second shortest, third shortest path, and so on). In this way, suboptimal solutions can be found if the optimal solution do not respect the preassigned safety constraints (clearance).

B. Path Simplification

Given the path's waypoints produced in the previous steps, a simplifying process is performed to reduce the course changes that the underwater vehicle must perform to reach the destination. In particular, the path can be simplified by removing a vertex if, and only if, the safety (clearance) constraints are respected, as shown with the following pseudo-code (the variable names are self-explanatory).

```
for i=1 to num_path_segments
  for j=1 to num_obstacles
    d(i)=distance(segment_i,obstacle_j);
  end
  dist_min_before=minimum(d);
end
for i=2 to (vertexes-1)
  remove_vertex_from_path(vertex(i))
  for i=1 to path_segments
    for j=1 to obstacles
      d(i)=distance(segment_i,obstacle_j);
    end
  dist_min_after=minimum(d);
  if dist_min_after<dist_min_before
    if dist_min_after<min_clearance
      reintroduce_vertex_into_path(vertex(i));
    end
  end
end
```

Listing 1: Path simplification pseudo-code: every vertex of the path is temporarily removed to see if the new path still respects the clearance constraints. If so, the vertex is permanently removed, since it is considered redundant.

C. Path Generation using 3D Dubins Path

If, in 2D, it has been proven that the Dubins path is the shortest path which connects two given points [21], in 3D the matter of defining the shortest path which connects a starting with a final points with given initial and final tangents, is more complicated [37]. Nevertheless, Dubins path[2] has been extensively used in many robotics applications, and many examples could be also found for applications in 3D. [38], [39], [40], [41], [42] are some examples of applications which mainly target Unmanned Aerial Vehicles (UAVs).

In this paper, the geometrical approach used in [41] is adapted to build a smooth path that respects the curvature constraints of an UUV (i.e. requiring that the radius of the circles which compose the curved segments of the path is higher than the inverse value of the maximum flyable curvature).

Giving a set of waypoints p_i (selected from the Voronoi roadmap, as in Subsection IV-A) and an initial and final direction, it is possible to obtain a Dubins path segment for every pair of successive points. The connection of those segments will produce the final path. Consider Figure 5, the centre of the circular segment can be obtained as:

$$o = p_f + rw, \tag{1}$$

where $w = \frac{W}{\|W\|}$ is the unit vector which is directed from p_f towards the centre of the circle o, and r is the given radius

[2]In this paper, *3D Dubins path* only indicates a path defined in the 3D-space, which is composed by straight and circular segments.

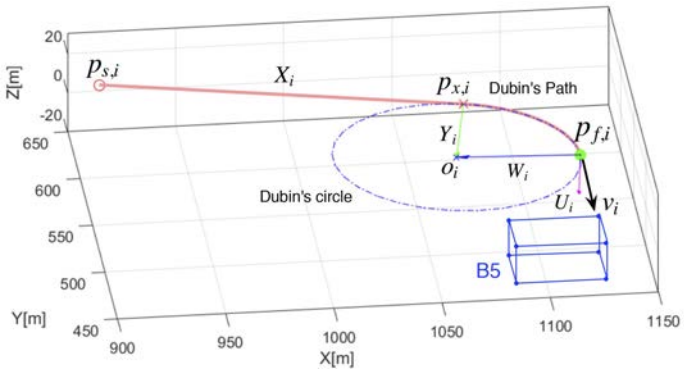

Figure 5: The last segment of the Dubins path included in the scenario of Figure 1 is shown here with its main geometrical components, as explained in Subsection IV-C. In the same figure, $p_{s,i}$ correspond to p_4, while $p_{f,i}$ correspond to P_f. The bounding box of the destination template (B5) is also depicted.

of the circle. The point which connects the straight segment with the circular one, can be calculated as:

$$p_x = o - ry = p_f + rw - ry, \tag{2}$$

where $y = \frac{Y}{\|Y\|}$ is the unit vector which is directed from p_x towards the centre of the circle o.

$$\begin{aligned} X = p_X - p_s &= p_f + rw - ry - p_s \\ &= p_f - p_s - r(x + v_2)\tan\frac{\theta_2}{2} \end{aligned} \tag{3}$$

where θ_2 is the turning angle of the circular segment. By setting $\cos\theta_2 = v_2 \cdot x$, and decomposing the equation along the three directions:

$$\begin{aligned} p_{f,x} - p_{s,x} - p_{X,x} - rx_x\tan\tfrac{\theta_2}{2} - rv_x\tan\tfrac{\theta_2}{2} &= 0 \\ p_{f,y} - p_{s,y} - p_{X,y} - rx_y\tan\tfrac{\theta_2}{2} - rv_y\tan\tfrac{\theta_2}{2} &= 0 \\ p_{f,z} - p_{s,z} - p_{X,z} - rx_z\tan\tfrac{\theta_2}{2} - rv_z\tan\tfrac{\theta_2}{2} &= 0 \end{aligned} \tag{4}$$

imposing the constraints $x = \frac{X}{\|X\|}$ and solving for p_X, it is possible to find all the geometrical elements described above and to draw the Dubins path. Further details about the geometrical construction and the mathematical solutions of such equations, can be found in [41].

Notice that, in this paper, the radius of the circular arcs composing the path varies, and it is directly proportional to the distance of the waypoints that connects: $r_i = \frac{||p_i - p_{i+1}||}{4}$.

V. Rules for Underwater Safe Navigation

In this section, safe underwater navigation rules for UUVs are proposed by adapting the COLREGS (from the marine industry), and the TCAS (from the aviation industry), with the purpose of avoiding collisions with other physical structures, natural objects, or other vehicles in the subsea environment [23], [43], [22]. These rules allow the replanning system to decide in the best way among replanning alternatives, under various collision scenarios.

A. Development of the Rules Set

Among the 38 rules, COLREGS contains five rules pertaining to collision avoidance of surface ships (rules 13, 14, 15, 16 and 17). These rules help the commander's decision process during overtaking, head-on, crossing, and give way scenarios between two vessels, and actions to be taken by a stand-on vessel. These rules are applied to marine vehicle operating on the sea surface (2D plane) and do not consider the vertical axis. To develop rules for the vertical plane, the TCAS rules (which pertain to the collision avoidance of aerial vehicles) are utilized to provide vertical separation and resolution advisories. While COLREGS promote maximization of horizontal distance to obstacle, the TCAS promote maximization of vertical separation (over a pretermined safe distances) between two aircrafts. When these two safety philosophies are applied to UUVs, high level safety navigation rules can be derived for 3D underwater applications.

In this paper, a moving obstacle is simulated to cross its path with the target UUV. When the UUV detects the obstacle as potential collision hazards, the path-replanning system produces a deviation from the original path, which agrees with the established set of rules.

A set of navigation rules provides decision support basis to the UUV during different collision scenarios, in particular will be here divided among rules to be considered for static obstacles, and rules to be considered with moving obstacles. The static obstacle (subsea structure or natural objects) can either be below the UUV or at the same altitude. The crossing obstacle can either move towards the UUV or away from it in the horizontal plane; moreover the relative position of the obstacle to the UUV can differ (higher, same, lower altitude).

Table I defines a subset of UUV navigation rules when they encounter static obstacles in the mission path. Table II defines the safe navigation rules in the dynamic obstacle case.

VI. Path-Replanning System

A scalable approach allows to use the same logic of the path-planning system (described in Section IV and Figure 3), also for the path-replanning system. The same approach has been also used, from the authors of this paper, in [18]. The main phases are summarized in the following, and refer to geometrical construction illustrated in Figure 6.

When the UUV detects an obstacle, the Closest Time of Approach (CTA), and the correspondent Closest Point of Approach (CPA), are calculated [44]:

$$t_C = \frac{(\boldsymbol{p}_{UUV} - \boldsymbol{p}_O)\cdot(\boldsymbol{v}_{UUV} - \boldsymbol{v}_O)}{||\boldsymbol{v}_{UUV} - \boldsymbol{v}_O||}, \tag{5}$$

$$d_C = ||(\boldsymbol{p}_{UUV} + \boldsymbol{v}_{UUV}t_C) - (\boldsymbol{p}_O + \boldsymbol{v}_O t_C)||, \tag{6}$$

where $\boldsymbol{p}_{UUV}, \boldsymbol{p}_O$ are respectively the position vectors of the UUV and of the obstacle, $\boldsymbol{v}_{UUV}, \boldsymbol{v}_O$ the velocity vectors of the UUV and of the obstacle, t_C is the CTA, while d_C is the CPA. As soon as the obstacle is detected within a certain accuracy[3], the Projected Obstacle Area (POA) [45] is defined

[3]In this paper, the obstacle's state estimation is not treated for space reason. The authors of this paper treated the topic for the 2D case in [18].

Obstacle position in horiz. plane (wrt UUV)	Obstacle position in vertical plane (wrt UUV)	Safe navigation rules
Front Left	Lower altitude	Turn right, climb.
Front Left	Same altitude	Turn right, climb.
Front	Lower altitude	Turn right, climb.
Front	Same altitude	Turn right, climb.
Front Right	Lower altitude	Turn left, climb.
Front Right	Same altitude	Turn left, climb.

Table I: Safe navigation rules in presence of a static obstacle.

Direction of movement	Obstacle position in horizontal plane (wrt UUV)	Obstacle position in vertical plane (wrt UUV)	Safe navigation rules
Obstacle moving in opposite direction of UUV	Crossing Left	Higher altitude	UUV descends, obstacle climbs.
	Crossing Left	Same altitude	UUV Climbs, obstacle descends.
	Crossing Left	Lower Altitude	UUV Climbs, obstacle descends.
	Crossing Right	Higher altitude	UUV descends, obstacle climbs.
	Crossing Right	**Same altitude**	**UUV Climbs, obstacle descends**.
	Crossing Right	Lower Altitude	UUV Climbs, obstacle descend.
Obstacle moving in same direction as UUV	Crossing Left	Higher altitude	UUV descends, obstacle climbs.
	Crossing Left	Same altitude	UUV descends, obstacle climbs.
	Crossing Left	Lower Altitude	UUV descends, obstacle climbs.
	Crossing Right	Higher altitude	UUV descends, obstacle climbs.
	Crossing Right	Same altitude	UUV descends, obstacle climbs.
	Crossing Right	Lower Altitude	UUV Climbs, obstacle descends.

Table II: Safe navigation rules in presence of a moving obstacle which is moving in the opposite/same direction as the UUV.

to cover the estimated positions that the obstacle can occupy from the moment of the first detection, to the CPA. The POA is a tetrahedron which represents a conservative estimation of the area that the UUV should keep at a certain (clearance) distance, in order to safely avoid collisions.

Once the POA of the obstacle is defined, the *replanning area* (i.e. the area in which the replanned segment will be calculated) must be found. The characteristics of this area are predefined, and should provide a proper compromise between the flexibility and the higher computational time that a bigger area would require. In particular, the vertexes of the replanning area are defined as in Figure 6. For instance, the lower left vertex is defined as:

$$\begin{aligned} V^b_{(1,x)} &= \min(0, o_{x,s}, o_{x,f}) - \Delta_{x,1} \\ V^b_{(1,y)} &= \min(o_{y,s}, o_{y,f}) - \Delta_{y,1} \\ V^b_{(1,z)} &= \min(0, o_{z,s}, o_{z,f}) - \Delta_{z,1} \end{aligned} \tag{7}$$

where $o_s = (o_{x,s}, o_{y,s}, o_{z,s})$ is the position of the obstacle at the first detection, $o_f = (o_{x,f}, o_{y,f}, o_{z,f})$ is the position of the obstacle at the CPA, $\Delta_{x,1}, \Delta_{x,2}, \Delta_{y,1}, \Delta_{y,2}, \Delta_{z,1}, \Delta_{z,2} > 0$ are positive spacing constants. All the other vertexes are defined similarly; this allows to have the a good spacing around the POA in all directions. For the following simulation, the spacing constants were defined as: $\Delta_{x,1} = \Delta_{x,2} = 50\text{m}, \Delta_{y,1} = \Delta_{y,2} = 40\text{m}, \Delta_{z,1} = \Delta_{z,2} = 10\text{m}$

By estimating the state of the obstacle (and knowing the state of the UUV), it is possible to select the right traffic rule to apply. In the case represented in Figure 6, the obstacle is *moving in the opposite direction of the UUV*, is *crossing right* and has the *same altitude*. Consequently the UUV should avoid it by increasing its altitude (this is underlined with bold letters in Table II). In order to achieve this, a *traffic rule box* (corresponding to the selected rule) is built inside the replanning box and considered as an extra obstacle, in order to exclude all the paths that would enter the forbidden area.

Finally, a Voronoi diagram is generated inside the replanning box. In order to summarize, the set of the generator vertexes for the Voronoi diagram will be composed by:

- the vertexes of all the bounding boxes of the obstacles which are inside the replanning box;
- the vertexes of the POA bounding box;
- the vertexes of the traffic rules' box;
- a set of random vertexes positioned on the faces of the replanning box and on the faces of the POA tetrahedron (as in Subsection IV-A).

Once the roadmap is calculated, the shortest available path is selected, waypoints are filtered and the path is smoothed (as in Subsections IV-A, IV-B and IV-C). Clearance is checked at every stage. Notice that the first and last waypoints of the replanned segments are found as the intersection points of the original path with the replanning box. This allows for a smooth convergence from the original path to the replanned one, and vice versa.

VII. Simulations

Results of the presented algorithms can be found throughout the entire length of the paper, and here they are summarized to provide a comprehensive exposition.

In the scenario presented in Figure 1, inspired from the Åsgard SPS, two docking stations are added at the bottom left part: D1 and D2. The same figure shows also the result of the path-planning which brings the UUV from the docking

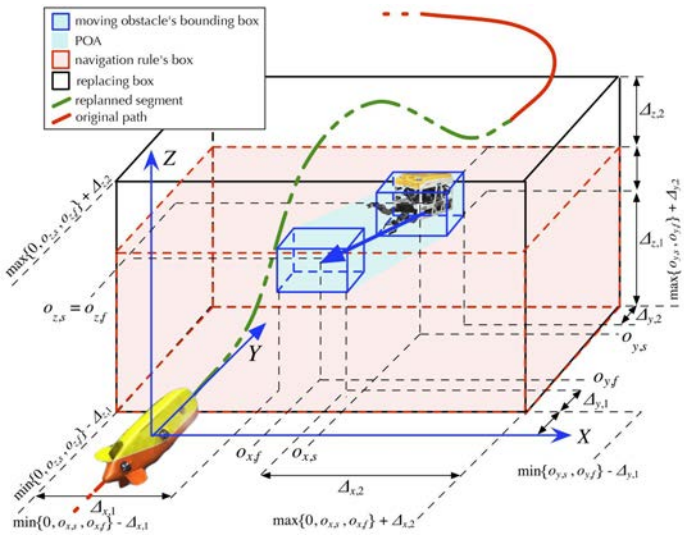

Figure 6: Main elements of the replanning system procedure, as explained in Section VI. The replanning (black), traffic rules (red), obstacle (blue) boxes are represented. Light blue tetrahedron represents the POA. The red path is deviated on the green dashed path, in order to avoid the detected obstacle.

station D1 to the template B5: the final, smooth, Dubins path is represented as a light red line, the initial waypoints $(p_s, p_1, p_2, p_3, p_4, p_5, p_f)$ are represented as empty red circles, the refined waypoints $(p_s, p_1, p_3, p_4, p_f)$ are shown as full red circles.

During the UUV's navigation, a moving obstacle (a vehicle which is returning to the docking station from the template B3) is detected in proximity of the B2 template. Since the CPA is too close to the UUV, the path is replanned as shown in Figure 7, applying the rules defined in Table II. This produces the new starting and final points of the replanned segments (respectively $P_{r,s}$ and $P_{r,f}$) and the intermediate initial and refined points as shown in the same figure as empty or full red circles. The replanned path smootly reconverges to the initial one (respectively the green and light red paths in Figure 7).

VIII. Conclusions

This paper presented a novel 3D dynamic path-planning system for Unmanned Underwater Vehicles (UUVs), where the term referred, in this paper, to a generic underactuated UUV with extended autonomy characteristics, intervention and docking ability, the latter giving permanent hovering possibilities. The proposed system was able to plan an initial, smooth, and flyable path on long distance and on a realistic scenario depicting a Subsea Production Systems (SPS) field layout.

The geometrical construction of the path and the process of replanning were presented. Moreover, a novel set of rules which helps to resolve collision-risk cases was proposed.

When encountering the moving obstacle, the replanning procedure was modified in order to exclude the possible replanning segments that were not compatible with the new set of safety rules. The replanning time has been consistently lower than $2.5s$ in every simulated replanning scenario, making the path replanning system a good candidate for future testing with full-scale, real-time applications.

Acknowledgments

This work has been carried out at the NTNU Centre for Autonomous Marine Operations and Systems (NTNU AMOS). The Norwegian Research Council is acknowledged as the main sponsor of AMOS through the Centres of Excellence funding scheme (project n.223254). The second and third authors were funded by the project Next Generation Subsea Inspection, Maintenance and Repair Operations (NextGenIMR), 234108. The first author would like to thank the PhD candidate Filippo Frontini for the help with Rhino modeling of the 3D models.

References

[1] Åsgard SPS. http://goo.gl/jDnum7. Accessed: 1-8-2016.

[2] A.J. Sørensen and M. Ludvigsen. Towards Integrated Autonomous Underwater Operations. *IFAC Workshop on Navigation, Guidance and Control of Underwater Vehicles.*, December 2015.

[3] M. Vagia, A.A. Transeth, and S.A. Fjerdingen. A literature review on the levels of automation during the years. What are the different taxonomies that have been proposed? *Applied ergonomics*, pages 190–202, 2016.

[4] G. Meinecke, V. Ratmeyer, and J. Renken. HYBRID-ROV - Development of a new underwater vehicle for high-risk areas. In *OCEANS'11 MTS/IEEE KONA*, pages 1–6, Sept 2011.

[5] A.D. Bowen, D.R. Yoerger, C. Taylor, R. McCabe, J. Howland, D. Gomez-Ibanez, J.C. Kinsey, M. Heintz, G. McDonald, D.B. Peters, B. Fletcher, C. Young, J. Buescher, L.L. Whitcomb, S.C. Martin, S.E. Webster, and M.V. Jakuba. The Nereus hybrid underwater robotic vehicle for global ocean science operations to 11,000m depth. In *OCEANS 2008*, pages 1–10, Sept 2008.

[6] Hydroid. Underwater mobile docking of autonomous underwater vehicles. *2012 Oceans*, pages 1–15, Oct 2012.

[7] A. Sans-Muntadas, E.F. Brekke, Ø. Hegrenaes, and K.Y. Pettersen. Navigation and Probability Assessment for Successful AUV Docking Using USBL. *10th IFAC Conference on Manoeuvring and Control of Marine Craft MCMC 2015*, 48(16):204 – 209, 2015.

[8] R.S. McEwen, B.W. Hobson, L. McBride, and J.G. Bellingham. Docking Control System for a 54-cm-Diameter (21-in) AUV. *IEEE Journal of Oceanic Engineering*, 33(4):550–562, Oct 2008.

[9] H. Singh, J.G. Bellingham, F. Hover, S. Lemer, B.A. Moran, K. von der Heydt, and D. Yoerger. Docking for an autonomous ocean sampling network. *IEEE Journal of Oceanic Engineering*, 26(4):498–514, 2001.

[10] J. Hegde, I.B. Utne, and I. Schjølberg. Applicability of Current Remotely Operated Vehicle Standards and Guidelines to Autonomous Subsea IMR Operations. In *ASME 2015 34th International Conference on Ocean, Offshore and Arctic Engineering*, volume 7, Jun 2015.

[11] J. Hegde, I.B. Utne, I. Schjølberg, and B. Thorkildsen. Application of fuzzy logic for safe autonomous subsea imr operations. *Safety and Reliability of Complex Engineered Systems*, Sep. 2015.

[12] Z. Zeng, L. Liana, K. Sammut, F. He, Y. Tang, and A. Lammas. A survey on path planning for persistent autonomy of autonomous underwater vehicles. *Ocean Engineering*, 110(A):303–313, 2015.

[13] S.M. LaValle. *Planning Algorithms*. Cambridge University Press, New York, NY, USA, 2006.

[14] A. Tsourdos, B. White, and M. Shanmugavel. *Cooperative Path Planning of Unmanned Aerial Vehicles*. Wiley, November 2010.

[15] A. Caiti. *Encyclopedia of Systems and Control*, chapter Motion Planning for Marine Control Systems, pages 1–6. Springer, 2014.

[16] G. Antonelli, S. Chiaverini, R. Finotello, and R. Schiavon. Real-time path planning and obstacle avoidance for RAIS: an autonomous underwater vehicle. *IEEE Journal of Oceanic Engineering*, 26(2):216–227, Apr 2001.

[17] M. Candeloro, A.M. Lekkas, A.J. Sørensen, and T.I. Fossen. Continuous Curvature Path Planning Using Voronoi Diagrams and Fermat's Spirals. *9th IFAC Conference on Control Applications in Marine Systems*, 9(1):132–137, 2013.

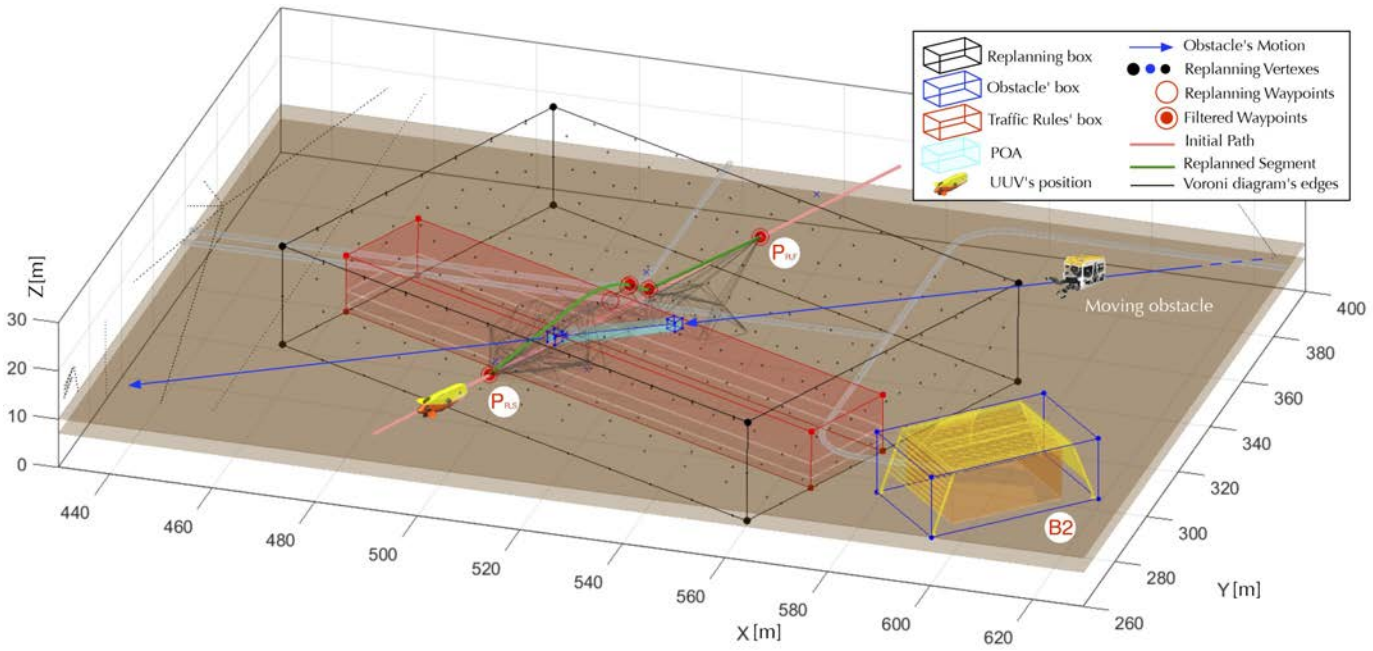

Figure 7: Simulation case of the replanning system. The UUV detects a vehicle returning from the template B3 (not represented in figure) and heading to a docking station. In order to avoid the collision, it replans the path producing the green segment, which overcome the obstacle by increasing the altitude of the vehicle, as dictated by the related traffic rule. The elements in the figure are explained in Figure 6. Black semi-transparents lines represent the Voronoi edges which generated the path. Starting and filtered waypoints are also represented.

[18] M. Candeloro, A.M. Lekkas, and A.J. Sørensen. A Voronoi-Diagram-Based, Dynamic Path-Planning System for Marine Underactuated Vessels. *Submitted to Control Engineering Practice*, 2016.

[19] J.S. Bellingham, M. Tillerson, M. Alighanbari, and J.P. How. Cooperative path planning for multiple UAVs in dynamic and uncertain environments. *Decision and Control, 2002, Proceedings of the 41st IEEE Conference on*, 3:2816–2822 vol.3, Dec 2002.

[20] I.R. Goralski and C.M. Gold. Maintaining the Spatial Relationships of Marine Vessels Using the Kinetic Voronoi Diagram. *Voronoi Diagrams in Science and Engineering, 2007. ISVD '07. 4th International Symposium on*, pages 84–90, July 2007.

[21] L.E. Dubins. On Curves of Minimal Length with a Constraint on Average Curvature, and with Prescribed Initial and Terminal Positions and Tangents. *American Journal of Mathematics*, 79(3):497–516, 1957.

[22] J.K. Kuchar and A.C. Drumm. The Traffic Alert and Collision Avoidance System (TCAS). *MIT Lincoln Laboratory Journal*, 16(2), 2007.

[23] International Maritime Organization. The International Regulations for Preventing Collisions at Sea. http://www.imo.org/en/About/Conventions/ListOfConventions/Pages/COLREG.aspx, July 1977.

[24] Gullfaks. http://goo.gl/FGPmDP. Accessed: 1-8-2016.

[25] Battelle UUV Docking and Replenishment Station (UDRS). http://goo.gl/GRrS7i. Accessed: 1-8-2016.

[26] Woods Hole Oceanographic Institution. Seafloor Docking Project. http://goo.gl/IoFSPi, 2012. Accessed: 1-8-2016.

[27] R.M. Ramberg, S.R.H. Davies, H. Rognoe, and O. Oekland. Steps to the Subsea Factory. In *Offshore Technology Conference*, Oct 2013.

[28] Eelume. http://eelume.com/. Accessed: 1-8-2016.

[29] P. Hedne. Subsea processing and transportation of hydrocarbons. http://goo.gl/j1AH8Q. Accessed: 1-8-2016.

[30] Statoil. The subsea factory. http://goo.gl/2PE5ms. Accessed: 1-8-2016.

[31] F. Aurenhammer. Voronoi diagrams - a survey of a fundamental geometric data structure. *ACM Computing Surveys*, 3:345–404, 1991.

[32] H. Ledoux. Computing the 3D Voronoi Diagram Robustly: An Easy Explanation. In *Voronoi Diagrams in Science and Engineering, 2007. ISVD '07. 4th International Symposium on*, pages 117–129, July 2007.

[33] K.Q. Brown. Voronoi diagrams from convex hulls. *Information Processing Letters*, 9(5):223 – 228, 1979.

[34] C.B. Barber, D.P. Dobkin, and H. Huhdanpaa. The Quickhull Algorithm for Convex Hulls. *ACM Trans. Math. Softw.*, 22(4):469–483, 1996.

[35] J.Y. Yen. An algorithm for finding shortest routes from all source nodes to a given destination in general networks. *Quarterly of Applied Mathematics*, 27:526530, 1970.

[36] E.W. Dijkstra. A note on two problems in connexion with graphs. *Numerische Mathematik*, 1:269–271, 1959.

[37] H.J. Sussmann. Shortest 3-dimensional paths with a prescribed curvature bound. In *Decision and Control, 1995., Proceedings of the 34th IEEE Conference on*, volume 4, pages 3306–3312 vol.4, Dec 1995.

[38] G. Ambrosino, M. Ariola, U. Ciniglio, F. Corraro, A. Pironti, and M. Virgilio. Algorithms for 3D UAV Path Generation and Tracking. In *Proceedings of the 45th IEEE Conference on Decision and Control*, pages 5275–5280, Dec 2006.

[39] K. Yang and S. Sukkarieh. 3D smooth path planning for a UAV in cluttered natural environments. In *2008 IEEE/RSJ International Conference on Intelligent Robots and Systems*, pages 794–800, 2008.

[40] G. Ambrosino, M. Ariola, U. Ciniglio, F. Corraro, E. De Lellis, and A. Pironti. Path Generation and Tracking in 3-D for UAVs. *IEEE Transactions on Control Systems Technology*, 17(4):980–988, July 2009.

[41] S. Hota and D. Ghose. Optimal geometrical path in 3d with curvature constraint. In *Intelligent Robots and Systems (IROS), 2010 IEEE/RSJ International Conference on*, pages 113–118, Oct 2010.

[42] Y. Lin and S. Saripalli. Path planning using 3D Dubins Curve for Unmanned Aerial Vehicles. In *Unmanned Aircraft Systems (ICUAS), 2014 International Conference on*, pages 296–304, May 2014.

[43] US Department of Transportation and Fedreal Aviation Administration. Introduction to TCAS II, Version 7.1. http://goo.gl/nnkmQn, 2011. Accessed: 1-8-2016.

[44] Y. Kuwata, M. T. Wolf, D. Zarzhitsky, and T. L. Huntsberger. Safe maritime autonomous navigation with colregs, using velocity obstacles. *IEEE Journal of Oceanic Engineering*, 39(1):110–119, Jan 2014.

[45] J. Larson, M. Bruch, and J. Ebken. Autonomous navigation and obstacle avoidance for unmanned surface vehicles. *Society of Photo-Optical Instrumentation Engineers (SPIE) Conference Series*, 6230:623007, 2006.

Article K

Glowing in the dark: discriminating patterns of bioluminescence from different taxa during the Arctic polar night

G. Johnsen, **M. Candeloro**, J. Berge and M. Moline

The article has been published in the journal
Polar Biology,
Volume 37 (5), pages 707–713. March 2014.

Polar Biol
DOI 10.1007/s00300-014-1471-4

ORIGINAL PAPER

Glowing in the dark: discriminating patterns of bioluminescence from different taxa during the Arctic polar night

Geir Johnsen · Mauro Candeloro · Jørgen Berge · Mark Moline

Received: 5 May 2013 / Revised: 19 February 2014 / Accepted: 20 February 2014

Abstract Research since 2009 has shown that despite almost total darkness during the Arctic polar night, there is much more biological activity than previously assumed, both at the sea surface, water column and sea floor. Here, we describe in situ monitoring of the bioluminescent fraction of the zooplankton community (dinoflagellates, copepods, krill and ctenophores) as a function of time and space. In order to examine the relative contribution of each selected taxon and any diurnal patterns in the relative signals, a time series platform capable of detecting in situ bioluminescent flashes was established in Kongsfjord, Svalbard, during the polar night in January 2013. Combined with laboratory-controlled measurements of animals collected next to the time series platform, we present both taxon-specific and community characteristics of the bioluminescence signal from a location at 79°N and from the middle of the polar night. Based on this 51-h time series, we conclude that the bioluminescent fraction of the zooplankton does not maintain a diurnal signal. Rather, the frequency of bioluminescence flashes from the entire bioluminescent community remained steady throughout the sampling period. Furthermore, we conclude that bioluminescence flash kinetic characteristics have a strong potential for in situ taxa recognition of zooplankton.

Keywords Arctic · Polar night · Marine zooplankton · Bioluminescence · Copepods · Krill · Ctenophores

This article belongs to the special PolarNight issue, coordinated by Ole Jørgen Lønne.

G. Johnsen (✉)
Applied Underwater Robotics Laboratory, Department of Biology, Norwegian University of Technology and Science (NTNU), Trondheim, Norway
e-mail: geir.johnsen@ntnu.no

G. Johnsen · J. Berge
Department of Arctic Biology, University Centre on Svalbard (UNIS), Longyearbyen, Norway

M. Candeloro
Applied Underwater Robotics Laboratory, Department of Marine Technology, Norwegian University of Technology and Science (NTNU), Trondheim, Norway

J. Berge
Faculty of Biosciences, Fisheries and Economy, Institute of Arctic and Marine Biology, University of Tromsø, Tromsø, Norway

M. Moline
School of Marine Science and Policy, University of Delaware, Newark, DE, USA

Introduction

During the last few decades, there has been a consistent and strong reduction in the sea ice extent in the Arctic Ocean (Sakshaug et al. 2009; Polyak et al. 2010). For its unique ecosystem, the sea ice is an important habitat for more than one thousand species of algae and invertebrates that have been recorded living in or on the underside of the ice, as well as the marine mammals and seabirds that find their main food there (Bluhm et al. 2011). In addition, the sea ice acts as a key regulator for important processes such as light penetration, water mass formation and temperature regulation. Hence, the Arctic sea ice extent and thickness is a "canary in the coal mine" with respect to global climate change in the high north (Polyak et al. 2010). Today we see an expanding activity and international interest in the marine environment in the Arctic with respect to natural resources such as oil, gas, minerals and fisheries. New

Published online: 07 March 2014

activities and sea-transport routes require new knowledge about ecosystem structure and dynamics for sound management and decision making (Sakshaug et al. 2009; Wang and Overland 2009; Hirche and Kosobokova 2011).

There has been a common assumption from the governmental authorities, nature management and the scientific community that during the polar night, there is low biological activity and biomass at all trophic levels throughout the water column and on the sea floor. Lately, however, the use of new underwater technology such as autonomous underwater vehicles (AUVs) and optical sensors have proven to be important for elucidating life and environmental conditions during the polar night (Berge et al. 2009, 2012; Båtnes et al. 2013). Also, we now know that several species of seabirds (Brünnichs guillemot, black guillemot, kittiwake, fulmar, little auk and glaucous gull) are overwintering in Arctic fjords (Weslawski et al. 1991; Berge et al. 2012, own observations) and actively feeding in the upper water column. Their prey comprises of different species of zooplankton (copepods, amphipods, ctenophores, krill) and fish (e.g., polar cod) indicating key trophic linkages persist at these locations.

This study focuses on the bioluminescent fraction of the zooplankton, which may be an important cue for visual predators such as seabirds and fish in their pursuit of prey. Bioluminescence (BL, light generated from an living organism measured as photons s^{-1}) is a characteristic feature of all the world's oceans, but has been documented to be of special importance in the abyssal zone (Haddock et al. 2010; Moline et al. 2013). In the Arctic, however, during the darkest part of the polar night at 79°N, a distinct and diurnal pattern of depth-dependent bioluminescence associated with zooplankton (diurnal vertical migration, DVM) has been demonstrated to be of particular importance in the upper 50 m of the water column (Berge et al. 2012). In order to investigate which species are actively bioluminescent during the polar night, a high-resolution in situ measurement platform as deployed over a 51-h period in order to measure and count the number of bioluminescence flashes in Kongsfjord, Svalbard, in mid January 2013. Correspondingly, bioluminescent organisms were sampled next to the platform for species-specific bioluminescence characteristics. Documented BL characteristics include maximum, average intensity, duration time until maximum of bioluminescence and BL cumulative sum was reached (see definitions, symbols and units in Table 1). Sampled specimens and bioluminescent taxa were immediately examined in a shipboard aquarium under subdued light. The species-specific bioluminescence characteristics, examined under controlled conditions in the laboratory on board, were related to the in situ measurements and used as an aid to positively identify the species responsible for the in situ bioluminescence.

Table 1 BL kinetic parameters used to discriminate between taxa

Parameter	Explanation	Unit
BL_{max}	Maximum intensity of BL	$\times 10^9$ photons s^{-1}
BL_{mean}	Average BL intensity	$\times 10^9$ photons s^{-1}
Σ_{max}	Cumulative sum of $BL_{0\ \%}$ until BL_{max}	$\times 10^9$ photons s^{-1}
T_{max}	Time to reach maximum BL	s
T_{high}	High intensity duration, BL20 % rise and 20 % decay	s
T_{decay}	Time from $BL_{20\ \%}$ decay to $BL_{0\ \%}$	s

The parameters are based on 60 Hz bioluminescence curve kinetics

Materials and methods

Instrumentation

The bathyphotometer (UBAT, Wet Labs, USA) consist of a water inlet and outlet using an impeller to pump the water into a detection chamber equipped with a photon multiplier tube (PMT) counting bioluminescence as photons s^{-1} after calibration according to Herren et al. (2005). The UBAT flow rate was 0.373 L s^{-1}. The impeller in the detection chamber of the bathyphotometer was used to induce bioluminescence. The controller software (BLINC, Wet Labs) was used as graphic user interface and for control of instrument (inserting calibration coefficient, pump RPM, flow RPM, PMT input/output voltage and raw counts).

The software was used to schedule BL recording times, i.e., schedule for repeating samples and sample length adjusting for battery power needed for 51-h TS at in situ temperatures.

The bathyphotometer provides the measurements as raw 1–60 A/D counts per second that were converted to bioluminescence values (BL, photons s^{-1}) after correction of instrument-specific photomultiplier tube (PMT) calibration coefficient provided by Wet Labs. The BP utilizes an impeller to continuously draw a measured volume of water into a chamber where bioluminescence was measured by the PMT at 60 Hz (see Herren et al. 2005; Berge et al. 2012; Moline et al. 2013 for details). The PMT calibration coefficient was different depending on gain setting.

Taxa-specific bioluminescence: laboratory experiments

The UBAT was used for detecting and characterizing the flash kinetics on living specimens in a laboratory aquarium on board the R/V *Helmer Hanssen* (University of Tromsø) January 9–21, 2013. The UBAT was connected to the DH4 data handler, logger and power unit (both Wet Labs) with baud rate PC-DH4 set to 115 kHz using the DH4 software. The DH4 was powered with 12 V (input power 12–15 V)

and a power cord connection with 12 V was connected from DH4 to UBAT.

In situ collection of zooplankton for onboard laboratory BL work was performed using WP2 zooplankton net (180 µm, 0.25 m^2 opening) and Mik-net (1,000 µm, 3 m^2 opening) close to the UBAT time series station (in situ temperature ranging from 0.54 to 0.89 °C and salinity 34.62–34.64 (recorded at 1 Hz).

Taxa (still in suspension in net flask) were immediately separated into polyethylene trays and stored in pre-filtered saltwater in a dark cooling room at 2–4 °C before transferred to 50 L aquarium filled with pre-filtered (180 µm) seawater (25 L of pre-washed polyethylene tanks) at in situ temperature. Prior to each specimen examined for BL, new and fresh, pre-filtered seawater at in situ temperature was used. A pre-washed bathyphotometer was submerged into the aquarium and examined species for species.

The bathyphotometer settings were the same for all species. Living specimens were gently put into the aquarium in front of the inlet of the bathyphotometer. The time for each species reaching the detector was noted to relate bioluminescence signal to number and bioluminescence characteristics of specimens. For each species, new and pre-filtered (in situ temperature) saltwater was put into the aquarium prior to experiments. Filtered seawater gave a BL_{max} (maximum intensity of BL) of 0–2 × 10^6 photons s^{-1}, indicating BL background signal of in the underwater bathyphotometer (UBAT). For each taxon, the following characteristics according to Table 1 was measured (Figs. 1, 2).

In situ measurements of bioluminescence

An underwater platform consisting of the UBAT and a SBE 49 Fastcat CTD (temperature, salinity and depth, Seabird Electronics, Washington, USA) were deployed 20 m below surface at a location in Kongsfjorden, Svalbard, with a bottom depth of 300 m. The platform was deployed January 15–17, 2013, over a total of 51 h of BL measurements (Figs. 3, 4, 5). The DH4 was used to control the sampling protocol; a programmed warm-up (10 s), a meter flush (20 s), a sampling period of 5 min, with an interval between samples of 10 min, and a low voltage cutoff of 10 V. During the last period of time series, we needed to reduce sampling period and raised the interval between samples to save battery power ensuring that the voltage did not drop below critical voltage (to avoid non-linear responses in BL measurements). For time series, all BL values are integrated per hour.

In order to assign the BL curves extracted from the time series data to specific taxa, the time series parameters were compared with the taxon-specific parameters (Table 2).

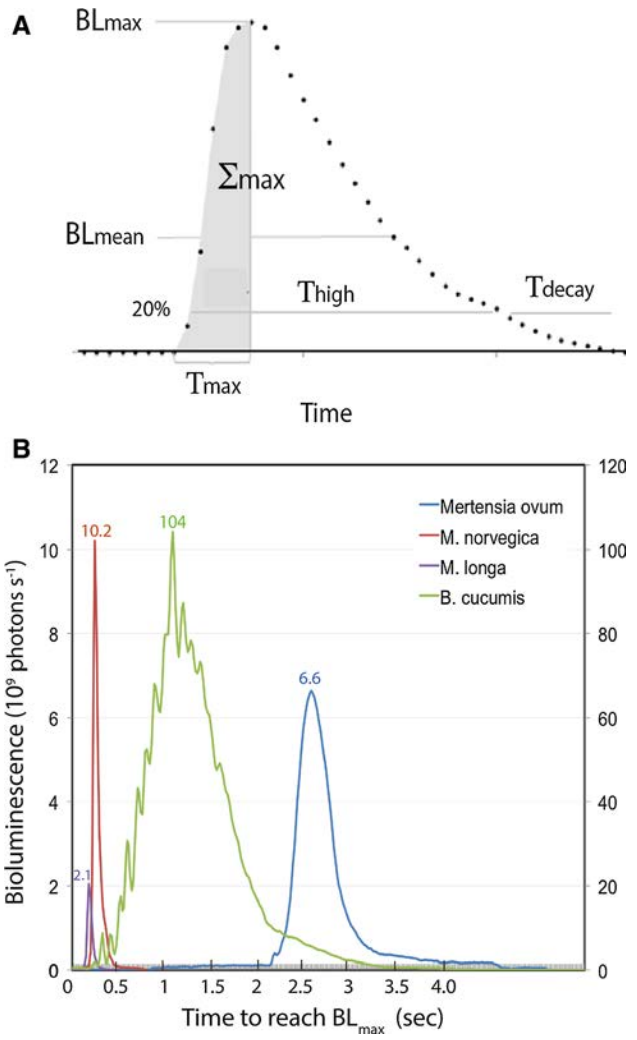

Fig. 1 Species-specific differences in bioluminescence characteristics. **a**. Graphic presentation of the bioluminescence parameters in Table 1: average BL intensity (BL_{mean}), maximum intensity of BL (BL_{max}), cumulative sum of $BL_{0\ \%}$ until BL_{max} (Σ_{max}), time to reach maximum BL (T_{max}), high intensity duration from 20 % of BL rise and decay level (T_{high}), and time from $BL_{20\ \%\ decay}$ to $BL_{0\ \%}$. Figure modified from Moline et al. (in press). **b**. Species-specific BL characteristics in *M. longa* (copepod), the ctenophores *M. ovum* and *B. cucumis*, and *M. norvegica* (krill). Note secondary Y axis for *B. cucumis* (10–50 X stronger BL intensity than the other species), the others species on primary Y axis. *Note* X axis include start to end of BL kinetics, numbers indicate BL max intensity

Taxa-specific BL kinetic signatures

In particular four parameters; maximum bioluminescence (BL_{max}), time to maximum bioluminescence (T_{max}), BL cumulative sum (Σ_{max}) and average bioluminescence (BL_{mean}) provided a BL kinetic signature that could be used to identify the species responsible (Figs. 1, 2; Table 1).

The first step was to automatically identify (see Eqs. 1–6) and store the BL kinetic signature of the taxa identified in situ

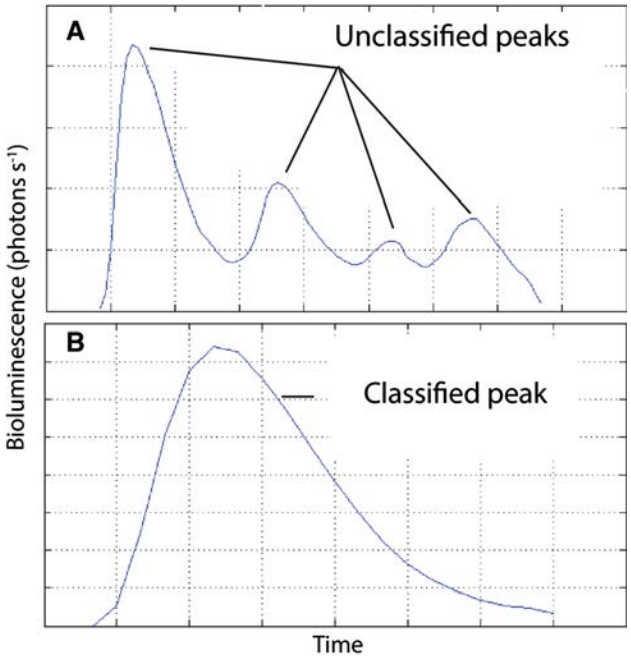

Fig. 2 Interpretation and recognizing in situ BL signatures. **a**. Indicates BL signature that is produced by more than one taxa (or several individuals of one taxa) shown by several peaks that cannot be recognized as a given taxa. **b** Represents a clear BL kinetic signature due to one taxa/specimen. The first signature (**a**) is manually removed from the dataset, while the second one (**b**) is selected to be recognized to a given taxa

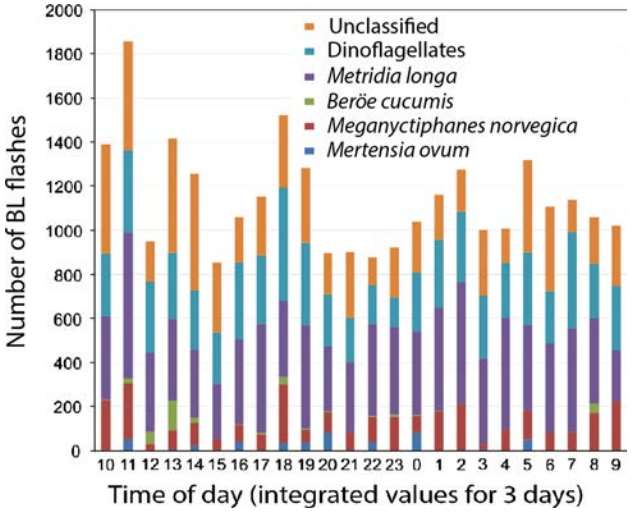

Fig. 3 Polar night time series of total species-specific (recognized) BL flashes over 3 days at 20 m depth in Kongsfjorden, Spitsbergen, January 15–17, 2013

(Figs. 3, 4, 5). A manual and visual analysis has been done to eliminate those signatures that were clearly representative of more than one taxa, and therefore difficult to identify and classify (Fig. 2a, b). All the selected data are then further processed and identified. The eliminated data will still take part in the statistical analysis to provide information about the "unidentified data." The BL kinetic signatures in Fig. 2 has been calculated for all the peaks measured during the time series at 20 m depth (Figs. 3, 4) and compared with the species-specific BL characteristics (Fig. 1; Table 1 elucidated during the laboratory experiments (5 taxa, Table 2). By putting specimens of different taxa into the UBAT, one by one, we detected BL and non-BL zooplankton.

This comparison has been done calculating an error (Eq. 1) that represents an imaginary "distance" between each BL signature and the taxon-specific signatures from the laboratory experiments. The error, e_{taxa_i}, was calculated as a simple weighted average of the four BL parameters errors:

$$e_{\text{taxa}_i} = \frac{w_1 \cdot e_{\text{BL}_{\max},\text{taxa}_i} + w_2 \cdot e_{T_{\max},\text{taxa}_i} + w_3 \cdot e_{\Sigma_{\max},\text{taxa}_i} + w_4 \cdot e_{\text{BL}_{\text{mean}},\text{taxa}_i}}{w_1 + w_2 + w_3 + w_4} \quad (1)$$

where taxa_i is one of the 5 recognized taxa of interest (Fig. 1; Table 2), $w_{1,\ldots,}\ w_4$ are the weights of the four parameters errors $e_{\text{BL}_{\max},\text{taxa}_i}, e_{T_{\max},\text{taxa}_i}, e_{\Sigma_{\max},\text{taxa}_i}, e_{\text{BL}_{\text{mean}},\text{taxa}_i}$ defined as (note that the formula is the same for all the parameters):

$$e_{\text{BL}_{\max},\text{taxa}_i} = \frac{\left|\text{BL}_{\max}^{\text{in situ}} - \text{BL}_{\max}^{\text{lab, taxa}_i}\right|}{\left\|\text{BL}_{\max}^{\text{in situ}}, \text{BL}_{\max}^{\text{lab, taxa}_i}\right\|_{\infty}} \quad (2)$$

Equation 2 is the normalized error between the maximum bioluminescence ($\text{BL}_{\max}$) of the BL kinetic signature of the unknown taxa measured in situ and the parameter of the kinetic BL signature of the taxa measured in laboratory. In this, we considered each parameter to have the same importance (the same weight in Eq. 1), that means: $w_{1,}\ w_{2,}\ w_{3,}\ w_4 = 1$.

After using Eq. 1 (see rewriting of Eq. 1 in Eq. 3 below) together with Eq. 4 for all the 5 taxa (taxa_i; comprising dinoflagellates, the copepod *Metridia longa*, the ctenophores *Mertensia ovum* and *Beröe cucumis*, and the krill species *Meganyctiphanes norvegica*), we ended up with five error values for each taxa, each one of them will represent the error recognizing the in situ signature of a specific taxa. Rewriting Eq. 1, we will have (Eq. 3):

$$e_{\text{taxa}_i} = \frac{e_{\text{BL}_{\max},\text{taxa}_i} + e_{T_{\max},\text{taxa}_i} + e_{\Sigma_{\max},\text{taxa}_i} + e_{\text{BL}_{\text{mean}},\text{taxa}_i}}{4} \quad (3)$$

The taxa providing the minimum recognition value of a given taxa (taxa_i, Eq. 3) will then recognize the in situ signature as described by Eq. 4:

$$\text{taxa} = \text{taxa: } \min\left\{e_{Metridia},\ e_{\text{Beroe}},\ e_{\text{Dinoflagellates}},\ e_{Mertensia},\ e_{\text{krill}}\right\} \quad (4)$$

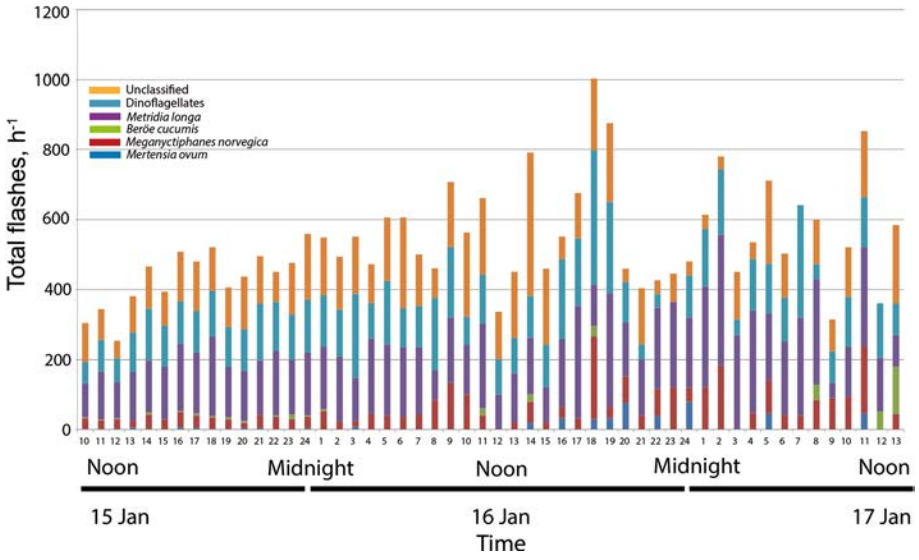

Fig. 4 Hourly (integrated values from 3 days) distribution of BL flashes and corresponding recognized fraction of species. From time series presented in Fig. 3

All unclassified flashes have deleted manually (using the approach shown in Fig. 2) from further analysis. The unrecognized BL signatures need further detailed experiments under controlled conditions, but is beyond the scope of this paper.

In the plot, the cumulative sum of BL related to the identified peaks has been integrated over the hours, divided between taxa and compared (Eqs. 5–6). Unclassified peaks have not been included in Fig. 5, but they will be considered in a further refinement to have a more complete overview about the total amount of light present in a certain hour.

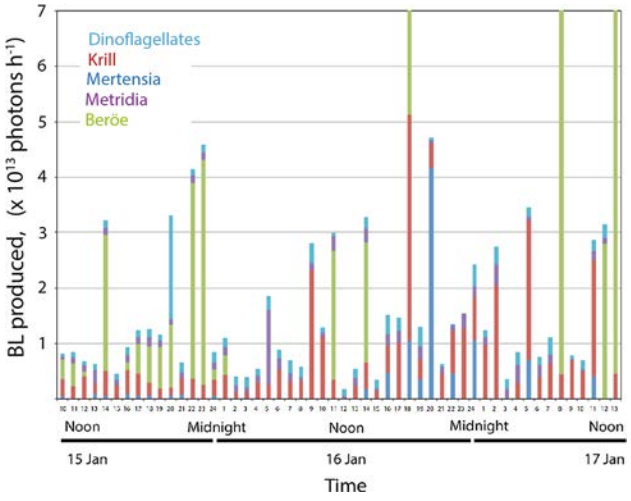

Fig. 5 Sum of measured bioluminescence produced by recognized taxa integrated in 1 h over 3 days (compare with number of flashes in Fig. 3). The total light emitted per recognized taxa indicates that highly bioluminescent species such as *B. cucumis* and the krill *M. norvegica*, despite being in low numbers relative to other BL taxa, may contribute significantly to the total bioluminescence produced in the water column during the polar night

The plotted data in Fig. 5 are the cumulative sum of the whole kinetic signature (from start to end of a BL flash curve defined in Fig. 1a) integrated over 1 h (Eqs. 5–6; Fig. 5):

$$\Sigma_{\mathrm{BL}} = \int_{t:\mathrm{StartKinSignature}}^{t:\mathrm{EndKinSignature}} (\mathrm{BL})\,\mathrm{d}t \tag{5}$$

$$\Sigma_{\mathrm{BL,integrated}} = \Sigma_{\mathrm{BL}} \cdot k_{\mathrm{hour}} \tag{6}$$

The integrating factor k_{hour} depends by the amount of sampled minutes over the hour, basically the integrating factor extrapolates the measured data per hour.

Results

Specific-specific characteristics in the laboratory

The four dominant bioluminescent taxa in the laboratory study included (with number of specimens in parentheses) *M. longa* (12), *M. ovum* (11), *B. cucumis* (5) and *Meganychtiphanes norvegica* (7), all of which were collected and identified from samples taken next to the in situ platform. All bioluminescent species (BL) gave $\mathrm{BL_{max}}$ ranging from 2 to 100 $\times$ 10^9 photons s^{-1}. Bioluminescence characteristics from monocultures of these were measured according to the following BL characteristics by means of BL maximum value, average value, maximum value time and rising time (see Fig. 1a; Table 2 for details).

Seven taxa were found to be non-bioluminescent in this study (number of individuals in parentheses): The pelagic amphipods *Themisto libellula* ($n = 14$) and *T. abyssorum*

Table 2 Bioluminescence kinetics of the four taxa producing BL in the laboratory using BL kinetic characteristic

BL groups ($\times 10^9$)	Unit	*M. longa*	*M. norvegica*	*M. ovum*	*B. cucumis*	Dinoflagellates
BL_{max}	$\times 10^9$ photons s^{-1}	2.05	10.2	6.64	104	0.32
BL_{mean}	$\times 10^9$ photons s^{-1}	0.25	0.9	0.66	15.5	1.59
Σ_{max}	$\times 10^9$ photons s^{-1}	3.82	19.5	84	1,870	8.39
T_{max}	s	0.20	0.27	2.63	1.12	0.051
T_{high}	s	0.11	0.12	0.65	1.38	nd
T_{decay}	s	0.25	0.48	2.25	3.65	nd

BL_{max}, maximum intensity of BL; BL_{mean}, average BL intensity; Σ_{max} cumulative sum of BL until maximum intensity is reached; T_{max}, time to reach maximum BL; T_{high}, high intensity duration, from 20 % rise and 20 % fall; and T_{decay}, from 20 % of max to 0 %. Values for dinoflagellates are taken from Moline et al. in press; nd, no data

($n = 8$), the arrow worms *Parasagitta elegans* ($n = 15$) and *Eukrohnia hamata* ($n = 15$), the calanoid copepod *Calanus glacialis* ($n > 100$), the krill *Thysanoessa* sp. ($n = 50$), and the pteropod *Clione limacina* (14).

These species gave a BL signal up to 3×10^6 photons s^{-1}, i.e., equivalent to the background signal of filtered water. In contrast, the BL_{max} values for the true bioluminescent taxa ranged from 2–10 $\times 10^9$ photons s^{-1}, 1,000 times the background signal.

Identification of in situ bioluminescence peaks

Based upon the taxon-specific bioluminescence characteristics (see Fig. 1; Table 2), five identified taxa were identified as active throughout the period. In total, more than 50 % of the peaks could unequivocally be assigned as being produced by *M. longa*, whereas dinoflagellates accounted for one-third of all identified peaks. The ctenophore *B. cucumis*, although numerically the least dominant, had a BL signal one order of magnitude stronger than any of the other taxa (Lapota et al. 1992a, b).

The total BL signal from the zooplankton community was measured in situ during a 51-h deployment of the bathyphotometer at 20 m depth (Figs. 2, 3, 5), covering three noon and two midnight periods. The variation in total number of measured peaks varied throughout the sampling period, no clear diurnal signal could be detected.

Discussion

A total of 2,981 BL flashes were detected during the 51-h time series. Two thousand seven hundred and fifteen different BL peaks were identified, based on the species-specific BL characteristics (see below) comprising *M. ovum* (20 flashes); *M. norvegica* (286 flashes), *B. cucumis* (30 flashes), *M. longa* (1,344 flashes) and dinoflagellates (1,031 flashes), see Fig. 2. During the second part of the deployment (January 16–17), at total of 266 were identified; *M. ovum* (10), *M. norvegica* (44), *B. cucumis* (6), *M. longa* (121) and dinoflagellates (81), Fig. 2. The latter group was identified by the bioluminescent characteristics of dinoflagellates (Table 1; Fig. 1).

Identification of biolum taxa based on the laboratory measurements

Time series of taxa-specific bioluminescent zooplankton was identified by means of the laboratory-based measurements of living specimens identified in Table 2. In situ BL zooplankton was dominated by *M. longa* with about 50 % of total bioluminescent flashes for both January 15–16 and 16–17, 2013. The second dominant BL group was the dinoflagellates with about 25–30 % of BL, followed by bioluminescent krill *M. norvegica*, and the two ctenophores *M. ovum* and *B. cucumis* (Table 3; Figs. 3, 4, 5). In contrast to other bioluminescent organism, *B. cucumis* gave green–yellow emission in contrast to the other BL species which gave a bright blue emission (seen by eye). All species gave a similar shape bioluminescent curves with smooth rise and decay characteristics, except for a jagged curve from *B. cucumis* (Fig. 1b). The jagged curvature was caused by

Table 3 Major bioluminescent taxa during TS measurements at 20 m depth in Kongsfjorden

Taxa	15–16 January specimens (% of total)[a]	16–17 January specimens (% of total)[b]
Dinoflagellates	1,031 (38)	81 (31)
Copepod (*M. longa*)	1,344 (49)	121 (46)
Krill (*M. norvegica*)	286 (11)	44 (17)
Ctenophore 1 (*M. ovum*)	20 (0.7)	10 (3.8)
Ctenophore 2 (*B. cucumis*)	30 (1.3)	6 (2.2)
Total specimens	2,711 (100)	262 (100)

[a] January 15–16, 2013, and [b] January 16–17, 2013. In situ temperature 0.54–0.89 °C

pulsating light through the bell-shaped animal giving varying BL_{max} through the measurements at 60 Hz (Fig. 1). Note that *B. cucumis* was virtually absent at 20 m depth at midnight, but could be quite numerous around noon (see noon day 3, Fig. 4). If total bioluminescence contribution is taken into consideration, highly BL taxa such as *B. cucumis* and *M. norvegica* may be a significant contributor to "light in the dark" (Fig. 5).

The bioluminescent fraction of the zooplankton community has previously been examined from the same site and at the same time of year, but using a different method deployed herein. Berge et al. (2012) reported on the bioluminescence measured by the same UBAT mounted on an AUV, concluding that bioluminescent dinoflagellates were conducting vertical migrations within the upper 30 m of the water column. Later, Moline et al. (in press) reanalyzed the same dataset and distinguished three main clusters of flashes, arguing that they represented three different groups of bioluminescent taxa. The BL flash kinetics from dinoflagellates (data from Kongsfjorden in January 2010) belongs the low-intensity BL_{max} group called G1 (Lapota et al. 1992a, b) which was the largest BL group recorded in these waters during polar night. Two other BL groups were recorded (BL group G2 and G3) in Moline et al. (in press), but these groups were not identified. In Table 3, BL_{max} indicates that *B. cucumis* can be put into BL G3, and the rest in BL group G2. However, Moline et al. (in press) also identified two other clusters, named group 1 and 2, respectively. Based on the laboratory-controlled bioluminescence characteristics of four other taxa defined herein (Table 2), we conclude that the group 3 in Moline et al. (in press) most likely represent *B. cucumis*. Especially the BL_{max} and BL_{mean} correspond with those herein described as characteristic of this large and common ctenophore (Majaneva et al. 2013). The second group (Group 2), however, does not unequivocally correspond to any of the four taxa characterized in Table 2, although the high Σ_{max} might indicate that this group is also a ctenophore—the smaller but more numerous *M. ovum*

In conclusion, we argue that the flash kinetics of bioluminescent zooplankton is a useful and easy way of characterizing zooplankton communities, particularly so at high latitudes during the otherwise challenging winter conditions. In general, bioluminescence of arctic zooplankton is in itself a poorly studied topic, one that may provide new and vital information concerning both ecological interactions and physical forcing of biological processes during the arctic winter. Specifically, our study demonstrates that the bioluminescence flash kinetics of arctic zooplankton has clear species-specific characteristics that allow for in situ identification of species.

Acknowledgments The work is part of the two NFR projects Circa (Project Number 214271/F20) and Marine Night (Project Number 226417/E10). Furthermore, the work was supported by the CoE AMOS at NTNU (NFR 223254). Thanks are given two three anonymous reviewers for constructive comments.

References

Båtnes AS, Miljeteig C, Berge J, Greenacre M, Johnsen G (2013) Quantifying the light sensitivity of *Calanus* spp. during the polar night: potential for orchestrated migrations conducted by ambient light from the sun, moon, or aurora borealis? Polar Biol DOI 10.1007/s00300-013-1415-4, Electronic supplementary material doi:10.1007/s00300-013-1415-4

Berge J, Cottier F, Last K, Varpe Ø, Leu E, Søreide J, Eiane K, Falk-Petersen S, Willis K, Nygård H, Voegedes D, Griffiths C, Johnsen G, Lorenzen D, Brierley AS (2009) A diel vertical migration of Arctic zooplankton during the polar night. Biol Lett. doi:10.1098/rsbl.2008.0484

Berge J, Båtnes AS, Johnsen G, Blackwell SM, Moline MA (2012) Bioluminescence in the high Arctic during the polar night. Mar Biol 159:231–237. doi:10.1007/s00227-011-1798-0

Bluhm BA, Gebruk AV, Gradinger R, Hopcroft RR (2011) Arctic marine biodiversity: an update of species richness and examples of biodiversity change. Oceanography 24:232–248

Haddock SHD, Moline MA, Case JF (2010) Bioluminescence in the sea. Annu Rev Mar Sci 2:443–493

Herren CM, Haddock SHD, Johnson C, Moline MA, Case JF (2005) A multi-platform bathyphotometer for fine-scale, coastal bioluminescence research. Limnol Oceanogr Methods 3:247–262

Hirche HJ, Kosobokova KN (2011) Winter studies on zooplankton in Arctic seas: the Storfjord (Svalbard) and adjacent ice-covered Barents Sea. Mar Biol 158:2359–2376

Lapota D, Rosenberger DE, Lieberman SH (1992a) Planktonic bioluminescence in the pack ice and the marginal ice zone of the Beaufort Sea. Mar Biol 112:665–675

Lapota D, Young D, Bernstein S, Geiger M, Huddell HDL, Case JF (1992b) Diel bioluminescence in heterotrophic and photosynthetic marine dinoflagellates in an Arctic fjord. J Mar Biol Assoc UK 72:733–744

Majaneva S, Berge J, Renaud PE, Vader A, Stübner E, Rao AM et al (2013) Aggregations of predators and prey affect predation impact of the Arctic ctenophore *Mertensia ovum*. Mar Ecol Progr Ser 476:87–100. doi:10.3354/meps10143

Moline MA, Oliver MJ, Orrico C, Zaneveld R (2013) Bioluminescence in the sea. In: Watson J, Zielinski O (eds) Subsea optics and imaging, Chapter 7. Woodhead Publishing Ltd., Cambridge, pp 134–170 608 pp

Moline MA, Berge J, Johnsen G, Båtnes A, Blackwell S (in press) Bioluminescence flash kinetics characterize pelagic community structure. J Plankton Res

Polyak L, Alley RB, Andrews JT, Brigham-Grette J, Cronin TM et al (2010) History of sea ice in the Arctic. Quat Sci Rev 29:1757–1778. doi:10.1016/j.quascirev.2010.02.010

Sakshaug E, Johnsen G, Kovacs K (2009) Ecosystem Barents Sea. Tapir Academic Press, Trondheim 587 pp

Wang M, Overland J (2009) A sea ice free summer Arctic within 30 years. Geophys Res Lett 36:L07502. doi:10.1029/2009GL037820

Weslawski JM, Kwasniewski S, Wiktor J (1991) Winter in a Svalbard fjord ecosystem. Arctic 44:115–123

Article L

Underwater vehicles for environmental management in coastal areas

M. Ludvigsen, T. Thorsnes, R.E. Hansen, A.J. Sørensen, G. Johnsen, P.A. Lågstad, Ø. Ødegård, **M. Candeloro**, S.M. Nornes, C. Malmquist

The article has been published in the proceedings of the
MTS/IEEE OCEANS 2015.
Genova, Italy, 18-21 May 2015.

Underwater vehicles for environmental management in coastal areas

Martin Ludvigsen
Centre for Autonomous Marine Operations and Systems (AMOS) Norwegian University of Science and Technology (NTNU), 7491 Trondheim, Norway.
martin.ludvigsen@ntnu.no

Terje Thorsnes, Geological Survey of Norway (NGU)
P.O. box 6315 Sluppen NO-7491 Trondheim
Norway

Roy E. Hansen, Norwegian Defence Research Establishment (FFI), P O Box 25, NO-2027 Kjeller, Norway

Asgeir J. Sørensen, Norwegian University of Science and Technology (NTNU), Centre for Autonomous Marine Operations and Systems (AMOS) 7491 Trondheim, Norway

Geir Johnsen, Norwegian University of Science and Technology (NTNU), 7491 Trondheim, Centre for Autonomous Marine Operations and Systems (AMOS) Norway

Petter A. Lågstad, Norwegian Defence Research Establishment (FFI), P O Box 25, NO-2027 Kjeller, Norway

Øyvind Ødegård, Norwegian University of Science and Technology (NTNU), 7491 Trondheim, Centre for Autonomous Marine Operations and Systems (AMOS) Norway

Mauro Candeloro, Norwegian University of Science and Technology (NTNU), 7491 Trondheim, Centre for Autonomous Marine Operations and Systems (AMOS) Norway

Stein M. Nornes, Norwegian University of Science and Technology (NTNU), 7491 Trondheim, Centre for Autonomous Marine Operations and Systems (AMOS) Norway

Christian Malmquist, Norwegian University of Science and Technology (NTNU), 7491 Trondheim, Norway

***Abstract* — Methods for using underwater vehicles for mapping and monitoring are developed continuously. These methods developed must be accurate, quantitative and repeatable while being as cost effective as possible. In 2011, 2012, 2013 and 2014 The Norwegian University of Science and Technology (NTNU) Applied Underwater Robotics Laboratory completed surveys in the Trondheim Fjord area. During these surveys methods relevant for addressing several of these challenges have been tested. We have tested Synthetic Aperture Sonar for establishing baselines for marine habitats and littering. In the sonar data cold-water coral habitats gave a significant signal. These observations were confirmed by video and hyperspectral imaging. We have also revisited the same areas and demonstrated the potential to detect changes. During our campaigns the sonar data has also been verified by ROV video and sampling. A dumping area in the fjord was mapped by the AUV mounted SAS and on a subsequent cruise the ROV was deployed for video survey, stereo photos and sediment sampling. Stereo models may prove an important tool where millimeter resolution and precision is attainable. Based on the experimental work presented in this paper, a proposal for underwater vehicles in environmental management of coastal areas is described.**

Keywords—ROV, AUV, Sonar, Photogrammetry

I. Introduction

Autonomous Underwater Vehicles (AUVs) has over the last 15 years evolved from experimental technology to commercially available systems, and some vendors and models have established substantial track records. But there is still a considerable potential for enhancing mapping and monitoring efficiency by increasing the use of underwater vehicles and autonomy in science and management. In this work we consider environmental management mapping and monitoring of the marine coastal environment and its development in terms like biological abundance, diversity, behaviour, industrial pollution, marine traffic, construction work, and global warming to make sustainable decisions for the community. NTNU has through the Applied Underwater Robotics Laboratory (AUR-Lab) developed technology for underwater vehicles and led several operations, both for engineering trials and scientific cruises. This paper discusses results from selected operations and how experiences gained can be used in environmental management.

The knowledge of the world beneath the surface can be considered limited compared to the terrestrial counterparts in

978-1-4799-8736-8/15/$31.00 ©2015 IEEE

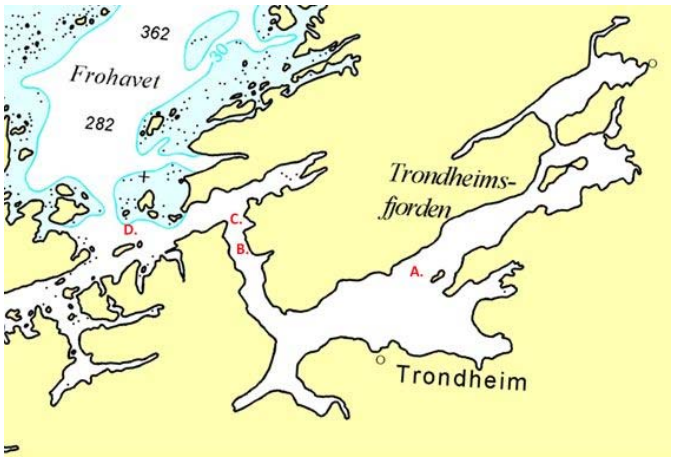

Fig. 1 Map showing the location discussed. A is the Tautra ridge, B is the Agdenes dumping field, C is the Agdenes threshold and D is the Nord Leksa site.

the coastal zone. It is more demanding to collect data in the underwater environment – many of the terrestrial techniques do not work underwater. The human footprint is ever increasing requiring continuous awareness of the conditions and development. Improved knowledge of the seabed and the water column can be considered profitable for the society, [1], [2].

In efficient management, the decisions are based on data and information. These data will be of high interest for many individual user groups, also outside the management. The technology for underwater mapping and monitoring is evolving continuously, increasing the possible knowledge of the sea and the coast, also for management.

In the described operations AUV and Remotely Operated Vehicle (ROV) surveys have been performed both for mapping and exploration for new objects and for monitoring of areas with known occurrences. In addition to high resolution seabed mapping, underwater vehicles can be used for collecting water

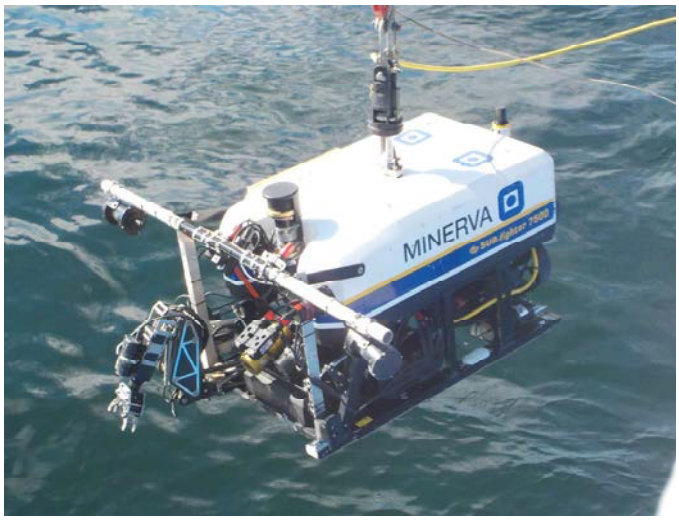

Fig. 2 ROV Minerva.is an observation ROV.

Fig. 3 The Hugin HUS AUV launch off the aft of RV Gunnerus.

column data such as temperature, salinity, current, cDOM (coloured Dissolved Organic Matter) and chlorophyll. The water column is dynamic and the measurement process becomes a trade of between temporal and spatial resolution, and vehicle and instrument capacity in terms of speed and range. An example is given in [3] where oxygen concentration is tracked in a dynamic environment. The seabed has lower dynamics and in this context many of them can be considered static, however Change Detection (CD) research using sonar images shows that also the seabed changes over time, [4].

A proposal using underwater vehicles in environmental management in coastal areas based on our experimental work is the contribution of this paper. NTNU AUR-Lab has used AUV-mounted sonars to map several sites in the Trondheim fjord, and some areas have been mapped twice allowing comparative study for monitoring. ROV mounted Underwater Hyperspectral Imager (UHI), stereo camera and photogrammetry models have also been shown with good results proving higher resolution. Both methods concern high resolution seabed mapping. In environmental management these maps can be used to: classify seabed to detect habitat types [5], detect changes in sedimentation, detect manmade seabed objects and map macro fauna.

II. Method

Over the last 4 years AUR-Lab has arranged a series of AUV and ROV operations [6], [7]. During the scientific cruises, the vehicles have been employed for seabed characterization, mapping of associated habitats, anthropogenic objects and historical artefacts. The base for these operations has been the 31 meter long research vessel Gunnerus, owned and operated by NTNU. Equipped with a Dynamic Positioning (DP) system, an EM 3002 Multi Beam Echosounder (MBE) and a high end USBL system (the HiPAP 500, trademark of Kongsberg Maritime) it provides services usually offered by larger ships.

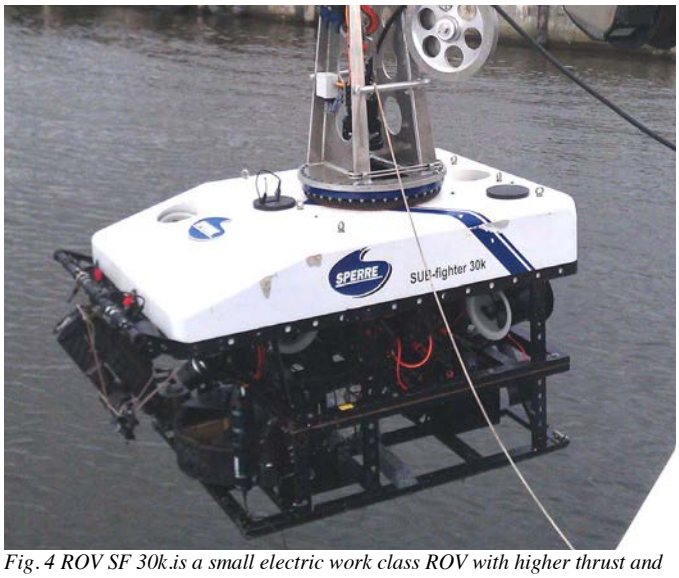

Fig. 4 ROV SF 30k.is a small electric work class ROV with higher thrust and payload capacity than the ROV Minerva.

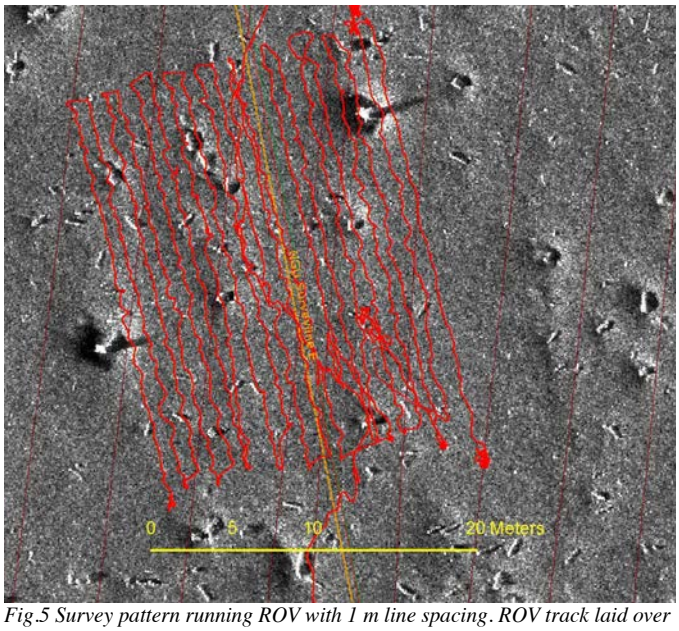

Fig.5 Survey pattern running ROV with 1 m line spacing. ROV track laid over SAS imagery of the seabed on the Agdenes dumping field (B in fig 1.).

A. Equipment

1) AUV Hugin HUS

The AUV Hugin HUS is operated by Norwegian Defence Research Establishment (FFI) and was mobilized for two operations onboard the RV Gunnerus, see fig 3. The vehicle weighs just below 1 ton and has typical range of 15- 24 hours depending on payload and speed. The navigation system is based on an advanced INS comprising Doppler Velocity Log (DVL), and USBL aiding. The Side Scan Sonar (SSS) and optical camera (TFish) were the primary payload sensors for our operations.

AUV Hugin has the Synthetic Aperture Sonar (SAS) HiSAS 1030 (trademark of Kongsberg Maritime), [8] installed. This system has incorporated interferometric processing providing bathymetric information. To allow SAS processing the system depends on precise motion data provided by the inertial system onboard the Hugin vehicle. For seabed imagery the coverage and resolution is specified to 2.6 km2/h and 3 x 3 cm. Bathymetry resolution is specified to 50 x 50 cm, but considerably finer results has been proved.

2) ROV Minerva

ROV Minerva is an observation class ROV equipped with five frequency controlled AC thrusters, see fig 2. The vehicle weighs approximately 500 kgs and is equipped with a simple 5 function hydraulic manipulator. A control system developed at NTNU AUR-Lab is connected to the ROV [9] providing advanced automated manoeuvres like station keeping and path following. This system is essential flying the vehicle in lawn-mower patterns with decimetre level cross track errors to ensure full overlap for sensors with small swath widths, like cameras for photomosaic or UHI. The vehicle is navigated using USBL installed on RV Gunnerus combined with DVL, INS and pressure sensor in an observer integrated in the control system. In the described scientific cruises, the vehicle has been equipped with video, UHI and stereo camera.

The UHI is a push broom hyperspectral imager, and the system is patented by the NTNU spin-off company Ecotone, [10]. In our operations, the system relied on 2 x 250 W halogen light sources. The instrument sampled at a 20 Hz rate, and moving the vehicle and the instrument in a line, an image is constructed analogous to the way SSS imagery are compiled of successive lines. The spectral resolution for the set up used was adjustable from 1 to 8 nm. 1600 spatial pixels containing 872 spectral bins were obtained for each image frame representing a line in the resulting imagery. The reflectance spectra of Objects Of Interest (OOI) can be detected. These spectra can then be compared to a library of known marine substances allowing us to identify the bio-geo-chemical composition of the material on the site.

Using two industrial block cameras, a stereo-rig was constructed. The camera blocks were mounted in housings and placed on an aluminium bar fixing their internal orientation. The cameras have only modest resolution, but high light sensitivity which is important in underwater imaging as we are usually light limited in our imaging process. Through the ROV's fibre optical communication link the cameras were triggered simultaneously from a computer on the surface.

3) ROV SF 30k

The ROV SF 30k is constructed of the same basis as the ROV Minerva having similar instrumentation and control systems, see fig 4. But the SF 30k ROV is considerably larger having a mass of approximately 2 tons and has a 7 function force feedback manipulator installed. The navigation and payload packages are identical to the Minerva.

B. Operations

The operations were comprehensive mobilizations and were organized as multi-client operations to maximize the outcome for AUR-Lab's multi-disciplinary user group. The areas were covered first using vessel mounted MBE or AUV mounted SSS for map or explore an area before detailed investigations were performed using the ROV.

Fig. 6 Photogrammetry model of manmade objects laying on the seabed.on the Agdenes dumping field (B in fig 1.). The object in the center of the figure is measured from the photogrammetry model to be 115 cm long and 30 cm in diameter.

In December 2012 AUR-Lab, FFI and its collaborators surveyed the Tautra ridge and several other sites in the Trondheim Fjord [7], see fig. 1. The ROV Minerva was deployed with video and UHI and provided ground-truthing for the sonar imagery. The operation was repeated in 2013 with identical AUV set up. The intention was prove repeatability and to test change detection on a cold-water coral reef, and the result is described in [11]. During the AUV operation in 2013, the Hugin HUS was also deployed on the Agdenes ridge, the Agdenes dumping field and the Nord Leksa cold-water coral reef [12], see fig. 7.

Based on the findings in the sonar data for the dumping area at Agdenes it was decided to mobilize the ROV SF 30k as the smaller ROV Minerva had previously proven insufficient in the strong current in this area. It appeared to be explosives from WWII on the site located in a geological erosion zone. The ROV was operated free flying with soft umbilical to the surface. The depth on the site was approximately 600 meters. During the operation, we performed three video transects with a total length of one kilometre. The transects were completed according to [13]. A box 20 x 25 meters was also surveyed with full seabed coverage using stereo camera rig and UHI in lawn-mower pattern with 1 meter line spacing, see fig 5.

C. Data processing

The data collected was compiled in a Geographical Information System (GIS). This allowed us to compare data signatures of features across the instruments, also providing guidance for the data interpretation. The SAS data were processed using the FOCUS processing suite and Reflection software (Kongsberg Maritime) before it was exported to the GIS data base. Both bathymetry and sonar imagery were exported. Target identification was completed using either Reflections or SonarWiz (Chesapeake Technology). Processing of the multi view photogrammetric models was completed using the software Photoscan (Agisoft). Thousands of images were processed to models with millimetre resolution.

D. Quality Assesment

The qualities of the data in the operations described are of two types, navigation accuracy and measurement accuracy. For the AUV survey in 2012 we experienced off-sets for the USBL positioning due to faulty calibration. The AUV survey at Tautra was hence completed using INS initialising on the surface with GPS. The approach required the DVL to have bottom lock all the time to ensure position accuracy. For the 2013 and 2014 campaigns, proper USBL calibration allowed USBL support for the ROV and AUV navigation.

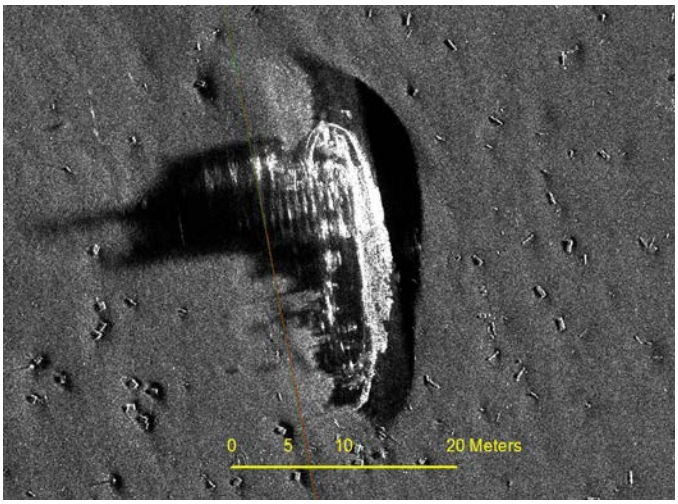

Fig. 7 Ship wreck in SAS data in the Agdenes dumping field (B in fig 1.).

III. Results

We found large areas of scleractinian corals on both the Nord-Leksa and the Agdenes ridge.

A. Tautra

The scleractinian cold-water coral colony on the Tautra ridge was mapped in 2012, 2.7 km^2 were covered. The surveys showed large portions of the seabed clothed with scleractinian corals on depths varying from 50 m to 200 meters. Research has been performed on these corals for centuries [12], but for the first time it is possible to determine the exact extent of these corals.

These two data sets from Tautra were used to develop and test change detection techniques for cold-water coral habitats [11]. The 2012 data hence was the baseline survey. Due to the temporal baseline (one year) and the rough topography incoherent co-registration was attempted aiming for pixel level co-registration. The preliminary results show the potential for

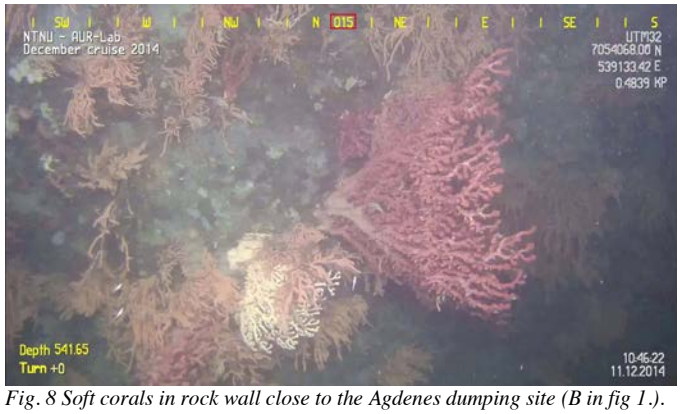

Fig. 8 Soft corals in rock wall close to the Agdenes dumping site (B in fig 1.). The depth is 540 m.

the change detection for monitoring corals, but also the challenges related to mapping rough terrain with high vehicle pitch and heave values combined with varying speed of sound. There was a significant correlation between the image difference and the topography. But large human impacts like anchor lines, dumping of objects or pipeline would give a distinct signature.

B. Agdenes

The dumping field at Agdenes is a geological erosion zone due to high seabed currents. The Norwegian Geological Survey had observed indications of seabed erosion in existing sonar data sets. Consulting oceanographic models of the area, the area appears to be a high current area. This was also confirmed during or ROV operations. High seabed currents were experience during our ROV operations.

The area covered was 2.2 km2 and had served as dumping field for several decades from the end of WWII and some decades on. In 2013 the Hugin AUV was deployed and the sonar imagery showed 25 ship wrecks and thousands of smaller object suspected to be explosives, see fig. 7. Optical imagery from the AUV showed object shaped like bombs and grenades.

Approximately 1000 m of video transect was completed using ROV SF 30k and approximately 940 anthropogenic objects were detected. The box 20 x 25 meters was mapped using UHI and stereo camera resulting in full coverage, see fig. 5. Using UHI, we were able to identify species by spectral analysis of the reflected light. The objects were corroded after long time on the seabed. In spite of the possible aggressive chemical substances inside the object, they were colonized by several species of soft and hard corals and other biota. One of the larger concerns was leakage of poisonous substances from the explosives dropped. Hence a sediment sample was collected using a push corer mounted on the ROV in the intermediate vicinity of an object.

The species are known from literature to settle in areas with high currents and this conform our experienced coincidence of current maxima and corals. However the occurrence of high currents makes this area attractive for cold-water corals. The sediments themselves does not allow settlement of corals, but the man-made objects were sufficiently hard to allow the corals to attach. Hence, a large portion of the objects were habitat for cold-water corals. In the north east direction, a vertical rock wall rises up from the seabed. The rock wall was visited with ROV and proved to be a rich coral colony with both hard and soft corals, see fig. 8. The species diversity was high. It is common to find corals on location exposed to current; hence the occurrence of corals in the exposed dumping field was not surprising.

Using the ROV, one of the ship wrecks was also visited. The wreck was most likely a condemned fishing vessel made from wood.

IV. Discussion

To support efficient management of vulnerable areas SAS imagery can be established as baseline for monitoring programs. In spite of the discussed challenges to CD techniques in complicated terrains, repeated surveys can be used for CD processing. This will reveal changes to structures like scleractinian coral communities caused by human activities on a level not obtainable with other techniques. A programme with frequent AUV surveys would hence provide information of human influence to these areas.

For specific sites like ship wrecks, dangerous objects or threatened biological structures, photogrammetric models can be established. Using repeated surveys and CD for such data sets the development of these objects can be held under control. From these results, the rate of decay can be estimated allowing for efficient assessment of the associated risks. UHI would provide valuable supplementary information to such investigations.

V. Conclusions

NTNU AUR-Lab, FFI, NGU and Ecotone AS have demonstrated advanced techniques for AUV and ROV surveys. Valuable data were collected during the cruises demonstrating their potential. The HiSAS imagery is sufficiently detailed to provide this base-line for cold-water corals. It is possible to classify and quantify the occurrence based on these data. Revisiting the areas and applying CD, it is also possible to detected and monitor human intervention like pipelines, dredge-line etc. Offering higher resolution modern multi view photogrammetry enables high level details allowing more detailed mapping and monitoring. This information can further be complemented using UHI analysing the chemical, biological or biological composition of the targets.

Acknowledgment

The results of this cruise were made possible by NTNU AUR-Lab and FFI and the authors are grateful to all cruise participants. The authors are also grateful to SINTEF Fisheries and Aquaculture for the current estimates provided by Ingrid Ellingsen. The authors would also like to thank the crew of RV Gunnerus for their invaluable help and positive attitude during the operations. NTNU, FFI, NGU, and Ecotone AS all contributed financially to enable this operation. This work was also supported by the Research Council of Norway through the Centres of Excellence funding scheme, project number 223254, AMOS.

References

[1] Leveson, I.: 'Socio-Economic Study: Scoping the Value of NOAA's Coastal Mapping Program': 'Report' (2012).

[2] PriceWaterCooperHouse: 'INFOMAR Marine Mapping Study – Options Apprisal Report,': 'Report' (PriceWaterCooperHouse, 2008.), pp.

[3] Clark, C.M., Hancke, K., Xydes, A., Hall, K., Schreiber, F., Klemme, J., Lehr, J., and Moline, M.: 'Estimation of Volumetric Oxygen Concentration in a Marine Environment with an Autonomous Underwater Vehicle', Journal of Field Robotics, 2013, 30, (1), pp. 1-16

[4] Midtgaard, Ø.: 'Change detection using synthetic aperture sonar imagery with variable time intervals.', in In Proceedings of the 1st Underwater Acoustic Conference, Corfu, Greece, June 2013.

[5] Harris, P.T., and Baker, E.: 'Seafloor geomorphology as benthic habitat: GeoHAB atlas of seaflorr geomorphic features and benthic habitats' (Elsevier, 2012.)

[6] Ødegård, Ø., Ludvigsen, M., Johnsen, G., Sørensen, A.J., Ekehaug, S., Dukan, F., and Moline, M.: 'Managing data from multiple sensors in an interdisciplinary research cruise'. Proc. CAA 2012 (Computer Applications and Quantitative Methods in Archaeology), Southamption, 26-30 March 2012

[7] Ludvigsen, M., Johnsen, G., Sørensen, A.J., Lågstad, P.A., and Ødegård, Ø.: 'Scientific Operations Combining ROV and AUV in the Trondheim Fjord', Marine Technology Society Journal, 2014, 48, (2), pp. 59-71

[8] Hansen, R.E., Saebo, T.O., Callow, H.J., Hagen, P.E., and Hammerstad, E.: 'Synthetic aperture sonar processing for the HUGIN AUV', In Proceedings of Oceans '05 Europe, volume 2, pages 1090-1094, Brest, France, June 2005.

[9] Sørensen, A.J., Dukan, F., Ludvigsen, M., De Almeida Fernandes, D., and Candeloro, M.: 'Development of Dynamic Positioning and Tracking System for the ROV Minerva', in Roberts, G.N., and Sutton, R. (Eds.): 'Further Advances in Unmanned Marine Vehicles' (Institution of Engineering and Technology, 2012), pp. 113-128

[10] Johnsen, G., Volent, Z., Dierssen, H., Pettersen, R., Ardelan, M.V., Søreide, F., Fearns, P., Ludvigsen, M., and Moline, M.: 'Underwater hyperspectral imagery to create biogeochemical maps of seafloor properties', in Watson, J., and Zielinski, O. (Eds.): 'Subsea optics and imaging' (Woodhead Publishing Ltd, 2013), pp. 608

[11] Hansen, R.E., Sæbø, T.O., Lorentzen, O.J., and Midtgaard, Ø.: 'Change detection in topographic structures using interferometric synthetic aperture sonar. ', in In Proceedings of the 2st Underwater Acoustic Conference, Rhodes, Greece, June 2014

[12] DONS, C. 1944. Norges korallrev. Det Kongelige Norske Videnskabers Selskabs Forhandlinger, 16, 37-82.

[13] Norge, Standard.: 'NS-EN 16260:2012 Water quality - Visual seabed surveys using remotely operated and/or towed observation gear for collection of environmental data ', (2012), pp.

Previous PhD theses published at the Department of Marine Technology

Previous PhD theses published at the Departement of Marine Technology (earlier: Faculty of Marine Technology) NORWEGIAN UNIVERSITY OF SCIENCE AND TECHNOLOGY

Report No.	Author	Title
	Kavlie, Dag	Optimization of Plane Elastic Grillages, 1967
	Hansen, Hans R.	Man-Machine Communication and Data-Storage Methods in Ship Structural Design, 1971
	Gisvold, Kaare M.	A Method for non-linear mixed -integer programming and its Application to Design Problems, 1971
	Lund, Sverre	Tanker Frame Optimalization by means of SUMT-Transformation and Behaviour Models, 1971
	Vinje, Tor	On Vibration of Spherical Shells Interacting with Fluid, 1972
	Lorentz, Jan D.	Tank Arrangement for Crude Oil Carriers in Accordance with the new Anti-Pollution Regulations, 1975
	Carlsen, Carl A.	Computer-Aided Design of Tanker Structures, 1975
	Larsen, Carl M.	Static and Dynamic Analysis of Offshore Pipelines during Installation, 1976
UR-79-01	Brigt Hatlestad, MK	The finite element method used in a fatigue evaluation of fixed offshore platforms. (Dr.Ing. Thesis)
UR-79-02	Erik Pettersen, MK	Analysis and design of cellular structures. (Dr.Ing. Thesis)
UR-79-03	Sverre Valsgård, MK	Finite difference and finite element methods applied to nonlinear analysis of plated structures. (Dr.Ing. Thesis)
UR-79-04	Nils T. Nordsve, MK	Finite element collapse analysis of structural members considering imperfections and stresses due to fabrication. (Dr.Ing. Thesis)
UR-79-05	Ivar J. Fylling, MK	Analysis of towline forces in ocean towing systems. (Dr.Ing. Thesis)
UR-80-06	Nils Sandsmark, MM	Analysis of Stationary and Transient Heat Conduction by the Use of the Finite Element Method. (Dr.Ing. Thesis)
UR-80-09	Sverre Haver, MK	Analysis of uncertainties related to the stochastic modeling of ocean waves. (Dr.Ing. Thesis)
UR-81-15	Odland, Jonas	On the Strength of welded Ring stiffened cylindrical Shells primarily subjected to axial Compression
UR-82-17	Engesvik, Knut	Analysis of Uncertainties in the fatigue Capacity of

		Welded Joints
UR-82-18	Rye, Henrik	Ocean wave groups
UR-83-30	Eide, Oddvar Inge	On Cumulative Fatigue Damage in Steel Welded Joints
UR-83-33	Mo, Olav	Stochastic Time Domain Analysis of Slender Offshore Structures
UR-83-34	Amdahl, Jørgen	Energy absorption in Ship-platform impacts
UR-84-37	Mørch, Morten	Motions and mooring forces of semi submersibles as determined by full-scale measurements and theoretical analysis
UR-84-38	Soares, C. Guedes	Probabilistic models for load effects in ship structures
UR-84-39	Aarsnes, Jan V.	Current forces on ships
UR-84-40	Czujko, Jerzy	Collapse Analysis of Plates subjected to Biaxial Compression and Lateral Load
UR-85-46	Alf G. Engseth, MK	Finite element collapse analysis of tubular steel offshore structures. (Dr.Ing. Thesis)
UR-86-47	Dengody Sheshappa, MP	A Computer Design Model for Optimizing Fishing Vessel Designs Based on Techno-Economic Analysis. (Dr.Ing. Thesis)
UR-86-48	Vidar Aanesland, MH	A Theoretical and Numerical Study of Ship Wave Resistance. (Dr.Ing. Thesis)
UR-86-49	Heinz-Joachim Wessel, MK	Fracture Mechanics Analysis of Crack Growth in Plate Girders. (Dr.Ing. Thesis)
UR-86-50	Jon Taby, MK	Ultimate and Post-ultimate Strength of Dented Tubular Members. (Dr.Ing. Thesis)
UR-86-51	Walter Lian, MH	A Numerical Study of Two-Dimensional Separated Flow Past Bluff Bodies at Moderate KC-Numbers. (Dr.Ing. Thesis)
UR-86-52	Bjørn Sortland, MH	Force Measurements in Oscillating Flow on Ship Sections and Circular Cylinders in a U-Tube Water Tank. (Dr.Ing. Thesis)
UR-86-53	Kurt Strand, MM	A System Dynamic Approach to One-dimensional Fluid Flow. (Dr.Ing. Thesis)
UR-86-54	Arne Edvin Løken, MH	Three Dimensional Second Order Hydrodynamic Effects on Ocean Structures in Waves. (Dr.Ing. Thesis)
UR-86-55	Sigurd Falch, MH	A Numerical Study of Slamming of Two-Dimensional Bodies. (Dr.Ing. Thesis)
UR-87-56	Arne Braathen, MH	Application of a Vortex Tracking Method to the Prediction of Roll Damping of a Two-Dimension Floating Body. (Dr.Ing. Thesis)

UR-87-57	Bernt Leira, MK	Gaussian Vector Processes for Reliability Analysis involving Wave-Induced Load Effects. (Dr.Ing. Thesis)
UR-87-58	Magnus Småvik, MM	Thermal Load and Process Characteristics in a Two-Stroke Diesel Engine with Thermal Barriers (in Norwegian). (Dr.Ing. Thesis)
MTA-88-59	Bernt Arild Bremdal, MP	An Investigation of Marine Installation Processes – A Knowledge - Based Planning Approach. (Dr.Ing. Thesis)
MTA-88-60	Xu Jun, MK	Non-linear Dynamic Analysis of Space-framed Offshore Structures. (Dr.Ing. Thesis)
MTA-89-61	Gang Miao, MH	Hydrodynamic Forces and Dynamic Responses of Circular Cylinders in Wave Zones. (Dr.Ing. Thesis)
MTA-89-62	Martin Greenhow, MH	Linear and Non-Linear Studies of Waves and Floating Bodies. Part I and Part II. (Dr.Techn. Thesis)
MTA-89-63	Chang Li, MH	Force Coefficients of Spheres and Cubes in Oscillatory Flow with and without Current. (Dr.Ing. Thesis
MTA-89-64	Hu Ying, MP	A Study of Marketing and Design in Development of Marine Transport Systems. (Dr.Ing. Thesis)
MTA-89-65	Arild Jæger, MH	Seakeeping, Dynamic Stability and Performance of a Wedge Shaped Planing Hull. (Dr.Ing. Thesis)
MTA-89-66	Chan Siu Hung, MM	The dynamic characteristics of tilting-pad bearings
MTA-89-67	Kim Wikstrøm, MP	Analysis av projekteringen for ett offshore projekt. (Licenciat-avhandling)
MTA-89-68	Jiao Guoyang, MK	Reliability Analysis of Crack Growth under Random Loading, considering Model Updating. (Dr.Ing. Thesis)
MTA-89-69	Arnt Olufsen, MK	Uncertainty and Reliability Analysis of Fixed Offshore Structures. (Dr.Ing. Thesis)
MTA-89-70	Wu Yu-Lin, MR	System Reliability Analyses of Offshore Structures using improved Truss and Beam Models. (Dr.Ing. Thesis)
MTA-90-71	Jan Roger Hoff, MH	Three-dimensional Green function of a vessel with forward speed in waves. (Dr.Ing. Thesis)
MTA-90-72	Rong Zhao, MH	Slow-Drift Motions of a Moored Two-Dimensional Body in Irregular Waves. (Dr.Ing. Thesis)
MTA-90-73	Atle Minsaas, MP	Economical Risk Analysis. (Dr.Ing. Thesis)
MTA-90-74	Knut-Aril Farnes, MK	Long-term Statistics of Response in Non-linear Marine Structures. (Dr.Ing. Thesis)
MTA-90-75	Torbjørn Sotberg, MK	Application of Reliability Methods for Safety Assessment of Submarine Pipelines. (Dr.Ing.

		Thesis)
MTA-90-76	Zeuthen, Steffen, MP	SEAMAID. A computational model of the design process in a constraint-based logic programming environment. An example from the offshore domain. (Dr.Ing. Thesis)
MTA-91-77	Haagensen, Sven, MM	Fuel Dependant Cyclic Variability in a Spark Ignition Engine - An Optical Approach. (Dr.Ing. Thesis)
MTA-91-78	Løland, Geir, MH	Current forces on and flow through fish farms. (Dr.Ing. Thesis)
MTA-91-79	Hoen, Christopher, MK	System Identification of Structures Excited by Stochastic Load Processes. (Dr.Ing. Thesis)
MTA-91-80	Haugen, Stein, MK	Probabilistic Evaluation of Frequency of Collision between Ships and Offshore Platforms. (Dr.Ing. Thesis)
MTA-91-81	Sødahl, Nils, MK	Methods for Design and Analysis of Flexible Risers. (Dr.Ing. Thesis)
MTA-91-82	Ormberg, Harald, MK	Non-linear Response Analysis of Floating Fish Farm Systems. (Dr.Ing. Thesis)
MTA-91-83	Marley, Mark J., MK	Time Variant Reliability under Fatigue Degradation. (Dr.Ing. Thesis)
MTA-91-84	Krokstad, Jørgen R., MH	Second-order Loads in Multidirectional Seas. (Dr.Ing. Thesis)
MTA-91-85	Molteberg, Gunnar A., MM	The Application of System Identification Techniques to Performance Monitoring of Four Stroke Turbocharged Diesel Engines. (Dr.Ing. Thesis)
MTA-92-86	Mørch, Hans Jørgen Bjelke, MH	Aspects of Hydrofoil Design: with Emphasis on Hydrofoil Interaction in Calm Water. (Dr.Ing. Thesis)
MTA-92-87	Chan Siu Hung, MM	Nonlinear Analysis of Rotordynamic Instabilities in Highspeed Turbomachinery. (Dr.Ing. Thesis)
MTA-92-88	Bessason, Bjarni, MK	Assessment of Earthquake Loading and Response of Seismically Isolated Bridges. (Dr.Ing. Thesis)
MTA-92-89	Langli, Geir, MP	Improving Operational Safety through exploitation of Design Knowledge - an investigation of offshore platform safety. (Dr.Ing. Thesis)
MTA-92-90	Sævik, Svein, MK	On Stresses and Fatigue in Flexible Pipes. (Dr.Ing. Thesis)
MTA-92-91	Ask, Tor Ø., MM	Ignition and Flame Growth in Lean Gas-Air Mixtures. An Experimental Study with a Schlieren System. (Dr.Ing. Thesis)
MTA-86-92	Hessen, Gunnar, MK	Fracture Mechanics Analysis of Stiffened Tubular Members. (Dr.Ing. Thesis)

MTA-93-93	Steinebach, Christian, MM	Knowledge Based Systems for Diagnosis of Rotating Machinery. (Dr.Ing. Thesis)
MTA-93-94	Dalane, Jan Inge, MK	System Reliability in Design and Maintenance of Fixed Offshore Structures. (Dr.Ing. Thesis)
MTA-93-95	Steen, Sverre, MH	Cobblestone Effect on SES. (Dr.Ing. Thesis)
MTA-93-96	Karunakaran, Daniel, MK	Nonlinear Dynamic Response and Reliability Analysis of Drag-dominated Offshore Platforms. (Dr.Ing. Thesis)
MTA-93-97	Hagen, Arnulf, MP	The Framework of a Design Process Language. (Dr.Ing. Thesis)
MTA-93-98	Nordrik, Rune, MM	Investigation of Spark Ignition and Autoignition in Methane and Air Using Computational Fluid Dynamics and Chemical Reaction Kinetics. A Numerical Study of Ignition Processes in Internal Combustion Engines. (Dr.Ing. Thesis)
MTA-94-99	Passano, Elizabeth, MK	Efficient Analysis of Nonlinear Slender Marine Structures. (Dr.Ing. Thesis)
MTA-94-100	Kvålsvold, Jan, MH	Hydroelastic Modelling of Wetdeck Slamming on Multihull Vessels. (Dr.Ing. Thesis)
MTA-94-102	Bech, Sidsel M., MK	Experimental and Numerical Determination of Stiffness and Strength of GRP/PVC Sandwich Structures. (Dr.Ing. Thesis)
MTA-95-103	Paulsen, Hallvard, MM	A Study of Transient Jet and Spray using a Schlieren Method and Digital Image Processing. (Dr.Ing. Thesis)
MTA-95-104	Hovde, Geir Olav, MK	Fatigue and Overload Reliability of Offshore Structural Systems, Considering the Effect of Inspection and Repair. (Dr.Ing. Thesis)
MTA-95-105	Wang, Xiaozhi, MK	Reliability Analysis of Production Ships with Emphasis on Load Combination and Ultimate Strength. (Dr.Ing. Thesis)
MTA-95-106	Ulstein, Tore, MH	Nonlinear Effects of a Flexible Stern Seal Bag on Cobblestone Oscillations of an SES. (Dr.Ing. Thesis)
MTA-95-107	Solaas, Frøydis, MH	Analytical and Numerical Studies of Sloshing in Tanks. (Dr.Ing. Thesis)
MTA-95-108	Hellan, Øyvind, MK	Nonlinear Pushover and Cyclic Analyses in Ultimate Limit State Design and Reassessment of Tubular Steel Offshore Structures. (Dr.Ing. Thesis)
MTA-95-109	Hermundstad, Ole A., MK	Theoretical and Experimental Hydroelastic Analysis of High Speed Vessels. (Dr.Ing. Thesis)
MTA-96-110	Bratland, Anne K., MH	Wave-Current Interaction Effects on Large-Volume Bodies in Water of Finite Depth. (Dr.Ing. Thesis)
MTA-96-111	Herfjord, Kjell, MH	A Study of Two-dimensional Separated Flow by a Combination of the Finite Element Method and

		Navier-Stokes Equations. (Dr.Ing. Thesis)
MTA-96-112	Æsøy, Vilmar, MM	Hot Surface Assisted Compression Ignition in a Direct Injection Natural Gas Engine. (Dr.Ing. Thesis)
MTA-96-113	Eknes, Monika L., MK	Escalation Scenarios Initiated by Gas Explosions on Offshore Installations. (Dr.Ing. Thesis)
MTA-96-114	Erikstad, Stein O., MP	A Decision Support Model for Preliminary Ship Design. (Dr.Ing. Thesis)
MTA-96-115	Pedersen, Egil, MH	A Nautical Study of Towed Marine Seismic Streamer Cable Configurations. (Dr.Ing. Thesis)
MTA-97-116	Moksnes, Paul O., MM	Modelling Two-Phase Thermo-Fluid Systems Using Bond Graphs. (Dr.Ing. Thesis)
MTA-97-117	Halse, Karl H., MK	On Vortex Shedding and Prediction of Vortex-Induced Vibrations of Circular Cylinders. (Dr.Ing. Thesis)
MTA-97-118	Igland, Ragnar T., MK	Reliability Analysis of Pipelines during Laying, considering Ultimate Strength under Combined Loads. (Dr.Ing. Thesis)
MTA-97-119	Pedersen, Hans-P., MP	Levendefiskteknologi for fiskefartøy. (Dr.Ing. Thesis)
MTA-98-120	Vikestad, Kyrre, MK	Multi-Frequency Response of a Cylinder Subjected to Vortex Shedding and Support Motions. (Dr.Ing. Thesis)
MTA-98-121	Azadi, Mohammad R. E., MK	Analysis of Static and Dynamic Pile-Soil-Jacket Behaviour. (Dr.Ing. Thesis)
MTA-98-122	Ulltang, Terje, MP	A Communication Model for Product Information. (Dr.Ing. Thesis)
MTA-98-123	Torbergsen, Erik, MM	Impeller/Diffuser Interaction Forces in Centrifugal Pumps. (Dr.Ing. Thesis)
MTA-98-124	Hansen, Edmond, MH	A Discrete Element Model to Study Marginal Ice Zone Dynamics and the Behaviour of Vessels Moored in Broken Ice. (Dr.Ing. Thesis)
MTA-98-125	Videiro, Paulo M., MK	Reliability Based Design of Marine Structures. (Dr.Ing. Thesis)
MTA-99-126	Mainçon, Philippe, MK	Fatigue Reliability of Long Welds Application to Titanium Risers. (Dr.Ing. Thesis)
MTA-99-127	Haugen, Elin M., MH	Hydroelastic Analysis of Slamming on Stiffened Plates with Application to Catamaran Wetdecks. (Dr.Ing. Thesis)
MTA-99-128	Langhelle, Nina K., MK	Experimental Validation and Calibration of Nonlinear Finite Element Models for Use in Design of Aluminium Structures Exposed to Fire. (Dr.Ing. Thesis)
MTA-99-	Berstad, Are J., MK	Calculation of Fatigue Damage in Ship Structures.

129		(Dr.Ing. Thesis)
MTA-99-130	Andersen, Trond M., MM	Short Term Maintenance Planning. (Dr.Ing. Thesis)
MTA-99-131	Tveiten, Bård Wathne, MK	Fatigue Assessment of Welded Aluminium Ship Details. (Dr.Ing. Thesis)
MTA-99-132	Søreide, Fredrik, MP	Applications of underwater technology in deep water archaeology. Principles and practice. (Dr.Ing. Thesis)
MTA-99-133	Tønnessen, Rune, MH	A Finite Element Method Applied to Unsteady Viscous Flow Around 2D Blunt Bodies With Sharp Corners. (Dr.Ing. Thesis)
MTA-99-134	Elvekrok, Dag R., MP	Engineering Integration in Field Development Projects in the Norwegian Oil and Gas Industry. The Supplier Management of Norne. (Dr.Ing. Thesis)
MTA-99-135	Fagerholt, Kjetil, MP	Optimeringsbaserte Metoder for Ruteplanlegging innen skipsfart. (Dr.Ing. Thesis)
MTA-99-136	Bysveen, Marie, MM	Visualization in Two Directions on a Dynamic Combustion Rig for Studies of Fuel Quality. (Dr.Ing. Thesis)
MTA-2000-137	Storteig, Eskild, MM	Dynamic characteristics and leakage performance of liquid annular seals in centrifugal pumps. (Dr.Ing. Thesis)
MTA-2000-138	Sagli, Gro, MK	Model uncertainty and simplified estimates of long term extremes of hull girder loads in ships. (Dr.Ing. Thesis)
MTA-2000-139	Tronstad, Harald, MK	Nonlinear analysis and design of cable net structures like fishing gear based on the finite element method. (Dr.Ing. Thesis)
MTA-2000-140	Kroneberg, André, MP	Innovation in shipping by using scenarios. (Dr.Ing. Thesis)
MTA-2000-141	Haslum, Herbjørn Alf, MH	Simplified methods applied to nonlinear motion of spar platforms. (Dr.Ing. Thesis)
MTA-2001-142	Samdal, Ole Johan, MM	Modelling of Degradation Mechanisms and Stressor Interaction on Static Mechanical Equipment Residual Lifetime. (Dr.Ing. Thesis)
MTA-2001-143	Baarholm, Rolf Jarle, MH	Theoretical and experimental studies of wave impact underneath decks of offshore platforms. (Dr.Ing. Thesis)
MTA-2001-144	Wang, Lihua, MK	Probabilistic Analysis of Nonlinear Wave-induced Loads on Ships. (Dr.Ing. Thesis)
MTA-2001-145	Kristensen, Odd H. Holt, MK	Ultimate Capacity of Aluminium Plates under Multiple Loads, Considering HAZ Properties. (Dr.Ing. Thesis)
MTA-2001-146	Greco, Marilena, MH	A Two-Dimensional Study of Green-Water

		Loading. (Dr.Ing. Thesis)
MTA-2001-147	Heggelund, Svein E., MK	Calculation of Global Design Loads and Load Effects in Large High Speed Catamarans. (Dr.Ing. Thesis)
MTA-2001-148	Babalola, Olusegun T., MK	Fatigue Strength of Titanium Risers – Defect Sensitivity. (Dr.Ing. Thesis)
MTA-2001-149	Mohammed, Abuu K., MK	Nonlinear Shell Finite Elements for Ultimate Strength and Collapse Analysis of Ship Structures. (Dr.Ing. Thesis)
MTA-2002-150	Holmedal, Lars E., MH	Wave-current interactions in the vicinity of the sea bed. (Dr.Ing. Thesis)
MTA-2002-151	Rognebakke, Olav F., MH	Sloshing in rectangular tanks and interaction with ship motions. (Dr.Ing. Thesis)
MTA-2002-152	Lader, Pål Furset, MH	Geometry and Kinematics of Breaking Waves. (Dr.Ing. Thesis)
MTA-2002-153	Yang, Qinzheng, MH	Wash and wave resistance of ships in finite water depth. (Dr.Ing. Thesis)
MTA-2002-154	Melhus, Øyvin, MM	Utilization of VOC in Diesel Engines. Ignition and combustion of VOC released by crude oil tankers. (Dr.Ing. Thesis)
MTA-2002-155	Ronæss, Marit, MH	Wave Induced Motions of Two Ships Advancing on Parallel Course. (Dr.Ing. Thesis)
MTA-2002-156	Økland, Ole D., MK	Numerical and experimental investigation of whipping in twin hull vessels exposed to severe wet deck slamming. (Dr.Ing. Thesis)
MTA-2002-157	Ge, Chunhua, MK	Global Hydroelastic Response of Catamarans due to Wet Deck Slamming. (Dr.Ing. Thesis)
MTA-2002-158	Byklum, Eirik, MK	Nonlinear Shell Finite Elements for Ultimate Strength and Collapse Analysis of Ship Structures. (Dr.Ing. Thesis)
IMT-2003-1	Chen, Haibo, MK	Probabilistic Evaluation of FPSO-Tanker Collision in Tandem Offloading Operation. (Dr.Ing. Thesis)
IMT-2003-2	Skaugset, Kjetil Bjørn, MK	On the Suppression of Vortex Induced Vibrations of Circular Cylinders by Radial Water Jets. (Dr.Ing. Thesis)
IMT-2003-3	Chezhian, Muthu	Three-Dimensional Analysis of Slamming. (Dr.Ing. Thesis)
IMT-2003-4	Buhaug, Øyvind	Deposit Formation on Cylinder Liner Surfaces in Medium Speed Engines. (Dr.Ing. Thesis)
IMT-2003-5	Tregde, Vidar	Aspects of Ship Design: Optimization of Aft Hull with Inverse Geometry Design. (Dr.Ing. Thesis)
IMT-	Wist, Hanne Therese	Statistical Properties of Successive Ocean Wave

2003-6		Parameters. (Dr.Ing. Thesis)
IMT-2004-7	Ransau, Samuel	Numerical Methods for Flows with Evolving Interfaces. (Dr.Ing. Thesis)
IMT-2004-8	Soma, Torkel	Blue-Chip or Sub-Standard. A data interrogation approach of identity safety characteristics of shipping organization. (Dr.Ing. Thesis)
IMT-2004-9	Ersdal, Svein	An experimental study of hydrodynamic forces on cylinders and cables in near axial flow. (Dr.Ing. Thesis)
IMT-2005-10	Brodtkorb, Per Andreas	The Probability of Occurrence of Dangerous Wave Situations at Sea. (Dr.Ing. Thesis)
IMT-2005-11	Yttervik, Rune	Ocean current variability in relation to offshore engineering. (Dr.Ing. Thesis)
IMT-2005-12	Fredheim, Arne	Current Forces on Net-Structures. (Dr.Ing. Thesis)
IMT-2005-13	Heggernes, Kjetil	Flow around marine structures. (Dr.Ing. Thesis
IMT-2005-14	Fouques, Sebastien	Lagrangian Modelling of Ocean Surface Waves and Synthetic Aperture Radar Wave Measurements. (Dr.Ing. Thesis)
IMT-2006-15	Holm, Håvard	Numerical calculation of viscous free surface flow around marine structures. (Dr.Ing. Thesis)
IMT-2006-16	Bjørheim, Lars G.	Failure Assessment of Long Through Thickness Fatigue Cracks in Ship Hulls. (Dr.Ing. Thesis)
IMT-2006-17	Hansson, Lisbeth	Safety Management for Prevention of Occupational Accidents. (Dr.Ing. Thesis)
IMT-2006-18	Zhu, Xinying	Application of the CIP Method to Strongly Nonlinear Wave-Body Interaction Problems. (Dr.Ing. Thesis)
IMT-2006-19	Reite, Karl Johan	Modelling and Control of Trawl Systems. (Dr.Ing. Thesis)
IMT-2006-20	Smogeli, Øyvind Notland	Control of Marine Propellers. From Normal to Extreme Conditions. (Dr.Ing. Thesis)
IMT-2007-21	Storhaug, Gaute	Experimental Investigation of Wave Induced Vibrations and Their Effect on the Fatigue Loading of Ships. (Dr.Ing. Thesis)
IMT-2007-22	Sun, Hui	A Boundary Element Method Applied to Strongly Nonlinear Wave-Body Interaction Problems. (PhD Thesis, CeSOS)
IMT-2007-23	Rustad, Anne Marthine	Modelling and Control of Top Tensioned Risers. (PhD Thesis, CeSOS)
IMT-2007-24	Johansen, Vegar	Modelling flexible slender system for real-time simulations and control applications
IMT-2007-25	Wroldsen, Anders Sunde	Modelling and control of tensegrity structures.

		(PhD Thesis, CeSOS)
IMT-2007-26	Aronsen, Kristoffer Høye	An experimental investigation of in-line and combined inline and cross flow vortex induced vibrations. (Dr. avhandling, IMT)
IMT-2007-27	Gao, Zhen	Stochastic Response Analysis of Mooring Systems with Emphasis on Frequency-domain Analysis of Fatigue due to Wide-band Response Processes (PhD Thesis, CeSOS)
IMT-2007-28	Thorstensen, Tom Anders	Lifetime Profit Modelling of Ageing Systems Utilizing Information about Technical Condition. (Dr.ing. thesis, IMT)
IMT-2008-29	Refsnes, Jon Erling Gorset	Nonlinear Model-Based Control of Slender Body AUVs (PhD Thesis, IMT)
IMT-2008-30	Berntsen, Per Ivar B.	Structural Reliability Based Position Mooring. (PhD-Thesis, IMT)
IMT-2008-31	Ye, Naiquan	Fatigue Assessment of Aluminium Welded Box-stiffener Joints in Ships (Dr.ing. thesis, IMT)
IMT-2008-32	Radan, Damir	Integrated Control of Marine Electrical Power Systems. (PhD-Thesis, IMT)
IMT-2008-33	Thomassen, Paul	Methods for Dynamic Response Analysis and Fatigue Life Estimation of Floating Fish Cages. (Dr.ing. thesis, IMT)
IMT-2008-34	Pákozdi, Csaba	A Smoothed Particle Hydrodynamics Study of Two-dimensional Nonlinear Sloshing in Rectangular Tanks. (Dr.ing.thesis, IMT/ CeSOS)
IMT-2007-35	Grytøyr, Guttorm	A Higher-Order Boundary Element Method and Applications to Marine Hydrodynamics. (Dr.ing.thesis, IMT)
IMT-2008-36	Drummen, Ingo	Experimental and Numerical Investigation of Nonlinear Wave-Induced Load Effects in Containerships considering Hydroelasticity. (PhD thesis, CeSOS)
IMT-2008-37	Skejic, Renato	Maneuvering and Seakeeping of a Singel Ship and of Two Ships in Interaction. (PhD-Thesis, CeSOS)
IMT-2008-38	Harlem, Alf	An Age-Based Replacement Model for Repairable Systems with Attention to High-Speed Marine Diesel Engines. (PhD-Thesis, IMT)
IMT-2008-39	Alsos, Hagbart S.	Ship Grounding. Analysis of Ductile Fracture, Bottom Damage and Hull Girder Response. (PhD-thesis, IMT)
IMT-2008-40	Graczyk, Mateusz	Experimental Investigation of Sloshing Loading and Load Effects in Membrane LNG Tanks Subjected to Random Excitation. (PhD-thesis, CeSOS)
IMT-2008-41	Taghipour, Reza	Efficient Prediction of Dynamic Response for Flexible amd Multi-body Marine Structures. (PhD-

		thesis, CeSOS)
IMT-2008-42	Ruth, Eivind	Propulsion control and thrust allocation on marine vessels. (PhD thesis, CeSOS)
IMT-2008-43	Nystad, Bent Helge	Technical Condition Indexes and Remaining Useful Life of Aggregated Systems. PhD thesis, IMT
IMT-2008-44	Soni, Prashant Kumar	Hydrodynamic Coefficients for Vortex Induced Vibrations of Flexible Beams, PhD thesis, CeSOS
IMT-2009-45	Amlashi, Hadi K.K.	Ultimate Strength and Reliability-based Design of Ship Hulls with Emphasis on Combined Global and Local Loads. PhD Thesis, IMT
IMT-2009-46	Pedersen, Tom Arne	Bond Graph Modelling of Marine Power Systems. PhD Thesis, IMT
IMT-2009-47	Kristiansen, Trygve	Two-Dimensional Numerical and Experimental Studies of Piston-Mode Resonance. PhD-Thesis, CeSOS
IMT-2009-48	Ong, Muk Chen	Applications of a Standard High Reynolds Number Model and a Stochastic Scour Prediction Model for Marine Structures. PhD-thesis, IMT
IMT-2009-49	Hong, Lin	Simplified Analysis and Design of Ships subjected to Collision and Grounding. PhD-thesis, IMT
IMT-2009-50	Koushan, Kamran	Vortex Induced Vibrations of Free Span Pipelines, PhD thesis, IMT
IMT-2009-51	Korsvik, Jarl Eirik	Heuristic Methods for Ship Routing and Scheduling. PhD-thesis, IMT
IMT-2009-52	Lee, Jihoon	Experimental Investigation and Numerical in Analyzing the Ocean Current Displacement of Longlines. Ph.d.-Thesis, IMT.
IMT-2009-53	Vestbøstad, Tone Gran	A Numerical Study of Wave-in-Deck Impact usin a Two-Dimensional Constrained Interpolation Profile Method, Ph.d.thesis, CeSOS.
IMT-2009-54	Bruun, Kristine	Bond Graph Modelling of Fuel Cells for Marine Power Plants. Ph.d.-thesis, IMT
IMT 2009-55	Holstad, Anders	Numerical Investigation of Turbulence in a Sekwed Three-Dimensional Channel Flow, Ph.d.-thesis, IMT.
IMT 2009-56	Ayala-Uraga, Efren	Reliability-Based Assessment of Deteriorating Ship-shaped Offshore Structures, Ph.d.-thesis, IMT
IMT 2009-57	Kong, Xiangjun	A Numerical Study of a Damaged Ship in Beam Sea Waves. Ph.d.-thesis, IMT/CeSOS.
IMT 2010-58	Kristiansen, David	Wave Induced Effects on Floaters of Aquaculture Plants, Ph.d.-thesis, CeSOS.

IMT 2010-59	Ludvigsen, Martin	An ROV-Toolbox for Optical and Acoustic Scientific Seabed Investigation. Ph.d.-thesis IMT.
IMT 2010-60	Hals, Jørgen	Modelling and Phase Control of Wave-Energy Converters. Ph.d.thesis, CeSOS.
IMT 2010- 61	Shu, Zhi	Uncertainty Assessment of Wave Loads and Ultimate Strength of Tankers and Bulk Carriers in a Reliability Framework. Ph.d. Thesis, IMT/ CeSOS
IMT 2010-62	Shao, Yanlin	Numerical Potential-Flow Studies on Weakly-Nonlinear Wave-Body Interactions with/without Small Forward Speed, Ph.d.thesis,CeSOS.
IMT 2010-63	Califano, Andrea	Dynamic Loads on Marine Propellers due to Intermittent Ventilation. Ph.d.thesis, IMT.
IMT 2010-64	El Khoury, George	Numerical Simulations of Massively Separated Turbulent Flows, Ph.d.-thesis, IMT
IMT 2010-65	Seim, Knut Sponheim	Mixing Process in Dense Overflows with Emphasis on the Faroe Bank Channel Overflow. Ph.d.thesis, IMT
IMT 2010-66	Jia, Huirong	Structural Analysis of Intect and Damaged Ships in a Collission Risk Analysis Perspective. Ph.d.thesis CeSoS.
IMT 2010-67	Jiao, Linlin	Wave-Induced Effects on a Pontoon-type Very Large Floating Structures (VLFS). Ph.D.-thesis, CeSOS.
IMT 2010-68	Abrahamsen, Bjørn Christian	Sloshing Induced Tank Roof with Entrapped Air Pocket. Ph.d.thesis, CeSOS.
IMT 2011-69	Karimirad, Madjid	Stochastic Dynamic Response Analysis of Spar-Type Wind Turbines with Catenary or Taut Mooring Systems. Ph.d.-thesis, CeSOS.
IMT - 2011-70	Erlend Meland	Condition Monitoring of Safety Critical Valves. Ph.d.-thesis, IMT.
IMT – 2011-71	Yang, Limin	Stochastic Dynamic System Analysis of Wave Energy Converter with Hydraulic Power Take-Off, with Particular Reference to Wear Damage Analysis, Ph.d. Thesis, CeSOS.
IMT – 2011-72	Visscher, Jan	Application of Particla Image Velocimetry on Turbulent Marine Flows, Ph.d.Thesis, IMT.
IMT – 2011-73	Su, Biao	Numerical Predictions of Global and Local Ice Loads on Ships. Ph.d.Thesis, CeSOS.
IMT – 2011-74	Liu, Zhenhui	Analytical and Numerical Analysis of Iceberg Collision with Ship Structures. Ph.d.Thesis, IMT.
IMT – 2011-75	Aarsæther, Karl Gunnar	Modeling and Analysis of Ship Traffic by Observation and Numerical Simulation. Ph.d.Thesis, IMT.

Imt – 2011-76	Wu, Jie	Hydrodynamic Force Identification from Stochastic Vortex Induced Vibration Experiments with Slender Beams. Ph.d.Thesis, IMT.
Imt – 2011-77	Amini, Hamid	Azimuth Propulsors in Off-design Conditions. Ph.d.Thesis, IMT.
IMT – 2011-78	Nguyen, Tan-Hoi	Toward a System of Real-Time Prediction and Monitoring of Bottom Damage Conditions During Ship Grounding. Ph.d.thesis, IMT.
IMT- 2011-79	Tavakoli, Mohammad T.	Assessment of Oil Spill in Ship Collision and Grounding, Ph.d.thesis, IMT.
IMT- 2011-80	Guo, Bingjie	Numerical and Experimental Investigation of Added Resistance in Waves. Ph.d.Thesis, IMT.
IMT- 2011-81	Chen, Qiaofeng	Ultimate Strength of Aluminium Panels, considering HAZ Effects, IMT
IMT- 2012-82	Kota, Ravikiran S.	Wave Loads on Decks of Offshore Structures in Random Seas, CeSOS.
IMT- 2012-83	Sten, Ronny	Dynamic Simulation of Deep Water Drilling Risers with Heave Compensating System, IMT.
IMT- 2012-84	Berle, Øyvind	Risk and resilience in global maritime supply chains, IMT.
IMT- 2012-85	Fang, Shaoji	Fault Tolerant Position Mooring Control Based on Structural Reliability, CeSOS.
IMT- 2012-86	You, Jikun	Numerical studies on wave forces and moored ship motions in intermediate and shallow water, CeSOS.
IMT- 2012-87	Xiang ,Xu	Maneuvering of two interacting ships in waves, CeSOS
IMT- 2012-88	Dong, Wenbin	Time-domain fatigue response and reliability analysis of offshore wind turbines with emphasis on welded tubular joints and gear components, CeSOS
IMT- 2012-89	Zhu, Suji	Investigation of Wave-Induced Nonlinear Load Effects in Open Ships considering Hull Girder Vibrations in Bending and Torsion, CeSOS
IMT- 2012-90	Zhou, Li	Numerical and Experimental Investigation of Station-keeping in Level Ice, CeSOS
IMT- 2012-91	Ushakov, Sergey	Particulate matter emission characteristics from diesel enignes operating on conventional and alternative marine fuels, IMT
IMT- 2013-1	Yin, Decao	Experimental and Numerical Analysis of Combined In-line and Cross-flow Vortex Induced Vibrations, CeSOS

IMT-2013-2	Kurniawan, Adi	Modelling and geometry optimisation of wave energy converters, CeSOS
IMT-2013-3	Al Ryati, Nabil	Technical condition indexes doe auxiliary marine diesel engines, IMT
IMT-2013-4	Firoozkoohi, Reza	Experimental, numerical and analytical investigation of the effect of screens on sloshing, CeSOS
IMT-2013-5	Ommani, Babak	Potential-Flow Predictions of a Semi-Displacement Vessel Including Applications to Calm Water Broaching, CeSOS
IMT-2013-6	Xing, Yihan	Modelling and analysis of the gearbox in a floating spar-type wind turbine, CeSOS
IMT-7-2013	Balland, Océane	Optimization models for reducing air emissions from ships, IMT
IMT-8-2013	Yang, Dan	Transitional wake flow behind an inclined flat plate-----Computation and analysis, IMT
IMT-9-2013	Abdillah, Suyuthi	Prediction of Extreme Loads and Fatigue Damage for a Ship Hull due to Ice Action, IMT
IMT-10-2013	Ramìrez, Pedro Agustìn Pèrez	Ageing management and life extension of technical systems- Concepts and methods applied to oil and gas facilities, IMT
IMT-11-2013	Chuang, Zhenju	Experimental and Numerical Investigation of Speed Loss due to Seakeeping and Maneuvering. IMT
IMT-12-2013	Etemaddar, Mahmoud	Load and Response Analysis of Wind Turbines under Atmospheric Icing and Controller System Faults with Emphasis on Spar Type Floating Wind Turbines, IMT
IMT-13-2013	Lindstad, Haakon	Strategies and measures for reducing maritime CO2 emissons, IMT
IMT-14-2013	Haris, Sabril	Damage interaction analysis of ship collisions, IMT
IMT-15-2013	Shainee, Mohamed	Conceptual Design, Numerical and Experimental Investigation of a SPM Cage Concept for Offshore Mariculture, IMT
IMT-16-2013	Gansel, Lars	Flow past porous cylinders and effects of biofouling and fish behavior on the flow in and around Atlantic salmon net cages, IMT
IMT-17-2013	Gaspar, Henrique	Handling Aspects of Complexity in Conceptual Ship Design, IMT
IMT-18-2013	Thys, Maxime	Theoretical and Experimental Investigation of a Free Running Fishing Vessel at Small Frequency of Encounter, CeSOS
IMT-19-2013	Aglen, Ida	VIV in Free Spanning Pipelines, CeSOS

IMT-1-2014	Song, An	Theoretical and experimental studies of wave diffraction and radiation loads on a horizontally submerged perforated plate, CeSOS
IMT-2-2014	Rogne, Øyvind Ygre	Numerical and Experimental Investigation of a Hinged 5-body Wave Energy Converter, CeSOS
IMT-3-2014	Dai, Lijuan	Safe and efficient operation and maintenance of offshore wind farms ,IMT
IMT-4-2014	Bachynski, Erin Elizabeth	Design and Dynamic Analysis of Tension Leg Platform Wind Turbines, CeSOS
IMT-5-2014	Wang, Jingbo	Water Entry of Freefall Wedged – Wedge motions and Cavity Dynamics, CeSOS
IMT-6-2014	Kim, Ekaterina	Experimental and numerical studies related to the coupled behavior of ice mass and steel structures during accidental collisions, IMT
IMT-7-2014	Tan, Xiang	Numerical investigation of ship's continuous- mode icebreaking in leverl ice, CeSOS
IMT-8-2014	Muliawan, Made Jaya	Design and Analysis of Combined Floating Wave and Wind Power Facilities, with Emphasis on Extreme Load Effects of the Mooring System, CeSOS
IMT-9-2014	Jiang, Zhiyu	Long-term response analysis of wind turbines with an emphasis on fault and shutdown conditions, IMT
IMT-10-2014	Dukan, Fredrik	ROV Motion Control Systems, IMT
IMT-11-2014	Grimsmo, Nils I.	Dynamic simulations of hydraulic cylinder for heave compensation of deep water drilling risers, IMT
IMT-12-2014	Kvittem, Marit I.	Modelling and response analysis for fatigue design of a semisubmersible wind turbine, CeSOS
IMT-13-2014	Akhtar, Juned	The Effects of Human Fatigue on Risk at Sea, IMT
IMT-14-2014	Syahroni, Nur	Fatigue Assessment of Welded Joints Taking into Account Effects of Residual Stress, IMT
IMT-1-2015	Bøckmann, Eirik	Wave Propulsion of ships, IMT
IMT-2-2015	Wang, Kai	Modelling and dynamic analysis of a semi-submersible floating vertical axis wind turbine, CeSOS
IMT-3-2015	Fredriksen, Arnt Gunvald	A numerical and experimental study of a two-dimensional body with moonpool in waves and current, CeSOS
IMT-4-2015	Jose Patricio Gallardo Canabes	Numerical studies of viscous flow around bluff bodies, IMT

IMT-5-2015	Vegard Longva	Formulation and application of finite element techniques for slender marine structures subjected to contact interactions, IMT
IMT-6-2015	Jacobus De Vaal	Aerodynamic modelling of floating wind turbines, CeSOS
IMT-7-2015	Fachri Nasution	Fatigue Performance of Copper Power Conductors, IMT
IMT-8-2015	Oleh I Karpa	Development of bivariate extreme value distributions for applications in marine technology,CeSOS
IMT-9-2015	Daniel de Almeida Fernandes	An output feedback motion control system for ROVs, AMOS
IMT-10-2015	Bo Zhao	Particle Filter for Fault Diagnosis: Application to Dynamic Positioning Vessel and Underwater Robotics, CeSOS
IMT-11-2015	Wenting Zhu	Impact of emission allocation in maritime transportation, IMT
IMT-12-2015	Amir Rasekhi Nejad	Dynamic Analysis and Design of Gearboxes in Offshore Wind Turbines in a Structural Reliability Perspective, CeSOS
IMT-13-2015	Arturo Jesùs Ortega Malca	Dynamic Response of Flexibles Risers due to Unsteady Slug Flow, CeSOS
IMT-14-2015	Dagfinn Husjord	Guidance and decision-support system for safe navigation of ships operating in close proximity, IMT
IMT-15-2015	Anirban Bhattacharyya	Ducted Propellers: Behaviour in Waves and Scale Effects, IMT
IMT-16-2015	Qin Zhang	Image Processing for Ice Parameter Identification in Ice Management, IMT
IMT-1-2016	Vincentius Rumawas	Human Factors in Ship Design and Operation: An Experiential Learning, IMT
IMT-2-2016	Martin Storheim	Structural response in ship-platform and ship-ice collisions, IMT
IMT-3-2016	Mia Abrahamsen Prsic	Numerical Simulations of the Flow around single and Tandem Circular Cylinders Close to a Plane Wall, IMT
IMT-4-2016	Tufan Arslan	Large-eddy simulations of cross-flow around ship sections, IMT

IMT-5-2016	Pierre Yves-Henry	Parametrisation of aquatic vegetation in hydraulic and coastal research,IMT
IMT-6-2016	Lin Li	Dynamic Analysis of the Instalation of Monopiles for Offshore Wind Turbines, CeSOS
IMT-7-2016	Øivind Kåre Kjerstad	Dynamic Positioning of Marine Vessels in Ice, IMT
IMT-8-2016	Xiaopeng Wu	Numerical Analysis of Anchor Handling and Fish Trawling Operations in a Safety Perspective, CeSOS
IMT-9-2016	Zhengshun Cheng	Integrated Dynamic Analysis of Floating Vertical Axis Wind Turbines, CeSOS
IMT-10-2016	Ling Wan	Experimental and Numerical Study of a Combined Offshore Wind and Wave Energy Converter Concept
IMT-11-2016	Wei Chai	Stochastic dynamic analysis and reliability evaluation of the roll motion for ships in random seas, CeSOS
IMT-12-2016	Øyvind Selnes Patricksson	Decision support for conceptual ship design with focus on a changing life cycle and future uncertainty, IMT
IMT-13-2016	Mats Jørgen Thorsen	Time domain analysis of vortex-induced vibrations, IMT
IMT-14-2016	Edgar McGuinness	Safety in the Norwegian Fishing Fleet – Analysis and measures for improvement, IMT
IMT-15-2016	Sepideh Jafarzadeh	Energy effiency and emission abatement in the fishing fleet, IMT
IMT-16-2016	Wilson Ivan Guachamin Acero	Assessment of marine operations for offshore wind turbine installation with emphasis on response-based operational limits, IMT
IMT-17-2016	Mauro Candeloro	Tools and Methods for Autonomous Operations on Seabed and Water Column using Underwater Vehicles, IMT